University of Dundee

University of Dundee

DOCTOR OF PHILOSOPHY

The functional and molecular characterisation of the novel DNA damage repair protein Bod1L

Davies, Alistair Michael

Award date:
2015

Link to publication

General rights
Copyright and moral rights for the publications made accessible in the public portal are retained by the authors and/or other copyright owners and it is a condition of accessing publications that users recognise and abide by the legal requirements associated with these rights.

- Users may download and print one copy of any publication from the public portal for the purpose of private study or research.
- You may not further distribute the material or use it for any profit-making activity or commercial gain
- You may freely distribute the URL identifying the publication in the public portal

Take down policy
If you believe that this document breaches copyright please contact us providing details, and we will remove access to the work immediately and investigate your claim.

Download date: 05. May. 2023

The functional and molecular characterisation of the novel DNA damage repair protein Bod1L

A thesis submitted in fulfilment of the requirements for the degree of Doctor of Philosophy

Alistair Michael Davies

College of Life Sciences, University of Dundee, United Kingdom

September 2015

Ph.D. Supervisor: Prof. Jason R Swedlow, University of Dundee

Internal Examiner: Prof. Ronald T. Hay, University of Dundee

External Examiner: Prof. Francis A. Barr, University of Oxford

Abstract

DNA damage induces MDC1 recruitment and establishes a signalling platform that mediates the DNA damage response (DDR). I show that Bod1L plays a central role in DDR by controlling MDC1 and PP2A-B56 localisation to damaged DNA. Bod1L depletion leads to micronuclei formation in undamaged cells and hypersensitivity to genotoxic stress. Bod1L binds to chromatin and is phosphorylated by ATM at sites of DNA damage. In Bod1L-depleted cells, ATM activity is normal, but there is over-accumulation of MDC1 at damaged sites caused by hyper-phosphorylation of MDC1-T4. I show that PP2A-B56 phosphatase can dephosphorylate MDC1-T4 following DNA damage and that MDC1 accumulation is limited by PP2A-B56. PP2A-B56 binds Bod1L exclusively in damaged cells and requires Bod1L for localisation to damaged DNA.

In addition to mediating repair, DNA damage triggers cell-cycle arrest, allowing adequate time for DNA repair to occur and to prevent transmission of any DNA lesion to daughter cells. The data presented in this thesis provides evidence that Bod1L acts as a regulator of Chk2 activation, acting to release Chk2 from the well-characterised inhibitory Chk2/PP2A-B56 phosphatase complex upon DNA damage, thus allowing the kinase to phosphorylate downstream substrates.

Overall, Bod1L makes three critical contributions to the DNA damage response: it promotes the initial targeting of MDC1, limits MDC1 accumulation by targeting PP2A-B56 to dephosphorylate MDC1-T4 and regulates the phosphorylation and activation of the transducer kinase Chk2.

Acknowledgements

First and foremost I would like to thank Prof. Jason Swedlow for his support and guidance throughout my PhD. Jason's support of my both my professional and personal development has helped me achieve countless goals throughout the course of my PhD and helped develop my future career aspirations. I would also like to thank Dr. Iain Porter for the wonderful supervision he has provided me with throughout my time in Dundee. Without Iain's direction and perseverance I think it unlikely that I would have had the great experience I was lucky enough to enjoy. I would like to thank all of the other members of the Swedlow lab, Dr. Katharina Schleicher, Michael Porter and Dr. Sandra Moser, who have given their time to help me in various different ways throughout my Ph.D., from guidance in the lab, to much needed coffee and lunch breaks. Furthermore, I would like to thank the members of the Griffis, Saurin and Tanaka labs, whose stimulating lab-meeting discussions and kind gifts of reagents have helped drive the project on during difficult times.

My thanks go out to the support I have received from my funding agency, the Wellcome Trust, without whom none of this work would have been possible. Whilst there are too many people to individually thank from the College of Life Sciences for their help, I would like to particularly highlight the excellent technical help and assistance I received from the Dundee Imaging Facility.

Last but by no means least, I would like to thank my wonderful fiancée Heather for all of her help, encouragement and unwavering support even through the toughest times. Whilst you may never read or fully understand what is written here, it is because of you that I could get this done.

Author's Declaration

I hereby declare that the following thesis is based on the results of investigations conducted by me, and that this thesis is of my own composition. Work other than my own is clearly indicated in the text by reference to the relevant researchers or their publications. This thesis has not, in whole or part, been previously accepted for a higher degree.

Signed (Alistair Michael Davies)

……

Date

……

Supervisor's Declaration

I certify that the work of which this thesis is a record was performed by Alistair Michael Davies. The conditions of the relevant Ordinance and Regulations have been fulfilled.

Signed (Prof. Jason R. Swedlow FRSE)

……

Date

……

Table of Contents

List of Figures

List of Tables

Abbreviations

3' UTR	3' untranscribed region
53BP1	p53-binding protein 1
A	Alanine
A.U.	Arbitrary units
AbDil	Antibody dilution buffer
ABRA1	BRCA1-A complex subunit Abraxas
ACA	Anti-centromeric antigen
Alt-EJ	Alternative end-joining
APC/C	Anaphase promoting complex/cyclosome
ARPP19	cAMP-regulated phosphoprotein 19
AT	Ataxia-Telangiectasia
ATLD	Ataxia-Telangiectasia-Like Disorder
ATM	Ataxia-Telangiectasia mutated
ATP	Adenosine triphosphate
ATR	Ataxia telangiectasia-mutated Rad3-related homolog
BIR	Break-induced replication
BL21	BL21 strain *E. coli* cells
BLM	Bloom syndrome protein
Bod1	Biorientation of chromosomes in cell division protein 1
Bod1L	Bod1-like protein 1
BRCA1	Breast cancer type 1 susceptibility protein
BRCA1-A	BRCA1 complex of proteins
BRCA2	Breast cancer type 2 susceptibility protein

CDC20/45	Cell division cycle protein 20/45
CDC25A/C	M-phase inducer phosphatase 1/3
CDC27	Cell division cycle protein 27
CDK1/2	Cyclin-dependent kinase 1/2
CENPA	Histone H3-like centromeric protein A
Chk1	Serine/threonine checkpoint protein kinase 1
Chk2	Serine/threonine checkpoint protein kinase 2
CIP2A	Cancerous inhibitor of PP2A
CK2	Casein Kinase 2
COMPASS	Complex proteins associated with SET1
CtIP	CtBP-interacting protein/ DNA endonuclease RBBP8
CycB/E	Cyclin B/E
D	Aspartate
D-Loop	Displacement loop
DAPI	4',6-diamidino-2-phenylindole
DDR	DNA damage response
DH5α	DH5α strain *E. coli* cells
dHJ(s)	Double-Holliday junction(s)
DNA	Deoxyribonucleic acid
DNA-PK	DNA-dependent protein kinase
DNA-PKcs	DNA-dependent protein kinase catalytic subunit
DNA2	DNA replication ATP-dependent helicase/nuclease 2
DSB(s)	DNA double-strand break(s)
DSE	DNA double-strand end
DTT	Dithiothreitol
E	Glutamate

E. coli	*Escherichia coli*
EDTA	Ethylenediaminetetraacetic acid
EGTA	Ethylene glycol tetraacetic acid
EME1	Crossover junction endonuclease EME1
EMEM	Eagle's minimum essential medium
ENSA	Alpha-endosulfine
EXO1	Exonuclease 1
EYA	Eyes absent phosphatase
FA	Fanconi Anaemia
FANCE	Fanconi anemia group E protein
FANCD2	Fanconi-associated nuclease 1
FHA domain	Forkhead-associated domain
FRAP	Fluorescence recovery after photobleaching
FRET	Förster resonance energy transfer
G1 Phase	Gap phase 1
G2 Phase	Gap phase 2
GADD34	Growth arrest and DNA damage induced gene 34
GEN1	Flap endonuclease GEN homolog 1
GFP	Green fluorescent protein
H2A	Histone H2A
H2AX	Histone variant H2AX
H3	Histone H3
H3Kx	Methylate histone H3 (Lysine x)
HeLa	Human cervical adenocarcinoma cells
HERC2	HECT & RLD domain containing E3-Ub ligase 2
HR	Homologous recombination

IF	Immunofluorescence
IP	Immunoprecipitation
IR	Ionising radiation
IRIF	Ionising radiation induced focus
K	Lysine
KLH	Keyhole limpet hemocyanin
Ku70/80	X-ray repair cross-complementing protein 5/6
L	Leucine
LB	Luria-Bertani liquid medium
M Phase	Mitotic cell cycle phase
MAD2	Mitotic arrest deficient protein 2
MCAK	Mitotic centromere-associated kinesin
MCM7	DNA replication licensing factor MCM7
MDC1	Mediator of DNA damage checkpoint protein 1
MDM2	E3 ubiquitin-protein ligase Mdm2
MDMX	Mdm2-like p53-binding protein
MeOH	Methanol
MMC	Mitomycin C
MMEJ	Microhomology end-joining
MOPS	3-(N-morpholino) propanesulfonic acid
MRE11	Double-strand break repair protein MRE11A
MRN	MRN complex (MRE11, RAD50, NBS1)
MUS81	Crossover junction endonuclease MUS81
NBS	Nijmegen breakage syndrome
NBS1	Nijmegen breakage syndrome protein 1
NFBD1	Nuclear Factor with BRCT domains (MDC1)

NHEJ	Non-homologous end-joining
NLS	Nuclear localisation signal
OA	Okadaic acid
p53	Cellular tumour antigen p53
PAGE	Polyacrylamide gel electrophoresis
PALB2	Partner and localizer of BRCA2
PARP	Poly(ADP-ribose) polymerase
PBS	Phosphate-buffered saline
PCR	Polymerase chain reaction
PFA	Paraformaldeyhe
PIAS1/4	Protein inhibitor of activated STAT1/4
PIKK	Phosphatidylinositol 3-kinase-related kinase
PLK1	Polo-like kinase 1
PNK	Polynucleotide kinase
PNUTS	PP1 nuclear targeting subunit
PP	Protein phosphatase
PP1	Protein phosphatase 1
PP2A	Protein phosphatase 2A
PP4	Protein phosphatase 4
PST-rich	Proline-Serine-Threonine rich region
PTIP	PAX-interacting protein 1
PTM(s)	Post-translational modification(s)
RAD50	DNA repair protein RAD50
RAD51	DNA repair protein RAD51 homologue 1
RAD54	DNA repair and recombination protein RAD54-like
RAP80	BRCA1-A complex subunit RAP80

RDS	Radioresistant DNA synthesis
RFP (TagRFP-t)	Red fluorescent protein
RIF1	Telomere-associated protein RIF1
RING domain	Really Interesting New Gene domain
RIPA	Radioimmunoprecipitation assay buffer
RNA	Ribonucleic acid
RNF168	E3 ubiquitin-protein ligase RNF168
RNF4	E3 ubiquitin-protein ligase RNF4
RNF8	E3 ubiquitin-protein ligase RNF8
ROI	Region-of-interest
ROS	Reactive oxygen species
RPA	Replication protein A
S	Serine
S-Phase	DNA synthesis cell cycle phase
S.O.C.	Super optimal broth with catabolite repression
SAC	Spindle assembly checkpoint
SDS	Sodium dodecyl sulfate
SDSA	Synthesis-dependent strand annealing
SDT-repeat	Serine-Aspartate-Threonine repeat domain
Shg1	Complex proteins associated with SET1 protein Shg1
si3'UTR	Cells treated with Bod1L 3'UTR siRNA
siB56	Cells treated with B56 pool siRNA
siBod1L	Cells treated with Bod1L siRNA
siCTR	Cells treated with control siRNA
SIM	Sumo-interacting motif
siRNA	Small interfering RNA

SLX1/4	Structure-specific endonuclease subunit SLX1/4
SSA	Single-strand annealing
SSB(s)	Single-strand break(s)
ssDNA	Single strand DNA
T	Threonine
tBRCT	Tandem BRCA1 carboxy-terminal domain
TBS	Tris-buffer saline
Tip60	Histone acetyltransferase KAT5
TIPRL	TIP41-like protein
TOPOII	Topoisomerase II
TOPOIII	Topoisomerase III
TQXF-cluster	Threonine-Glutamine-x-Phenylalanine cluster
Tris	Tris(hydroxymethyl)aminomethane
Ub	Ubiquitination site
UBC13	Ubiquitin-conjugating enzyme E2 N
UDR	Ubiquitination-dependent recruitment motif
UIM	Ubiquitin-interacting motif
UV	Ultraviolet light
WB	Western blot
WSTF	Williams-Beuren syndrome transcription factor
WT	Wild-type
XLF	Non-homologous end-joining factor 1
XRCC1/4	X-ray repair cross-complementing protein 1/4
YFP	Yellow fluorescent protein
Z-stack	Sequential images taken at different focal planes
γH2AX	Phosphorylated histone H2AX (S139)

Chapter 1 – Introduction

1.1 DNA and DNA replication

Deoxyribonucleic acid (DNA) is a molecule responsible for carrying the genetic code necessary for the development, function and survival of the cell. In order to pass on this genetic information from one generation to the next, cells must precisely replicate their genomes before each cell division, ensuring that the genetic code passed on to each daughter cell is an exact copy of the maternal DNA. To ensure that DNA is replicated only once during the cell cycle, a complex mechanism exists, which couples the synthesis of new DNA to the progression of the cell cycle (Walter and Newport, 2000). Due to their size, eukaryotic genomes are replicated from many replication origins distributed along multiple chromosomes during S-phase of the cell cycle, allowing for the replication of large amounts on DNA in a relatively short period of time (Diffley, 2011).

To regulate the replication origins that are used during S-phase, thus ensuring that origins are not fired inappropriately, a pre-replicative (pre-RC) complex is formed during G1 phase of the cell cycle. This process involves the hierarchical assembly of a number of replication proteins, including the origin recognition complex (ORC), Cdt1 protein, Cdc6 protein, and mini-chromosome maintenance proteins (Mcm2-7) (Bell and Dutta, 2002). As this complex can only be assembled on chromatin during G1 phase of the cell cycle, it prevents the re-replication of DNA from occurring during S-phase, thus maintaining the high fidelity duplication of the genomic code (Blow and Dutta, 2005). During transition of the cell cycle from G1 to S-phase, the cyclin-dependent protein

kinase 1 (CDK1), together with the Cdc7/Dbf4 kinase (DDK) transition the pre-RC complex into an active replication fork (Diffley, 2011). During this process, Cdc6 is lost from the complex and Cdc45 and GINS are loaded onto the MCM2-7 proteins. This Cdc45-MCM-GINS (CMG) helicase complex, in association with additional accessory proteins, is required for DNA unwinding, allowing for replication of the leading and lagging DNA strands (Costa et al., 2011).

Once the cell passes into S-phase, the initiation complex becomes the replisome, which is responsible for coordination of DNA replication. The CMG helicase complex unwinds DNA and 5'-3' replication of the DNA is performed by DNA polymerase α/ε (leading strand) and DNA polymerase δ (lagging strand) in a complex consisting of a number of accessory factors. As these DNA polymerases require a primer on which to commence DNA synthesis, DNA polymerase α acts to synthesise such a primer in association with an RNA primase, on both leading and lagging strands prior to DNA synthesis by either Pol ε or Pol δ (McCulloch and Kunkel, 2008). As DNA replication of the lagging strand by Pol δ is discontinuous due to the continual unwinding of the maternal DNA, multiple DNA fragments are generated by the DNA-synthesis action of Pol δ. These 100-400 nucleotide fragments are termed Okazaki fragments. The short flaps created between each of the discontinuous fragments following ligation, are cleaved by structure-specific endonucleases and the remaining nicks ligated by DNA ligase 1 (Burgers, 2009). Following replication of the entire genome during S-phase, any damaged DNA or replication errors are corrected during the following G2-phase, following which a single copy of the genome is segregated into each daughter cell during mitosis.

1.2 Causes and types of DNA damage

As alluded to in the previous section, the DNA is under constant threat of damage from both endogenous sources such as replication errors, as well as exogenous sources such as radiation or genotoxic chemicals. These threats have the potential to result in the formation of a number of different DNA lesions. These can range from very common but minor lesions such as single-strand breaks (SSBs) and oxidative damage, to severe and highly toxic DNA double-strand breaks (DSBs), which pose a serious threat to the genomic stability of the cell (Hoeijmakers, 2009)(Figure 1.1). Left unrepaired, or repaired improperly, this genomic instability can combine with other genetic and epigenetic events to influence the oncogenic potential of the cell, possibly leading to tumorgenesis and the formation of cancerous lesions (Hanahan and Weinberg, 2000). So important is maintaining genomic stability, that it underlines the six biological capabilities acquired during the development of human tumours (Hanahan and Weinberg, 2011), with elevated levels of DNA damage commonly detected in early tumours (Bartkova et al., 2005). To overcome the vast array of DNA lesions that occur often simultaneously within the cell, a number of different pathways have evolved to counteract potential genomic instability. These complex mechanisms act in synchrony to detect and signal the presence of a DNA lesion; working in harmony to prevent cell-cycle progression and allow adequate time for DNA repair. Collectively these mechanisms have been termed the DNA damage response (DDR). Failing proper repair, the mechanism triggers cellular apoptosis or senescence to prevent the transmission of the DNA lesion to daughter cells (Ciccia and Elledge, 2010; Jackson and Bartek, 2009).

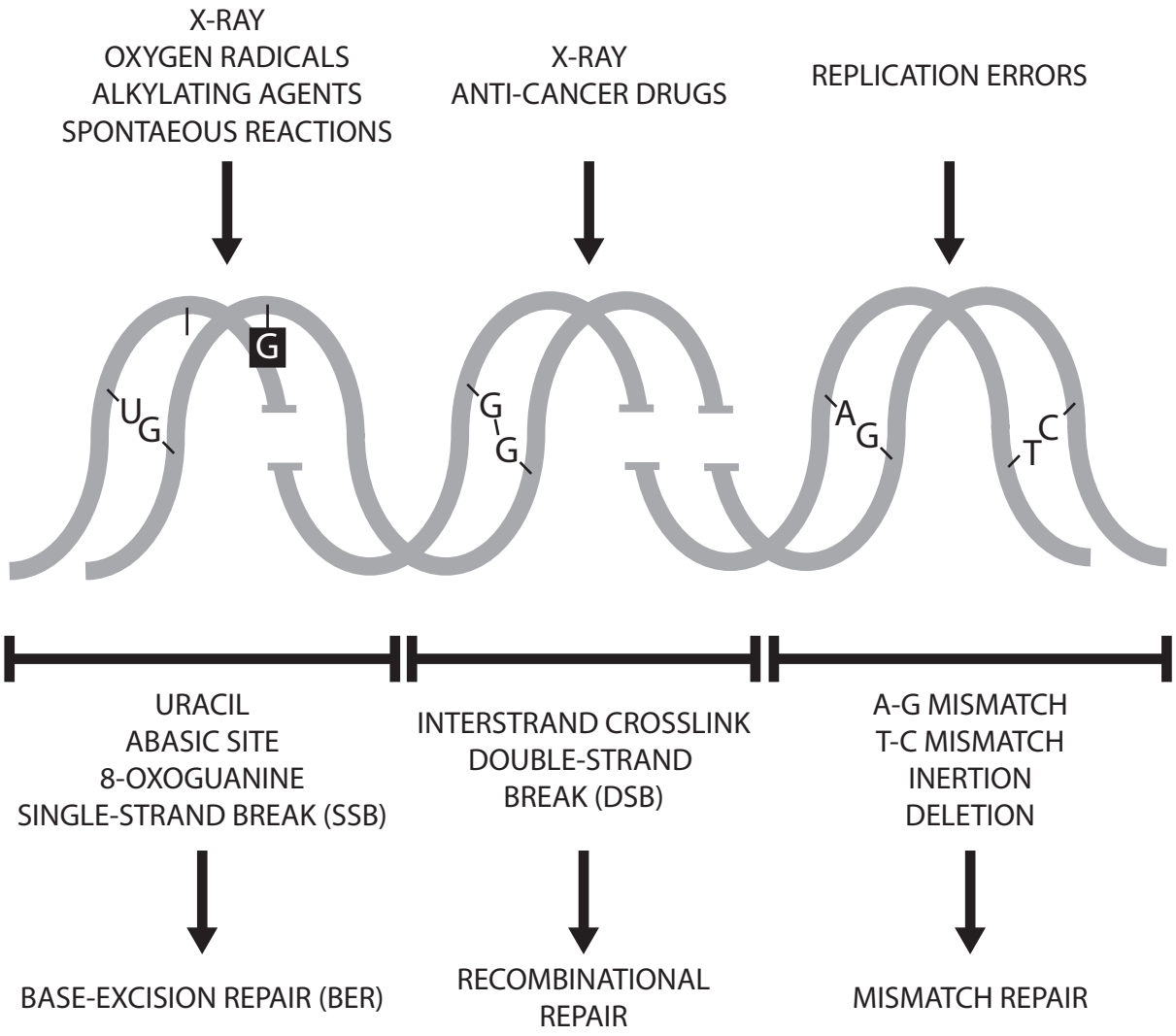

Figure 1.1: Types of DNA damage and repair mechanisms

Common forms of genotoxic stresses and poisons, along with examples of lesions induced by these agents. The DNA repair mechanism aligned with each type of damage is highlighted below. Adapted from (Hoeijmakers, 2001)

The importance of the DDR in the prevention of tumorgenesis is highlighted by the number of mutations in critical DDR components, such as p53 and ATM, present in early stage tumours (Negrini et al., 2010). Thus it is likely that tumour progression overcomes the barrier of DDR activation through mutations in critical DDR components, allowing rapid proliferation despite the presence of genomic instability (Bartek et al., 2007). Whilst mutations in these key components can drive tumorgenesis and proliferation, it renders cells harbouring such mutations hyper-sensitive to DNA damaging agents due to a lack of robust repair pathways (Helleday et al., 2008). Targeting cells with compromised DNA repair, for example the use of Poly(ADP-ribose) polymerase (PARP) inhibitors in cells with BRCA1/2 mutation, results in profound chromosomal instability, cell cycle arrest and subsequent apoptosis (Farmer et al., 2005). The use of such compounds, in combination with traditional chemotherapies has been successful in the treatment of previously resistant or difficult to treat cancers (Cheung-Ong et al., 2013; Lord and Ashworth, 2012).

1.3 ATM mediated DNA damage response

1.3.1 DNA double-strand break and the Phosphoinositide 3-kinase family

As mentioned previously, of the various different forms of DNA lesion bought about from endogenous and exogenous sources, the DNA double strand break is the most toxic to the cell, with a single DSB enough to induce apoptosis and cell death (Jackson, 2002). These breaks are generated when the two complementary strands on DNA are broken in close enough proximity that the chromatin structure and base-pairing are insufficient to keep the two DNA strands together (Jackson, 2002). This physical dissociation, coupled with base-pair damage mean that simple DNA ligation is insufficient for repair, with

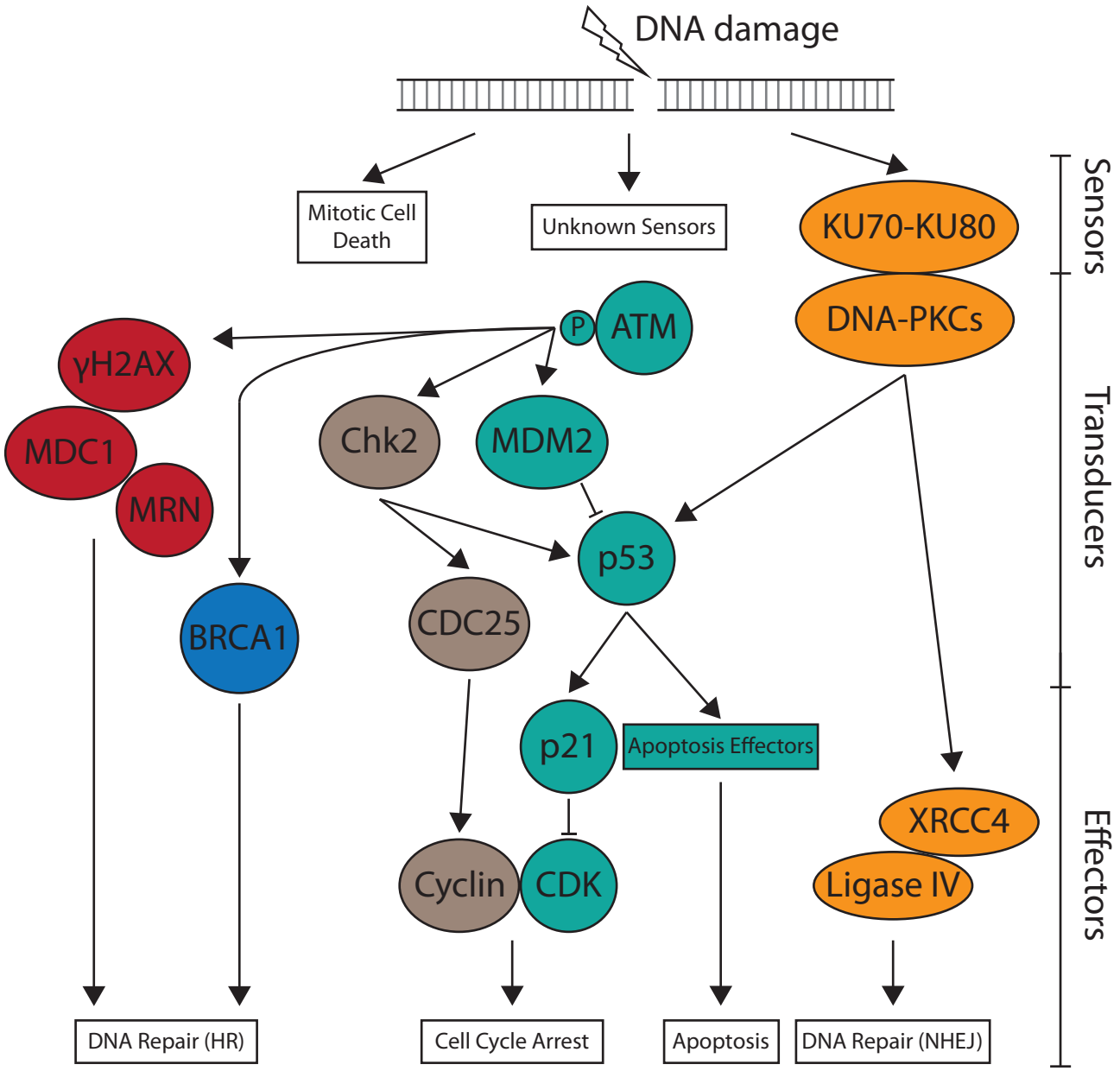

Figure 1.2: The cellular response to DNA damage

Schematic representation of the cellular response to DNA damage, divided into sensor, transducer and effector proteins. ATM is activated in response to damaged DNA, whose downstream phosphorylation activates a range of transducer proteins. Transducer protein activation leads to downstream interaction or modulation of effector proteins leading to a range of cellular effects to the initial damage event. Adapted from (Chen and Stubbe, 2005)

complex processing needed before repair can be carried out. Whilst DSBs can be caused by a variety of exogenous sources, such as ionising radiation (IR) and chemicals used for chemotherapy (Hoeijmakers, 2001), such breaks are often generated deliberately or accidently during a defined biological process (Jackson, 2002) (Figure 1.1). These processes include the deliberate generation of DSBs for V(D)J recombination, a process which occurs in developing B-/T-lymphocytes to generate antigen binding diversity (Fugmann et al., 2000). As well as deliberate DSB formation, these toxic breaks can also be generated naturally when replication forks encounter blocking lesions (such as reactive oxygen species (ROS)) leading to fork collapse (Shrivastav et al., 2008).

The repair of DSBs is mediated by the activity of the phosphatidylinositol 3-kinase-related kinase (PI3K) family, primarily by DNA-dependent protein kinase (DNA-PK) and Ataxia-telangiectasia mutated (ATM), which act to sense and transduce the DDR signalling to the effector proteins (Figure 1.2). ATM is responsible for the phosphorylation of over 700 downstream proteins in response to DNA damage, giving scope to the scale and involvement of the DDR in almost all cellular processes (Matsuoka et al., 2007). An additional PI3K family member, Ataxia-telangiectasia mutated and rad3-related kinase (ATR) is principally involved in the repair of single-stranded DNA breaks occurring as a result of replication stress (Brown and Baltimore, 2003). ATM and DNA-PK are both involved in the repair of DSBs, with the later functioning within the non-homologous end-joining pathway discussed in section 1.4.2.

1.3.2 The ATM mediated signalling response to DSBs

Upon the formation of a DSB, the MRN complex consisting of MRE11, RAD50 and NBS1 is rapidly recruited to the broken DNA ends, which acts to both tether the free DNA ends and recruit ATM (Lamarche et al., 2010). Through a C-terminal binding motif on NBS1, inactive ATM is recruited to the newly formed DSB, where it is subsequently activated by ATP-driven conformational changes in the MRN complex (Falck et al., 2005; Lee et al., 2013; Uziel et al., 2003). In the absence of DNA damage, the ATM kinase exists as an inactive dimer (Shiloh and Ziv, 2013). Recruitment of ATM to DSBs by MRN facilitates the autophosphorylation of ATM at S367, S1893, S1981 and S2996, in addition to the histone acetyltransferase Tip60 dependent acetylation on K3016, which result in the activation of the kinase (Bakkenist and Kastan, 2003; Kozlov et al., 2011; 2006; Sun et al., 2005). The MRN complex is also required for targeting Tip60 to H3K9me3, which is required to activate the acetyltransferase activity of Tip60 (Sun et al., 2009). These multiple post-translational modifications (PTMs) cause the inactive ATM dimer to dissociate, leading to the formation of active monomers (Shiloh and Ziv, 2013)(Figure 1.3).

Once activated, one of the first targets of ATM is histone H2AX, a histone variant of H2A that includes a longer C-terminal tail containing a conserved SQEY-COOH motif (Rogakou et al., 1998). Phosphorylation of the conserved S139 by ATM, in addition to the dephosphorylation of Y142 by the EYA phosphatase, initiates the recruitment of a number of downstream factors to the DSB, which can be visualised as a microscopic focus (Cook et al., 2009; Lukas et al., 2003; Rogakou et al., 1999). Phosphorylated γH2AX provides a binding

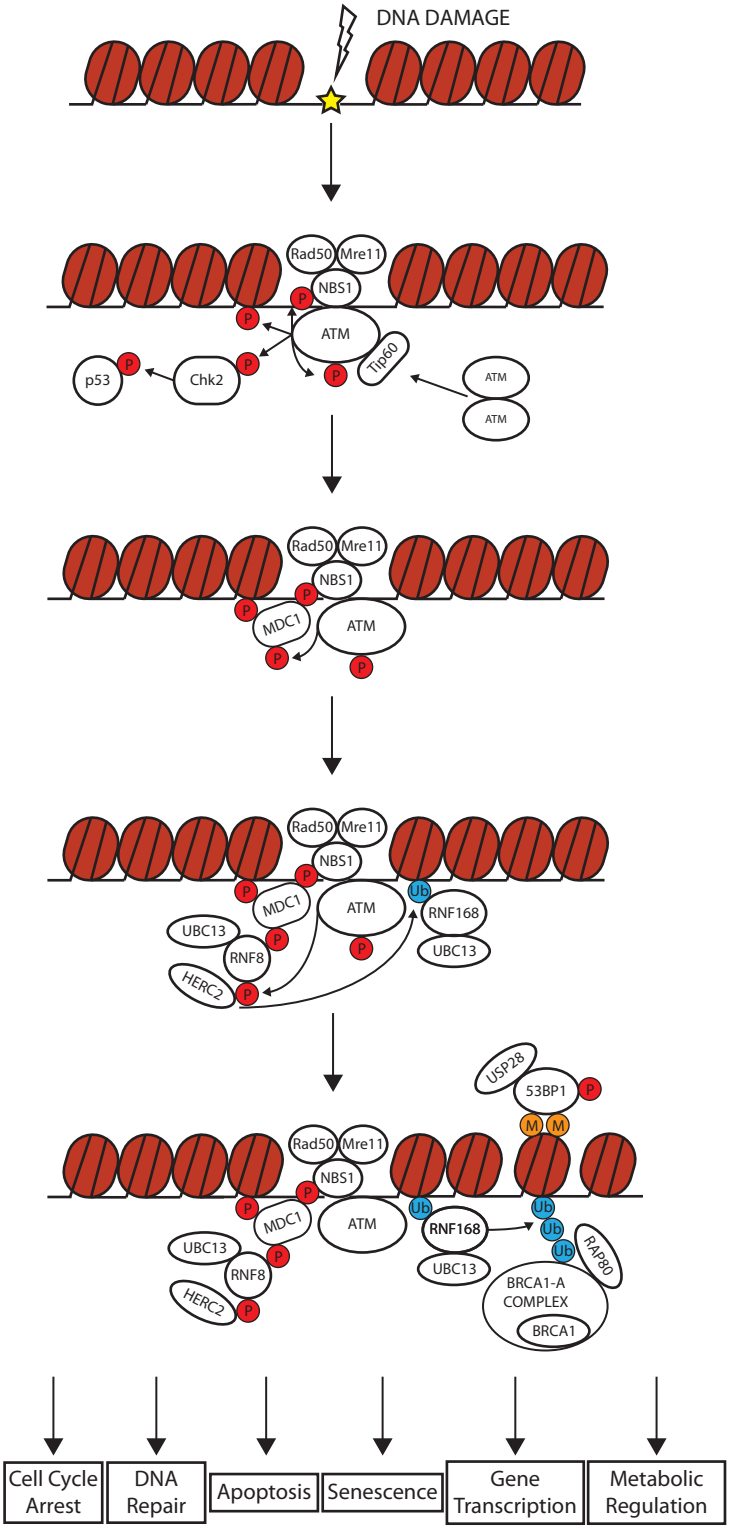

Figure 1.3: Multi-step signalling pathway of DNA double strand break recognition

Double strand break formation leads to the activation and of ATM via MRN complex and TIP60. Phosphorylation of Chk2 and p53 leads to cell cycle arrest. Phosphorylation of the histone variant H2AX initiates the γH2AX signalling cascade resulting in the direct and indirect recruitment of MDC1, RNF8/RNF168, BRCA1-A complex and 53BP1. The formation of these protein complexes at sites of DNA damage lead to the cellular processes outlined at the bottom of the figure Adapted from (Bohgaki et al., 2010; Ciccia and Elledge, 2010)

platform for a major phospho-scaffold protein Mediator of damage checkpoint 1 (MDC1), which interacts with γH2AX via its tandem BRCA1 carboxy-terminal (tBRCT) domain (Stucki et al., 2005). The principle purpose for the recruitment of MDC1 to DNA lesions is to act as a phosphoscaffold for the recruitment of a number of downstream proteins. MDC1 binds to NBS1 via the SDT-repeat domain of MDC1 and the FHA domain of NBS1, which serves to re-recruit the MRN complex to sites of damage (Chapman and Jackson, 2008; Melander et al., 2008; Spycher et al., 2008; Wu et al., 2008). MDC1 binding to the MRN complex at DSBs allows for the recruitment of additional ATM to DSBs via a positive feedback loop. The increased ATM recruitment serves to amplify the γH2AX phosphorylation and signalling in the region surrounding the DSB (Lou et al., 2006). This local increase in activated ATM also enables the phosphorylation of a number of key transducer kinases, such as Chk2 and p53, which act to control the cell cycle during the DDR (Ahn et al., 2000; 2002; Lukas et al., 2004b)(Figure 1.2). The control of cell-cycle during the DDR is discussed in depth in section 1.6.

In addition to the ATM-dependent recruitment of MRN to DSBs, MDC1 also functions to recruit a number of additional components to sites of damage. MDC1 is phosphorylated directly by ATM at the TQXF cluster, which promotes binding to the FHA domain of the E3 ubiquitin ligase RNF8 (Huen et al., 2007; Kolas et al., 2007; Mailand et al., 2007). RNF8, along with HERC2 and UBC13, are responsible for the ubiquitination (Lys-63) of H2A and H2AX in the chromatin region flanking the break (Bekker-Jensen et al., 2009; Mailand et al., 2007). This facilitates the recruitment of RNF168 to these ubiquitylated histones. RNF168, together with UBC13, catalyses the monoubiquitination of

the histones specifically on K13-15, which results in the conjugation of K63 ubiquitin chains at these sites (Mattiroli et al., 2012). As well as acting as a binding platform, ubiquitination of H2A and H2AX surrounding the DSB is believed to relax the chromatin structure, facilitating the recruitment of additional repair factors such as p53-binding protein 1 (53BP1) and Breast cancer susceptibility gene 1 (BRCA1) (Doil et al., 2009; Kolas et al., 2007; Stewart et al., 2009). In addition, the SUMO E3-ligases PIAS1 and PIAS4 are recruited to DSBs via their SAP domains and have been shown to be important in the robust recruitment of 53BP1, BRCA1 and RNF168 to damage sites (Galanty et al., 2010).

Recruitment of 53BP1 to DSBs is unusual in that initial recruitment of the protein is dependent on histone H4 di-methylated lysine 20 (H4K20me2) and histone H3 di-methylated lysine 79 (H3K79me2), rather than direct protein-protein interaction. These histone marks are revealed following the chromatin relaxation mediated by RNF8 and RNF168 (Botuyan et al., 2006; Huyen et al., 2004; Sanders et al., 2004)(Figure 1.3). It has also been shown that the direct ubiquitination of 53BP1 by RNF168 is important for proper 53BP1 recruitment to DSBs (Bohgaki et al., 2013). These methylated histones are recognised by the Tudor domain of 53BP1 (Zgheib et al., 2009). In addition, acetylation by Tip60 limits 53BP1 association with damaged chromatin, a mechanism believed to control the relative DSB chromatin occupancy and repair activities of BRCA1 and 53BP1 (Tang et al., 2013). Recently an additional regulatory mechanism has been identified, which acts to prevent 53BP1 recruitment to DSBs during mitosis. Phosphorylation of 53BP1 at T1609 and S1618 in the well-conserved ubiquitination-dependent recruitment (UDR) motif prevents 53BP1 recruitment

to H2A (Lee et al., 2014; Orthwein et al., 2014). This mechanism exists to prevent Aurora B kinase–dependent sister telomere fusions that produce di-centric chromosomes and aneuploidy when the DSB machinery is active during mitosis (Orthwein et al., 2014). Once recruited at DSBs, 53BP1 has a multifaceted role. 53BP1 is a key regulator of DSB repair pathway choice. During G1, it promotes non-homologous end-joining (NHEJ)-mediated DSB repair by supressing DNA end resection (Bunting et al., 2010). This pathway choice is mediated by mutual antagonism with breast cancer 1 (BRCA1). During S-G2 phase of the cell cycle, BRCA1 and CtIP promote DNA end-resection and thus homologous recombination-mediated DSB repair (Escribano-Diaz et al., 2013). Whilst the function of 53BP1 at DSB is understood, the mechanism into how 53BP1 blocks resection in G1 and how this is counteracted by BRCA1-CtIP to promote HR repair in S/G2 phase remains unknown (Panier and Boulton, 2013).

The K63-ubiquitin chains generated by the activity of RNF8 and RNF168 are also recognised by the ubiquitin-interacting motif (UIM) of RAP80, which recruits the BRCA1-A complex, through an interaction with the scaffold protein ABRA1 (Ciccia and Elledge, 2010; Huen et al., 2007; Kolas et al., 2007; Wang and Elledge, 2007). The recruitment of BRCA1-A to DSBs is also dependent on sumoylation. The SUMO E3-ligases PIAS1 and PIAS4 are recruited to DSBs via their SAP domains. PIAS4 is believed to stimulate the ubiquitin ligase activity of RNF8/UBC13, thus promoting recruitment of RNF168 and therefore BRCA1-A to sites of damage. PIAS1 is believed to directly sumoylate BRCA1 to stimulate its ubiquitin ligase activity (Galanty et al., 2010; Morris et al., 2010). RAP80 also contains a SUMO-interacting motif (SIM) which has been shown to be

necessary for DSB recruitment (Guzzo et al., 2012). Furthermore, RNF4, a SUMO-targeted ubiquitin E3-ligase that synthesises hybrid SUMO-ubiquitin chains, localises to DSBs and is critical for the recruitment of RAP80 and BRCA1 to sites of DNA damage (Guzzo et al., 2012). Loss of RNF4 results in defective loading of replication protein A (RPA) and Rad51 onto ssDNA, suggesting the importance of this protein in DSB repair (Yin et al., 2012). Once recruited to DSB, the BRCA1-A complex is involved in the DNA damage repair and the activation of cell-cycle checkpoints (Huen et al., 2009).

1.4 DNA double strand break (DSB) repair

Eukaryotic cells typically repair DSBs by one of two primary mechanisms: non-homologous end-joining (NHEJ) or homologous recombination (HR). Typical DSBs caused by doses of ionising radiation or structure-specific nucleases can be repaired using either pathway due to the availability of both DNA ends. DSBs caused by replication fork collapse are primarily repaired by HR, as these fork collapses produce a one-sided DSB, known as a double-strand end (DSE) (Rothstein et al., 2000; Shrivastav et al., 2008). The DSE has no second end to re-join and as such this break is incompatible with repair by NHEJ. Inappropriate activation of the NHEJ repair pathway following replication fork collapse is associated with detrimental genome rearrangements and cell death (Saberi et al., 2007).

NHEJ does not require sequence homology and as such is active throughout the cell cycle, therefore this repair pathway constitutes the major DSB repair mechanism in eukaryotic cells (Lieber, 2010). Whilst somewhat of a generalisation, this method of repair is termed “error-prone”, as the lack of homologous sequence surrounding the break risks potential nucleotide loss

during the repair process. In contrast to this, repair of DSBs by HR is considered “error-free”, as the mechanism utilises homologous sequences to align the DSB ends prior to ligation and thus limit any risk of nucleotide loss (Aparicio et al., 2014). Whilst repair by HR is possible during both the S and G2 phase of the cell cycle, recent evidence suggests that HR is only favoured during S-phase, with NHEJ the preferred mechanism to repair DSBs during the remaining cell cycle (Aparicio et al., 2014; Shahar et al., 2011; Shibata et al., 2011). Indeed the findings suggest that the principle role for HR repair is mainly in the repair of challenging DSBs, in contrast to uncomplicated lesions that are frequently repaired by NHEJ (Shahar et al., 2011; Shibata et al., 2011). Interestingly, lower organisms with mutations in key HR components show a much higher degree of radiosensitivity compared with mammalian cells with similar mutations. This suggests that a certain degree of redundancy is incorporated into the mammalian DNA repair system, unsurprising given the importance of maintaining genomic stability (Kakarougkas and Jeggo, 2014).

Several factors can determine the repair pathway chosen to repair a detected DSB. As discussed above, HR repair is only possible during S and G2 phase of the cell cycle and as such DSBs occurring during G1 are primarily repaired using NHEJ. DSBs detected during mitosis display diminished DNA repair, with the DSBs marked for repair after mitotic exit (Giunta and Jackson, 2011). Recent evidence suggests that this process protects the uncapped telomeric ends from the DSB repair machinery (Orthwein et al., 2014). Another critical mediator of repair pathway choice is the stability of DNA ends following a DSB. The initiation of 5’-3’ resection of DNA ends commits cells to HR repair, preventing repair by NHEJ (Chapman et al., 2012; Symington and Gautier,

2011). In addition to cell-cycle stage and stability of DNA ends, the interplay between 53BP1 and BRCA1 is crucial as a determinant of pathway choice. RIF1 and PTIP are recruited to DSBs via an interaction with ATM-phosphorylated 53BP1 (Callen et al., 2013; Escribano-Diaz et al., 2013; Munoz et al., 2007). RIF1/PTIP/53BP1 can then act to restrict BRCA1 accumulation at damage sites outside the S/G2 phases of the cell cycle, thus promoting repair by NHEJ. During S/G2 phases, BRCA1/CtIP can accumulate at the site surrounding the DSB and can render this region permissive to end resection, thus promoting repair by HR. Exactly how RIF1/PTIP/53BP1 can exclude BRCA1/CtIP from breaks during G1 remains unclear (Panier and Boulton, 2013).

1.4.1 Homologous Recombination

As mentioned above, BRCA1 has been shown to be critical for the initiation of DNA repair by HR. The protein acts to recruit and activate a number of proteins which facilitates repair (Chapman et al., 2012). The presence of single-strand DNA at the DSB end is necessary to initiate the search for sequence homology, which is generated by the nucleolytic degradation of the 5' strand of a DSB end, exposing a single-stranded 3' DNA terminus, in a process termed end resection (Aparicio et al., 2014). Resection is initiated by the MRN complex, which binds the DNA ends through RAD50 and resects the DNA via the action of MRE11. MRE11 cooperates with CtIP, a protein which is proteolytically degraded during G1 phase, to generate 3' ssDNA overhangs through a combination of endonucleolytic cleavage, followed by 3'-5' exonucleolytic processing (Shibata et al., 2014). Proteolytic degradation of CtIP during G1 phase acts as a further safeguard to ensure that HR can only occur during S/G2 phases (Germani et al., 2003). The initial processing of DNA ends by MRE11/CtIP provides a

substrate for the exonucleases EXO1 and DNA2 together with the helicase BLM, which act synergistically to unwind DNA and continue the DNA resection (Nimonkar et al., 2011).

The exposed ssDNA is coated with RPA, forming an RPA-ssDNA nucleoprotein filament. The binding of RPA serves to prevent the degradation or annealing of the ssDNA strand and also act to promote downstream DNA-processing protein recruitment, assembly and interaction (Chen et al., 2013; Fan and Pavletich, 2012; Zou et al., 2006). Rad51 is then recruited by BRCA2/PALB2 to the nucleoprotein filament, which displaces RPA from the ssDNA, resulting in Rad51-ssDNA nucleoprotein filament formation (Xia et al., 2006). These filaments, along with the ATPase Rad54, undergo homology searching and invade the homologous sister chromatid, forming a displacement-loop (D-loop) structure which contains the novel heteroduplex DNA and the displaced strand of donor DNA (Alexeev et al., 2003; Renkawitz et al., 2014).

Once formed, the D-loop is extended by DNA polymerases using the homologous strand as template. This DNA synthesis leads to the dissociation of Rad51 from heteroduplex DNA (Solinger et al., 2002). During the post-synapsis phase, the D-loop can be removed and the break resolved in a number of different ways. In the presence of a second DNA end, the predominant pathway for DSB repair is synthesis-dependent strand annealing (SDSA). Newly synthesised DNA is displaced from the D-loop and annealed to the resected DNA of the second end (Pâques and Haber, 1999). The process, thought to be promoted by the RTEL helicase following Rad51 displacement (Barber et al., 2008), removes the need for cross-overs and as such removes any potential

risk of genomic rearrangements (Heyer et al., 2010). If the original break occurred as a result of fork-collapse then the DSE created cannot undergo repair by SDSA as there is no resected second end to anneal to. Such breaks undergo a process termed break-induced replication (BIR), whereby the reassembly of a new replication fork at RAD51-generated D loop intermediates occurs (Llorente et al., 2008). Whilst this process repairs such breaks effectively, restoring the integrity of the chromosome, it can lead to loss of heterozygosity of all genetic information distal to the DSB (Heyer et al., 2010). A third alternative pathway for repair, involves the formation of double-Holliday junctions (dHJs), which form following ligation of the invading strand with the second end captured by D-loop branch migration (Nimonkar and Kowalczykowski, 2009). The dHJ formed can then be dissolved by the BLM/TOPOIIIα complex, or cleaved by the structure-specific endonucleases GEN1, MUS81/EME1, or SLX1/SLX4, producing either a crossover or non-crossover product (Ciccia and Elledge, 2010; Fekairi et al., 2009; Ip et al., 2008; Munoz et al., 2009; Svendsen et al., 2009). Aside from resolution of the dHJs by BLM/TOPOIIIα, resolution by GEN1, MUS81/EME1 or SLX1/SLX4 can lead to a loss of heterozygosity and can cause genomic rearrangements. As such resolution of dHJs by these structure-specific nucleases is highly regulated (Ciccia and Elledge, 2010).

1.4.2 Non-homologous end joining (NHEJ)

NHEJ, the major repair pathway for DSBs, is active throughout the cell cycle as the repair process is not reliant on a homologous DNA strand to act as template. DSB DNA ends are rapidly bound (within seconds) by the Ku70/Ku80 heterodimer, which may assist in tethering the broken DNA ends (Kim et al., 2005). Once bound, the Ku heterodimer translocates inwards, facilitating the

loading and activation of the catalytic subunit of the PIKK kinase, DNA-PK (DNA-PKcs) (Mahaney et al., 2009; Yoo and Dynan, 1999). The translocation of Ku allows the DNA-PK to interact across the DSB in a “synaptic complex”, which stimulates the kinase activity of DNA-PK and tethers the DNA ends together (DeFazio et al., 2002). The presence of DNA is also necessary for the full activation of the DNA-PK kinase activity (Gottlieb and Jackson, 1993). Active DNA-PK then phosphorylates a number of targets on SQ/TQ sites, including the Ku70/80 heterodimer, XRCC4 and Artemis, as well as autophosphorylation which is believed to be required for its release from DSBs *in vivo* (Douglas et al., 2002; Lee et al., 2004; Ma et al., 2005a; Mahaney et al., 2009). DNA breaks that contain non-ligatable ends are first processed by the Artemis/APLF nucleases which possesses DNA-PK-dependent endonuclease and DNA-PK-independent 5’-3’ exonucleases activity (Iles et al., 2007; Ma et al., 2005b). In addition, polynucleotide kinase (PNK) is also involved in DNA end-processing, possessing both 3’-DNA phosphatase and 5’-DNA kinase activities, allowing removal of non-compatible/non-ligatable end groups from DNA ends (Mahaney et al., 2009).

Once processed, DNA ends are ligated by DNA ligase IV in complex with XRCC4, with the help of the stimulatory factor XLF (Ahnesorg et al., 2006). XRCC4 possesses no enzymatic activity, instead acting as a scaffold to recruit ligation factors such as DNA ligase IV to the break and stimulate their activity to seal the break (Grawunder et al., 1997; Nick McElhinny et al., 2000).

1.4.3 Annealing-dependent repair pathways

Whilst the majority of DSBs are repaired by one of the two repair pathways detailed above, other modes of repair are observed in normal and pathological

settings. These alternative end-joining (Alt-EJ) pathways are often activated if one of the two major pathways becomes compromised. In a situation where HR repair is compromised, for example in BRCA1/2 deficient cells, microhomology-mediated end-joining (MMEJ) and single-strand annealing (SSA) can repair a DSB whose resection has rendered the break incompatible with NHEJ repair (Aparicio et al., 2014). These pathways undergo base pairing between strands of exposed homologous sequences on separate ssDNA overhangs, followed by further processing to fill in any gaps and ligate the nicks. Short homologous tracks are generally repaired by MMEJ, with longer tracks relying on SSA (Deriano and Roth, 2013). Both MMEJ and SSA pathway operate in the absence of classical NHEJ factors such as Ku70/80, XRCC4 and DNA ligase IV (Hartlerode and Scully, 2009), yet are reliant on the resection activity of the MRN-CtIP complex to expose regions of microhomology (Bennardo et al., 2008). DNA ligation is believed to be carried out using DNA ligase III/XRCC1, with some additional contribution from DNA ligase I (Dueva and Iliakis, 2013). Whilst these alterative repair pathways are capable of repairing DNA breaks in the absence of HR or NHEJ components, it is believed that the use of these pathways is associated with the formation of pathological chromosomal deletions and translocations in cancer cells (Della-Maria et al., 2011; Greenman et al., 2007).

1.4.4 Pathologies associated with defective DSB repair

A robust and functional response to DNA damage is critical to maintain cell viability and help prevent genomic instability and the downstream consequences of this. The importance of the DNA repair pathways is highlighted by the clinical severity of mutations in any of the key components of the DDR. Several mutations in the number of key DDR proteins have been

identified, with many clinical features of these mutations overlapping (Figure 1.4).

One of the best characterised of the conditions associated with defective DSB repair is Ataxia-Telangiectasia (AT), a neurodegenerative disease that presents during early childhood (Gatti et al., 2001). The prominent neurological sign of AT is a significant loss of cerebellar function, which results in increasing uncoordinated or ataxic movements and ocular telangiectasia (dilated eye blood vessels) (McKinnon, 2004). In addition to the well-characterised neurodegeneration and neurological clinical features, patients with AT also display a number of cellular features, including radiosensitivity and heightened susceptibility to lymphoreticular cancer such as leukaemia and lymphoma (Frappart and McKinnon, 2006; Gumy-Pause et al., 2003). AT arises as a result of mutations in the *ATM* gene. Whilst over 400 unique mutations have been reported for ATM in AT patients, extending the full length of the gene, almost all of these mutations are truncating or slice-site mutations that give rise to short, unstable ATM proteins (Lavin, 2008). Given a lack of functional ATM and the important role that this kinase plays in maintaining genomic stability, it is unsurprising that patients diagnosed with AT are prone to chromosomal instability and cancer predisposition. It still remains unclear as to whether the other pathophysiologies associated with AT arise as a direct result of unrepaired DNA damage, and the subsequent cell death, or indirectly due to the build-up of oxidative stress as a consequence of the persistence of breaks in DNA (Lavin, 2008).

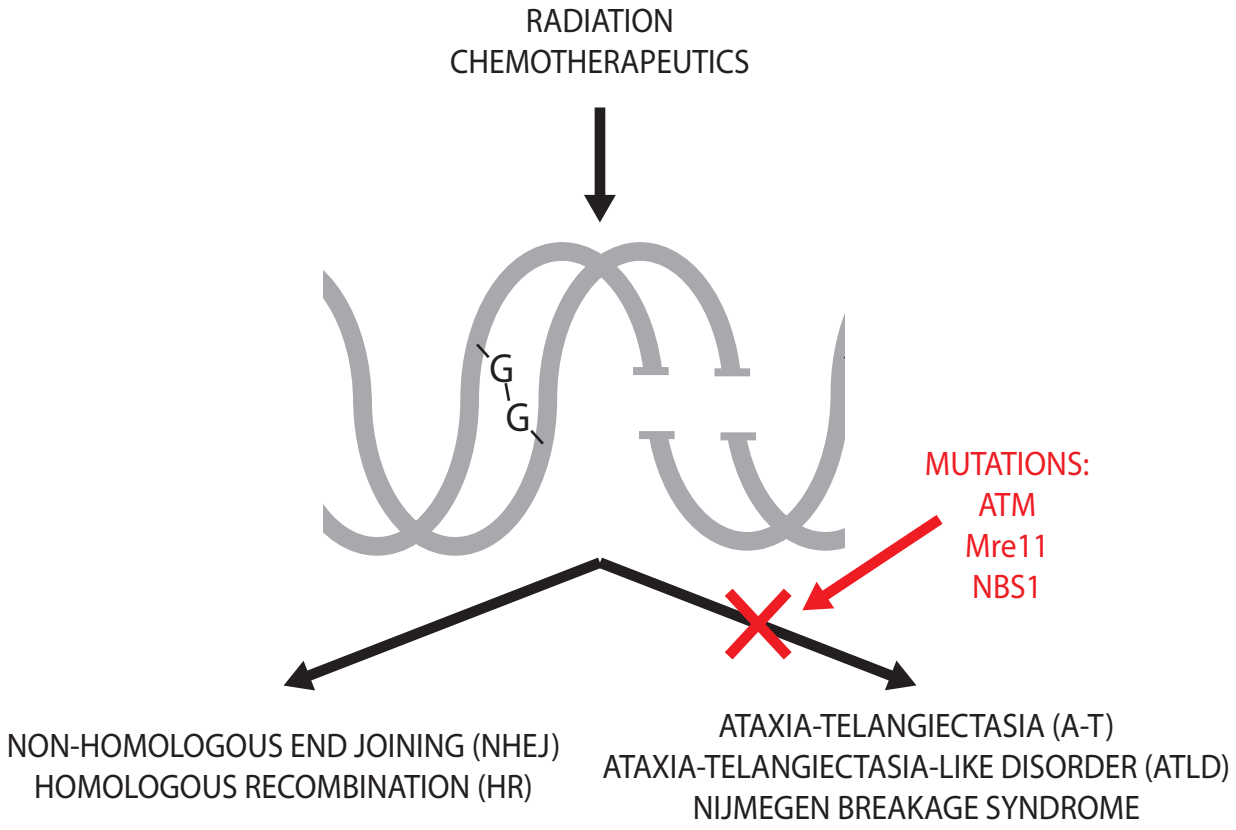

Figure 1.4: Pathologies resulting as a consequence of improper DNA damage repair

Representation of the consequences of mutated ATM, Mre11 or NBS1 on robust DNA repair. Mutation in ATM and Mre11 lead to Ataxia-Telangiectasia or Ataxia-Telangiectasia-Like-Disorder (ATLD) respectively. Mutations in NBS lead to Nijmegen Breakage Syndrome. Adapted from (McKinnon, 2009).

A syndrome similar in clinical presentation to AT is Ataxia-Telangiectasia-Like Disorder (ATLD), characterised by a hypomorphic mutation in the MRE11 gene (Stewart et al., 1999). The cellular features of ATLD are extremely similar to AT and include radiosensitivity, radioresistant DNA synthesis (RDS; suggestive of defective cell-cycle arrest) and an abrogation of the ATM signalling pathway (Stewart et al., 1999). Whilst ATLD patients suffer from the progressive cerebellar ataxia seen with AT patients, they show no telangiectasia and the onset of neurological effects is much later in presentation, suggestive that the condition is less severe than AT (Taylor et al., 2004). Whilst the ATLD is extremely rare in comparison to AT, with only 6 cases currently identified (Pitts et al., 2001), the similarity in clinical presentation and cellular pathophysiology of the two conditions suggest that disruption of any part of the early repair machinery can have severe consequences on human health (Taylor et al., 2004).

Whereas mutation in ATM and MRE11 produce very similar clinical and cellular traits, mutation in another component of the MRN complex, NBS1, termed Nijmegen breakage syndrome (NBS), leads to a subtly different clinical presentation (Shiloh, 1997; Varon et al., 1998). In addition to similar cellular pathophysiology to AT/ATLD such as radiosensitivity, immunodeficiency and increased cancer risk, NBS patients also display characteristic facial appearance, microcephaly and growth retardation (Digweed and Sperling, 2004). Over 90% of patients are homozygous for the same mutation which causes a deletion of five base pairs, leading to a frame shift and truncated form of NBS1 (Digweed and Sperling, 2004). One question that remains unanswered is why do NBS patients not get cerebellar degeneration that is commonly

associated with AT and ATLD patients, despite these proteins functioning in overlapping pathways. It has been hypothesised that the hypomorphic mutant NBS1 protein expressed in all NBS patients retains sufficient function to prevent progressive Purkinje and granule loss associated with the development of progressive cerebellar ataxia, yet the function of this protein is not sufficient to maintain robust DDR (Reynolds and Stewart, 2013). In addition, it has been proposed that the lack of functional ATM in AT patients prevents ATM/p53 dependent apoptosis from occurring, allowing relatively normal brain development even in the presence of unrepaired DSBs. In NBS patients, functional ATM can activate the apoptotic pathway in response to the genomic instability arising from truncated NBS1 due to the intact NBS1 C-terminal ATM interacting domain, leading to neuronal cell death during development and the downstream development of microcephaly (Reynolds and Stewart, 2013; Shull et al., 2009).

1.5 Key initial components of the DNA damage repair machinery

In response to DNA-damage, a large macromolecular assembly of proteins forms at the chromatin flanking the break. The formation of this protein cluster is highly ordered and occurs in a strictly hierarchical fashion, with regulation of protein interactions controlled by a variety of PTMs including phosphorylation, ubiquitination and sumoylation (Bekker-Jensen and Mailand, 2010). A number of key proteins that are recruited to the break during the early phases of the DDR mediate these PTMs and are critical in maintain a robust response to DNA damage (Jungmichel and Stucki, 2010).

1.5.1 MDC1

MDC1 (previously referred to as Nuclear Factor with BRCT Domains (NFBD1)) is a large phospho-scaffold binding protein involved in mammalian cell DNA damage repair. MDC1 was functionally characterised in a number of independent studies that highlighted a key role for the protein in the recruitment of DNA repair factors to DNA lesions, in addition to regulating downstream signalling associated with DNA damage response and checkpoint signalling (Goldberg et al., 2003; Lou et al., 2003; Peng, 2003; Shang et al., 2003; Stewart et al., 2003; Xu, 2003).

1.5.1.1 MDC1 structure and functional domains

1.5.1.1.1 Fork-head associated (FHA) domain

MDC1 is a large, 2,089 amino acid nuclear protein with distinct functional domains, which are critical for protein-protein interactions with DNA damage repair and signalling components (Figure 1.5A). At the extreme N-terminus of MDC1 is a conserved fork-head associated (FHA) domain, whose precise function remains largely inconclusive. Loss of this phospho-specific interaction module from MDC1 leads to a multitude of DNA damage repair defects including compromised repair and checkpoint signalling defects, suggesting the importance of this FHA domain (Lou et al., 2003; 2006; Zhang et al., 2005). One of the first proteins identified as interacting with the MDC1-FHA was the phosphorylated phospho-T68 Chk2 (Lou et al., 2003). The study demonstrated that phospho-T68 could immunoprecipitate with MDC1 from cell extracts, with the FHA domain of MDC1 critical in this interaction. Suppression of MDC1 expression resulted in defective S-phase checkpoint activation and reduced apoptosis, consistent with the role of Chk2 in the damage response (Zannini et

al., 2014). This phenotype could only be rescued with exogenously expressed MDC1 containing the FHA domain (Lou et al., 2003). Whilst this study demonstrated an interaction between MDC1 and Chk2 in response to DNA damage, subsequent studies have been unable to detect Chk2 accumulation at DNA damage foci, despite strong MDC1 localisation (Lukas et al., 2003). In addition, the process of auto- and trans-phosphorylation that activates Chk2, results in the loss of the 'priming' phospho-T68 phosphorylation (Ahn and Prives, 2002), which was shown as critical for the MDC1-Chk2 interaction (Lou et al., 2003). This suggests that the interaction between the two proteins may be very transient, or temporally restricted, with more work needed to understand the functional consequences of such an interaction (Jungmichel and Stucki, 2010). MDC1 has also been shown to be loosely associated with ATM, an interaction which is reduced upon exposure to IR (Stewart et al., 2003). This interaction was later shown to be mediated through the FHA domain of MDC1 (Lou et al., 2006). The study demonstrated that MDC1 bound to both γH2AX and ATM to form a positive feedback loop, promoting the further phosphorylation of γH2AX, thus amplifying the DNA damage response. Loss of MDC1, prevented active ATM from accumulating at DNA lesions as determined using immunofluorescence, which led to defective ATM signalling and IR sensitivity (Lou et al., 2006). Several independent studies have demonstrated that the FHA domain of MDC1 is required for robust HR repair, with this domain required for interaction with Rad51 (Xie et al., 2007; Zhang et al., 2005). Whilst MDC1 and Rad51 do not co-localise at DNA lesions (Goldberg et al., 2003), suppression of MDC1 expression resulted in impaired Rad51 foci formation and hypersensitivity to MMC (Zhang et al., 2005).

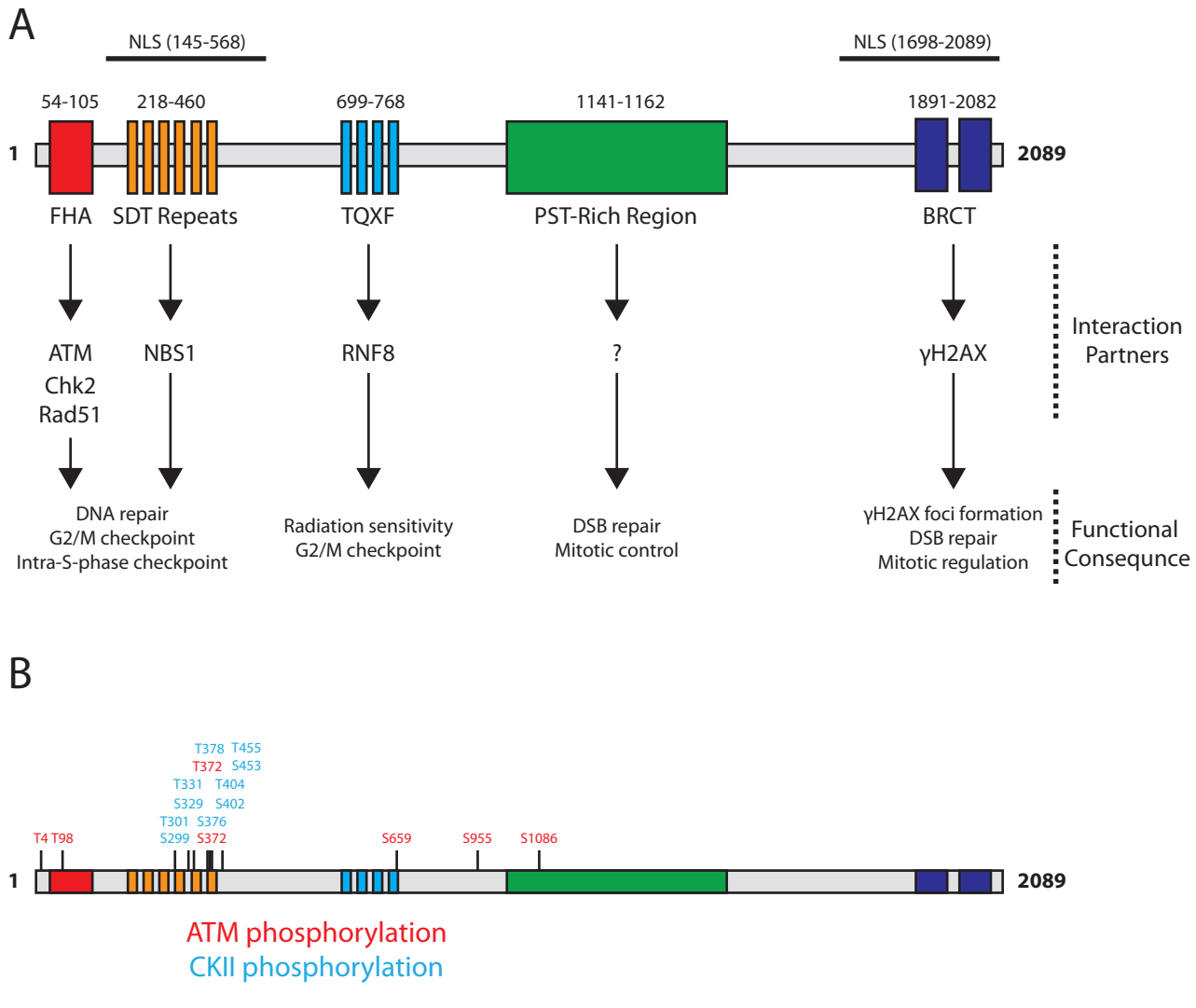

Figure 1.5: Schematic illustration of MDC1 domains and modifications

(A) Schematic representation of the identified domains and interaction partners of MDC1. MDC1 contains an N-terminal FHA interaction domain responsible for oligomerisation and signalling. Clusters of SDT and TQXF repeats are responsible for facilitating key interactions responsible for DNA repair and checkpoint arrest. A large proline-serine-threonine rich region plays an unknown role in regulating DNA repair. Two C-terminal BRCT domains are crucial for γH2AX signalling and mitotic regulation. Adapted from (Jungmichel and Stucki, 2010).

(B) Schematic representation of selected phosphorylation modifications identified for MDC1. ATM phosphorylations are coloured in red, CKII phosphorylations are coloured in blue. Phosphorylation data compiled from (Matsuoka et al., 2007; Spycher et al., 2008).

A recently identified phosphorylation site at the extreme N-terminus of the MDC1 FHA domain has been shown by multiple independent studies to be required for MDC1 dimerisation at DNA lesions, with the function of MDC1 as a scaffold at sites of damage dependent on this dimerisation/oligomerisation. Phosphorylation of the MDC1 FHA domain at T4, primarily by ATM, stimulates the dimerisation of MDC1 and accumulation of downstream DDR factors at sites of DNA damage (Jungmichel et al., 2012; Liu et al., 2012; Luo et al., 2011). The subsequent increase in local density of MDC1 at DNA lesions promotes accumulation of activated ATM at sites flanking DNA damage, further facilitating ATM-dependent phosphorylation of H2AX and the amplification of DNA damage signals (Lou et al., 2006). Despite these observations, it remains largely unclear what impact the attenuation of MDC1 dimerisation has on the cells ability to promote DNA repair and checkpoint activation.

1.5.1.1.2 SDT-repeat domain

Distal to the FHA domain of MDC1 lies the SDT-repeat region, consisting of conserved repeats of 8-10 amino acids comprising serine and threonine residues embedded in an acidic sequence environment (Jungmichel and Stucki, 2010). The acidophilic casein kinase 2 (CK2) phosphorylates multiple sites within this region, promoting the damage-independent interaction between the SDT-repeat of MDC1 and the FHA and BRCT domains of NBS1 (Chapman and Jackson, 2008; Melander et al., 2008; Spycher et al., 2008; Wu et al., 2008). Expression of MDC1 lacking the SDT-repeat region leads to reduced MRN staining at IRIF, suggesting that whilst the interaction between MDC1 and NBS1 is not essential for the initial recruitment of the MRN complex to sites of DNA damage, sustained interaction at the DNA lesions is dependent on MDC1 binding (Chapman and Jackson, 2008; Jungmichel and Stucki, 2010). Figure

1.5B demonstrates the number of CK2 phosphorylation sites present in the SDT-repeat region of MDC1 as identified by mass-spectrometry; a number of which have been shown as important for maintenance of the MDC1-NBS1 interaction (Spycher et al., 2008). Progressive attenuation of the SDT-repeat region of MDC1 prevents binding to NBS1, with a reduction in associated NBS1 dependent on the number of S/T to A mutations present (Melander et al., 2008; Spycher et al., 2008). Consistent with this, mutations in either the FHA or BRCT domain of NBS1 abolish the interaction and impair the localisation of the MRN to IRIF (Lloyd et al., 2009; Wu et al., 2008). Although the interaction between MDC1 and NBS1 has been well studied, the functional consequence of the interaction remain elusive. One school of thought is that MDC1-MRN interaction may act to enhance the DSB-induced signalling via a positive feedback loop, promoting phosphorylation of distal chromatin regions and thus increasing the protein density at DNA lesions (Spycher et al., 2008). Other groups are more specific in suggesting that the interaction is required for intra S-phase checkpoint activation in response to damage (Wu et al., 2008); a role with which MDC1 has previously been linked (Goldberg et al., 2003; Stewart et al., 2003).

1.5.1.1.3 TQXF-Cluster

C-terminal to the SDT-repeats, is a cluster of four TQ motifs which are followed by a phenylalanine at the +3 position, referred to as the TQXF cluster (Coster and Goldberg, 2010). This region has been shown to bind the E3 ubiquitin ligase RNF8, with the FHA domain of RNF8 binding to the phosphorylated threonine residues (Huen et al., 2007; Kolas et al., 2007; Mailand et al., 2007). In addition to an FHA domain, RNF8 also contains a RING domain, the function of which is critical for BRCA1 and 53BP1 recruitment to DNA lesions. Mutation or deletion of this domain prevented the poly-ubiquitination of histones H2A and

H2AX at DNA lesions and prevented BRCA1 and 53BP1 recruitment (Huen et al., 2007; Kolas et al., 2007; Mailand et al., 2007). Phosphorylation of MDC1 at the TQXF cluster is ATM mediated and damage dependent, thus recruitment of RNF8 to sites of DNA damage occurs in a damage-dependent manner. Like the SDT-repeat domain on MDC1, a redundancy of phosphorylation sites exists, with binding of RNF8 to MDC1 at the TQXF-cluster requiring only a single phosphorylated threonine residue (Coster and Goldberg, 2010; Kolas et al., 2007). A recent study found that an additional level of control exists to regulate the MDC1 and RNF8 interaction during mitosis. Previous observation had shown that RNF8 was not recruited to sites of DNA damage during early mitosis, with full DDR only occurring in the following G1 phase (Giunta et al., 2010; Giunta and Jackson, 2011). This idea was further explored to show that the during mitosis, the mitotic kinase CDK1 phosphorylates RNF8 outside of the FHA domain, preventing RNF8 binding to phosphorylated MDC1 in response to DNA damage during mitosis (Orthwein et al., 2014). Blocking CDK1 phosphorylation of RNF8 restored the interaction with MDC1, subsequently activating DNA repair during mitosis, which paradoxically is deleterious due to DNA repair occurring at telomeres, resulting in telomeric fusion (Orthwein et al., 2014)

1.5.1.1.4 Proline-Serine-Threonine (PST)-rich domain

The precise role of the poorly conserved Proline-Serine-Threonine (PST)-rich region of MDC1 remains elusive, with a number of independent studies demonstrating differing roles for this domain of MDC1 (Jungmichel and Stucki, 2010). MDC1 has previously been reported to play a role in mitosis, with the protein heavily phosphorylated during the mitotic cell cycle phase (Figure 1.5B) (Dephoure et al., 2008). MDC1 has been shown to bind with a subunit of the

anaphase-promoting complex/cyclosome (APC/C), an interaction dependent upon the C-terminal BRCT and PST-rich domain. This interaction regulates normal metaphase-to-anaphase transition via modulation of APC/C E3 ubiquitin ligase activity (Coster et al., 2007; Townsend et al., 2009). Mutated MDC1 lacking the PST-rich region was unable to bind APC/C *in vitro* and was unable to rescue the metaphase mitotic block caused by siRNA depletion of endogenous MDC1 (Townsend et al., 2009). In addition to a probable role in controlling MDC1 function during mitosis, the PST-rich region has also been implicated in the regulation of DNA repair by both NHEJ (Lou et al., 2004) and HR repair (Xie et al., 2007). In regulating NHEJ, it was proposed that MDC1 binds the DNA-PK complex, with down regulation of MDC1 by siRNA resulting in defective phospho-DNA-PKcs foci formation and defective NHEJ repair (Lou et al., 2004). In addition, more recent work has demonstrated a function of the MDC1 PST-rich domain in maintaining robust HR repair. Whilst deletion of the PST-rich domain did not affect MDC1 recruitment to γH2AX, DNA repair by HR was compromised (Xie et al., 2007). More work is needed to elucidate the precise mechanism by which deletion of the PST-rich region leads to compromised HR repair.

1.5.1.1.5 Tandem BRCA1 carboxy-terminal (tBRCT) domains

The most C-terminal functional regions of MDC1 are the tandem BRCA1 carboxy-terminal (tBRCT) domains, deletion of which abrogates MDC1 foci formation in response to DNA damage (Shang et al., 2003). Several independent studies showed that the tBRCT domain of MDC1 displayed high specificity for the ATM-phosphorylated C-terminus of histone H2AX, allowing the downstream protein recruitment associated with MDC1 at DNA lesions (Lee et al., 2005; Lou et al., 2006; Stucki et al., 2005). Although the binding of γH2AX

is likely the principle function of the tBRCT domains, other binding partners have been associated with this domain. As mentioned previously, MDC1 interacts with a phosphorylated subunit of the APC/C complex, phospho-CDC27, which occurs through both the PST-rich domain and the tBRCT domain (Coster et al., 2007). As the C-terminal phosphorylation motif of CDC27 is similar to γH2AX, it is likely that both proteins bind MDC1 via the same mechanism (Coster and Goldberg, 2010). In addition to the evidence that the tBRCT domain binds to γH2AX and components of the APC/C, some tentative evidence exists that MDC1 binds 53BP1 through the same region. One exploratory study established that 53BP1 and MDC1 interact directly through the tBRCT domain of MDC1 and residues 1288 –1409 of 53BP1, in the presence of DNA damage. They went on to demonstrate that the interaction is required for 53BP1 focus formation (Eliezer et al., 2008). Subsequent studies have gone on to show that RNF168 also interacts with 53BP1 in damaged cells, with the loss of RNF168 attenuating the 53BP1–MDC1 interaction (Bohgaki et al., 2013). Consistent with this, the interaction of exogenous 53BP1 and MDC1 was enhanced in the presence of exogenous RNF168 protein, suggesting that RNF168 interacts with 53BP1 and MDC1, which facilitates the formation of a protein complex that includes these three proteins (Bohgaki et al., 2013).

1.5.1.2 MDC1 and DNA repair

The process of DNA repair begins with the rapid assembly of a number of DDR proteins at the chromatin regions flanking the break. The initial recruitment of proteins to the DNA lesion leads to substantial downstream amplification, which promotes the recruitment, retention and activation of downstream DDR components, leading to DNA repair (Coster and Goldberg, 2010). The process of converting initially small protein recruitment to a signal large enough to

trigger full activation of the DDR is critical and largely dependent on the activity of the phospho-scaffold protein MDC1 (Lou et al., 2006).

As discussed previously, ATM-dependent phosphorylation of the C-terminal tail of histone variant H2AX at chromatin regions flanking the double-strand break initiates the signalling cascade associated with DNA repair, providing a binding platform for MDC1 through the tBRCT domain (Lee et al., 2005; Stucki et al., 2005). In addition to the well-characterised S139 phosphorylation of γH2AX, an additional modification has been shown to promote DNA repair in damaged cells. WSTF (Williams–Beuren syndrome transcription factor) phosphorylates Y142 of H2AX in undamaged cells, preventing interaction of γH2AX with downstream DDR components. Upon damage, the novel phosphatase EYA dephosphorylates this residue, which promotes the interaction between phosphorylated S139 γH2AX and MDC1 (Cook et al., 2009; Xiao et al., 2008) It has been shown that the γH2AX-MDC1 interaction serves a dual purpose. Firstly, MDC1 acts to facilitate the recruitment of down-stream repair proteins to sites of DNA damage (Stucki and Jackson, 2006). Loss of MDC1 prevents the retention of NBS1 and 53BP1 at damage sites (Bekker-Jensen, 2005; Lukas et al., 2004a), and also ATM via the interaction with the MRN complex (Falck et al., 2005). Secondly, the interaction between γH2AX and MDC1 is vital for signal amplification at IRIF. Through an interaction with γH2AX at the tBRCT domains and ATM at the FHA domains, MDC1 accumulates activated ATM flanking the sites of DNA damage, facilitating further ATM-dependent phosphorylation of H2AX and the amplification of DNA damage signals (Lou et al., 2006). Indeed, loss of MDC1 prevents this localised amplification, resulting in reduced γH2AX S139 phosphorylation and compromised protein recruitment

to IRIF (Lou et al., 2006; Stucki et al., 2005). Once recruited to DNA lesions, MDC1 is phosphorylated directly by ATM at the TQXF cluster, which promotes binding to the FHA domain of the E3 ubiquitin ligase RNF8 (Huen et al., 2007; Kolas et al., 2007; Mailand et al., 2007). The recruitment of RNF8 to DNA lesions is important to generate the ubiquitin-conjugates required for 53BP1 and BRCA1 recruitment to the IRIF, with disruption of the MDC1-RNF8 interaction leading to loss of 53BP1 and BRCA1 recruitment (Huen et al., 2007; Mailand et al., 2007).

Whilst the role of MDC1 in recruitment and amplification at DNA lesions is well explored, the function of MDC1 in DNA repair is less well understood. In DNA repair by NHEJ, it was shown that MDC1 binds the DNA-PK complex, with down regulation of MDC1 resulting in defective phospho-DNK-PKcs foci formation and defective NHEJ repair (Lou et al., 2004). In addition, MDC1 has been shown to be necessary robust HR repair, via a direct interaction with Rad51 (Xie et al., 2007; Zhang et al., 2005). Whilst MDC1 and Rad51 do not co-localise at DNA lesions (Goldberg et al., 2003), suppression of MDC1 expression resulted in increased Rad51 degradation, coupled with impaired Rad51 foci formation and hypersensitivity to MMC (Zhang et al., 2005).

Unlike γH2AX, which is extensively targeted by Ser/Thr protein phosphatases following resolution of damage (discussed in depth later) (Freeman and Monteiro, 2010), very little is known about dephosphorylation of MDC1. MDC1 has been shown to be removed from DNA foci via ubiquitin mediated degradation (Shi et al., 2008). Sumoylation of MDC1 by PIAS4 at lysine 1840 targets the protein for ubiquitination and degradation by the E3 ligase RNF4

(Galanty et al., 2012; Yin et al., 2012). Consistent with mis-localisation and persistence of DNA foci, mutation of the MDC1 K1840 resulted in impaired RPA and Rad51 accumulation at IRIF and defective homologous recombination (Luo et al., 2012).

1.5.1.3 MDC1 involvement in cell cycle control, apoptosis and mitosis

In addition to the key function of MDC1 in recruitment of DDR proteins to sites of damage and amplification of ATM signalling, MDC1 has also been implicated in the function of the intra-S-phase checkpoint. Loss of MDC1 resulted in a defective intra-S-phase checkpoint (Stewart et al., 2003), with cells displaying radio resistant DNA synthesis (RDS) (Goldberg et al., 2003; Lou et al., 2003), consistent with DNA synthesis occurring despite the presence of damaged DNA (Falck et al., 2001). Two parallel pathways regulate the intra-S-phase checkpoint, both regulated by ATM. ATM phosphorylation of Chk2 at T68 induces the destruction of CDC25A, which locks the CDK2/CycE S-phase promoting complex in an inactive form (Falck et al., 2002). Several independent studies have demonstrated that MDC1 binds phosphorylated Chk2, implicating MDC1 in the pathway (Lou et al., 2003; Wu et al., 2012). In addition ATM phosphorylation of NBS1, resulting in activation of the MRN complex, can also lead to activation of the intra-S-phase checkpoint, however the precise molecular mechanism remains unclear (Falck et al., 2002). It has been shown that disruption of NBS1-MDC1 binding results in a failure of NBS1 accumulation at DNA lesions and impairment of intra-S-phase checkpoint activation (Wu et al., 2008). In summary, whilst it is clear that MDC1 plays a key a critical role in the regulation or activation of the intra-S-phase checkpoint, the precise molecular mechanism for this remains unclear.

A growing body of evidence exists which supports the idea that MDC1 is able to supress apoptosis during the DNA damage response, allowing time for DNA repair. MDC1 was demonstrated to bind p53 through the tBRCT domain, with over-expression of MDC1 resulting in the inhibition of ATM-dependent phosphorylation of p53 at S15, leading to destabilisation of the protein and a reduction in the transcription of pro-apoptotic genes (Nakanishi et al., 2007). A subsequent study also revealed that MDC1 binds to and stabilises MDM2 through the tBRCT domain, with stabilised MDM2 then able to target p53 for ubiquitination and proteosomal degradation (Inoue et al., 2008).

As mentioned previously, MDC1 has been reported to play a role in mitosis, with strong evidence that the protein is heavily phosphorylated during the mitotic cell cycle phase (Figure 1.5B) (Dephoure et al., 2008). The anaphase-promoting complex/cyclosome (APC/C) is responsible for the proteasome-mediated degradation of cell cycle regulators during mitosis and is required for sister separation during anaphase and mitotic exit (McLean et al., 2011; Vodermaier, 2004). MDC1 has been shown to bind with a subunit of APC/C, an interaction dependent upon the C-terminal BRCT and PST-rich domain (Coster et al., 2007; Townsend et al., 2009). Mutated MDC1 lacking the PST-rich region was unable to bind APC/C *in vitro* and was unable to rescue the metaphase mitotic block caused by siRNA depletion of endogenous MDC1 (Townsend et al., 2009). In addition to promoting mitotic progression, MDC1 has also been implicated in the regulation of the spindle assembly checkpoint (SAC). The Goldberg group demonstrated that following SAC activation, ATM phosphorylates histone H2AX at mitotic kinetochores, which promotes MDC1

localisation to mitotic kinetochores (Eliezer et al., 2014). The study went on to show that kinetochore localised MDC1 was needed for kinetochore localisation of the inhibitory mitotic checkpoint complex components, Mad2 and Cdc20, and for the maintenance of the mitotic checkpoint complex integrity (Eliezer et al., 2014). Whilst the precise function of MDC1 at kinetochores remains unclear; the involvement of MDC1 in the SAC does propose a possible link between the DDR and cell cycle regulation.

1.5.2 The MRN Complex

The MRN complex, consisting of the core components MRE11, RAD50 and NBS1, plays a critical role in sensing damaged DNA, propagating resultant signalling and repairing the damaged DNA (Czornak et al., 2008). The different activities of the MRN complex are functionally distinct and are dependent on key regions and domains of the various components (Buis et al., 2008). The importance of the complex in robust DNA repair is highlighted by the number of conditions arising as a result of genetic mutations in any of the components as discussed previously. Indeed, null mutations in any of the three genes leads to embryonic lethality in mice (Luo et al., 1999; Xiao and Weaver, 1997; Zhu et al., 2001).

1.5.2.1 MRN complex components

1.5.2.1.1 MRE11

MRE11 is an 80 kDa protein which acts as the core of the MRN complex, interacting independently with both NBS1 and RAD50, whilst also forming homodimers and multimers with itself (D'Amours and Jackson, 2002; Desai-Mehta et al., 2001). The MRE11 dimer acts as the core MRN complex, binding two molecules of RAD50, with the MRE11-RAD50 complex finally binding a

single molecule of NBS1 (van der Linden et al., 2009). The N-terminal region of MRE11 contains four phosphoesterase motifs which are necessary for the 3'-5' double-strand DNA exonuclease activity and single-stranded/double-stranded endonuclease activity (Paull and Gellert, 1998; Trujillo et al., 1998). This activity has been demonstrated as being structure specific, with MRE11 nuclease activity most active at blunt ended or 3'-recessed DNA (Trujillo and Sung, 2001). Both the exo- and endonuclease activity of MRE11 can be regulated via the binding of the other MRN components RAD50 and NBS1. Rad50 binding to MRE11 stimulates both exo- and endonuclease activity, whilst NBS1 binding only stimulates the endonuclease activity of MRE11 (Paull and Gellert, 1999; Trujillo and Sung, 2001).

1.5.2.1.2 RAD50

RAD50 is a large, 150 kDa protein which contains walker A and B nucleotide-binding motifs at both the N- and C-terminal ends, which have been shown to be crucial for MRN function (D'Amours and Jackson, 2002). RAD50 shares structural similarity with the 'structural maintenance of chromosome' (SMC) proteins, which act to regulate chromatid cohesion. The principle function of RAD50 is to bind DNA ends and hold them in close proximity (de Jager et al., 2001). In the presence of ATP, the two walker A and B motifs facilitate RAD50 binding and unwinding of DNA (Chen et al., 2005a; de Jager et al., 2002). Once bound, a central hinge region between the two walker A and B motifs allows the protein to fold onto itself forming a functional ATP-binding domain (Hopfner et al., 2000). The presence of ATP forces the RAD50-MRE11 complex into a state that promotes the intercomplex interaction required for DNA tethering (Moreno-Herrero et al., 2005). The importance of such DNA tethering is clear and there have been several suggestions as to how this tethering activity can promote

survival in response to DSB. It has been suggested that the tethering of DNA ends could facilitate the search for homology regions, crucial for HR repair. In addition it has also been suggested that the DNA tethering may prevent physical separation of chromatid fragments and promote the local activity of DNA ligases during NHEJ repair (Chen et al., 2001; D'Amours and Jackson, 2002).

1.5.2.1.3 NBS1

The NBS1 protein lacks any enzymatic activity but is essential for the recruitment of the MRN complex to the nucleus and sites of DNA damage via the NLS present in NBS1 (Desai-Mehta et al., 2001). The presence of the N-terminal FHA and tBRCT domains of NBS1 allows interaction and recruitment of key DDR factors to DSBs, which includes CtIP and MDC1 (Lloyd et al., 2009; Williams et al., 2009). The interaction between MDC1 and NBS1 has been shown to be necessary for chromatin retention of the MRN complex at DNA lesions (Chapman and Jackson, 2008; Spycher et al., 2008). In addition, the C-terminal end of NBS1 contains an ATM interacting motif which facilitates the recruitment and activation of ATM at sites of DNA damage (Falck et al., 2005; Lee and Paull, 2005; You et al., 2005).

1.5.2.2 MRN complex and ATM activation

The ATM kinase plays a central role in the signalling associated with the response to DNA damage. The MRN complex plays a crucial role both in the recruitment of ATM to sites of DNA damage and the subsequent activation of the kinase locally at DSB (Uziel et al., 2003). ATM binding to such sites is dependent on functional MRE11, with initial MRN recruitment to DSB possibly dependent on Rad17 activity (Uziel et al., 2003; Wang et al., 2014).

The ability of the MRN complex to activate ATM has been demonstrated *in vitro*, with inactive ATM dimers activated in the presence of DNA and MRN (Lee and Paull, 2005). The unwinding of DNA ends by MRN was essential for this ATM activation, consistent with observations that ssDNA acts as a conserved signal for DNA damage (D'Amours and Jackson, 2002; Lee and Paull, 2005). More recent work has demonstrated that the ATP-bound form of MRN is the critical conformation for ATM activation (Lee et al., 2013). Whilst it is likely that the core MRE11-RAD50 complex is necessary for ATM activation, it has been reported that the C-terminal region of NBS1 is critical for ATM interaction and localisation, with wild type MRN not necessary for the MRN-ATM interaction (Falck et al., 2005). Interestingly, IR treatment does not enhance the ATM-MRN complex formation, instead the study found that DNA ends stabilises the interaction (Falck et al., 2005).

1.5.2.3 MRN complex involvement in DNA damage repair

In addition to a role in recruiting and activating ATM, the MRN complex also plays a role in DNA repair which is independent of ATM activation (Buis et al., 2008). Whilst it has previously been reported that the MRN complex associates at DNA lesions via an interaction with γH2AX (Kobayashi et al., 2002), more recent studies have consistently reported that the MRN complex binds to MDC1 at DSB, likely through FHA domain of NBS1 (Lukas et al., 2004a). Consistent with this, abrogation of MDC1 binding to γH2AX prevents MRN recruitment to sites of DNA damage, suggesting that MDC1-MRN are directly interacting (Lou et al., 2006; Lukas et al., 2004b). Several studies demonstrated that the SDT-repeat region of MDC1 bound to the FHA domain of NBS1, facilitating this binding (Chapman and Jackson, 2008; Melander et al., 2008; Spycher et al.,

2008). The MRN complex bound to DNA ends can then act to tether the break facilitating repair by NHEJ or alternatively initiate resection prior to repair by homologous recombination. MRE11 together with CtIP initiates 5'-3' resection (which is continued by EXOI/DNA2 in conjunction with the BLM helicase), allowing for downstream RPA coating and subsequent processing (Gravel et al., 2008; Renkawitz et al., 2014).

1.6 Transducer kinases and cell-cycle control during DSB repair

1.6.1 Cell-cycle checkpoints in response to DNA damage

The DNA damage checkpoint network is composed of a number of DNA damage sensor kinases (the PI3Ks such as ATM and DNA-PK), transducer kinases (such as Chk1/Chk2) and effector molecules (such as p53), whose substrates and activities mediate cell cycle arrest at various stages of the cell cycle, DNA repair, and cell death via apoptosis (Figure 1.2) (Bartek and Lukas, 2007). It has long been understood that the DNA damage response temporarily halts cell growth and proliferation, allowing time for precise DNA repair, after which normal cell homeostasis is restored. However it is becoming more apparent that the activity is a much more two-way process; with cell cycle machinery acting to regulate the DDR via repair pathway choices, and *vice versa*, with the precise mechanism of DDR arrest of the cell cycle dependent on cell cycle stage (Shaltiel et al., 2015).

The basic mammalian cell cycle consists of four distinct phases. The first of these phases is S-phase (synthesis) during which the genome of the cell is duplicated to provide an exact copy for subsequent daughter cells. This is followed by G2 (gap phase 2), during which protein synthesis is performed to

ensure a viable proteome for both daughter cells. The daughter cells are produced during the M-phase (mitotic), in which DNA is condensed into chromosomes, which separate forming two identical daughter cells. Finally, G1 (gap phase 1) allows the newly formed daughter cells to synthesise proteins and grow in size in preparation for the new S-phase (Hartwell and Kastan, 1994). A number of checkpoints exist between the various cell cycle stages, to ensure that progression is only permitted if relevant criteria are met. In addition to these homeostatic checkpoints, a number of DNA damage dependent checkpoints are present to ensure that the cell cycle is stalled to aid in DNA repair (Figure 1.6) (Houtgraaf et al., 2006). The figure highlights the three main checkpoints which can be activated in response to DNA damage: G1/S checkpoint, intra S-phase checkpoint and G2/M checkpoint. Whilst all three checkpoints temporarily stall the cell cycle during different phases, they operate via a common set of sensor kinases, transducer kinases and effector molecules (Tasat and Yakisich, 2010; Wang et al., 2009b).

The precise function and activity of the sensor kinases ATM and DNA-PK have been covered in detail in previous sections of this chapter. This section will look to explore the complex signal transduction associated with the transducer kinases Chk1 and Chk2, incorporating the multifaceted role of the effector molecule p53 during the arrest of the cell cycle in response to DNA damage.

1.6.2 Chk1

Checkpoint kinase 1 (Chk1) is responsible for the phosphorylation of key regulators of the cyclin dependent kinases (CDK) in response to DNA damage, resulting in the inactivation of CDK and blockade of cell cycle progression (Patil et al., 2013). Chk1 protein is highly conserved between eukaryotic species and

contains an N-terminal kinase domain in addition to a SQ/TQ cluster domain (Sanchez et al., 1997). Damaged DNA leads to the activation of the PI3K kinase ATR, which phosphorylates Chk1 at S317 and S345, resulting in activation of the kinase and initiation of the downstream signal transduction (Liu et al., 2000; Zhao and Piwnica-Worms, 2001). It has been shown that the N-terminal kinase domain of Chk1 is constitutively active, with ATR phosphorylation driving conformational change which allows the kinase domain to interact with Chk1 substrates (Patil et al., 2013). Phosphorylation by Chk1 can promote to DNA repair pathway choices, activate any of the three cell-cycle checkpoints or inhibit p53-dependent apoptosis in damaged cells (Dai and Grant, 2010; Roos and Kaina, 2006).

Arrest of the cell cycle by Chk1 is achieved via the phosphorylation of the CDC25 family of phosphatases. Chk1 is capable of phosphorylating two (A and C) mammalian isoforms, dependent on the checkpoint activated (Sanchez et al., 1997). Phosphorylation of CDC25A by Chk1 at S123 leads to ubiquitination of CDC25A followed by proteosomal degradation. Loss of CDC25A phosphatase activity results in sustained inhibitory phosphorylation of CDK1 and CDK2 leading to activation of G1/S, intra S-phase and G2/M checkpoints (Donzelli and Draetta, 2003; Mailand et al., 2000). Activated Chk1 also phosphorylates CDC25C at S216, creating a binding site for 14-3-3 proteins that leads to CDC25C nuclear export (Peng et al., 1997; Pines, 1999). Lack of active CDC25C phosphatase in the nucleus prevents CDK1/Cyclin B dephosphorylation and thus activates the G2/M checkpoint (Sanchez et al., 1997). In addition to arresting the cell cycle in response to DNA damage, Chk1

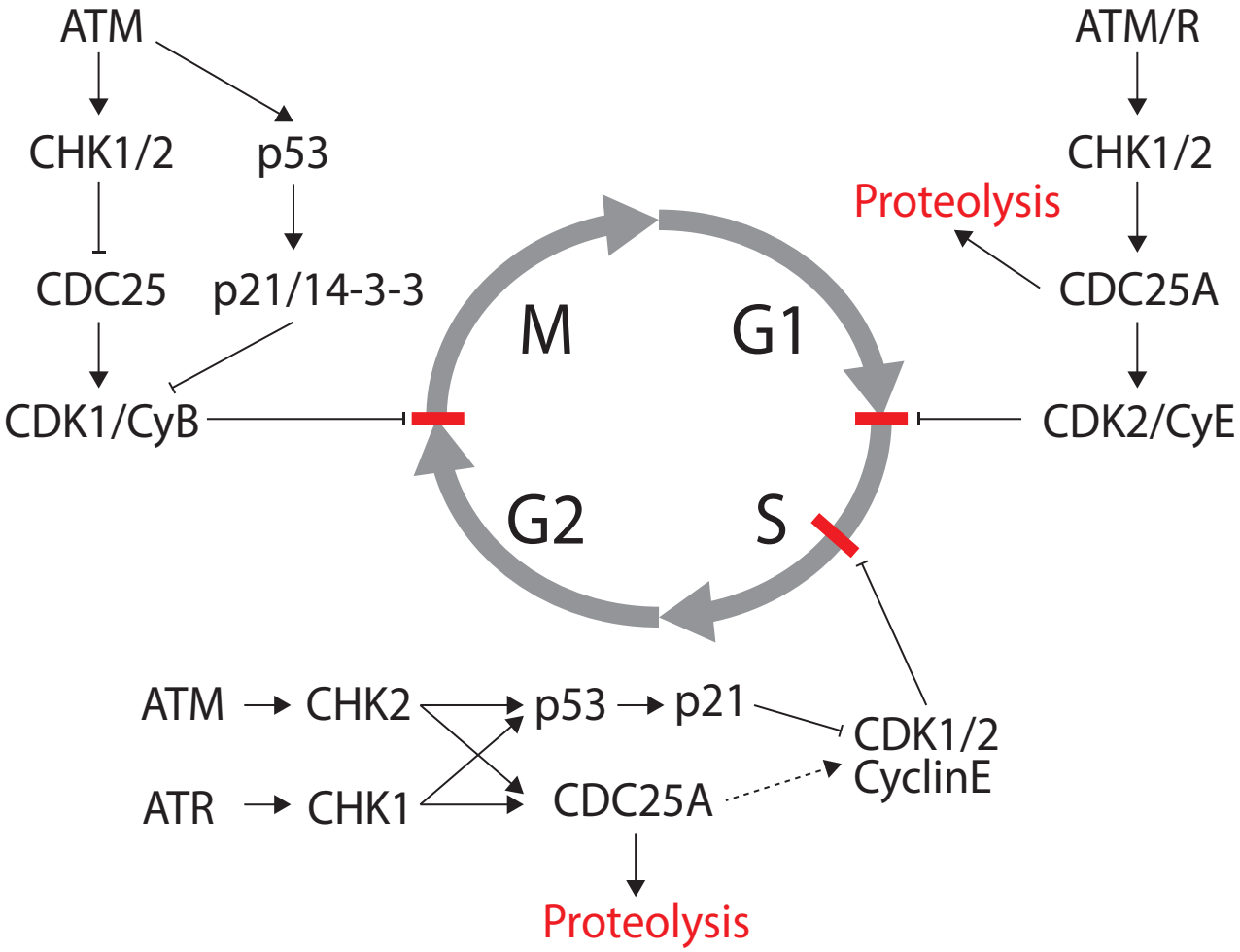

Figure 1.6: Activation of cell cycle checkpoints following DNA damage

Schematic representation of cell cycle shows three major checkpoints in the cell cycle following DNA damage: G1/S checkpoint, Intra S-phase checkpoint and G2/M checkpoint. Compiled from (Tasat and Yakisich, 2010; Wang et al., 2009b).

is also able to slow DNA replication in a CDC25/CDK independent manner, by regulating the association between Cdc45 and Mcm7 at origins of replication (Liu et al., 2006).

Chk1 participates not just in the arrest of cell cycle progression upon damage, but also in the repair process itself, phosphorylating key repair proteins upon activation by ATM or ATR. Phosphorylation of the Fanconi Anaemia complex protein FANCE at T346 and S374 facilitates the repair of DNA inter-strand cross link damage by promoting interaction with FANCD2 at DNA lesions (Wang et al., 2007). Chk1 is also a key regulator of genomic stability by HR repair, via an interaction with Rad51. Chk1 interacts with, and phosphorylates Rad51 at T309 promoting recruitment of Rad51 to DNA lesions (Sørensen et al., 2005). In addition, Chk1 phosphorylates the BRCA2 C-terminal domain at T3387; a modification which is critical role in regulating the binding of Rad51 to BRCA2 and subsequent recruitment of Rad51 to DNA lesions (Bahassi et al., 2008). Cells depleted of Chk1, or expressing a phosphorylation-deficient mutant, failed to form Rad51 foci and displayed persistent, unrepaired DNA double-strand breaks (Smith et al., 2010).

Multiple studies have revealed that Chk1 inhibition or depletion led to a significant increase in cell death after treatment with genotoxic stress suggesting a possible role for Chk1 inhibition of apoptosis upon DNA damage via ATM and ATR dependent suppression of caspase 2 and caspase 3 activation (Myers et al., 2009; Sidi et al., 2008). This presents Chk1 as a promising cancer therapy target, as inactivation or inhibition of Chk1 kinase activity could promote p53-independent activation of apoptosis in p53 deficient

cancerous cells (Zhou and Bartek, 2004). Combination therapy of Chk1 inhibitors with either anti-mitotics (Xiao et al., 2005) or DNA-damaging irradiation treatment, enhanced therapeutic efficacy (Koniaras et al., 2001). Clinical data further validates evidence that targeting Chk1 may have positive clinical outcomes. A patient with an advanced, gemcitabine-resistant, pancreatic tumour was treated with MMC and responded positively for over 36 months due to the tumour carrying mutations in PALB2 which disrupted key BRCA1 and BRCA2 interactions (Villarroel et al., 2011).

1.6.3 Chk2

Chk2 is the second transducer kinase to play an important role during the DNA damage response to mediate cell cycle arrest at various stages of the cell cycle, DNA repair, and cell death via apoptosis (Bartek and Lukas, 2007). Chk2 is principally involved in the response to DSBs, mediated by the activity of ATM (Zannini et al., 2014). Chk2 contains an N-terminal SQ/TQ cluster, the site of phosphorylation by PIKK-kinases, in addition to an FHA interaction domain and a C-terminal kinase domain (Ahn et al., 2004). ATM principally activates Chk2 in response to DNA damage. Active ATM phosphorylates inactive monomeric Chk2 at T68, which induces a conformational change inducing Chk2 dimerisation through binding to the FHA domain of another Chk2 monomer (Ahn et al., 2000; 2002). The process of dimerisation triggers extensive Chk2 autophosphorylation of the kinase domain (Guo et al., 2010), in addition to phosphorylation of the active loop at T383, T387 and S516 (Schwarz et al., 2003). This process of auto- and trans-phosphorylation activates the kinase and the resultant active Chk2 splits to form active monomers, resulting in the loss of the ‘priming’ phospho-T68 phosphorylation (Ahn and Prives, 2002). Phosphorylation of Chk2 at this site is highly dynamic and regulated by the

action of Ser/Thr protein phosphatases, which will be discussed later in this chapter. Chk2 phosphorylates in excess of 24 proteins at a RxxS or RxxT motif in response to DNA damage (Seo et al., 2003), which can act to promote DNA repair, activate the G2/M or S-phase checkpoint or promote apoptosis should damage be deemed un-repairable (Zannini et al., 2014).

Much like ATR-regulated Chk1, ATM-regulated Chk2 can phosphorylate both CDC25A and CDC25C, preventing the phosphatase activity and thus stalling cell cycle progression (Donzelli and Draetta, 2003). Indeed, following activation by ATM, Chk2 can also phosphorylate CDC25C on S216, creating a binding site for 14-3-3 scaffold proteins, resulting in CDC25C nuclear export (Peng et al., 1997; Pines, 1999). Lack of active CDC25C phosphatase in the nucleus prevents CDK1/Cyclin B dephosphorylation at T14 and thus activates the G2/M checkpoint (Sanchez et al., 1997). In the presence of DNA damage, activated Chk2 also phosphorylates CDC25A at S123, which targets the phosphatase for proteosomal degradation (Falck et al., 2001). This loss of functional CDC25A activity results in the sustained phosphorylation and inhibition of phospho-T14-CDK2, activating the G1/S checkpoint. In addition, the lack of active CDK2/Cyclin E and Cdc45 loading inhibits both early and late origins resulting in an intra S-phase arrest (Donzelli and Draetta, 2003). Robust signalling of the ATM-Chk2-CDC25A-CDK2 pathway is critical to prevent radio-resistant DNA synthesis (Falck et al., 2001; 2002). As well as activating the G1 checkpoint through phosphorylation and degradation of CDC25A, Chk2 phosphorylates p53 at S20 in response to DNA damage, leading to stabilisation of p53 and transcription of p21, which inhibits CDK2 and sustains the G1/S checkpoint (Chehab et al., 2000; Hirao et al., 2000; Mirzayans et al., 2012).

In a manner similar to Chk1, Chk2 phosphorylates BRCA2 at T3387, which disrupts the BRCA2-Rad51 constitutive interaction, promoting Rad51 recruitment to DNA lesions (Bahassi et al., 2008). In addition, Chk2 phosphorylates BRCA1 at S988 which further facilitates the recruitment of Rad51 to sites of damage, in addition to supressing the NHEJ repair pathway (Lee et al., 2000). The promotion of HR repair over NHEJ repair is dependent mainly upon BRCA1 phosphorylation by Chk2 and is not dependent on ATM phosphorylation of BRCA1 (Zhang et al., 2004). As well as regulating the recruitment of Rad51 to DNA lesions, Chk2 phosphorylation has also recently been shown to control heterochromatin remodelling at sites of damage to allow for the recruitment of repair factors. Chk2 dependent phosphorylation of Krüppel-associated box (KRAB)-associated protein 1 (KAP1) at S473 attenuated binding of KAP1 with the heterochromatin packaging factor heterochromatin protein 1-β (HP1-β). Release of HP1-β relaxes the chromatin structure, leading to chromatin restructuring at sites of DNA damage (Hu et al., 2012).

Unlike Chk1, DNA damage dependent phosphorylation by Chk2 promotes apoptosis in cells where the amount of DNA damage is irreparable (Ciccia and Elledge, 2010). Chk2 control apoptosis through phosphorylation of p53, which serves as a regulator of the apoptotic process that can modulate key control points in both the extrinsic and intrinsic pathways (Fridman and Lowe, 2003). Damage-dependent phosphorylation of p53 at multiple C-terminal phosphorylation sites stabilises the p53 protein and causes the dissociation and degradation of the p53 inhibitor MDMX (Chen, 2012; Ou et al., 2005). Indeed,

direct phosphorylation of MDMX by Chk2 promotes binding of MDMX with 14-3-3 proteins, preventing normal localisation between the nucleus and cytoplasm, resulting in MDM2-dependent degradation of MDMX (Chen et al., 2005b; LeBron et al., 2006). Due to the pro-apoptotic role of Chk2 in response to genotoxic stress, the use of Chk2 inhibitors as single or combination therapy in cancer has yielded mixed results. On the one hand, inhibition of Chk2 prevents cell-cycle checkpoint activation and repair pathway choice, which would have a negative effect on cell survival; yet conversely, preventing apoptotic induction through p53 may be detrimental. Despite this, several recent studies have demonstrated that inhibition of Chk2 in combination with standard chemotherapies led to improved clinical outcome in multiple cancer types (Duong et al., 2013; Gutiérrez-González et al., 2012). Chk2 specificity is challenging to achieve, with many compounds also active on Chk1, as such most clinical success with such combination therapy has been achieved using dual-specificity transducer kinase inhibitors (Garrett and Collins, 2011).

1.7 The role of Serine/Threonine protein phosphatases in response to DNA damage

1.7.1 Overview of phosphatases in the DDR

There are multiple phosphatases involved in the DNA damage response which act at all stages in the process. A mass-spectrometry based approach to assess the nuclear phospho-proteome during the DNA damage response identified 594 unique phosphorylation events upon damage, but in addition observed a considerable number of sites that underwent DNA damage-induced dephosphorylation (Bennetzen et al., 2010). This evidence highlights the importance of the phosphatases in all stages of DDR; from initiating DNA-

damage repair by dephosphorylation of protein targets, to reversal of the damage-induced phosphorylation events upon resolution of DNA damage repair. Figure 1.7 demonstrates the complexity and cross-talk that exists between the phosphatases and phosphorylation targets. The large number of phosphatases linked with specific process, such as the dephosphorylation of γH2AX is intriguing, with some groups suggesting that these phosphatases do not act redundantly, rather each might respond to different types of DNA damage (Nakada et al., 2008).

Despite the extensive research that has gone into PI3K signalling in response to DNA damage (reviewed in (Jackson and Bartek, 2009)), understanding of phosphatase activity in this process is rudimentary (Freeman and Monteiro, 2010). Whilst figure 1.7 demonstrates that many phosphatases involved in DDR have been described, it is as yet unknown which phosphatase or phosphatases are associated with a number of the critical DNA damage protein complexes such as MDC1 and MRN. This section will outline the unique and complementary roles played by the phosphatases involved with DNA damage repair.

1.7.2 PP1

The Serine/Threonine Protein Phosphatase 1 (PP1) is one of multiple protein phosphatases to play a key role during multiple phases of the DNA damage response. Mammalian cells possess three closely related PP1 catalytic subunits, PP1α, PP1γ and PP1δ that differ in sequence mainly in their C-

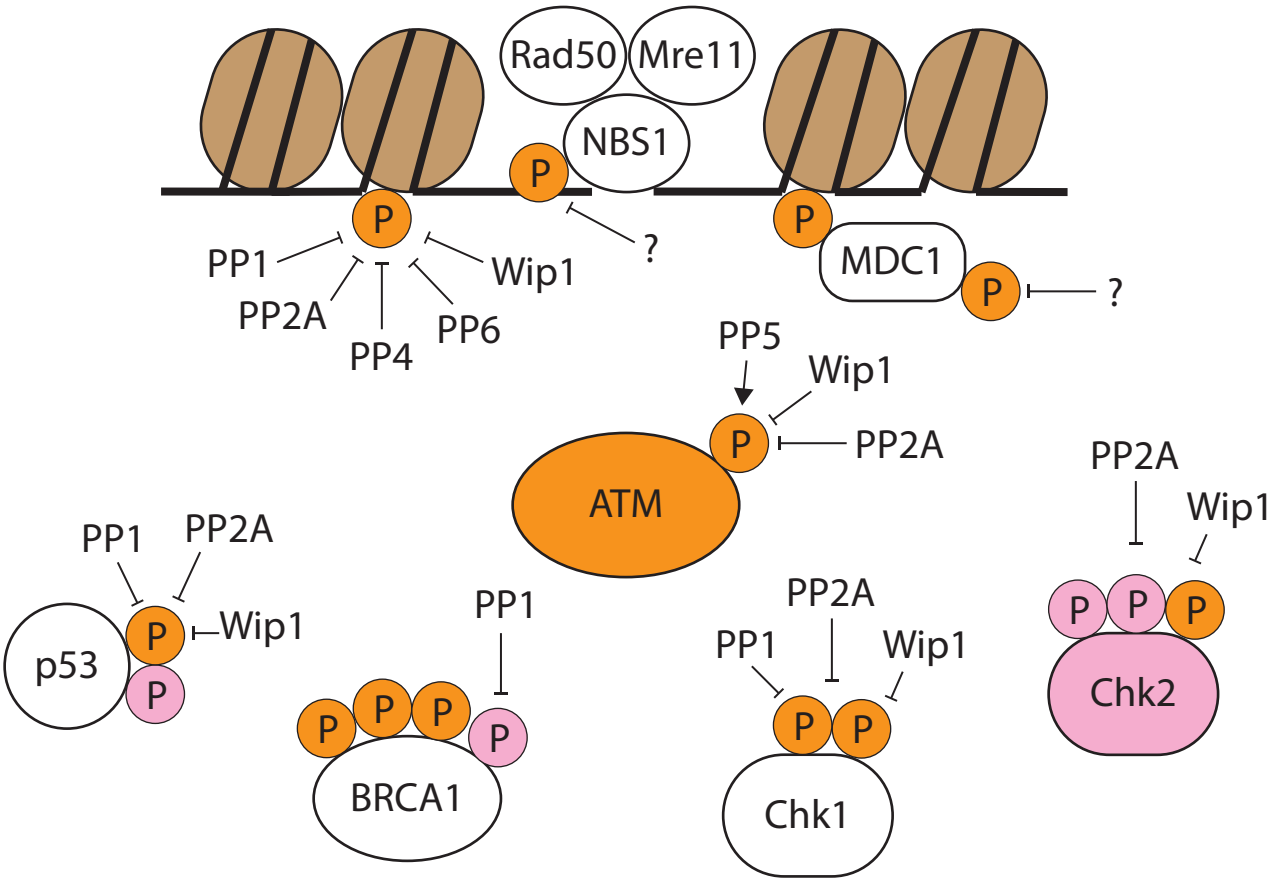

Figure 1.7: The multiple targets of the Ser/Thr phosphatases in DNA damage repair

Regulation of DNA damage repair signalling proteins by the Ser/Thr family of protein phosphatases. Phosphorylations in orange are ATM targets, phosphorylations in pink are Chk2 targets. Adapted from (Freeman and Monteiro, 2010).

terminal and N-terminal sequence (Cohen, 2002). The different PP1 catalytic isoforms are expressed fairly ubiquitously across multiple tissue types, however these different isoforms of PP1 have been shown to display distinct subcellular localisation (Andreassen et al., 1998). There does appear to be some redundancy in PP1 function, with regard to the different PP1-complexes formed. Studies in mice have demonstrated that mice with PP1$\gamma^{-/-}$ deletion are viable but display male infertility. This suggests that although PP1α may compensate for the loss of PP1γ during early embryonic development, the PP1γ complex is critical for functional spermiogenesis in these animals (Varmuza, 1998).

Like many of the Ser/Thr protein phosphatases, PP1 activity and specificity is controlled mainly through association with a large number of regulatory subunits that can modulate catalytic activity as well as drive specific sub-cellular localisation (Bollen et al., 2010). Unlike holocomplexes of PP2A, the regulatory subunits of PP1 do not appear to share recognisable sequence similarities; instead they contain a PP1C binding motif RVxF, allowing binding of the regulatory subunit to the hydrophobic groove of the catalytic subunit. Interestingly, several PP1 substrates also contain this consensus motif, allowing binding to the PP1 catalytic subunit (Wakula et al., 2003).

PP1 phosphatase targets multiple proteins and pathways involved in the DNA damage response. The importance of the phosphatase at DNA lesions is demonstrated by a recent study which demonstrated that simultaneous inhibition of PP1 and PP2A activated DNA damage signalling in *xenopus* egg extracts, despite the absence of actual DNA damage (Peng et al., 2010). In addition, this study demonstrated that the PP1γ interacting protein Repoman

(Recruits PP1 onto mitotic chromatin at anaphase) extensively co-localised with ATM on chromatin, with inhibition of either PP1γ or Repoman enhancing ATM activation in response to DNA damage. This suggests that the levels of PP1γ/Repoman present on chromatin determines the threshold for the initiation of DNA damage signalling. It also appears that PP1, in combination with another regulatory subunit, 'Inhibitor-2', is phosphorylated by ATM upon DNA damage leading to dissociation of the PP1 catalytic subunit from inhibitor-2 resulting in increased cellular PP1 activity (Guo et al., 2002a; Tang et al., 2008). Although the necessity for 'primed' and active PP1 early in the DDR is clear, the physiological effect of such activity remains ambiguous. Both studies did however conclude that the early DNA damage-induced PP1 activity may play a role in inhibiting Aurora A activity, thus preventing histone H3 phosphorylation and G2/M progression (Guo et al., 2002a; Tang et al., 2008).

An example of a PP1 interaction that is critical for maintaining robust HR-mediated DNA damage repair, is the interaction of PP1α with BRCA1, mediated through the RVxF motif (Yu et al., 2008). PP1 has been shown to dephosphorylate BRCA1 at the S988 Chk2 phosphorylation site, in addition to the S1524 ATM site, with over-expression of the PP1 phosphatase preventing the hyper-phosphorylation of BRCA1 in response to DNA damage (Liu et al., 2002; Yu et al., 2008). Mutation of the PP1-BRCA1 binding site negatively affected HR-mediated DNA repair and reduced the localisation of Rad51 to DNA lesions (Hsu, 2007; Yu et al., 2008). PP1 Nuclear Targeting Subunit (PNUTS) is another abundant nuclear PP1 binding factor, which binds to the α and γ isoforms of PP1C via the RVxF motif, specifically at telomeric regions of chromatin (Allen et al., 1998; Landsverk et al., 2005; Trinkle-Mulcahy et al.,

2006). Studies have shown that PNUTS is rapidly recruited to sites of DNA damage, with loss of the protein leading to activation of the G2 cell-cycle checkpoint (Landsverk et al., 2010). In addition, multiple DNA damage markers including γH2AX, 53BP1, RPA and Rad51 persist for prolonged periods of time in cells depleted of PNUTS, coupled with a loss of clonogenic survival. PNUTS has also been shown to interact with the telomeric protein TRF2 (Kim et al., 2009), a member of the shelterin complex of proteins, necessary for the inactivation of the DDR at telomeric DNA ends (Sfeir and de Lange, 2012). Given that several TRF2-interacting components are implicated in the DDR, the association of PNUTS with TRF2 may suggest that PNUTS/PP1α/γ may be involved in inhibition of specific damage repair pathways at telomeres (Kim et al., 2009; Küntziger et al., 2014).

Finally, PP1 also plays a crucial role in the control of key signalling pathways during the DNA damage response via interaction with regulatory interacting proteins. DNA damage induced p53 dephosphorylation at S15 and S37 is believed to be controlled by PP1, mediated through the interaction of PP1 with PNUTS and GADD34 (Growth arrest and DNA damage-induced gene 34) (Haneda et al., 2004; Lee et al., 2007; Li et al., 2006). Inhibition of PP1 dramatically increased dephosphorylation at S15/S37 and PP1 was shown to dephosphorylate these residues both *in vitro* and *in vivo*, decreasing the transcriptional activity associated with p53 (Li et al., 2006).

1.7.3 PP2A

One of the most ubiquitous protein phosphatases involved in the DNA damage response is the Ser/Thr-specific phosphoprotein phosphatase PP2A. PP2A exists as a heterotrimeric complex consisting of a catalytic subunit (PPP2CA

and PPP2CB), a regulatory subunit and a structural subunit (PPP2R1A and PPP2R1B)(Figure 1.8A-D) (Janssens et al., 2008). The regulatory subunit is believed to confer the specificity to the PP2A holocomplex, directing interactions and localisation (Janssens et al., 2008; Westermarck and Hahn, 2008). Structural assessment of the differing PP2A heterotrimers reveals clear structural diversity of the holocomplex dependent on regulatory subunit composition (Figure 1.8E-F). Unlike the catalytic and structural subunits, multiple classes of regulatory subunits can form holocomplexes. Four distinct families of regulatory subunit have been identified (B/B55, B'/B56, B''/PR72, B'''/striatin), with the B56 containing holoenzyme complexes the best studied with regard to DNA damage repair (Janssens et al., 2008; Lee and Chowdhury, 2011; McCright et al., 1996). Each of the PP2A-B56 subunits are highly conserved throughout higher eukaryotic species, with some evidence of over-lapping functions and compensation upon gene deletion (Sommer et al., 2015). The individual B-subunits are expressed at a much lower copy number than the core catalytic-structural dimer, with the regulatory subunits undergoing rapid degradation when not complexed with the structural subunit (Ruediger et al., 1994; Strack et al., 2004). Despite the abundant expression of PP2A, protein levels are tightly controlled to prevent the potentially lethal uncontrolled activity of PP2A in cellular processes (Baharians and Schönthal, 1998; Sents et al., 2012).

In general, PP2A function is controlled by either post-translational modification of the various subunits that control holocomplex assembly, or via the activity of a number of cellular PP2A inhibitory proteins (Janssens et al., 2008). A diverse range of inhibitory proteins have been shown to modulate PP2A function in cell

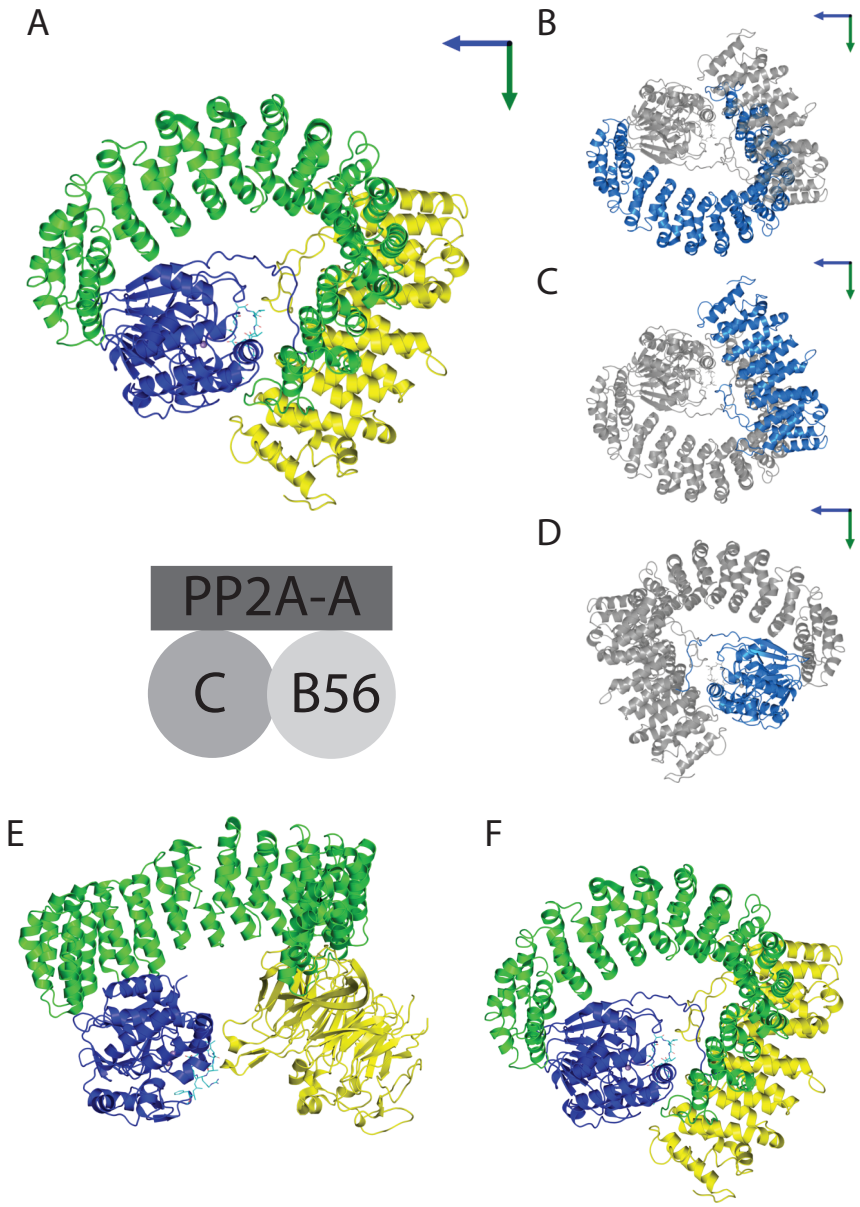

Figure 1.8: Crystal structure of the PP2A-B56 Ser/Thr phosphatase holo-complex

(A) Crystal structure and cartoon representation of the PP2A-B56 holoenzyme. Structural (*A*) α-isoform subunit is coloured in green. Regulatory (*B56*) B56γ subunit is shown in yellow. Catalytic (*C*) α-isoform is coloured in blue. Stick model of the non-competitive inhibitor of PP2A, microcystein-LR, is shown bound to catalytic subunit. Manganese co-factors are shown in purple bound to catalytic subunit (PDB: 2iae).

(B) Structural α-isoform highlighted in blue.

(C) Regulatory B56γ subunit highlighted in blue.

(D) Catalytic α-isoform highlighted in blue.

(E, F) Comparison of the structural variance between the PP2A-B56γ holo-enzyme complex (E) and the PP2A-B55 containing complex (F)(PDB: 3dw8). B56α and B55 regulatory subunits are coloured in yellow. Structural α-isoform subunit is coloured in green. Catalytic α-isoform is shown in blue.

signalling pathways (I2/SET, CIP2A) (Li et al., 1996) and during mitotic progression (Bod1, ENSA, ARPP19) (Gharbi-Ayachi et al., 2010; Mochida et al., 2010; Porter et al., 2013), as well as playing an important role in DNA damage and repair signalling, opposing ATM/ATR-dependent phosphorylation events (TIPRL) (McConnell et al., 2007). The numerous roles of PP2A within the DNA damage response, in addition to other cellular processes, are a principle reason for its appeal as an anti-cancer target for novel pharmaceuticals. Multiple PP2A inhibitors in phase I clinical trials have recently been shown to hypersensitise tumour cells to DNA damaging agents, identifying this pathway as a promising combination therapy in cancer treatment (Chang et al., 2015; Lv et al., 2014; Wei et al., 2013).

PP2A has been shown to play a key role in regulating ATM during the DNA damage response. Khanna and colleagues found that treatment of cells with Okadaic acid (OA) at doses that only inhibit PP2A, induces autophosphorylation of ATM on S1981 in the absence of DNA damage (Goodarzi et al., 2004). They went on to demonstrate that ATM interacts with the structural subunit of PP2A, with ATM immunoprecipating a functional PP2A complex, suggesting that the PP2A complex keeps ATM in a dephosphorylated state, a result confirmed by the Sablina group (Kalev et al., 2012). In line with these observations, inhibition of PP2A using OA, induced ATM autophosphorylation in undamaged cells (Yan et al., 2010). Ionising radiation induced a dissociation of ATM and PP2A, resulting in the inactivation of PP2A and the autophosphorylation of ATM at S1981. This is consistent with previous observations that activation of ATM in response to IR, caused dissociation of the B55 regulatory subunit from the core PP2A dimer (Guo et al., 2002b), thus suggesting a mechanism for ATM to

control PP2A activity. Following activation of the kinase, ATM is able to directly phosphorylate and specifically regulate the B56γ and B56δ PP2A heterotrimers, resulting in the PP2A-B56γ mediated inhibition of cell proliferation and dephosphorylation of p53 (Shouse et al., 2011).

In addition to PP6, PP2A positively regulates the DNA-PK activity upon DNA damage, acting to dephosphorylate Ku70 and Ku80, which leads to increase DNA-PK activity and promotion of the NHEJ repair pathway (Douglas et al., 2001; Wang et al., 2009a). DNA damage induced by camptothecin leads to the physical association of PP2A with Ku70/80, resulting in the dephosphorylation of both subunits as well as DNA-PKcs, removing the inhibitory autophosphorylations and promoting the formation of a functional kinase complex on DNA (Chan and Lees-Miller, 1996; Wang et al., 2009a).

Potentially linked with the interaction between PP2A and ATM, PP2A, along with a number of additional Ser/Thr protein phosphatases, dephosphorylates γH2AX upon the resolution of DNA damage (Chowdhury et al., 2005). PP2AC co-localises with γH2AX at IRIF leading to prolonged γH2AX phosphorylation and defective DNA repair (Chowdhury et al., 2005). More recent work observed that the PP2A-B56ε was the heterotrimeric regulatory subunit responsible for γH2AX dephosphorylation, with the B56ε containing hetero-trimer translocating from the cytoplasm to the nucleus upon treatment with camptothecin. Specific depletion of the B56ε isoform led to defective cell-cycle checkpoint control in addition to compromised HR repair measured by comet assay. (Li et al., 2015). The large number of phosphatases linked with γH2AX dephosphorylation is intriguing, with some groups suggesting that these phosphatases do not act

redundantly, rather each might respond to different types of DNA damage (Nakada et al., 2008).

As mentioned previously, under normal homeostatic conditions, the activity of p53 is supressed. DNA damage associated post-translational modification of p53 stabilises the protein, activating down stream signalling pathways (Levine, 1997; Vousden and Lu, 2002). In response to DNA damage, the catalytic subunit of PP2A, in a complex with the regulatory subunit B56, physically binds p53, mediating the dephosphorylation of p53 at multiple phosphorylation, thus stabilising the protein and promoting downstream p53 signalling (Dohoney et al., 2004; Li et al., 2007; Mi et al., 2009a). Inhibition of PP2A using small-molecule inhibitors (Gordon et al., 2015), or depletion of subunits of the holocomplex attenuated p53 dephosphorylation, reduced p53 stabilisation and reduced downstream signalling (Li et al., 2007; Mi et al., 2009a). 14 tumour-derived PP2A-B56γ mutations were recently identified in human cancer cells, although little frequency data for such mutations suggests that these occur rarely. The mutations prevented the PP2A holocomplex from binding to and dephosphorylating p53, thus losing the tumour suppressive function of the phosphatase (Nobumori et al., 2013). The process of PP2A-p53 binding is regulated by ATM, which phosphorylates both p53 at S15 and PP2A-B56γ3 at S510, promoting interaction. This process also serves to upregulate B56γ3 expression upon DNA damage by blocking MDM2-mediated B56γ3 ubiquitination (Shouse et al., 2011; 2008).

Upon DNA damage, ATM phosphorylates Chk2 at phospho-T68, enabling FHA-dependent dimerisation and subsequent activation (Ahn et al., 2004). Several

studies have demonstrated binding of Chk2 with both PP2A-B56γ and PP2A-B56α in the absence of DNA damage, mediating dephosphorylation of phospho-T68 Chk2 by PP2AC (Dozier et al., 2004; Freeman et al., 2010; Liang et al., 2006). This interaction is hypothesised to keep Chk2 in an inactive state under basal ATM kinase activity (Carlessi et al., 2010). Activation of ATM in response to genotoxic stress led to damage-dependent deactivation of this interaction and negative feedback loop, allowing the phosphorylation of Chk2 by ATM and subsequent downstream signalling (Freeman et al., 2010). Indeed, inhibition of PP2A using LB100, led to phosphorylation and activation of CDC25C/CDK1, a known Chk2 target, suggesting that in the absence of active PP2A, Chk2 is erroneously activated (Wei et al., 2013). PP2A also antagonises the ATR-dependent phosphorylation of the transducer kinase Chk1 at S317 and S345, with PP2A simultaneously regulated by phosphorylated Chk1 (Leung-Pineda et al., 2006). Existing in an ATR-Chk1-PP2A regulatory feedback loop, ATR phosphorylates Chk1 upon damage, which is then subject to regulation by Chk1-regulated PP2A via a decrease in the transcription of cancerous inhibitor of PP2A (CIP2A) (Khanna et al., 2013). This feedback loop functions to keep Chk1 largely inactive during homeostatic conditions, but primed to respond to DNA damage (Khanna et al., 2013; Leung-Pineda et al., 2006).

1.7.4 PP4

PP4 is a phosphatase which is structurally and functionally similar to PP2A, consisting of a catalytic subunit in complex with one of a number of regulatory subunits (PP4R1, PP4R2, PP4R3α, PP4R3β and PP4R4) (Chen et al., 2008). There is multiple instances of redundancy between PP2A and PP4, consistent with the similarity between the phosphatase sequences (Freeman and Monteiro, 2010). PP4C exhibits differing localisation that is dependent on

regulatory subunit, much the same as PP2A. PP4C/R3β is primarily localised to the nucleus and does not co-localise with γH2AX foci post-damage (Chowdhury et al., 2008). Despite this, the PP4 holocomplex has been shown to carry out a number of roles during the DNA damage response, both during early foci formation phases, to later resolution of DNA damage complexes. During complex assembly and homologous repair, a PP4 complex containing the PP4R2 regulatory subunit mediates an interaction between the PP4C subunit and RPA2, allowing efficient dephosphorylation of RPA2, thus promoting efficient Rad51 loading (Lee et al., 2010). Several recent studies have also highlighted the role for PP4 in regulating protein recruitment to DNA lesions dependant upon cell cycle stage. The PP4C/R3β complex dephosphorylates PLK1 phosphorylation sites on 53BP1, promoting recruitment of the protein to chromatin during G1 phase of the cell cycle (Lee et al., 2014). Failure to maintain this phosphorylation balance on 53BP1 led to mitotic defects associated with telomeric fusion events occurring as a result of DSB repair of telomeres (Lee et al., 2014; Orthwein et al., 2014).

During the resolution of DNA damage complexes, PP4 has been shown as essential for the dephosphorylation of γH2AX at repaired sites of DNA damage in both yeast and mammalian cells (Nakada et al., 2008). In addition, a PP4C-PP4R3β complex is also responsible for dephosphorylation of phospho-S824 KAP-1, regulating the role of KAP-1 in chromatin compaction and gene expression, promoting the progression of cell cycle post-DNA damage (Lee et al., 2012; Liu et al., 2014). Depletion of PP4 leads to prolonged G2/M checkpoint after DNA damage repair along with prolonged chromatin relaxation.

1.7.5 PP5

The precise and full function of PP5 in the DDR is currently unclear, most in part due the low basal activity and expression of the phosphatase (Chen and Cohen, 1997; Chinkers, 2001). The principle function of PP5 identified so far is the modulation of the PIKK kinase activity in response to DNA damage. Unlike PP2A and Wip1, PP5 functions to activate the response to DNA damage via ATM. PP5 was found to physically bind ATM in a damage inducible manner (Ali et al., 2004), with a depletion of PP5, or expression of catalytically-dead phosphatase, leading to attenuated ATM signalling, reduction in the phosphorylation of ATM targets and loss of the intra S-phase checkpoint arrest (Ali et al., 2004; Yong et al., 2007). The precise mechanism for this finding remains unclear, however one explanation is that PP5 may dephosphorylate a hitherto unknown inhibitory phosphorylation site on ATM, promoting the activation of the kinase (Peng and Maller, 2010).

PP5 has also been shown to exhibit more specific effect on DDR, aside from changes to global ATM signalling upon DNA damage. A recent study using the yeast two-hybrid-system identified a damage-dependent interaction between 53BP1 and PP5, which controlled the phosphorylation status of 53BP1 in response to DNA damage (Kang et al., 2009). Loss of this interaction prevented the dephosphorylation of phospho-S25/S1778 53BP1 resulting in persistent DNA damage foci and compromised NHEJ repair.

1.7.6 PP6

In comparison to the other protein phosphatases described within this chapter, little has been investigated into the role of PP6 in the DNA damage response. Like PP5, PP6 is classified as a PP2A-like phosphatase due to similarity with

the catalytic subunit of PP2A and sensitivity to catalytic site inhibitors such as Okadaic acid and microcystin (Honkanen and Golden, 2002). The phosphatase exists as a heterotrimer consisting of a catalytic subunit (PP6C), a regulatory subunit (PP6R1, PP6R2 and PP6R3) plus an ankyrin repeat subunit (ARS-A, ARS-B and ARS-C) (Stefansson and Brautigan, 2006; Stefansson et al., 2008).

The DNA-dependent protein kinase catalytic subunit (DNA-PKcs) plays a critical role in the repair of DSB by NHEJ and is autophosphorylated in response to ionising radiation (Hammel et al., 2010). Various independent studies have reported that activated DNA-PKcs interacts with the intact PP6 holocomplex, with depletion of PP6C or regulatory subunits leading to hypersensitivity to IR and delayed release from the G2/M checkpoint (Douglas et al., 2010; Mi et al., 2009b). In addition, RNAi silencing of PP6C led to sustained phosphorylation of γH2AX at DNA lesions and compromised HR repair (Douglas et al., 2010; Zhong et al., 2011). Consistent with this, bacterially expressed PP6C-complexes exhibit phosphatase activity against γH2AX *in vitro* (Zhong et al., 2011). There does appear to be some discrepancy over whether the DNA-PKcs and PP6 interaction is damage-dependent and whether this interaction is necessary for DNA-PK activation following DNA damage. One study revealed that the binding between the two proteins increases following IR and promotes the activation of DNA-PK in response to DNA damage (Mi et al., 2009b). However a more recent study demonstrated that the PP6-DNA-PK interaction is constitutive and is not affected by the presence of DNA damage; with the interaction instead facilitating the recruitment PP6 to sites of damage, modulating the dephosphorylation of γH2AX (Douglas et al., 2010). Further investigation is needed to address the reason for these conflicting models.

In addition, mutations in the catalytic subunit of PP6, PPP6C, have been shown to act as drivers for the development of melanoma. PPP6C is mutated in between 9-12% of melanoma samples, with such mutations compromising assembly of the PP6 holoenzyme and subsequent phosphatase activity (Hammond et al., 2013). Cells with mutated PPP6C (H114Y), display elevated Aurora A activity, which results in chromosome instability and DNA damage generated by Aurora-A associated micronucleation (Hammond et al., 2013).

1.7.7 Wip1

Wip1 (wild-type p53-inducible phosphatase 1), also known as PPM1D, is a member of the PP2C family of protein phosphatases. Unlike the phosphoprotein phosphatase (PPP) family (PP1/PP2A etc.), the PP2C phosphatases lack regulatory subunits, with specificity instead determined by specific regulatory and targeting domains. In addition, the catalytic activity of these protein phosphatases in unaffected by PPP inhibitors such as Okadaic acid and microcystin (Fiscella et al., 1997). Wip1 targets multiple DNA damage repair proteins via the pSQ/pTQ motif which are phosphorylated in response to DNA damage by ATM or ATR (Yamaguchi et al., 2007). The importance of this phosphatase is demonstrated by the evidence that Wip1 is an oncogene that is amplified and overexpressed in multiple human cancer types, including breast and ovarian carcinomas (Lu et al., 2008).

It appears that a major function of Wip1 is in the reversal of cell cycle checkpoints and signalling pathways, resuming normal homeostatic function following the completion of DNA damage (Shimada and Nakanishi, 2013). Wip1 constitutively interacts with ATM and dephosphorylates ATM at S1981 upon resolution of DNA damage (Shreeram et al., 2006). In line with this

function, depletion of Wip1 led to constitutively active ATM in the absence of DNA damage, with overexpression of Wip1 suppressing ATM activation at DNA lesions. The evidence of Wip1 as a negative regulator of ATM is further strengthened with mice studies demonstrating that deletion of Wip1 in $ATM^{-/-}$ mice partially rescued many of the ATM deficiency phenotypes associated with these animals, such as radiosensitivity and fertility defects (Darlington et al., 2011).

Whilst the precise mechanistic events leading up to DNA repair remain well understood, the process of deactivating these mechanisms and returning cells to their homeostatic state is poorly understood. Multiple independent recent publications have highlighted the role of Wip1 in the direct dephosphorylation of γH2AX upon resolution of DNA damage, promoting the dissolution of DNA damage foci (Cha et al., 2010; Macurek et al., 2010; Moon et al., 2010). Fluorescently labelled Wip1 localised at IRIF, with overexpression of Wip1 leading to a decrease in the number and intensity of γH2AX foci, resulting in the delayed recruitment of DNA repair factors (Macurek et al., 2010). In addition, overexpression of Wip1 delayed the repair of DSB as determined using comet assays (Cha et al., 2010).

Wip1 has also been shown to play a critical role in the regulation of key signalling cascades in response to DNA damage. Wip1 expression upon DNA damage is driven in a p53 dependent manner (Bulavin et al., 2002; Song et al., 2010). In a negative feedback mechanism, Wip1 then dephosphorylates p53 at S15 and the E3-ubiquitin ligase MDM2 at S395, both sites phosphorylated by ATM in response to DNA damage (Lu et al., 2005). These dephosphorylations

collectively enhance the MDM2 affinity for p53, destabilise the p53 protein and leading to its proteolysis by MDM2, thus relieving the cell-cycle arrest associated with the DNA damage response (Lu et al., 2007). Another key cell cycle related function of Wip1 is the dephosphorylation of Chk1 following the resolution of DNA damage. Wip1 dephosphorylates the ATR-mediated S345, resulting in decreased Chk1 activity which correlates with a reduction in intra S-phase and G2/M checkpoint signalling (Lu et al., 2005). A physical interaction between Wip1 and Chk2, dependent on ATM phosphorylation of phospho-T68 Chk2, has also shown to be critical in the reversal of cell cycle checkpoints following damage resolution (Yoda et al., 2006). Wip1 dephosphorylates phospho-T68 Chk2, promoting cell cycle progression. Knockdown of Wip1, or expression of a phosphatase-deficient mutant (D314A), resulted in sustained phosphorylation of Chk2 and subsequently prevented cell cycle progression post-damage (Fujimoto et al., 2005). Consistent with these observations, ectopic expression of Wip1 prevented Chk2 activation and the subsequent contribution of the kinase to the G2/M checkpoint (Oliva-Trastoy et al., 2006).

1.8 Bod1L and the Bod1 family of proteins

1.8.1 Identification and function of Bod1

Bod1 and Bod1L are members of the Fam44 family of previously unknown function proteins (Figure 1.9A). An additional family member, Fam44C shares a strong degree of sequence homology with Fam44B (Bod1), however its function remains unknown (Figure1.10B) (Porter et al., 2007). Fam44A (Bod1L) also shares a region of N-terminal homology with Bod1, however it contains an additional large C-terminal extension of approximately 300 kDa. This large C-

terminal extension does not appear to relate to any other known protein, or share sequence homology with known protein groups.

Work from a previous independent study identified Bod1 from a *Xenopus laevis* proteomic screen looking to identify novel factors required for proper chromosome segregation (Porter et al., 2007). The screen utilised *in vitro* assembled chromosomes and observed by immunofluorescence that Bod1 localises to kinetochores and mitotic spindle poles during mitosis. Using RNA interference (RNAi), the authors found that when Bod1 protein levels were depleted, elongated mitotic spindles with severe bi-orientation defects were detected. More detailed examination of the phenotype revealed that Bod1 knockout did not affect the microtubule-kinetochore interaction nor the activity or localisation of the Aurora B kinase, but rather led to defects in the correct localisation and phosphorylation of the microtubule depolymerase mitotic centromere- associated kinesin (MCAK).

A more recent study, following on from work describing Bod1 as critical for correct bi-orientation during mitosis, highlighted the sequence similarity between Bod1 and the PP2A-B55 inhibitors Ensa and Arpp-19 (Porter et al., 2013). Ensa and Arpp-19 have been identified as inhibitors of PP2A-B55 and are critical in allowing activity of Cdk1/CyclinB and promoting entry into mitosis (Gharbi-Ayachi et al., 2010; Mochida et al., 2010). The reports identifying Ensa and Arpp-19 as PP2A-B55 inhibitors described a critical aspartate residue that is conserved in the Bod1 sequence (Gharbi-Ayachi et al., 2010). The Bod1 study showed that in addition to this conserved aspartate residue, an upstream Cdk site that is not present in Ensa and Arpp-19 is critical for Bod1 activity as a

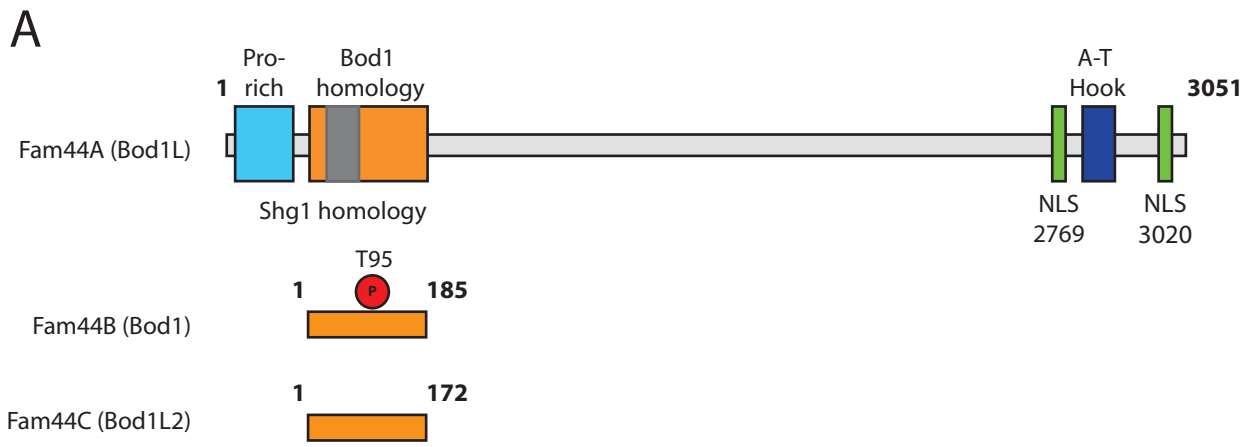

B

```
Fam44B      MATNPQPQPPPPAPPPPPPQPQPQPPPPPPGP-----------------GAGPGAG----
Fam44A      -------------------------MADGGGGGGTGAVGGGGTSQASAGAATGATGASG
Fam44C      -------------------------MADGGGGGSG-------------GAGPASTRASG

Fam44B      ---GAGGAGAGAGDPQLVAMIVNHLKSQGLFDQFRRDCLADVDTKPAYQNLRQRVDNFVA
Fam44A      GGGPINPASLPPGDPQLIALIVEQLKSRGLFDSFRRDCLADVDTKPAYQNLRQKVDNFVS
Fam44C      GGGPINPASLPPGDPQLIAIIVGQLKSRGLFDSFRRDCKADVDTKPAYQNLSQKADNFVS
                ↓  ↓D98
Fam44B      NHLATHTWSPHLNKNQLRNNIRQQVLKSGMLESGIDRIISQVVDPKINHTFRPQVEKAVH
Fam44A      THLDKQEWNPTMNKNQLRNGLRQSVVQSGMLEAGVDRIISQVVDPKLNHIFRPQIERAIH
Fam44C      THLDKQEWNPPANDNQLHDGLRQSVVQSGRSEAGVDRISSQVVDPKLNHIFRPQIEQIIH

Fam44B      EFLATLNHKEEGSGNTAPDDEKPDTSLITQGVPTPGPSANVANDAMSILETITSLNQEAS
Fam44A      EFLAAQKKAAVPAPPPEPEGQ-----------DPPAPSQDTS------------------
Fam44C      EFLVAQKEAAVPALPPEPEGQ-----------DPPAPSQDTS------------------
```

Figure 1.9: The Fam44 family of proteins

(A) Schematic representation of the annotated domains of the Fam44 family of proteins. The T95 phosphorylation site identified on Bod1 has been highlighted.

(B) Alignment of the three Fam44 family members. Black arrows indicate the residues shown to be important for PP2A-B56 inhibition by Fam44B (Bod1) (Porter et al., 2013).

specific inhibitor of kinetochore associated PP2A-B56 during mitosis. Loss of Bod1 from mammalian cells releases the inhibition of the PP2A-B56 phosphatase, resulting in the loss of phospho-epitopes at the kinetochore during mitosis. The authors demonstrate that this hyperactivity of PP2A-B56 results in the delocalisation of the critical kinetochore components Plk1 and Sgo1, resulting in the bi-orientation phenotype observed. During normal mitotic conditions, Bod1 acts as an additional level of regulatory control over the PP2A-B56 phosphatase ensuring specificity of action. Intriguingly, although the critical aspartate (D98) and upstream CDK site (T95) are conserved between Fam44B (Bod1) and Fam44C, these two residues are not conserved in Bod1L in any species investigated (Figure 1.9B). This is despite the surrounding sequence of all three family members being highly conserved.

1.8.2 Shg1/COMPASS domain

Post-translational modifications described previously, such as phosphorylation by ATM and the down-stream ubiquitin modifications mediated by E3-ubiquitin ligases such as RNF8 and RNF168, all occur in response to damage, specifically at DNA lesions. Unlike these modifications, histone methylation involved in the DNA damage response appears to occur more constitutively throughout the cell-cycle.

Contained within the Bod1-homology domain of Bod1L (and the family member Bod1) is a region of homology with the Complex proteins associated with SET1 protein (COMPASS) component Shg1. The COMPASS complex, first identified in *saccharomyces cerevisiae*, is responsible for histone H3 lysine 4 (H3K4) methylation and is evolutionary highly conserved (Shilatifard, 2012). In yeast cells, the sole methyltransferase, Set1p, assembles with a number of accessory

proteins (Sdc1p, Swd1p, Swd2p, Spp1p, Swd3p, Shg1p and Bre2p) to generate the COMPASS complex (Miller et al., 2001). In higher eukaryotic cells, at least six H3K4 methyltransferases have been identified (Set1a, Set1b, MLL1-5) leading to the formation of six COMPASS-like complexes (Eissenberg and Shilatifard, 2010; Shilatifard, 2012). The individual methyltransferases share common accessory proteins, consisting of Wdr5, Rbbp5, Ash2l and Dpy30, with specificity likely determined by the methyltransferase present in the complex (Dehe et al., 2006; Dou et al., 2006).

Both mono- (me) and tri-methylation (me3) of H3K4 have been shown to be involved in the DNA damage response in both yeast and mammalian cells. As mentioned previously, histone methylation appears to occur constitutively, with the active removal of H3K4me3 occurring at sites of damage identified by γH2AX staining. A recent study by the Friedl group demonstrated that the anti-correlation of H3K4me3 and γH2AX staining increases with time post-irradiation, suggesting that the histone methylation is actively removed over time (Seiler et al., 2011). Studies in yeast have revealed that in cells with a Δ*set1* mutation preventing H3K4 methylation, are defective in NHEJ repair and show compromised S-phase progression in the presence of replication stress (Faucher and Wellinger, 2010). Both these examples, in addition to other work, highlight the function of H3K4 modification in altering chromatin structure at sites of DNA damage to allow for robust repair (Nakamura et al., 2011).

As alluded to previously, the six mammalian COMPASS complexes contain a multiple accessory subunits, a number of which are found unanimously across all of the COMPASS complexes (Dehe et al., 2006; Dou et al., 2006). The

precise function of each of these subunits remains unknown, however a complex of subunits lacking the methyltransferase Set1 homologue were demonstrated as displaying intrinsic methyltransferase activity toward H3K4, suggestive that a degree of redundancy may exist within each COMPASS complex (Patel et al., 2009). Recent data has shown that Bod1L interacts with one key accessory subunit, Ash2L, suggestive of Bod1L being part of the Ash2L containing H3K4 methyltransferase complex. In addition, the study also identified that H3K4 methyltransferase complexes bind to the Bod1L promoter, implying that regulation of chromatin structure at Bod1L locus might be important to regulating the H3K4 di- and tri-methylation (Ciotta, 2011). A more recent study identified both Bod1 and Bod1L as interacting partners of the Dpy30 (WRAD) complexes, with Bod1L and Bod1 exclusively present in Set1A/Set1B methyltransferase complexes (van Nuland et al., 2013). This study also identified a Set1B independent interaction between Bod1 and Bod1L, implying that these two proteins may form a heterodimer. Given the inclusion of Bod1L in methyltransferase complexes, coupled with the Shg1 homology, both of these studies proposed that Bod1L may function as the higher eukaryotic paralogue of yeast Shg1 (Ciotta, 2011; van Nuland et al., 2013).

1.8.3 Bod1L is required to suppress deleterious resection of stressed replication forks

A recently published paper from the Stewart group identified Bod1L as a component of pathway that safeguards genome stability following replication stress (Higgs et al., 2015). Loss of Bod1L resulted in sensitivity to replication stress, resulting in catastrophic genome instability. They showed that Bod1L functions downstream of BRCA2 to stabilise Rad51 nucleofilaments at damaged replication forks, protecting such damaged forks and preventing

resection by DNA2. As Rad51 localisation to forks is unaffected following Bod1L depletion, this strongly suggests that Bod1L acts to stabilise these filaments once formed. Whilst this study reveals an interesting functional consequence of Bod1L depletion, little mechanistic detail is discussed regarding the position and function of Bod1L in the pathway and therefore the implications and future direction of the study are hard to gauge. In addition, no replication or DNA damage defects could be detected in cells only depleted of Bod1L, indeed all phenotypes observed in the study were induced using agents that lead to replication stress, particularly MMC. Whilst the use of such agents is useful in exacerbating subtle phenotypes, if the principle function of Bod1L was to safeguard genome stability following replication stress, one would expect a more pronounced phenotype occurring as a result of endogenous replication stress. The authors do however demonstrate that Bod1L interacts with a number of key components of the DDR, including MRE11 and BRCA2, suggestive of a potential additional role of this protein in repair of damaged DNA.

1.9 Aims and objectives

The maintenance of genomic integrity by DNA repair is of critical importance for cell survival. DSBs are among the most adverse forms of DNA damage and failure to properly repair these breaks may lead to genomic instability, gene deletions and cancer (Bartkova et al., 2005; Ciccia and Elledge, 2010; Jackson and Bartek, 2009). The cell therefore maintains several elaborate systems to rapidly detect and repair DNA damage, whilst delaying cell cycle progression (Lukas et al., 2004b; Melo and Toczyski, 2002; Zhou and Elledge, 2000). As such, one of the objectives of this study will be to determine whether Bod1L functions to delay the cell cycle upon DNA damage.

As outlined above, the recognition and repair of DNA lesions is accomplished by the concentration of signalling and repair factors in the vicinity of the damage, leading to the formation of DNA damage foci (Lukas et al., 2005). ATM-dependent phosphorylation of the histone variant H2AX (γH2AX) is the principal and critical step for subsequent down-stream accumulation of signalling and repair factors at DNA lesions (Celeste et al., 2003; Paull et al., 2000; Rogakou et al., 1998). MDC1 directly binds γH2AX (Stucki and Jackson, 2006), and is the critical recruitment platform for most other proteins involved in signalling and repair at sites of damage (Jungmichel and Stucki, 2010; Stucki et al., 2005). Analysis of global ATM and ATR substrates, as well as ultradeep phosphoproteome mass-spectrometry revealed multiple phosphorylation sites on Bod1L (Matsuoka et al., 2000; Sharma et al., 2014). In light of this evidence, coupled with the preliminary data from the lab suggesting that Bod1L depletion leads to genomic instability and published data on Bod1L (Higgs et al., 2015), this study will look to investigate the role of Bod1L in controlling the focal assembly of early DNA repair factors at sites of DNA damage.

Multiple protein phosphatases have been implicated in the repair of DNA damage, involved in both the formation of DNA damage foci as well as the disassembly of foci following repair (Chowdhury et al., 2005; Freeman and Monteiro, 2010; Li et al., 2015; Nakada et al., 2008). Specifically, PP2A-B56 isoforms are required for dephosphorylation of γH2AX (Chowdhury et al., 2005; Li et al., 2015) with the loss of PP2A activity resulting in persistent γH2AX foci and impaired DNA damage repair. In addition to a role in modulating foci formation, PP2A has also been implicated in the inhibition of cell proliferation

and the cell cycle following DNA damage (Li et al., 2007). There is also strong recent evidence that treatment of cells with chemical inhibitors of PP2A causes defects in cell cycle arrest leading to improper DNA damage repair and cell death (Lu et al., 2009). Given the already established role of Bod1 as an inhibitor of PP2A-B56 function, coupled with the strong degree of homology between Bod1 and Bod1L, this study will look to investigate whether Bod1L, like Bod1, interacts with the Ser/Thr phosphatase PP2A-B56. There is already precedence for the involvement of phosphatase inhibitors during the DNA damage response, with the cellular PP2A inhibitor TIPRL having been shown to play an important role in DNA damage and repair signalling, opposing ATM/ATR-dependent phosphorylation events (McConnell et al., 2007; Smetana and Zanchin, 2007)

To summarise, in light of this background information and preliminary data, the aims and objectives of this study were:

i. *Investigate the role of Bod1L during the DNA damage response*
ii. *Identify whether Bod1L, like Bod1, interacts with the Ser/Thr phosphatase PP2A-B56*
iii. *Understand whether Bod1L plays a role in cell-cycle control following DNA damage*

Chapter 2 - Experimental Procedures

2.1 Tissue Culture

2.1.1 Cell Lines and Culture

All cell lines were maintained in a standard EMEM medium (Lonza) and supplemented with 10% v/v foetal bovine serum (FBS)(Lonza), 2 mM L-glutamine (Life Technologies), 100 U/mL Penicillin and 100 mg/mL Streptomycin (Life Technologies). U2OS cells stably expressing a DR-GFP cassette construct were maintained in the standard cell culture medium supplemented with 2 μg/mL puromycin (Sigma). U2OS cells stably expressing GFP-MDC1 were maintained in the standard cell culture medium supplemented with 400 μg/mL G-418 (Life Technologies). Individual cell culture details can be found in table 2.1. For adherent cells, 0.05% trypsin-EDTA with phenol red (Life Technologies) was added to lift cells for passaging. All cell lines were maintained at 37°C at 5% CO_2 in a humidified incubator. At passage 20, cells were disposed of and fresh cells were defrosted from liquid nitrogen storage. Liquid nitrogen storage media consisted of 90% FBS and 10% DMSO (Sigma).

2.1.2 DNA and RNA transfections

2.1.2.1 siRNA transfection

Cells were seeded in 6-well tissue culture dishes (TPP) and incubated until 90% confluence was reached in culture medium that does not contain penicillin or streptomycin. Cells were transfected with 8 – 24 nM siRNA duplexes (concentration is optimisation dependant), or equal concentration medium-GC control siRNA (Life Technologies) using Lipofectamine 2000 (Life

Technologies). Standard manufacturers protocol was followed for transfections. After 16-24 hours, cells were split into fresh media. Cells were assessed for knockdown 48 hours after transfection.

2.1.2.2 DNA transfection

Cells were seeded in 6-well tissue culture dishes and incubated until 70-90% confluence was reached. Cells were transfected with 0.3-1 μg DNA per well (concentration is optimisation dependant) using Effectene transfection reagent (Qiagen) following standard manufacturers protocol. The following day, cells were split into fresh culture medium and expression was assessed after 48 hours. DNA constructs used in this study are listed in table 2.5.

2.1.2.3 siRNA and DNA co-transfection

For rescue experiments, endogenous protein was depleted by siRNA and exogenous fusion protein was expressed from plasmid DNA. Cells were seeded in 6-well tissue culture dishes and incubated until 80% confluence was reached in culture medium that does not contain penicillin or streptomycin. Cells were transfected with siRNA as described previously. After 16-24 hours, fresh media containing penicillin and streptomycin was added and cells were transfected with DNA as described previously. After 12 hours, cells were split into fresh media. Cells were assessed for knockdown and exogenous protein expression 24 hours after DNA transfection.

2.1.3 Generation of stable cell lines

pDRGFP was a gift from Maria Jasin (Addgene plasmid # 26475) (Pierce et al., 1999). HeLa DR-GFP cells were generated by transfecting HeLa S3 cells with pDRGFP plasmid using Effectene as described above. 2 μg/mL puromycin (Life

Technologies) was used to select for cells that had stably integrated the plasmid. Single clones were selected, transfected with I-Sce-I plasmid and screened for GFP by direct microscope observation.

Full length Homo Sapiens MDC1 (NP_055456.2) (Yin et al., 2012)(A kind gift from the Hay group, Dundee) cloned from HeLa Kyoto cDNA was fused to eGFP or mCherry generating pEGFP-MDC1 (pA414) and pmCherry-MDC1 (pA495). U2OS GFP-MDC1 cells were generated by transfecting U2OS cells with GFP-MDC1 plasmid using METAFECTENE PRO (Biontex). After G418 selection (400µg/ml)(Calbiochem), GFP-MDC1 expression was confirmed by direct microscope observation.

pCDNA5-B56γ1-YFP (a kind gift from the Saurin Group, Dundee) was created by PCR of B56γ1 from pCEP-4xHA-B56γ1 (Addgene plasmid #14534; deposited by D. Virshup, Duke-NUS Graduate Medical School, Singapore) and ligation into pCDNA5 vector using Not1 and Apa1 restriction sites. HeLa Flp-in cells (a gift from S. Taylor, University of Manchester, UK) were transfected with pCDNA5-YFP-B56γ1 and pOG44 (Invitrogen) using Fugene HD (Promega) and positive clones were selected using Hygromycin B. PP2A-B56γ1-YFP expression was induced with 1 μg/mL of doxycycline for ≥16 h.

2.1.4 Clonogenic survival assay

HeLa or U2OS cells were transfected with siRNA and DNA as described above and seeded 2000 cells per 10 cm dish. Experiments were carried out in triplicate for each condition. Compounds were added for 16 hours before wash-out and fresh media addition. Cells were left to propagate for 10-12 days before

plates were dried and then stained with a 2/1/1 ddH_2O/MeOH (VWR)/Crystal violet solution (Sigma). Colonies were counted using a GelCount colony counter (Oxford Optronix) and percentage survival was calculated.

2.1.5 DR-GFP Assay

U2OS cells stably expressing a cassette in which a unique I-Sce-I restriction site was placed between tandem mutant copies of GFP were transfected with control or Bod1L siRNA. After 48 hours cells were transfected with I-Sce-I vector plus DMSO or 10 μM KU59933. After 24 hours cells were fixed in PFA and analysed with microscopy for GFP expression.

2.1.6 Drug treatments and Ionising Radiation

Chemicals were dissolved in DMSO (Sigma) to a stock concentration of between 100 μM – 10 mM. Etoposide (Sigma) was used at a working concentration of 10 μM. Monastrol (Tocris) was used at a concentration of 100 nM. Nocodazole (CalBioChem) was used at a concentration of 100 ng/mL. Cisplatin (Sigma), Mitomycin C (SantaCruz), Camptothecin (Donated by Rouse group, University of Dundee) and 6-Thioguanine (Sigma) were all used at the concentration ranges indicated.

Irradiation of samples was carried out using an IBL 437C Gamma Irradiator with a Cesium^{137} gamma source. The typical dose delivered was 5 Gy unless otherwise stated, at an approximate rate of 2 Gy/min. Note that all non-irradiated samples were treated with a mock-irradiation to mimic any results arising as a result of temperature shock. Recovery from irradiation or mock-irradiation was at 37°C.

Table 2.1 Cell culture cell line maintenance

Cell Line	ATCC Number	Culture Medium	Cell Passaging	Notes
HeLa (S3)	CCL-2.2	EMEM, 10% FBS, 2 mM L-Glutamine, 100 U/ml Penicillin, 100 mg/ml Streptomycin	Split 1:10 every 4 days. Maintained between passage number 1 and 20.	
HeLa-DRGFP	-	EMEM, 10% FBS, 2 mM L-Glutamine, 100 U/ml Penicillin, 100 mg/ml Streptomycin, 2 µg/ml puromycin	Split 1:10 every 4 days. Maintained between passage number 1 and 20.	
HeLa-PP2A-B56alpha-GFP "211C"	-	EMEM, 10% FBS, 2 mM L-Glutamine, 100 U/ml Penicillin, 100 mg/ml Streptomycin	Split 1:10 every 4 days. Maintained between passage number 1 and 20.	Gift from Foley Lab
RPE1-PP2A-B56delta-GFP	-	EMEM, 10% FBS, 2 mM L-Glutamine, 100 U/ml Penicillin, 100 mg/ml Streptomycin	Split 1:10 every 4 days. Maintained between passage number 1 and 20.	Gift from Foley Lab
HeLa-PP2A-A -GFP "204E"	-	EMEM, 10% FBS, 2 mM L-Glutamine, 100 U/ml Penicillin, 100 mg/ml Streptomycin	Split 1:10 every 4 days. Maintained between passage number 1 and 20.	Gift from Foley Lab
HeLa-PP2A-B56γ1-YFP	-	EMEM, 10% FBS, 2 mM L-Glutamine, 100 U/ml Penicillin, 100 mg/ml Streptomycin	Split 1:10 every 4 days. Maintained between passage number 1 and 20.	Gift from Saurin Lab
U2OS	HTB-96	EMEM, 10% FBS, 2 mM L-Glutamine, 100 U/ml Penicillin, 100 mg/ml Streptomycin	Split 1:5 every 4 days. Maintained between passage number 1 and 20.	
U2OS-MDC1-GFP	-	EMEM, 10% FBS, 2 mM L-Glutamine, 100 U/ml Penicillin, 100 mg/ml Streptomycin, 400 µg/ml G418	Split 1:5 every 4 days. Maintained between passage number 1 and 20.	Gift from Hay Lab
U2OS-LacO	-	EMEM, 10% FBS, 2 mM L-Glutamine, 100 U/ml Penicillin, 100 mg/ml Streptomycin	Split 1:4 every 4 days. Maintained between passage number 1 and 20.	Gift from Saurin Lab
HeLa (Kyoto)-CENPA-GFP	-	EMEM, 10% FBS, 2 mM L-Glutamine, 100 U/ml Penicillin, 100 mg/ml Streptomycin	Split 1:10 every 4 days. Maintained between passage number 1 and 20.	Gift from Jaqaman Lab

2.2 Molecular Biology

2.2.1 Primer design

All primers were ordered with a synthesis scale of 25 nmole and pre-purified via de-salting. Primers were reconstituted in TE buffer to a stock concentration of 100 μM and kept at -20°C.

Primers for PCR reactions varied according to application but were generally kept between 20-30 nucleotides in length, with a GC content of between 40-60%. Unique restriction sites were inserted into primer sequence where necessary. Primer T_m for PCR reactions was calculated using the following calculation:

$$T_m=(\text{sum A+T}) \times 2 + (\text{sum G+C}) \times 4°C$$

Primers for sequencing reactions followed similar design guidelines to PCR primers, however the T_m was kept close to 60°C. In addition to this, primers were designed with at least one G or C at the 3' end of the primer. Homopolmeric (e.g. CCCCC) and sequence repeats were also avoided where possible. A list of primers used in this study can be found in table 2.4.

2.2.2 Polymerase chain reaction (PCR)

PCR reactions were performed in 25 μL reactions using an Eppendorf Mastercycler Gradient Thermal Cycler. 10 ng of template DNA was combined with 200 μM dNTPs (Thermo), 500 nM forward and reverse primers, 1 X Phusion reaction buffer and 0.4U Phusion HotStart II DNA polymerase (Thermo). PCR reactions with Bod1L had the addition of 8% v/v DMSO (Sigma) and 1.6 M Bettaine (Sigma) to help reduce secondary structure. PCR cycling

program was optimised for each reaction, however in general the programme consisted of an initial denaturation at 98°C for 3 minutes, proceeded by 25-30 cycles of 98°C for 30 seconds, T_m°C for 30 seconds (with T_m the calculated melting temperature of primer pair used), 72°C for 30 seconds/Kb followed by 72°C for product length + 20%.

2.2.3 DNA sequencing and concentration determination

DNA sequencing was performed in-house using the Dundee sequencing service (http://www.dnaseq.co.uk/, accessed between 09/11 – 05/15) DNA concentrations from PCR reactions or restriction digests were measured using a Nanodrop 1000 spectrophotometer (Thermo). The Nanodrop was blanked with EB Buffer (Qiagen) before 1 μL of DNA in EB buffer was measured and the concentration noted. $A_{260/280}$ was also measured to assess DNA purity. Samples with an $A_{260/280}$ differing from ~1.8 were rejected.

2.2.4 Agarose gel electrophoresis

Restriction digested DNA and PCR products were visualised via agarose gel electrophoresis. 0.8% w/v Agarose gels were cast using Ultrapure agarose (Life Technologies) in TAE buffer. Ethidium bromide (EtBr)(Sigma) was added to the partially cooled agarose at a final concentration of 0.5 μg/mL. Samples were combined with 10 X loading dye to a final concentration of 1 X and run alongside a 0.1-10 Kb DNA ladder (New England Biolabs). Samples were run at 110V for 45 minutes. Gels were visualised using the Gel-Doc system (BioRad).

2.2.5 Restriction digests

Restriction digests were carried out for cloning or verification of DNA fragment size. All restriction enzymes were purchased from New England BioLabs and

where possible High-Fidelity versions were used. Reactions were performed at 37°C for 1 hour and consisted of between 0.5 and 4 μg DNA and 10-20 units of restriction enzyme. Double digests were performed where necessary in a compatible buffer. Where no compatible reaction buffer was available, sequential reactions were performed, passing the DNA through a QIAquick PCR purification column (Qiagen) for buffer exchange.

For plasmid backbone, where necessary, samples were treated with Calf intestinal alkaline phosphatase (CIP)(New England Biolabs) at a final concentration of 10U/reaction to dephosphorylate 5' and 3' ends and help prevent relegation.

2.2.6 Bacterial Transformation

2.2.6.1 Bacterial culture medium and plates

LB broth and LB agar plates were purchased pre-prepared from the in-house media kitchen and stored for a maximum of one month at 4°C. Ampicillin was added to LB and LB-agar at a final concentration of 100 μg/mL. Kanamycin was added to LB and LB-agar at a final concentration of 50 μg/mL.

2.2.6.2 Bacterial transformation

Chemically competent DH5α and BL21 *E. coli* cells were purchased in-house (MRC-PPU/DSTT). For circular plasmid DNA, 0.2 μL of DNA or ddH_2O as control was gently mixed with 50 μL competent *E. coli* cells. For ligation products from molecular cloning, 4 μL of DNA or ddH_2O was gently mixed with 50 μL competent *E. coli* cells. Cells were incubated on ice for 30 minutes before heat-shock at 42°C for 30 seconds and then 2 minutes recovery on ice. 950 μL

S.O.C. medium (Life Technologies) was added to the cells and mixture was incubated with shaking at 37°C for 1 hour. 100 μL of cells were then plated onto antibiotic selection plates. The remaining mixture was spun-down at 7,500 r.c.f. for 5 minutes before re-suspending in 100 μL fresh S.O.C. This was then plated onto another LB-agar plate containing the selection antibiotic. Colonies were allowed to grow overnight at 37°C before colonies were picked and grown in liquid culture.

2.2.7 Molecular cloning

A list of all DNA constructs used in this study can be found in table 2.5.

2.2.7.1 Standard cloning

DNA to be inserted into the plasmid vector was amplified using PCR method described above. PCR products were run on 0.8% w/v agarose gel and DNA was visualised using EtBr. Bands corresponding the to the correct size were excised from the gel and prepared using a QIAquick gel extraction kit (Qiagen). Both the PCR amplified insert as well as the target vector were digested with two unique cutting restriction enzymes (New England BioLabs/Thermo) in order to generate complementary sticky DNA overhangs for ligation. Insert and target vector were ligated using T4 DNA ligase (New England BioLabs) using an insert:vector ratio of 4:1. Ligation reaction was performed at 16°C overnight or at room temperature for 2 hours. 5 μL ligated DNA product was then transformed into competent cells.

2.2.7.2 Gibson Assembly cloning

Gibson assembly protocol (New England BioLabs) was used to ligate site directed mutagenesis fragments. Standard manufacturers protocol was followed.

PCR primers were designed to contain 30 nucleotide homologous overlapping regions to ensure full sequence coverage of final product. PCR reactions were performed as described above. PCR product was run on 0.8% w/v agarose gel and bands were excised and prepared using QIAquick gel extraction kit. As per the manufacturers protocol, 0.2 pmol DNA for each fragment was added to the reaction mix and an optimal ligation an optimal ligation ratio of 2:1 insert to backbone was used. Samples were incubated at 50°C for 60 minutes before bacterial transformation was carried out. Positive and negative controls were included to ensure specificity and functionality of Gibson assembly master mix.

2.2.7.3 Site-directed mutagenesis

Site-directed mutagenesis was performed using the Q5 site-directed mutagenesis kit (New England BioLabs).

Non-overlapping primer design allows for exponential amplification of region of interest. Mutagenic substitutions are created by incorporating the mutagenic nucleotide into the centre of the forward primer, with the reverse primer designed so that the 5’ ends of the primers anneal back-to-back. Mutagenic primers were designed using the following web-app: http://nebasechanger.neb.com/ (Accessed 09/14 – 09/15). PCR reaction was

carried out as described above, using the Q5 Hot Start High-Fidelity DNA polymerase (New England BioLabs).

1 μL PCR product was run on 0.8% w/v agarose gel to ensure successful PCR. PCR product was then treated with KLD enzyme mix (Kinase:Ligase:DpnI) to ligate linear DNA and digest methylated DNA template. Ligated DNA was then transformed into competent bacteria.

2.2.8 Preparation of plasmid DNA

2.2.8.1 Mini-prep of plasmid DNA

Single bacterial colonies were picked from LB-agar selection plates and spiked into pre-warmed LB broth containing the relevant antibiotic. Samples were incubated with shaking overnight at 37°C. Once turbid, samples were spun-down at 6,000 r.c.f. for 5 minutes to pellet bacteria. Preparation of plasmid DNA was carried out using a QIAprep kit (Qiagen). Purified plasmid DNA was analysed using a Nanodrop 1000 to determine concentration and purity. DNA was stored in EB buffer at -20°C.

2.2.8.2 Maxi-prep of plasmid DNA

For larger scale production of plasmid DNA, single bacterial colonies were picked and spiked into pre-warmed LB broth containing the relevant antibiotic. Samples were incubated with shaking for 10-12 hours at 37°C. Starter culture was then diluted 1:1000 into 250 mL of LB broth containing antibiotic. Cells were then grown at 37°C for 12–16 h with vigorous shaking. Bacterial cells were harvested by centrifugation at 6000 r.c.f. for 15 min at 4°C. A Qiagen plasmid maxi-prep kit was then used to purify plasmid DNA and standard manufacturers

protocol was followed. Air-dried plasmid DNA was re-suspended in EB buffer and analysed using a Nanodrop 1000 to determine concentration and purity. DNA was aliquoted and stored at -20°C.

2.2.8.3 Preparation of glycerol stocks

Bacteria expressing various plasmid DNA constructs were stored as glycerol stocks. In short, 750 μL of starter culture was combined with 250 μL 50% v/v autoclaved glycerol (VWR) and stored at -80°C.

2.3 Biochemistry

2.3.1 Protein concentration determination

Protein concentration of cellular lysate, recombinant protein and purified antibodies were determined using Bradford protein assay (BioRad). A series of standards ranging from 0-10 μg/mL were made up using either BSA for protein concentration determination, or rabbit IgG for antibody concentration determination. Standards were combined with Bradford solution diluted 1:5 in ddH_2O and a standard curve was generated. Protein or antibody samples were added to diluted Bradford solution, incubated for 5 minutes and absorption was measured at 595 nm. Protein concentrations were calculated from the standard curve using Microsoft Excel.

2.3.2 Cell lysis and sample preparation

2.3.2.1 Radioimmunoprecipitation assay (RIPA) buffer

Fresh RIPA buffer was prepared fresh and kept on ice. Adherent cells were grown to the desired confluence before culture medium was aspirated and cells were washed once with ice-cold PBS. RIPA buffer was added directly to the

cells and left to incubate at 4°C for 10 minutes. After incubation, cells were lifted from culture dish using a sterile cell scraper (Greiner) and centrifuged at ~20,000 r.c.f. at 4°C for 10 minutes to pellet cellular debris. Supernatant was snap-frozen in liquid nitrogen and stored short-term at -20°C or long-term at -80°C.

2.3.2.2 Fractionation lysis

Fraction lysis buffers were prepared fresh and kept on ice. Adherent cells were grown to the desired confluence before culture medium was aspirated and cells were washed once with ice-cold PBS. Buffer A was added to cells and left to incubate at 4°C for 20 minutes. After incubation, cells were very gently lifted from culture dish using a sterile cell scraper (Greiner) and centrifuged at 1,400 r.c.f. at 4°C for 10 minutes. Supernatant was carefully aspirated, labelled as 'cytoplasmic fraction' and snap frozen. Pellet was re-suspended in buffer A+ and incubated for 1 minute at 37°C. EDTA was immediately added to a final concentration of 2 mM and lysate was incubated on ice for 5 minutes. Lysate was then centrifuged at 1,400 r.c.f. at 4°C for 5 minutes. Supernatant was carefully aspirated, labelled as 'nucleoplasmic fraction' and snap frozen. Pellet was re-suspended in buffer B and incubated for 1 minute at room temperature. Lysate was then centrifuged at 15,000 r.c.f. at 4°C for 10 minutes. Supernatant was then aspirated, labelled as 'chromatin fraction' and snap frozen. Protein lysates were stored short-term at -20°C or long-term at -80°C.

2.3.3 SDS-polyacrylamide gel electrophoresis (SDS-PAGE)

Pre-cast Bolt or NuPAGE SDS-PAGE gels (Life Technologies) were selected according to protein of interest. Typically proteins larger than 300 kDa were run

using 3-8% Tris-Acetate gels, with most other proteins run using 4-12% Bis-Tris gels. Protein concentration of samples was determined by Bradford assay and typically 20-40 μg of protein was run per well. Protein samples were prepared with LDS NuPAGE sample buffer (Life Technologies), supplemented with 5% v/v β-mercaptoethanol (Sigma). Samples were boiled for 5 minutes before centrifugation at 2,700 r.c.f. at 4°C for 2 minutes. Samples were run alongside a pre-stained high-molecular weight marker (Life Technologies) as well as an un-stained standard molecular weight marker (BioRad). Gels were run at 90V for 20 minutes followed by 180V (NuPAGE) or 165V (Bolt) for 50 minutes. Proteins were visualised on gels using SimplyBlue Safestain (Life Technologies) following manufacturers protocol.

2.3.4 Immunoblotting

2.3.4.1 Standard protein immunoblotting

Proteins were separated by size by SDS-PAGE and then transferred to either 0.2 μm pore-size nitrocellulose membranes or 0.2 μm pore-size PVDF membranes (GE Healthcare). Chilled 20X transfer buffer (Life Technologies) was diluted down to working concentration and supplemented with 10% v/v methanol (VWR). Transfer was carried out at 80V for 2 hours at room temperature. Protein transfer efficiency was determined by staining membranes in Ponceau S stain (Sigma) diluted in 1% v/v acetic acid (VWR). Excess Ponceau S stain was removed by washing in 1% v/v acetic acid until protein bands were visible. Prior to blocking, all Ponceau S stain was removed by washing for 5 minutes in TBS-Tween20.

To minimise non-specific binding, membranes were blocked by incubation in either 5% w/v non-fat milk in TBS-Tween20 (non phospho-antibodies)(Marvel) or 10% v/v Roti-Block in TBS-Tween20 (phospho-antibodies)(Carl Roth) at room temperature for 1 hour. Blocking solution was removed by a brief wash in TBS-Tween20 before addition of primary antibody. Antibodies were diluted in AbDil solution. Details of antibody dilution can be found in table 2.3. Following primary antibody incubation, membranes were washed 3 x 5 minutes in TBS-Tween20. Membranes were then incubated with secondary antibody conjugated with horseradish peroxidase (HRP) in 5% w/v low-fat milk, according to details in table 2.3. Following secondary antibody incubation, membranes were washed 3 x 5 minutes in TBS-Tween20. Membranes were incubated in Clarity ECL substrate (BioRad) according to manufacturers protocol and signal was detected using either X-ray film (Kodak) or the Odyssey CLx infrared detection system (LI-COR).

2.3.4.2 Immunoblotting of large (>300 kDa) proteins

For large proteins, a modified protocol was used for immunoblotting to ensure maximum transfer. Samples were boiled for 2 x 5 minutes with a brief vortex between each boil. Standard protein immunoblotting was followed except a modified Laemlli buffer was used for transfer, supplemented with 7.5% v/v methanol. Transfer was carried out at 4°C for 16-20 hours at 30V. The buffers and apparatus used for the blotting were all SDS-free to ensure maximum transfer efficiency.

2.3.4.3 Strip and re-blotting

When necessary, membranes were stripped of primary and secondary antibodies and re-probed with fresh antibody. A modified stripping buffer

(Yeung and Stanley, 2009) was added to membranes for 10 minutes at room temperature with agitation. After incubation, membranes were washed 3 x 5 minutes in TBS-Tween20 before blocking and standard immunoblotting protocol was followed.

2.3.5 GFP-Trap Immunoprecipitation

2.3.5.1 Generation of GFP-trap beads

Transformed BL21 *E. coli* expressing LAMA GFP-Trap fused to a GST tag were kindly donated by the Lamond Lab, University of Dundee.

A single colony was used to inoculate 5 mL LB broth (containing 100 μg/mL ampicillin) and was grown for 12 hours at 37°C with shaking. The starter culture was used to inoculate 500 mL of pre-warmed auto-induction media (containing 100 μg/mL ampicillin). This was incubated for 6 hours at 30°C. The temperature was then decreased to 25°C and bacteria were grown for 24 hours with shaking. Cells were harvested by centrifugation at 4,500 r.c.f at 4°C for 45 minutes with slow deceleration.

The cell pellet was re-suspended in 50 μL of PBS for every 1 mL of culture volume. Complete-EDTA free protease inhibitors (Roche) were added to the PBS prior to re-suspension. Lysozyme (Sigma) was added to a final concentration of 1 mg/mL and cells were incubated at 4°C with rotation for 30 min. Triton X-100 (VWR) was added to a final concentration of 1% v/v rotated for 5 minutes at 4°C.

Cell lysate was sonicated on ice with the program set to 5 seconds bursts with 5 second rests at 15% power for 5 minutes. Lysate was incubated at 4°C with rotation for 15 minutes before sonication was repeated. Cell lysate was centrifuged at 20,000 r.c.f. in a JLA25.50 rotor for 30 minutes at 4°C to pellet cellular debris.

Glutathione sepharose 4B slurry (Thermo) was pre-equilibrated by washing in 50 mL of PBS. Beads were centrifuged at 3000 r.c.f. for 4 minutes at 4°C with slow deceleration to preserve bead pellet. The protein lysate was then combined with the washed glutathione sepharose 4B and incubated overnight on a rotating wheel at 4°C. The bead/lysate solution was centrifuged at 3000 r.c.f. for 4 minutes at 4°C with slow deceleration and beads were washed twice with 50 mL of PBS. After washing, beads were re-suspended in PBS.

A 10 mL plastic column (Thermo) was washed with 30 mL PBS at room temperature. Beads in PBS were added to column and washed with 20 mL of TBS followed by 20 mL of thrombin cleavage buffer. 20U of thrombin (Sigma) was added to approximately 2-3 mL of cleavage buffer in the column. 3 μL of 0.5% w/v xylene cyanol (Sigma) was added to the column and pipetted to mix (added to enable visualisation of mixing and elution). Column was incubated overnight at room temp. Thrombin cleavage buffer was added to the column to elute cleaved fusion protein. Flow-through was collected until no more xylene cyanol was visible in the column.

Column flow through containing LAMA GFP-Trap was washed with PBS and concentrated using a 5 kDa centrifugal concentrator (Millipore). Protein concentration was measured by Bradford assay.

LAMA GFP-Trap protein was coupled to NHS-Activated Magnetic Beads (Thermo) following manufacturers instructions. GFP-Trap beads were stored in PBS + 0.05% w/v sodium azide (Sigma) for up to one year at 4°C.

2.3.5.2 GFP-Trap Immunoprecipitation protocol

Cells stably expressing or transiently expressing GFP fusion proteins were lysed using the fractionation lysis protocol and chromatin fractions were used for immunoprecipitation reactions. Cells expressing an empty GFP vector were used as a control condition. 10% of the sample was retained before the IP to be used as input control. GFP-Trap beads were washed 3 X 2 minutes in PBS before cell lysate was added to beads and incubated at 4°C for 1 hour with rotation. Beads were washed 3 X 5 minutes in IP wash buffer before LDS NuPAGE sample buffer was added, supplemented with 5% v/v β-mercaptoethanol. Samples were boiled for 5 minutes, gently vortexed and then boiled for a further 5 minutes. Samples were then spun at 2,700 r.c.f. at 4°C for 2 minutes and then either run on SDS-PAGE gel or stored at -80°C.

2.3.6 Generation of Bod1L non-phospho antibody

Peptide antibodies and non-phospho antibodies were designed and generated according to (Field et al., 1998). Bod1L antibody peptide was designed by Iain Porter (Swedlow group, University of Dundee) and immunised in rabbit. Full antigenic peptide sequence was NH_2-CLYSKYYSDSDDELTVEQRRQS-COOH (>80% purity)(Pepceuticals).

2.3.6.1 Coupling peptides to resin for affinity purification

Peptide was coupled covalently to resin in order to affinity purify the antigenic serum. All steps were carried out in a 5 ml poly-prep chromatography column (Biorad). 5 ml of Affigel-10 resin was washed and then activated with 5% v/v ethylene diamine (Sigma) in ddH_2O to generate Amino-Affigel. Amino groups were then converted to iodoacetyl groups via the addition of 7 mg IAA-NHS ester (Sigma) per ml of resin. Resin was washed thoroughly using 0.1 M sodium phosphate buffer (pH 7.8) before 5 mg of peptide (dissolved in DMSO at 100 mg/ml) was added to the resin and mixed gently overnight at 4°C. Residual iodoacetate groups were blocked by the addition of 0.2 % v/v β-mercaptoethanol. Resin was then consecutively washed with 0.1 M $NaHCO_3$, 1 M Na_2CO_3, ddH_2O, 0.2 M glycine-HCl (pH 2.0) and TBS in order to remove non-covalently bound peptide. Resin was re-equilibrated and stored in TBS + 0.1% w/v NaN_3.

2.3.6.1 Purification of anti-peptide antibody

Serum was diluted 1:1 with TBS and filtered through a 0.2 μm non-cellulose filter (Sartorius Stedim). Diluted serum was then loaded 10 times over the column and then washed with TBS. Column was washed 10 times with 0.5 M NaCl, 20 mM Tris-HCl (pH 7.4) and 0.2% v/v Triton-X100 before a further wash with TBS. Antibody was eluted from the column using a low pH buffer consisting of 0.15 M NaCl, 0.2 M Glycine-HCl (pH 2.0). 500 μL fractions were collected into eppendorf tubes containing 0.1 mL of 2 M Tris-HCl (pH 8.5). Column pH was re-equilibrated with a TBS wash and stored in TBS + 0.1% w/v NaN_3. Individual fractions were spotted onto nitrocellulose and protein content was visualised with Ponceau S. Protein containing fractions were pooled and

dialysed into TBS overnight. NaN_3 concentration was bought up to 0.1% v/v and antibodies were stored at either 4°C or -20°C in 50% v/v glycerol.

2.3.7 Generation of Bod1L pS1145 and pS1710 antibodies

2.3.7.1 Design of phospho-peptide

To maximise the likelihood of generating a successful antibody, peptides were designed with an overall net charge of -2 (https://www.genscript.com/ssl-bin/site2/peptide_calculation.cgi - accessed 09/14). A surface accessibility plot was generated to ensure that the modified pS residue was likely to be exposed. As figure 2.1 shows, the pS residue is exposed in both peptides.

The antigenic phospho-peptide sequence for the pS1145 site was NH_2-CDNRNNN[pS]QQDID-COOH. The antigenic phospho-peptide sequence for the pS1710 site was NH_2-CEEVDG[pS]QGNMMR-COOH.

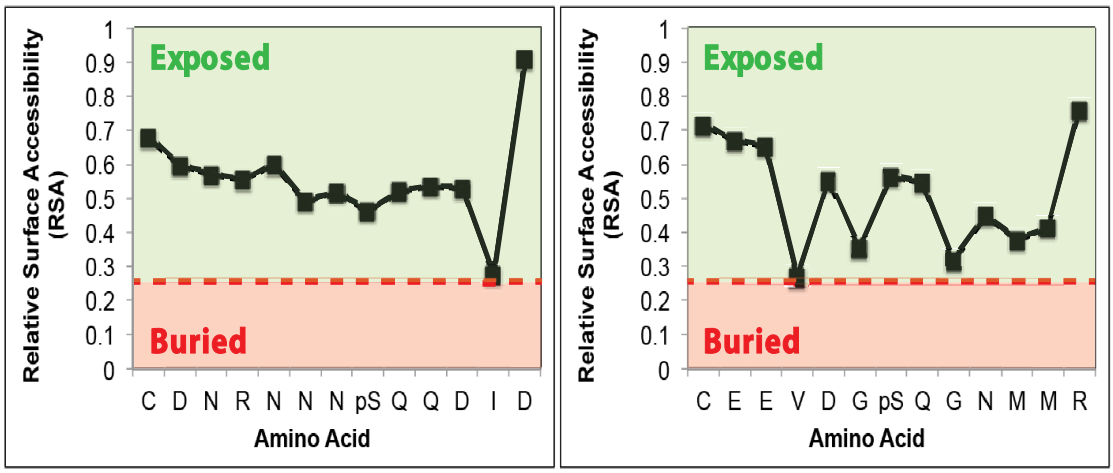

Figure 2.1 Surface accessibility plot for Bod1L phospho-peptide

Relative Surface Accessibility (RSA) was calculated using NetSurfP1.1. Residues (Petersen *et al.*, 2009). Individual amino acids were classified as exposed or buried based on the cut-off value assigned by the algorithm.

2.3.7.2 Thiol coupling of phospho-peptides to KLH

In order to generate the maximum possible antigenic effect in the sheep, the phospho-peptides were coupled with Keyhole Limpet Haemocyanin (KLH)(Millipore). Two sheep were used per phospho-peptide to limit any possible sheep-to-sheep variation in the immune response to the peptides. For the four injections needed to immunise the sheep, 100 mg of KLH was dissolved in 2 mL ddH_2O and dialysed overnight in 0.1 M sodium phosphate (pH 7.8). After dialysis, aggregates were removed from the solution by centrifugation. KLH-solution was warmed to room temperature and 1/9th volume 100 mg/mL IAA-NHS in DMSO was added. In dark, 4°C conditions, the solution was loaded into a large gel-filtration column containing Bio-Gel P-10 resin (Biorad) and equilibrated with 0.1 M sodium phosphate (pH 7.8). The KLH containing fractions (greyish-green colour) were pooled and 10 mg phospho-peptide was added and incubated for 8 hours at 4°C with gentle rotation. pH was checked and adjusted to 7.2-7.8 if necessary. KLH coupled peptide was diluted to 5 ml (final concentration 2 mg/mL) with 0.15 M NaCl, aliquoted and frozen ready for immunisation.

2.3.7.3 Immunisation protocol in sheep

As mentioned previously, two sheep were immunised per phospho-peptide to limit any possible sheep-to-sheep variation in the immune response to the peptides. The sheep were immunised with the KLH-peptide four times in total, and three bleeds were taken according to the immunisation schedule shown in table 2.2.

Procedure	Initial Immunisation	Booster Injection	Bleed 1	Booster Injection	Bleed 2	Booster Injection	Bleed 3
Day	0	28	35	56	63	84	91

Table 2.2 Immunisation schedule for Bod1L phospho-antibody generation

Immunisation and bleeds were carried out by the Scottish National Blood Transfusion Service (Midlothian, Scotland). Terminal bleeds on sheep were not performed.

Sera collected from each donation were run on a western blot on control samples and samples depleted of Bod1L by siRNA to assess whether a band could be identified. The strongest band was seen in the third bleed for each sheep and as such this sera was used for further affinity purification.

2.3.7.4 Coupling of phospho-peptides and non-phospho-peptides to resin for affinity purification

To generate Bod1L phospho-antibodies, HiTrap NHS activated HP columns (GE Healthcare) were used to affinity purify the sera. To prepare the columns for affinity purification, columns were first washed with 6 mL ice-cold 1 mM HCl before 1 mL peptide-containing solution was loaded into column. Peptide-containing solution consisted of 5 mg peptide in 1 mL coupling buffer (0.1 M $NaHCO_3$, 0.5 M NaCl (pH 8.3)). Column containing peptide was incubated at room temperature for 60 minutes. Un-reacted NHS groups were then blocked by washing column with 10 mL blocking buffer (0.5 M ethanolamine, 0.5 M NaCl (pH 8.3)). Column was then incubated for 30 minutes at room temperature in blocking buffer. Column was consecutively washed with 10 mL of 10 mM Tris-HCl (pH 8.0), 10 mL of 0.1 M glycine (pH 2.0), 10 mL of 10 mM Tris-HCl (pH 8.0) and 10 mL of 0.1 M triethylamine (pH 11.5). Washes were repeated before column was washed with 30 mL PBS. Column was stored at 4°C in a storage buffer containing 0.05 M Na_2HPO_4 and 0.1% w/v NaN_3 (pH 7.0).

2.3.7.5 Purification of phospho-antibody

Serum from each of the immunised sheep was purified on a column coupled with the non-phospho peptide, followed by a subsequent purification on a column coupled with the phospho-peptide. The non-phospho peptide column binds any antibodies that are specific to the epitope but not the phospho-epitope. The eluted antibodies from this column were designated as pan-specific and were used as an internal control. The column coupled with the phospho-specific peptide would therefore only bind the phospho-specific antibodies left in the serum, thus acting to enrich this pool of antibody in the eluate from the column.

Approximately 15 mL serum was diluted 1:1 with 2 X PBS and filtered through a 0.2 μm non-cellulose filter. Serum solution was re-circulated through the column using a peristaltic pump overnight at 4°C. Column was washed with approximately 50 mL wash buffer (0.5 M NaCl, 0.1% v/v Triton-X100 in PBS) until no protein could be detected in the flow through by Bradford assay. Column was then washed with 50 mL PBS. Antibody was eluted using 0.1 M glycine (pH 2.6), collecting 1 mL of eluate into eppendorfs containing 100 μL 2M Tris-HCl (pH 8.5). Column was washed with 50 mL of 10 mM Tris-HCl (pH 8.0), followed by 50 mL PBS before being stored at 4°C in a storage buffer containing 0.05 M Na_2HPO_4 and 0.1% w/v NaN_3 (pH 7.0).

Individual eluates were spotted onto nitrocellulose and protein content was visualised with Ponceau S. Protein containing fractions were pooled and dialysed into PBS overnight. NaN_3 concentration was bought up to 0.1% v/v and antibodies were stored at either 4°C or -20°C in 50% v/v glycerol.

2.3.8 In vitro kinase assays

2.3.8.1 GFP-MDC1 in vitro ATM kinase assay

ATM was immunoprecipitated with anti-ATM antibody (Abcam ab78) from cells dosed with 5 Gy IR and allowed to recover for 60 minutes. Cells were lysed in lysis buffer containing 20 mM Tris Acetate (pH 7.5), 1 mM EGTA, 1 mM EDTA, 10 mM Na-β-glycerophosphate, 5 mM Na-pyrophosphate, 1 mM Na-orthovanadate, 50 mM NaF, 1 mM microcystin, 0.27 M sucrose and 1 % v/v Triton-X-100. Immunoprecipitates were washed three times with lysis buffer and three times with a kinase buffer containing TADB (6.7 mM Tris–HCl (pH 7.5), 13 mM EGTA, 2 mM DTT), IB (10 mM Na_2HPO_4 (pH 7.4), 100 mM KCl, 1 mM $MgCl_2$) and magnesium/ATP cocktail (27.5 mM $MgCl_2$, 0.183 mM ATP, 4 mM 3-(N-morpholino) propanesulfonic acid (pH 7.2), 9.17 mM β-glycerolphosphate, 1.83 mM EGTA, 0.37 mM sodium orthovanadate, 0.37 mM DTT). Immunoprecipitated ATM was combined with GFP-MDC1 purified using GFP-trap protocol outlined in section 2.3.5 and incubated at 30°C for 45 minutes. Kinase reactions were stopped with SDS−PAGE loading dye and reaction mixtures were separated by SDS−PAGE. Transferred ATM and substrates were visualised using anti phospho-ATM (S9181), anti-phospho MDC1 (T4) and anti-MDC1 antibodies.

2.3.8.2 Bod1L-T in vitro DNA-PK kinase assay

Purified DNA-PKcs, Ku70/80 and Calf-thymus DNA was a kind gift from the Lees-Miller lab (Calgary, Canada). *In vitro* kinase assays were carried out as described (Yu et al., 2003). In short, purified DNA-PKcs (30 ng) and Ku70/80 (10 ng) were incubated in 20 μL of kinase buffer containing 50 mM Tris–HCl (pH 8.0), 10 mM $MgCl_2$, 1 mM DTT, 0.2 mM EGTA, 0.1 mM EDTA, 10 μg/ml sonicated calf thymus DNA, and 300 ng GST-Bod1L-T or 300 ng GST-Bod1L-

T^{S1710A} and incubated for 45 minutes at 30°C. Kinase reactions were stopped with SDS−PAGE loading dye and reaction mixtures were separated by SDS−PAGE. Transferred substrates were visualised using anti phospho-Bod1L (S1710A), anti-GST and anti-KU80 antibodies.

2.3.9 In vitro GFP-MDC1 phosphatase assay

Phosphatase assay was performed as described in (Porter et al., 2013). In brief, PP2A-B56δ-GFP was immunoprecipitated from RPE1 cells stably expressing the PP2A-B56δ-GFP construct (Foley et al., 2011). Beads were washed with a stringent wash buffer (300 mM NaCl, 1% v/v NP-40). GFP-MDC1 was immunoprecipitated from U2OS cells stably expressing GFP-MDC1, treated with 10 μM etoposide for 16 hours. GFP-MDC1 and PP2A-B56δ-GFP were mixed and resuspended in PPase reaction buffer +/- 2 nM Okadaic acid (50 mM HEPES, 1 mM dithiothreitol (DTT), 1 mM EDTA and 0.1% v/v NP40). Samples were incubated for 45 minutes at 30°C before run on SDS-PAGE gel and probed with anti-phospho MDC1 (T4), anti-GFP and anti-PP2A-C antibodies.

2.4 Imaging

2.4.1 Fixative preparation

2.4.1.1 3.7% w/v Paraformaldehyde (PFA)

10 μL 10M KOH (Sigma) was added to 3.5 mL ddH_2O. To this, 1.85 g of paraformaldehyde was added and agitated in a water bath set to 90°C for 5 minutes. After solution had cleared, it was passed through a 0.2 μm filter (Millipore) and 10 μL 10M HCl was added to neutralise pH. Solution was made up to 45 mL with ddH_2O to generate a paraformaldehyde solution with a final

concentration of 3.7% w/v. PFA solution was warmed to 37°C and used immediately.

2.4.1.2 70% v/v EtOH

Absolute ethanol (VWR) was diluted with ddH_2O until a concentration of 70% v/v was achieved. 70% EtoH was stored at -20°C until immediately before use, at which point it was transferred to a container containing dry-ice to keep temperature of ethanol solution low.

2.4.2 Immunofluorescence

2.4.2.1 Standard immunofluorescence staining

Cells were seeded onto borosilicate glass cover slips, thickness 1.5 (VWR). Once desired confluence was reached, media was aspirated and cells were fixed in 3.7% v/v PFA for 7 minutes at 37°C at 5% CO_2 in a humidified incubator. Fixative was aspirated and cells were briefly washed in PBS-T before incubation in PBS-T for 5 minutes at 37°C at 5% CO_2 in a humidified incubator. An additional 5-minute incubation in PBS-T was carried out at room temperature before coverslips were blocked with 1% v/v normal donkey serum (Sigma) in AbDil for 1 hour at room temperature or overnight at 4°C. Coverslips were washed once in TBS-T before primary antibody was added for 1 hour at room temperature diluted in AbDil. Details of antibody dilution can be found in table 2.3. Coverslips were gently washed twice in TBS-T, before the corresponding-species fluorescently labelled secondary antibody diluted 1:150 in AbDil (Jackon ImmunoResearch) was added for 1 hour. Coverslips were washed twice in TBS-T and then twice in TBS before 4',6-diamidino-2-phenylindole (DAPI)(Sigma) was added to coverslips at a final concentration of

1 μg/mL in TBS for 5 minutes. Cells were washed twice in TBS before mounting onto microscope slides (VWR) with mounting medium. Coverslip edges were sealed with nail-varnish and stored at -20°C in the dark.

2.4.2.2 Chromosome spreads

Cells were seeded onto borosilicate glass cover slips, thickness 1.5 and grown to desired confluence. 14 hours prior to fixation, nocodazole (CalBioChem) was added to a final concentration of 100 ng/mL. After incubation with nocodazole, cells were swollen in swelling media for 20 minutes at room temperature (40% fresh cell culture media, 60% ddH_2O passed through 0.45 μm filter (Millipore) and 100 ng/mL nocodazole). Coverslips were then centrifuged at 2,400 r.c.f. for 4 minutes on blotting paper (GE Healthcare) to spread the chromosomes. Standard immunofluorescence staining was then carried out.

2.4.3 Image acquisition

2.4.3.1 Fixed wide-field microscopy

Three-dimensional wide-field image data sets were primarily acquired using a DeltaVision Elite imaging system (GE Healthcare) equipped with an Olympus IX71 inverted microscope with high precision stage, and light delivery optics. Microscope was fitted with solid-state illumination source and CoolSNAP HQ2 CCD camera. In addition, microscope was fitted with a Quantifiable Laser Module (QLM) and environmental chamber for live-cell photo-manipulation. Depending on application, imaging was carried out using a 100X/1.4NA Plan-Apochromat oil immersion objective, 60X/1.42NA Plan-Apochromat oil immersion objective, 40X/0.6NA Plan Fluor objective or a 40X/1.2NA Plan-Apochromat oil immersion objective.

Image data sets were acquired in a single sitting and Z-stacks were collected using Nyquist sampling. Images were deconvolved using softWoRx software (GE Healthcare).

2.4.3.2 Live cell microscopy

For live cell microscopy, cells were seeded into glass bottom LabTek imaging dishes (Thermo) and incubated until desired cell confluence was reached. Once desired confluence was reached, media was aspirated and cells were washed with PBS at 37°C. L-15 media (Lonza) with 10% v/v FBS was added to cells and dish was moved to pre-warmed environmental chamber of microscope. Cells were imaged as described above, with care taken to minimise exposure times and prevent temperature fluctuations.

2.4.3.3 Laser stripe damage

To generate laser micro-irradiation stripes, cells were seeded into glass bottom LabTek imaging dishes (Thermo) and incubated until approximately 60% confluent. Media was aspirated and cells were washed with PBS at 37°C. L-15 media (Lonza) with 10% v/v FBS and 0.5 μg/ml Hoechst 33342 (Sigma) was added to cells and dish was incubated for 30 minutes at 37°C at 5% CO_2 in a humidified incubator. Cells were moved to pre-warmed environmental chamber of microscope. Laser micro-irradiation stripes were generated using a 60X/1.42NA oil immersion objective using a 30 mW 406 nm laser at 20% power with exposure time of 0.1 seconds. Striped cells were either imaged as described above or incubated for 30 minutes post before being fixed and immuno-stained.

2.4.3.4 Fluorescence Recovery After Photobleaching (FRAP)

Cells were prepared for live cell imaging as described previously. For FRAP experiments the microscope was set-up to acquire 3 pre-FRAP images and 32 post images using adaptive timing. Expected half-life was optimised for each experimental condition, total imaging ranged between 2-20 minutes. FRAP of GFP fusion proteins was performed using 60X/1.42NA oil immersion objective, 1 second 50 mW 488 nm laser exposure at 100% power. FRAP of RFP/mCherry fusion proteins was performed using 60X/1.42NA oil immersion objective, 2 second 50 mW 532 nm laser exposure at 100% power.

2.4.3.5 Förster Resonance Energy Transfer (FRET)

Cells were prepared for live cell imaging as described above. Fusion proteins expression GFP and TagRFP-t were used as an acceptor Photobleaching FRET pair. Imaging was carried out using a Zeiss 710 confocal microscope fitted with an environmental chamber set to 37°C. Photobleaching was performed using 60X/1.42NA oil immersion objective, 1 second 20 mW 543 nm laser exposure at 100% power, which reduced TagRFP-t signal by 60-70% of maximum.

2.4.4 Flow cytometry

Cells were transfected with siRNA as described previously and then incubated in 10 μM Etoposide for 14 hours. Cells were harvested by trypsinisation and washed twice in PBS. Cells were transferred to FACS tubes (Greiner) and fixed in 1 mL ice-cold 70% v/v EtOH. Cells were transferred to -20°C for 24 hours. Cells were washed twice in PBS + 1% w/v Bovine Serum Albumin (BSA)(Sigma). Cells were then pelleted and re-suspended in 500 μL staining buffer and incubated at room temperature protected from light for 20 minutes.

Cells were analysed using a FACS Calibur (Becton Dickinson) and data was analysed using FlowJo software.

2.4.5 Data analysis

2.4.5.1 Image quantification

Images acquired using a DeltaVision Elite microscope were deconvolved in SoftWoRx software and imported into OMERO for processing (Allan et al., 2012). Regions of interest (ROI) were drawn around cells for processing using either the built-in software in OMERO or the “Box-It” tool of the OMERO.mtools suite. Using the ‘Intensity Measure’ tool in the OMERO.mtools suite, cells to be analysed were segmented using Otsu thresholding and a minimum object size was set. The fluorescence signal for multiple channels was measured within the segmented mask and background signal was determined using a 2-pixel annulus derived from a 1-pixel gap around the mask. Quantified fluorescence intensity was expressed as the summed fluorescence intensity for each channel within the mask, subtracting the product of the mask size and average background intensity calculated from the 2-pixel annulus.

2.4.5.2 Statistics

Statistical tests were performed using SigmaPlot 12 (Sysat Software Inc.) or SPSS statistics V22 (IBM). A Kolmogorov–Smirnov test was performed to determine the distribution of the dataset. For normally distributed data, a student t-test was performed. For non-parametric data sets, a Wilcoxon–Mann–Whitney test was used. Data was a p-value ≥0.05 was determined as non-significant. A p-value score of between 0.01 and 0.05 was determined as

significant (*), between 0.01 and 0.001 as very significant (**) and ≤0.001 as extremely significant (***).

2.4.6 Intra S-phase checkpoint assay

To determine the integrity of the intra S-phase checkpoint, HeLa cells were transfected with control, PP2A-B56, Bod1L or PP2A-B56 + Bod1L siRNA. After 48 hours, cells were irradiated with 0, 5 or 10 Gy and left to recover for 1 hour at 37°C. BrdU (Life Technologies) was added incubated for a further 1 hour. Cells were fixed in PFA and BrdU intensity was determined by microscopy.

2.5 Software and bioinformatics

DNA sequence analysis, cloning design and DNA sequencing data was all carried out using CLC workbench 6 (CLC Bio). Pair-wise alignments were carried out using EMBOSS Needle (EMBL-EBI) and multiple sequence alignments were undertaken using Clustal OMEGA (EMBL-EBI). Potential post-translational modifications on Bod1L were identified using ELM (Dinkel et al., 2013) and Phosphosite Plus (Cell Signalling). Wide-field microscopy images were deconvolved using SoftWoRx software (GE Healthcare). All microscopy images and metadata were imported and saved using OMERO. Analysis was carried out using OMERO and a MatLab-based plug-in for OMERO, OMERO.mtools (Michael Porter, University of Dundee). Statistical tests were performed using SigmaPlot 12 and SPSS V22. All figures and diagrams were generated using Photoshop CS5.1 (Adobe) and Illustrator CS5.1 (Adobe).

2.6 Buffers, Reagents and Chemicals

2.6.1 Chemicals and Reagents

Unless otherwise stated, all chemical compounds were dissolved in DMSO (Sigma) to a stock concentration of between 100 μM – 10 mM. Etoposide (Sigma) was stored at a stock concentration of 10 mM used at a working concentration of 10 μM for 16 hours. Monastrol (Tocris) or S-trityl-L-cysteine (STLC)(Enzo Life Sciences) were used to induce mitotic arrest overnight at a concentration of 100 nM or 5 μM respectively. Nocodazole (CalBioChem) was stored at a stock concentration of 1 mM and used at a concentration of 100 ng/mL for 12 hours. MG132 (CalBioChem) was stored at a stock concentration of 10 mM and used at a final concentration of 10 μM for 1 hour. KU59933 (Selleck) was stored at a stock concentration of 10 mM and used at a working concentration of 10 μM for 1 hour. Cisplatin (Sigma), Mitomycin C (in EtOH)(SantaCruz), Camptothecin (Donated by Rouse group, University of Dundee) and 6-Thioguanine (Sigma) were all used at the concentration ranges indicated for clonogenic survival assays.

Dithiothreitol (DTT)(Sigma) was made at a stock concentration of 1 M, aliquoted and stored at -20°C. DTT was used at a final concentration of 1 mM Microcystin-LR (Carol McIntosh, University of Dundee) was stored at -80°C at a stock concentration of 1 mM and used at a final concentration of 1 μM. Phenylmethanesulfonylfluoride (PMSF)(Thermo) was stored at a stock concentration of 0.2 M at -20°C in 100% EtOH and used at a final concentration of 0.1 μM.

For bacterial growth, Ampicillin was added to LB and LB-agar at a final concentration of 100 μg/mL. Kanamycin was added to LB and LB-agar at a final concentration of 50 μg/mL. Chloramphenicol was added to LB and LB-agar at a final concentration of 100 μg/mL. Isopropyl β - D - 1 - thiogalactopyranoside (IPTG)(Sigma) was used for protein expression induction at a final concentration of 0.1 mM. LPC was prepared by combining a 10 mg/mL solution of leupeptin, pepstatin and Aprotinin (Sigma) in DMSO. LPC solution was aliquoted and stored at -20°C and used at a final concentration of 10 μg/mL.

Tissue culture medium antibiotics were added at the final concentrations indicated in table 2.1. G-418 (SelleckChem) was stored at a stock concentration of 100 mg/mL at 4°C for no longer than 1 month. Puromycin (Life Technologies) was stored at a stock concentration of 1 mg/mL and stored at -20°C.

2.6.2 Buffers

Antibody Dilution Buffer (AbDil)

0.25% v/v Tween-20 (VWR), 2% w/v BSA (Sigma), 0.1% w/v NaN_3 (Sigma) in 1 X TBS

Electrophoresis loading buffer

1 X LDS NuPAGE sample buffer (Life Technologies) diluted in ddH_2O, supplemented with 5% v/v β-mercaptoethanol (Sigma).

Flow cytometry staining buffer

50 μg/mL Propidium Iodide (PI)(Sigma), 50 μg/mL ribonuclease A (RNase A)(Sigma), 1% w/v BSA in 1 X PBS.

Fractionation buffer A

10 mM HEPES (pH7.9)(Sigma), 10 mM KCl (Sigma), 1.5 mM $MgCl_2$ (Sigma), 1 mM DTT, 10 μg/mL LPC, 0.1 mM PMSF, 0.34 M sucrose (VWR), 10% v/v Glycerol (VWR), 0.1% v/v Triton X-100 in 1 X PBS.

Fractionation buffer A+

10 mM HEPES (pH7.9)(Sigma), 10 mM KCl (Sigma), 1.5 mM $MgCl_2$ (Sigma), 1 mM DTT, 10 μg/mL LPC, 0.1 mM PMSF, 0.34 M sucrose (VWR), 10% v/v Glycerol (VWR), 0.1% v/v Triton X-100, ~ 50 U benzonase nuclease (Thermo), 1 mM $CaCl_2$ in 1 X PBS.

Fractionation buffer B

3 mM EDTA (Sigma), 0.2 mM EGTA (Sigma), 1 mM DTT, 10 μg/mL LPC in 1 X PBS.

IP wash buffer

20 mM Tris-HCl (pH7.4), 200 mM NaCl, 1 mM EGTA, 0.1% v/v Triton X-100 in 1 X PBS

Laemmli buffer (10 X stock)

250 mM Tris-Base (Sigma), 2 M Glycine (Sigma) in ddH_2O.

LB (Luria-Bertani) liquid medium (ordered in-house)

10 g/L Tryptone, 10 g/L NaCl, 5g/L Yeast extract in ddH_2O

LB Agar (ordered in-house)

20 g/L Agar, 10 g/L Tryptone, 10 g/L NaCl, 5g/L Yeast extract in ddH_2O

10 X DNA Loading dye

25% v/v Ficoll-PM400 (Sigma), 100 mM Tris-HCl (pH 7.4), 100 mM EDTA, ~ 1 mg Bromophenol blue (SantaCruz) in ddH_2O.

Mounting medium

0.5 % w/v p-Phenylenediamine (Sigma), 20 mM Tris-HCl (pH8.8), 90% v/v glycerol in ddH_2O and stored at -80°C protected from light.

1 X Phosphate-buffered saline (PBS)

137 mM NaCl, 2.7 mM KCl, 10 mM Na_2HPO_4 (Sigma), 1.8 mM KH_2PO_4 (Sigma) in ddH_2O.

PBS-Triton X-100 (PBS-T)

137 mM NaCl, 2.7 mM KCl, 10 mM Na_2HPO_4, 1.8 mM KH_2PO_4, 0.1% v/v Triton X-100 in ddH_2O.

Radioimmunoprecipitation assay buffer (RIPA)

1% v/v Triton X-100, 0.1% w/v SDS (Sigma), 50 mM Tris HCl (pH 7.4), 150 mM NaCl, 0.5% Sodium Deoxycholate (Sigma), 1 mM EDTA, 1 mM Microcystein-LR (Carol McIntosh, University of Dundee), 1% v/v β-mercaptoethanol, 10 μg/mL LPC in ddH_2O.

SDS-PAGE loading buffer

1 X LDS buffer (Life Technologies)(Consists of: 106 mM Tris-HCl, 141 mM Tris Base, 2% w/v LDS, 10% Glycerol, 0.51 mM EDTA, 0.22 mM SERVA Blue G250, 0.175 mM Phenol Red), 5% v/v β-mercaptoethanol in ddH_2O.

SDS-PAGE MOPS running buffer

50 mM MOPS (Life Technologies), 50 mM Tris Base, 0.1% w/v SDS, 1 mM EDTA in ddH_2O. Buffer adjusted to pH 7.7 and stored at room temperature.

SDS-PAGE Tris-Acetate running buffer

50 mM Tricine (Life Technologies), 50 mM Tris Base, 0.1% w/v SDS in ddH_2O. Buffer adjusted to pH 8.24 and stored at 4°C.

TAE (50 X stock solution)

2.5 M Tris-Acetate, 50 mM EDTA in ddH_2O.

Tris-buffered saline (TBS)

150 mM NaCl, 50 mM Tris-HCl (pH 7.4) in ddH_2O.

TBS-Triton X-100 (TBS-T)

150 mM NaCl, 50 mM Tris-HCl (pH 7.4), 0.1% v/v Triton X-100 in ddH_2O.

TBS-Tween20

150 mM NaCl, 50 mM Tris-HCl (pH 7.4), 0.1% v/v Tween-20 in ddH_2O.

Tris-EDTA (TE) Buffer

10 mM Tris-HCl (pH 8.0), 1 mM EDTA in ddH_2O.

Thrombin cleavage buffer

50 mM Tris-HCl (pH 8.0), 10 mM $CaCl_2$ in ddH_2O.

Thrombin storage buffer

20 mM Tris-HCl (pH8.0), 50% v/v Glycerol in ddH_2O.

Transfer buffer

1 X NuPAGE transfer buffer (Life Technologies), 10% v/v Methanol (VWR) in ddH_2O.

Western blot stripping buffer (Adapted from (Yeung and Stanley, 2009))

6 M GnHCl (Sigma), 0.2% v/v IGEPAL CA630 (NP40)(Sigma), 20 mM Tris-HCl (pH 7.5) in ddH_2O. Stored at room temperature and used for up to one month.

2.7 Antibodies, Primers, DNA constructs and siRNA

2.7.1 Antibodies

Antibodies were aliquoted and stored according to manufacturers instruction at either 4°C, -20°C or -80°C in TBS containing 0.1% w/v Na-Azide. Antibodies generated in the lab were stored at various temperatures and then tested for affinity to determine storage conditions.

Table 2.3 Immunoblotting and immunostaining antibodies

Protein Target	Species	Manufacturer	WB dilution	IF dilution
MDC1	Mouse	Abcam	1:200	1:200
Bod1L	Rabbit	Generated by Swedlow Lab	1:250	-
pBod1L (S1710)	Goat	Generated by Swedlow Lab	1:250 (+1:50 non-phospho peptide)	1:250 (+1:50 non-phospho peptide)
pBod1L (S1145)	Goat	Generated by Swedlow Lab	1:250 (+1:50 non-phospho peptide)	1:250 (+1:50 non-phospho peptide)
MDC1	Rabbit	Bethyl	1:1000	1:500
pChk2 (T68)	Rabbit	Abcam	1:500	-
Rad51	Rabbit	SantaCruz	-	1:500
pMDC1 (S329/T331)	Rabbit	Gift from Steve Jackson, Cambridge	1:500	1:500
pMDC1 (T4)	Rabbit	Abcam	1:500	1:500
Phospho-(Ser/Thr) ATM/ATR Substrate Antibody	Rabbit	Cell Signalling	1:500	-
gamma-H2AX (S139)	Rabbit	Millipore	1:1000	1:500
GFP	Mouse	Roche	1:1000	1:1000
Anti-Centromere Auto-antisera (ACA)	Human	Gift from Sara Marshall, Dundee	-	1:1000
Histone-H3	Rabbit	Cell Signalling	1:1000	-
FANCD2	Rabbit	Abcam	1:1000	-
ATM	Mouse	Abcam	1:1000	-
NBS1	Rabbit	Abcam	1:1000	-
PP2A-B56 (B')	Rabbit	Millipore	1:1000	-
pCDC25A (S124)	Rabbit	Abcam	1:500	-
pATM (S1981)	Rabbit	Abcam	1:2000	1:2000
Chk2	Rabbit	Abcam	1:5000	-
GAPDH	Mouse	Abcam	1:10000	-
Vinculin	Mouse	Sigma	1:20000	-
Anti-Mouse HRP	Donkey	GE Healthcare	1:10000	
Anti-Rabbit HRP	Donkey	Cell Signalling	1:5000	
Anti-Sheep HRP	Donkey	Sigma	1:2500	
Anti-Mouse FITC/TRITC/Cy5	Donkey	Jackson ImmunoResearch	-	1:150
Anti-Rabbit FITC/TRITC/Cy5	Donkey	Jackson ImmunoResearch	-	1:150
Anti-Human FITC/TRITC/Cy5	Donkey	Jackson ImmunoResearch	-	1:150
Anti-Goat FITC/TRITC/Cy5	Donkey	Jackson ImmunoResearch	-	1:150

2.7.2 Primer sequences

The following primers were used during this study. All primers were made up to a stock concentration of 100 μmole in TE buffer and stored at -20°C.

Table 2.4 Primer sequences

Primer Name	Manufacturer	Sequence (5' to 3')	Notes
Bod1L_seq_nt408	Invitrogen #E6055F07	TCA GGT TGT GGA CCC AAA G	Bod1L gene forward sequencing primer
Bod1L_seq_nt496	Invitrogen #E6055F02	CTT TGT GAT TTA GCG TGG CC	Bod1L gene reverse sequencing primer
Bod1L_seq_nt1193	Invitrogen #E6055F08	CTG ATG TGG ATG GAC TTA CAG	Bod1L gene forward sequencing primer
Bod1L_seq_nt1999	Invitrogen #E6055F09	GTA CAG GAA GAG ACT GAC AC	Bod1L gene forward sequencing primer
Bod1L_seq_nt2821	Invitrogen #E6055F10	CCA GAC AAG GAG AAG AAC ACA G	Bod1L gene forward sequencing primer
Bod1L_seq_nt3451	Invitrogen #E6055F11	TAT AAG CCA GGC CGT GGA AC	Bod1L gene forward sequencing primer
Bod1L_seq_nt4293	Invitrogen #E6055F12	GAA TGG CAA GAA GGA TGG C	Bod1L gene forward sequencing primer
Bod1L_seq_nt5106	Invitrogen #E6055G01	AAG CAG TGA AGA GGT GGA TG	Bod1L gene forward sequencing primer
Bod1L_seq_nt5898	Invitrogen #E6055G02	TGA AGT GAC ACC AGT TCC AG	Bod1L gene forward sequencing primer
Bod1L_seq_nt6759	Invitrogen #E6055F03	TGG CAT CAT CTC TAC GAG C	Bod1L gene forward sequencing primer
Bod1L_seq_nt7491	Invitrogen #E6055F04	GAA TGC TAA CTC ACC TGC C	Bod1L gene forward sequencing primer
Bod1L_seq_nt8250	Invitrogen #E6055F05	CGG TCA CAG TGT TGA AGC AG	Bod1L gene forward sequencing primer
Bod1L_seq_nt9012	Invitrogen #E6055F06	ATC CAC CAC CAG ATC AGA G	Bod1L gene forward sequencing primer
Bod1L_Frag1_seq_rev	In house #69124	CTG TGT TGC CAC TTC CTT	Bod1L_Frag1 reverse sequencing primer
TagRFP-t_Seq_End_fwd	Invitrogen #M5015A08	CTG GGG CAC AAA CTT AAT GG	TagRFP-t forward sequencing primer
TagRFP-t_Seq_End_rev	Invitrogen #E2252B01	GAC GTA GGT CTC TTT GTC G	TagRFP-t reverse sequencing primer
pCMV5 Fwd	Dundee DNA sequencing service	CGC AAA TGG GCG GTA GGC GTG	CMV forward sequencing primer
pCMV5 Rev	Dundee DNA sequencing service	CCT CCA CCC CAT AAT ATT ATA GAA GGA CAC	CMV reverse sequencing primer
CMV_seq_fwd	In house #69125	TGG CAT TAT GCC CAG TAC	CMV forward sequencing primer
pEGFP-N1	Dundee DNA sequencing service	CATGGTCCTGCTGGAGTTCGTGAC	eGFP forward sequencing primer
pEGFP-N1R	Dundee DNA sequencing service	GGC CGT TTA CGT CGC CGT CC	eGFP reverse sequencing primer
pmCherry-C1-Fwd	Dundee DNA sequencing service	GTT GGA CAT CAC CTC CCA CAA CGA G	mCherry forward sequencing primer
pmCherry-N1-Rev	Dundee DNA sequencing service	GGG CGG CCC TCG CCC TCG CCC TCG	mCherry reverse sequencing primer
MBP seq fwd	Invitrogen #E6040F03	GAT GAA GCC CTG AAA GAC GCG CAG	MBP forward sequencing primer
eGFP_fwd_XhoI	Invitrogen #E9793F08	ATA CTC GAG ATG GTG AGC AAG GGC	PCR of eGFP for Bod1L-GFP
eGFP_rev_SacII	Invitrogen #E9793F09	CGA TAC CGC GGT TAC TTG TAC AGC TC	PCR of eGFP for Bod1L-GFP
TagRFP-T_fwd_XhoI	Invitrogen #M2721G11	ATA CTC GAG ATG GTG TCT AAG GGC G	PCR of TagRFP-t for Bod1L-TagRFP-t
TagRFP-T_rev_SacII	Invitrogen #M2721G12	ATA CCG CGG TTA CTT GTA CAG CTC G	PCR of TagRFP-t for Bod1L-TagRFP-t
TagRFP-t_Seq_End_fwd	Invitrogen #M5015A08	CTG GGG CAC AAA CTT AAT GG	PCR of TagRFP-T for TagRFP-t-Bod1L
Bod1L_Frag_1_fwd_new	Invitrogen #M0034E09	CAG AGC TCG TTT AGT GAA CCG TCA G	PCR of Bod1L-N
Bod1L_Frag_1_rev_new	Invitrogen #M0034E10	AAA CCG CGG GGA AGT GGA GTC TTT ATC ACT CTT A	PCR of Bod1L-N
Bod1L_Frag_2_fwd_new	Invitrogen #M0144F03	GCA AGA TCT ATG TCC ACT TCC ACC AGG CTT GAG AGA AAG	PCR of Bod1L-T
Bod1L_Frag_2_rev_new	Invitrogen #M0144F04	GCA CCG CGG TAC AGA GGT GAT GAT GTC CTC A	PCR of Bod1L-T
Bod1L_Frag_3_fwd	Invitrogen #E8891D04	GCA AGA TCT ATG GGC CTG GTC GGG GGT AGT TAC GAT	PCR of Bod1L-C
Bod1L_Frag_3_rev	Invitrogen #E8891D05	GCA CCG CGG TCG CTT CGC TTT TTT CAC AG	PCR of Bod1L-C

Bod1L_2769_3020_fwd	Sigma #HA05524785	GGG CTG GAG CAG GTC CTA AAA GAA AAA GAA AGC AGC ATT ATC TCG CTG GAC CTT CTA TCA AGC GCA AGA GAG AAG TCA GCG CAG GTG CGG CCG CTG CTG GAG CG	Insert for 2769_3020 NLS
Bod1L_2769_3020_rev	Sigma #HA05524786	GAT CCG CTC CAG CAG CGG CCG CAC CTG CGC TGA CTT CTC TCT TGC GCT TGA TAG AAG GTC CAG CGA GAT AAT GCT GCT TTC TTT TTC TTT TAG GAC CTG CTC CAG CCC GC	Insert for 2769_3020 NLS
LacI_Bod1L_insert_fwd	Invitrogen #Q1276G07	GGC CGC GCT GCT AGA TCT GCT GCT CTC GAG ATA AGC TCT GCA	PCR of Bod1L into LacI-GFP vector
LacI_Bod1L_insert_rev	Invitrogen #Q1276G08	GAG CTT ATC TCG AGA GCA GCA GAT CTA GCA GCG C	PCR of Bod1L into LacI-GFP vector
LacI_Frag1_fwd	Invitrogen #Q7805A09	GAA TTC GTC GAC TGG ATC CGG TAC CGA GGA G	PCR of Bod1L-N into LacI Vector
LacI_Frag1_rev	Invitrogen #Q7805A10	CAA CTT TCT CTC AAG CCT GGT GGA AGT GGA	PCR of Bod1L-N into LacI Vector
LacI_Frag2_fwd	Invitrogen #Q7805A11	TCC ACT TCC ACC AGG CTT GAG AGA AAG TTG	PCR of Bod1L-T into LacI vector
LacI_Frag2_rev	Invitrogen #Q7805A12	AAG AAC ATC GTA ACT ACC CCC GAC CAG GCC	PCR of Bod1L-T into LacI vector
LacI_Frag3_fwd	Invitrogen #Q7805B01	GGC CTG GTC GGG GGT AGT TAC GAT GTT CTT	PCR of Bod1L-C into LacI vector
LacI_Frag3_rev	Invitrogen #Q7805B02	TCG CTT CGC TTT TTT CAC AGG GGC TTC CTC	PCR of Bod1L-C into LacI vector
Bod1L_S1145E_fwd	Invitrogen #Q8633B12	CAA TAA TAA TGA GCA GCA AGA CAT TGA CTC	Bod1L S1145A mutation primer
Bod1L_S1145E_rev	Invitrogen #Q8633B10	CGG TTG TCT TGG GTT TTA G	Bod1L S1145A mutation primer
Bod1L_S1710E_fwd	Invitrogen #Q8633C01	GGT GGA TGG CGA GCA GGG AAA TAT G	Bod1L S1710A mutation primer
Bod1L_S1710E_rev	Invitrogen #Q8633B11	TCT TCA CTG CTT ATA GAT CC	Bod1L S1710A mutation primer

2.7.3 DNA constructs

All DNA constructs were stored in TE buffer at -20°C at a concentration of between 200-1000 ng/μL.

Table 2.5 DNA constructs

Name	Description	Notes
Bod1L-GFP	Full length Bod1L, labelled at C-terminus with eGFP	Bod1L-tGFP purchased fom Origene (NM_148894). tGFP substituted for eGFP
GFP-Bod1L	Full length Bod1L, labelled at N-terminus with eGFP	-
Bod1L-TagRFPt	Full length Bod1L, labelled at C-terminus with TagRFP-t	-
TagRFPt-Bod1L	Full length Bod1L, labelled at N-terminus with TagRFP-t	-
Bod1L-N_2769_3020	Bod1L amino acid 1-1009, labelled at C-terminus with eGFP	-
Bod1L-T_2769_3020	Bod1L amino acid 1007-2038, labelled at C-terminus with eGFP	-
Bod1L-C_2769_3020	Bod1L amino acid 2002-3051, labelled at C-terminus with eGFP	-
LacI_GFP	LacI fused to eGFP with MCS intact	Gift from Saurin Group, Dundee
LacI_GFP_Bod1L	LacI_GFP fused to full length Bod1L	-
LacI_GFP_Bod1L-N	LacI_GFP fused to full length Bod1L-N	-
LacI_GFP_Bod1L-T	LacI_GFP fused to full length Bod1L-T	-
LacI_GFP_Bod1L-C	LacI_GFP fused to full length Bod1L-C	-
Bod1L-GFP_S1145A	Full length Bod1L with an S to A mutation at position 1145, labelled at C-terminus with eGFP	-
Bod1L-GFP_S1710A	Full length Bod1L with an S to A mutation at position 1710, labelled at C-terminus with eGFP	-
mCherry-MDC1	Full length MDC1, labelled at N-terminus with mCherry	Gift from Hay Group, Dundee
PP4C-GFP	Full length PP4C, labelled at C-terminus with eGFP	Purchased from DSTT (#DU19835), Dundee
H2B-RFP	Full-length Histone H2B labelled at C-terminus with RFP	Gift from M. Posch (Swedlow Group)
pCBASceI	I-SceI endonuclease expression vector with mammalian promoter to introduce a DSB at a genomic I-SceI site.	pCBASceI was a gift from Maria Jasin (Addgene plasmid # 26477)
Bod1L_T_GST_WT	Bod1L amino acid 1007-2038, labelled at C-terminus with GST	-
Bod1L_T_GST_^{S1710A}	Bod1L amino acid 1007-2038, labelled at C-terminus with GST with S1710A point mutation	-

2.8.4 siRNA sequences

A table containing details of siRNA used in this study is shown below. siRNA oligos were resuspended and stored in TE buffer at -20°C.

Table 2.6 siRNA sequences

Protein Target	Sense sequence	Manufacturer + Chemistry	Notes
Bod1L	5'-CAGUGCUGCUAGGGCUUCAACAGAA-3'	LifeTechnologies - Stealth	This siRNA was used throughout the study
Bod1L_Cterm	5'-CAUCUAGCAGCAAACUGAAAGUAAU-3'	LifeTechnologies - Stealth (HSS177930)	Used to assess on target activity
Bod1L_3'UTR	5'-UGGGAUUUCCCAAUGUGACACAUCA-3'	LifeTechnologies - Stealth	-
FANCD2	Unknown - Pool of 3-5 target-specific 19-25 nt siRNAs	SantaCruz (sc-35356)	-
PP4-Catalytic (PPP4C)	5'-GGCCAGAGAGAUCUUGGUAUU-3'	Dharmacon	(Chowdhury et al., 2008)
PP2A-B56α (PPP2R5A)	5'-GCUCAAAGAUGCCACUUCA-3'	Eurofins-MWG	(Foley et al., 2011)
PP2A-B56β (PPP2R5B)	5'-CGCAUGAUCUCAGUGAAUA-3'	Eurofins-MWG	(Foley et al., 2011)
PP2A-B56γ (PPP2R5C)	5'-GGAUUUGCCUUACCACUAA-3'	Eurofins-MWG	(Foley et al., 2011)
PP2A-B56δ (PPP2R5D)	5′-UCCAUGGACUGAUCUAUAA-3′	Eurofins-MWG	(Foley et al., 2011)
PP2A-B56ε (PPP2R5E)	5'-UUAAUGAACUGGUGGACUA-3'	Eurofins-MWG	(Foley et al., 2011)
Control	Stealth RNAi siRNA Control, Medium GC Content	LifeTechnologies - Stealth	-
BRCA2	5′-GAAACGGACUUGCUAUUUA-3′	Dharmacon	(Edwards et al., 2008)

Chapter 3 - Bod1L is required for a robust DNA damage response

This chapter seeks to explore the novel protein, Biorientation Of Chromosomes In Cell Division Protein 1-Like (Bod1L), a member of the same protein family as Bod1, the mitotic PP2A-B56 inhibitor (Porter et al., 2007; 2013). The experiments described in the following chapter aim to explore the functional and molecular characterisation of Bod1L.

Results

Bod1L is a conserved chromatin protein

Our group has previously identified and characterised the PP2A-B56α/δ-specific inhibitor Bod1, which is required for the establishment of proper bi-orientated kinetochore-microtubule attachment during mammalian cell mitosis (Porter et al., 2007; 2013). We identified an uncharacterised protein, Bod1L/FAM44A/KIAA1327 (referred to forthwith as Bod1L) in the human sequence databases which contained a region of ~80% homology with Bod1 (Figure 3.1A, B). This region of Bod1 homology with Bod1L is well conserved throughout higher eukaryotic species, but no evidence of Bod1L at a protein level can be detected in lower eukaryotes (Figure 3.1C). Despite the similarity of this region of sequence, loss of Bod1L did not affect normal mitotic progression (Porter et al., 2007).

B

```
Bod1L      MATNPQPQPPPPAPPPPPPQPQPQPPPPPPGPGAGPGAGG--------------------
Bod1       --------------------------MADGGGGGTGAVGGGGTSQASAGAATGATGASG

Bod1L      ----AGGAGAGAGDPQLVAMIVNHLKSQGLFDQFRRDCLADVDTKPAYQNLRQRVDNFVA
Bod1       GGGPINPASLPPGDPQLIALIVEQLKSRGLFDSFRRDCLADVDTKPAYQNLRQKVDNFVS

Bod1L      NHLATHTWSPHLNKNQLRNNIRQQVLKSGMLESGIDRIISQVVDPKINHTFRPQVEKAVH
Bod1       THLDKQEWNPTMNKNQLRNGLRQSVVQSGMLEAGVDRIISQVVDPKLNHIFRPQIERAIH

Bod1L      EFLATLNHKEEGSGNTAPDDEKPDTSLITQGVPTPGPSANVANDA
Bod1       EFLAAQKKAAVPAPPPEPEGQD-----------PPAPSQDTS---
```

C

```
Mouse      LKSQGLFDQFRRDCLADVDTKPAYQNLRQRVDNFVANHLATHTWSPHLNKNQLRNNIRQQ
Rat        ----------------------PAYQNLRQRVDNFVANHLATHTWSPHLNKNQLRNNIRQQ
Chicken    LKSQGLFDQFRRDCLADVDTKPAYQNLRQRVDNFVCNHLATHTWSPHLNKNQLRNNIRQQ
Xenopus    LKSQGLFDQFRRDCLADVDTKPAYQNLRQRVDNFVASHLASHTWSPHLNKNQLRNNIRQQ
Bovine     LKSQGLFDQFRRDCLADVDTKPAYQNLRQRVDNFVANHLATHTWSPHLNKNQLRNNIRQQ
Human      LKSQGLFDQFRRDCLADVDTKPAYQNLRQRVDNFVANHLATHTWSPHLNKNQLRNNIRQQ
Macaque    LKSQGLFDQFRRDCLADVDTKPAYQNLRQRVDNFVANHLATHTWSPHLNKNQLRNNIRQQ

Mouse      VLKSGMLESGIDRIISQVVDPKINHTFRPQVEKAVHEFLATLNHKEEAAGSTAPDDEKPE
Rat        VLKSGMLESGIDRIISQVVDPKINHTFRPQVEKAVHEFLATLNHKEETAGSTAPDDEKLE
Chicken    VLKSGMLESGIDRIISQVVDPKINHTFRPQVEKAVHEFLATLNHKEEAGPSTAPSEEKMD
Xenopus    VLKSGMLESGIDRIISQVVDPKINHLFRPQVEKVVKEYLAMMNNKEDGNVNTEQNEERSE
Bovine     VLKSGMLESGIDRIISQVVDPKINHTFRPQVEKAVHEFLATLSHKEDTSGSTAPEDEKPD
Human      VLKSGMLESGIDRIISQVVDPKINHTFRPQVEKAVHEFLATLNHKEEGSGNTAPDDEKPD
Macaque    VLKSGMLESGIDRIISQVVDPKINHTFRPQVEKAVHEFLATLNHKEEASGNTAPDDEKPD

Mouse      SSV-ITQGAPAPGPSANVASDAMSILETITSLNQEANAARASTEMSNAKVSERTSRKLSS
Rat        SSV-ITQGAPAPGPSANVASDAMSILETITSLNQEANAARASTEMSNAKASERISRKLSS
Chicken    ASV-AVQGVSTTAPSGNVASDAMSILETITSLNQEASAARASTDNSSSKNSDKAAKRLLS
Xenopus    ASISVPGSLPAVGPSTNVASDAMSILETISSLNQEATAARAFIETPNNKNSDKVSKRTIQ
Bovine     SST-ITQGVPAPGPSANVASDAMSILETITSLNQEASAARASTETSNAKTSERMSKKTPS
Human      TSL-ITQGVPTPGPSANVANDAMSILETITSLNQEASAARASTETSNAKTSERASKKLPS
Macaque    SSL-ITQGVPAPGPSANVANDAMSILETITSLNQEASAARASTETSNAKTSERASKKLPS
```

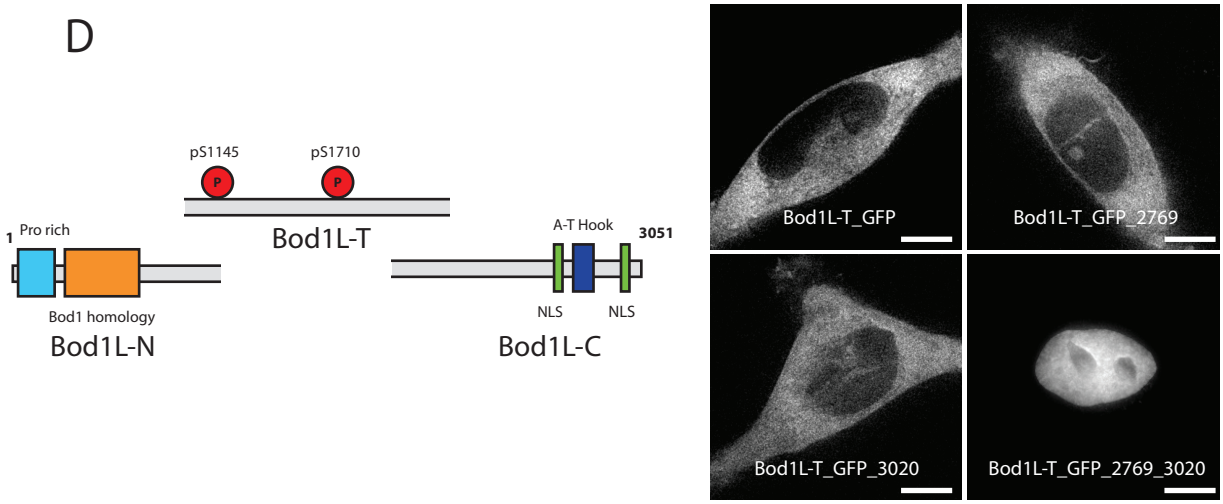

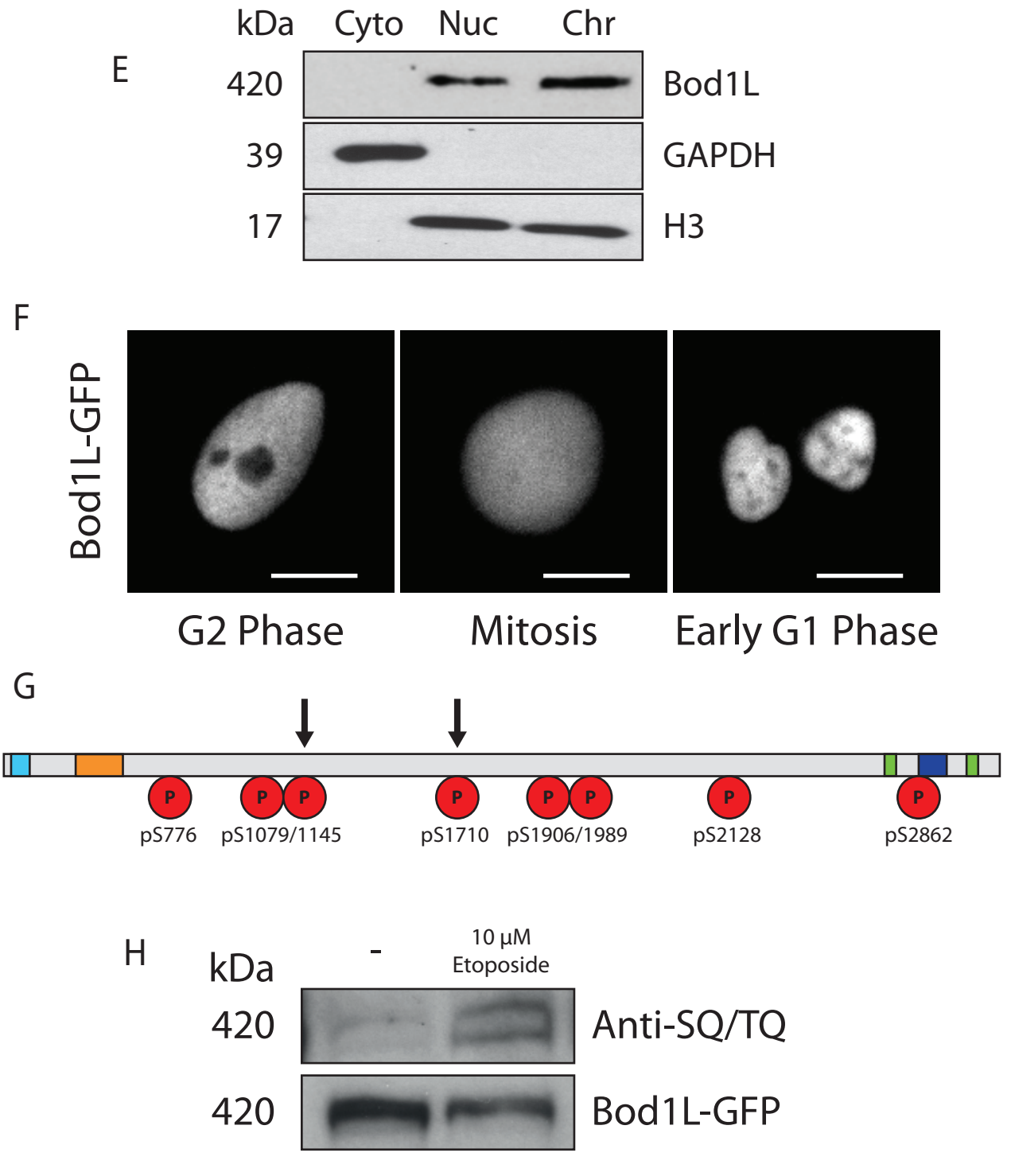
E
kDa
Cyto
Nuc
Chr
420
Bod1L
39
GAPDH
17
H3
F
Bod1L-GFP
G2 Phase
Mitosis
Early G1 Phase
G
P
pS776
pS1079/1145
pS1710
pS1906/1989
pS2128
pS2862
H
kDa
-
10 µM
Etoposide
420
Anti-SQ/TQ
420
Bod1L-GFP

Figure 3.1: Bod1L is a conserved chromatin associated protein

(A) Schematic representation of the domain architecture of Bod1L. Proline rich region, Bod1 homology domain, putative ATM phosphorylation sites, a C-terminal pair of nuclear localisation signals and an A-T hook domain are indicated.

(B) Alignment of the Bod1L N-terminus to Bod1. Identical residues are coloured red and similar residues are coloured in blue. The red box highlights a non-conserved proline rich region in Bod1L.

(C) Multiple species alignment of the Bod1 homology region of Bod1L. Identical residues are coloured red and similar residues are coloured in blue.

(D) Graphic representation of Bod1L-GFP labelled fragments, containing Bod1L NLS sequence. Bod1L-N corresponds to aa1 to aa1009. Bod1L-T corresponds to aa1007 to aa2038. Bod1L-C corresponds to aa2002 to aa3051. HeLa cells were transfected with plasmid DNA for the central trunk fragment of Bod1L (Bod1L-T)(clock-wise from top left): lacking either NLS sequence, containing only the 2769 sequence, containing only the 3020 sequence, containing both 2769 and 3020 sequence. Representative images show maximum intensity projections of GFP signal. NLS insertion site between ORF and GFP fluorescent protein. Scale bars, 10 microns.

(E) Immunoblots of sub-cellular fractionated HeLa cell lysates were probed with antibodies to Bod1L, GAPDH and histone H3.

(F) Representative maximum intensity projections of a HeLa cell transfected with a Bod1L-GFP construct during G2 phase, mitosis and in early G1 phase of the cell cycle. Scale bars, 10 microns.

(G) Schematic representation of experimentally determined ATM phosphorylation sites on Bod1L (http://www.phosphosite.org/ - accessed May 2015). Residues indicated by black arrow (S1145 and S1710) identified in (Matsuoka et al., 2007).

(H) Immunoblots of HeLa cell lysates treated with 10 μM Etoposide and probed with antibodies to GAPDH and Phospho-(Ser/Thr) ATM/ATR substrate.

In addition to a region of Bod1 homology, bioinformatic analysis also revealed a highly-proline rich region at the extreme N-terminus of Bod1L (Figure 3.1B, red box). This region contains 69% proline residues, but importantly contains consecutive sequences of 6 or more prolines which have been shown to be involved in DNA binding (Morgan and Rubenstein, 2013). Although the precise function of such proline-rich domains remains poorly understood, these domains have been extensively shown to promote key protein-protein interactions (Kay et al., 2000; Williamson, 1994). These domains are a target of the SH3-domain containing proteins. SH3 domains are 50–70 amino acids in length and are often present in eukaryotic signal transduction proteins such as CDC25 (Musacchio et al., 1992; Pawson, 1995). In addition, SH3-Proline domain signalling has shown to play an important role in a number of cellular process, such as the response to DNA damage (Shafman et al., 1997).

Given a protein of its size, the amino acid sequence of Bod1L contains few other annotated domains to indicate function (Figure 3.1A). I identified the presence of an A-T hook domain at the C-terminus of Bod1L, flanked by predicted nuclear localisation signals (NLS)(Figure 3.1A) (Brameier et al., 2007). The AT-hook is a short DNA-binding motif which is prevalent in many eukaryotic chromatin binding proteins (Aravind and Landsman, 1998). I demonstrated that both predicted NLS sequences (aa2769 and aa3020) are needed for proper nuclear localisation of synthetic Bod1L fragments (Figure 3.1D). Loss of either NLS leads to cytoplasmic expression of Bod1L protein fragments, suggesting that Bod1L is no longer chromatin bound.

To verify the effect of the AT-hook domain and multiple NLS on Bod1L cellular localisation, a rabbit antibody was raised against an N-terminal peptide of Bod1L corresponding to amino acid 476-496. Biochemical analysis of fractionated HeLa cell lysates using this antibody unsurprisingly showed localisation of Bod1L in the nucleoplasmic and chromatin fraction (Figure 3.1E). I generated a full-length Bod1L-eGFP construct to determine Bod1L localisation throughout the cell cycle (Figure 3.1F). Live-cell analysis of HeLa cells transfected with Bod1L-GFP revealed nuclear/chromatin localisation during all cell cycle phases except mitosis, during which Bod1L-GFP appears to dissociate from chromatin before rapidly re-associating during early cytokinesis/G1-phase. Whilst the data in figure 3.1F suggests that Bod1L is cytoplasmic during mitosis, it cannot be ruled out that a pool of Bod1L may still bind chromatin during this mitotic phase.

Bod1L is highly phosphorylated, particularly in response to DNA damage

Bioinformatic analysis revealed Bod1L as a highly modified protein using data collated from multiple phospho-proteomic studies (http://www.phosphosite.org/proteinAction.do?id=20501 - accessed 09/2011 – 09/2015). One such proteomic screen identified multiple ATM (Ataxia Telangiectasia Mutated)/ATR (ATM and Rad3-related) dependent phosphorylation sites on Bod1L, with the most prevalent sites at pS1145 and pS1710 (Matsuoka et al., 2007) (Figure 3.1G, S1145 and S1710 highlighted with arrow). Other subsequent studies have also confirmed the modification at these specific sites, further validating their probability (Sharma et al., 2014). To confirm whether these ATM/ATR phosphorylations on Bod1L were damage

dependent, I probed Bod1L-GFP immunoprecipitates treated with the Topo II isomerase inhibitor, etoposide, with an antibody against phosphorylated SQ/TQ (Figure 3.1H). I observed increased signal in the upper band of damaged lysate which aligned with the Bod1L-GFP signal, suggestive that Bod1L is phosphorylated by ATM/ATR is response to DNA damage.

Loss of Bod1L leads to severe genomic instability

The bioinformatic data regarding annotated Bod1L domains and modifications suggested a role for Bod1L in the maintenance of genomic stability. In order probe this potential role further; we designed siRNA targeting the N-terminal region of Bod1L (siRNA designed by Iain Porter, Swedlow Group). The siRNA led to a significant reduction of Bod1L protein levels after 48 hours (Figure 3.2A). I performed fluorescence microscopy on fixed HeLa cells treated with Bod1L siRNA, staining for DNA using DAPI (Figure 3.2B). Loss of Bod1L from HeLa cells led to severe genomic instability including the formation of micronuclei, anaphase bridging and abnormal nuclear morphology changes, suggestive of defective DNA repair (Constantinescu et al., 2010).

In response to DNA damage, multiple signalling cascades are initiated which lead to the recruitment of DDR factors to DNA lesions. In addition, multiple pathways are activated to arrest the cell-cycle whilst DNA is repaired (Sancar et al., 2004). To determine if Bod1L played a role in cell cycle progression, HeLa cells were depleted of Bod1L and cell cycle analysis was performed using flow cytometry, which revealed no change in normal cell cycle progression (Figure 3.2C). HeLa cells treated with etoposide arrested correctly during S-phase both in the presence and absence of Bod1L (Figure 3.2C). These results taken

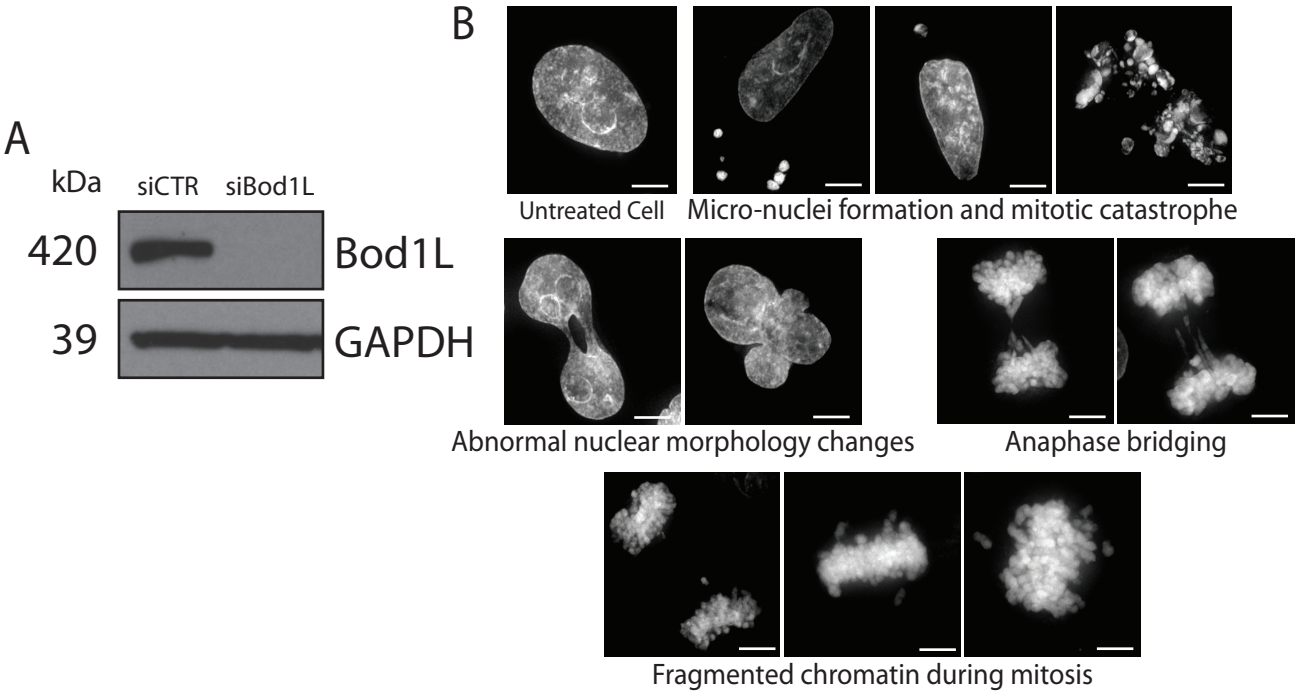

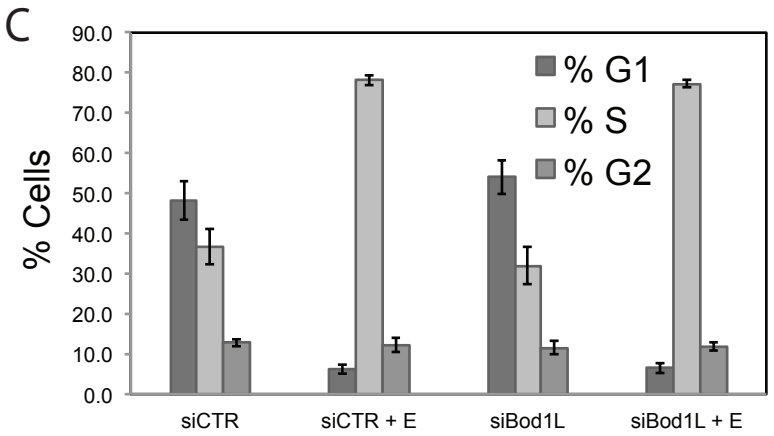

Sample	% G1	% S	% G2
siCTR	48.3	36.8	12.7
siCTR + E	6.1	78.1	12.3
siBod1L	54.0	32.0	11.5
siBod1L + E	6.5	77.2	11.9

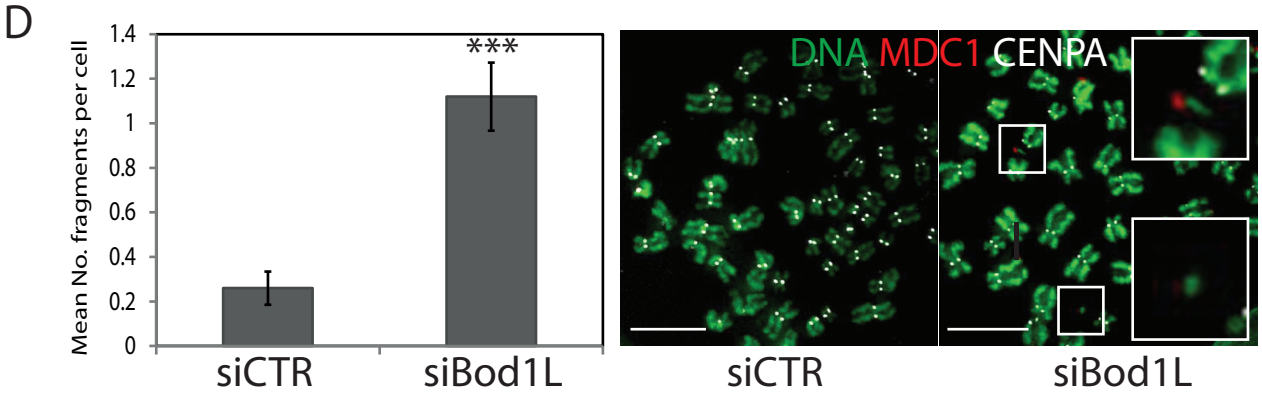

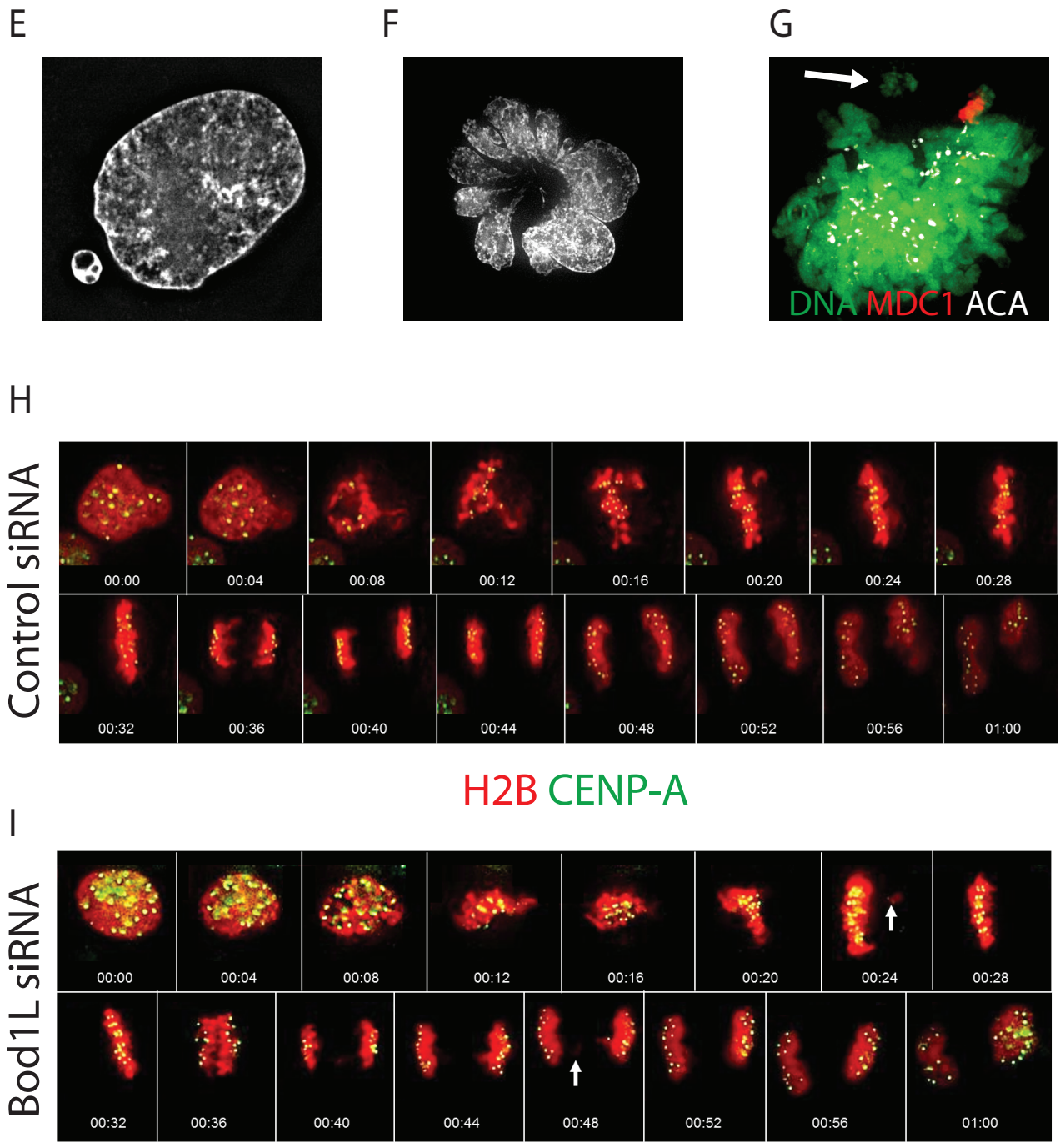
E
F
G
DNA MDC1 ACA
H
Control siRNA
00:00
00:04
00:08
00:12
00:16
00:20
00:24
00:28
00:32
00:36
00:40
00:44
00:48
00:52
00:56
01:00
H2B CENP-A
I
Bod1L siRNA
00:00
00:04
00:08
00:12
00:16
00:20
00:24
00:28
00:32
00:36
00:40
00:44
00:48
00:52
00:56
01:00

Figure 3.2: Loss of Bod1L from human cells leads to genomic instability and fragmented, acentric chromatin during mitosis

(A) Immunoblot of HeLa cell lysates transfected with control or Bod1L siRNA and probed with antibodies to Bod1L and GAPDH.

(B) Morphological analysis of HeLa cells transfected with control or Bod1L siRNA. Cells were fixed with PFA and stained with DAPI to detect DNA.

(C) Flow cytometry analysis of HeLa cells 48 hours post transfection with control or Bod1L siRNA plus 10 μM etoposide. Representative graph of 3 independent experiments. 2.5% cells were excluded as apoptotic/debris. Error bars represent 1 S.D.

(D) Representative images of chromosome spreads of nocodazole-arrested HeLa-CENPA-GFP cells 48 hours after transfection with control or Bod1L siRNA. MDC1, CENPA-GFP, and DNA are shown in red, white and green, respectively. Insets show examples of acentric chromatin fragments after Bod1L depletion. Mean number of chromosome fragments were determined (10 cells/condition, two independent experiments). Scale bar, 5 microns.

(E, F) Morphological analysis of U2OS cells transfected with control or Bod1L siRNA. Cells were fixed with PFA and stained with DAPI to detect DNA. Scale bar, 5 microns.

(G) U2OS cells were transfected with siBod1L. After 48 hours, cells were fixed in PFA and immunostained. MDC1, CENPA-GFP, and DNA are shown in red, white and green, respectively. Arrow indicates fragmented, acentric chromatin. Scale bar, 5 microns.

(H, I) HeLa cells stably expressing CENPA-GFP were transfected with control (H) or Bod1L (I) siRNA. After 24 hours, cells were transfected with an H2B-RFP construct. Cells were imaged during mitosis with single z-section images acquired at 4 minute time intervals. CENPA-GFP is shown in green and H2B-RFP is shown in red. Arrow in (I) top row shows fragment of chromatin containing centromere, arrow in (I) lower row shows acentric chromatin fragment.

together indicate that Bod1L is unlikely to play a critical role in cell cycle checkpoint control during the DNA damage response.

Bod1L depletion results in formation of fragmented, acentric chromatin during mitosis

Figure 3.2B revealed that loss of Bod1L led to micronuclei formation, most likely due to fragmented and acentric chromatin present during mitosis occurring as a result of unrepaired DNA damage. To examine this further, I performed chromosome spreads of HeLa cells treated with siBod1L. Micrographs once again revealed the presence of fragmented chromatin upon Bod1L depletion. Quantification of micrographs revealed an increased frequency of acentric chromatin fragments in cells depleted of Bod1L (Figure 3.2D), again indicative of defective DNA damage repair. All of the chromatin fragments detected after Bod1L depletion lacked CENPA-GFP staining, indicating that these fragments were acentric and were not misaligned chromosomes (Figure 3.2D, inset). Depletion of Bod1 from cells produces elongated mitotic spindles with severe bi-orientation defects, resulting in mitotic catastrophe and cell death (Porter et al., 2007). The lack of centromeric-positive misaligned chromosomes during mitosis, suggests that Bod1L and Bod1 are functionally distinct. In addition, many of the fragments are also positive for the DNA damage repair protein MDC1, suggesting that these fragments originate from unrepaired DNA damage. Importantly, the presence of fragmented, acentric chromatin, in addition to micronuclei and multi-lobed nuclei, were recapitulated in multiple cell lines (HeLa, U2OS), strengthening the hypothesis that these changes are directly due to loss of Bod1L and these phenotypes are not cell line specific (Figure 3.2E-G).

To verify that the fragmented chromatin seen in figure 3.2D was due to loss of Bod1L and not due to experimental process, live cell analysis was performed on HeLa cells stably expressing CENPA-GFP and transiently expressing H2B-RFP (Figure 3.2H-I). Although mitotic timing was unaffected following Bod1L depletion; lagging chromosomes and more importantly, fragmented chromatin, could be detected in cells following Bod1L depletion (white arrows).

Cells display hypersensitivity to specific genotoxic stresses in the absence of Bod1L

Defective DNA repair leads to hypersensitivity to agents that induce DNA damage. Induction of different forms of DNA lesion can help identify the pathways in which unknown proteins play a role.

Depletion of Bod1L with siRNA caused U2OS cells to become hypersensitive to a range of different DNA damaging agents. Cells depleted of Bod1L displayed severe hypersensitivity to the Topoisomerase II inhibitor etoposide, which causes DSBs by forming a ternary complex with topoisomerase II and DNA, preventing religation of DNA ends during an intermediary step, thus forming DSBs (Figure 3.3A). Loss of Bod1L also lead to mild sensitivity to ionising radiation, a treatment that also generates double-strand breaks (Figure 3.3B). These data collectively suggest that Bod1L is required for cell survival.

Depletion of Bod1L resulted in no added sensitivity to the Topoisomerase I inhibitor, camptothecin (Figure 3.3C). Treatment with camptothecin results in the conversion of single-strand breaks to double-strand breaks during S-phase.

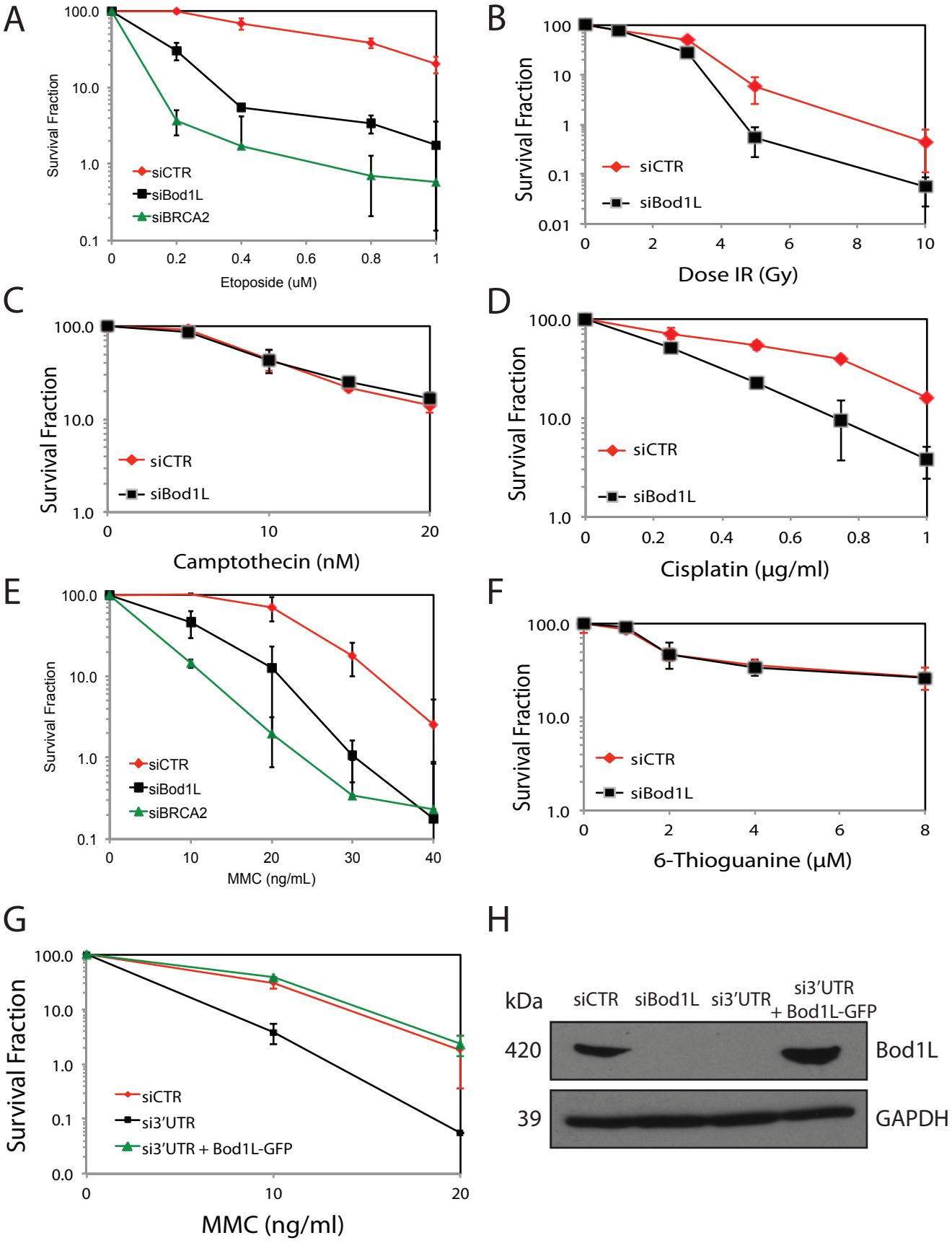
A
Survival Fraction
100.0
10.0
1.0
0.1
0
0.2
0.4
0.6
0.8
1
Etoposide (uM)
siCTR
siBod1L
siBRCA2
B
Survival Fraction
100
10
1
0.1
0.01
0
2
4
6
8
10
Dose IR (Gy)
siCTR
siBod1L
C
Survival Fraction
100.0
10.0
1.0
0
10
20
Camptothecin (nM)
siCTR
siBod1L
D
Survival Fraction
100.0
10.0
1.0
0
0.2
0.4
0.6
0.8
1
Cisplatin (µg/ml)
siCTR
siBod1L
E
Survival Fraction
100.0
10.0
1.0
0.1
0
10
20
30
40
MMC (ng/mL)
siCTR
siBod1L
siBRCA2
F
Survival Fraction
100.0
10.0
1.0
0
2
4
6
8
6-Thioguanine (µM)
siCTR
siBod1L
G
Survival Fraction
100.0
10.0
1.0
0.1
0.0
0
10
20
MMC (ng/ml)
siCTR
si3'UTR
si3'UTR + Bod1L-GFP
H
kDa
siCTR
siBod1L
si3'UTR
si3'UTR
+ Bod1L-GFP
420
Bod1L
39
GAPDH

Figure 3.3: Bod1L depletion results in sensitivity to selective genotoxic stresses

(A-F) Clonogenic survival assays of U2OS cells transfected with Control, Bod1L or BRCA2 (Etoposide/MMC) siRNA. Etoposide, MMC, Cisplatin, Camptothecin and 6-Thioguanine were added 48 hours after transfection at the indicated concentrations and cells propagated for 10 - 12 days. Cells were treated with IR 48 hours after transfection at the indicated dose and cells propagated for 10 - 12 days. For each siRNA, cell viability of untreated cells is defined as 100%. 3 repeats/condition, two independent experiments. Data represented as mean ± SEM.

(G) Clonogenic survival assay of HeLa cells transfected with control siRNA, 3'UTR-Bod1L siRNA or 3'UTR-Bod1L siRNA plus Bod1L-GFP. 48 hours post transfection MMC was added at the indicated concentration. 3 repeats/condition, two independent experiments. Data represented as mean ± SEM.

(H) Immunoblots of cells transfected as in (G) and probed for Bod1L and GAPDH.

The absence of camptothecin sensitivity could be explained by the low concentration of camptothecin used, thus not highlighting any sensitivity that may occur following loss of Bod1L.

In addition to displaying sensitivity to the DSB-inducing stresses, depletion of Bod1L also resulted in hypersensitivity to the intra-strand cross linker cisplatin, as well as the inter-strand cross linker Mitomycin-C (MMC)(Figure 3.3D, E). This severe hypersensitivity to such genotoxic stress suggests a role for Bod1L in the repair pathways associated with such lesions. Treatment of BRCA2 depleted cells with either MMC or etoposide also led to a hypersensitivity phenotype as previously reported (Yuan et al., 1999). Comparison of cell survival following both Bod1L or BRCA2 depletion and treatment with MMC or etoposide revealed that BRCA2 loss led to greater sensitivity than depletion of Bod1L (Figure 3.3A, E). This suggests that BRCA2 may play a more important role in the repair of DNA damage than Bod1L, or alternatively is involved in multiple repair or signalling pathways associated with the DDR.

Cells deficient in mismatch repair have previously been shown to display resistance to treatment with 6-thioguanine (Swann et al., 1996). Figure 3.3F demonstrates that treatment of Bod1L depleted cells with 6-thioguanine led to no additional sensitivity above control treated cells. The lack of resistance to 6-thioguanine treatments in siBod1L cells suggests that Bod1L is unlikely to be involved in mismatch repair.

In order to determine whether the hypersensitivity phenotypes were specifically due to loss of Bod1L, siRNA was designed to target the endogenous Bod1L 3’

untranscribed region (UTR), thus depleting endogenous Bod1L but not exogenously expressed Bod1L. To demonstrate that the hypersensitivity phenotypes were specific to Bod1L depletion, HeLa cells expressing Bod1L-GFP (expression levels of Bod1L-GFP were >70%) were treated with MMC and siRNA targeting the Bod1L 3'-UTR. As figure 3.3G shows, treatment of cells with Bod1L 3'UTR led to severe sensitivity to MMC, recapitulating the results seen using U2OS cells. Expression of exogenous Bod1L-GFP to approximately endogenous protein levels, (Figure 3.3H) led to a complete recovery of sensitivity, confirming that the observed phenotypes were directly due to a loss of Bod1L.

A fluorescence reporter assay reveals compromised repair by homologous recombination following Bod1L depletion

Given the hypersensitivity displayed by Bod1L depleted cells to genotoxic agents which lead to double-strand break formation, I wanted to determine whether Bod1L depleted cells were defective for homologous repair of these breaks. I utilised the recombination substrate DR-GFP, to fluorescently assay a gene conversion event that replicates repair of a double strand break in cells treated with siBod1L (Pierce et al., 1999). In short, the DR-GFP cassette contains a modified GFP gene (SceGFP) that contains a unique I-SceI restriction site. When I-SceI is expressed in cells containing a stably integrated DR-GFP cassette, a single double-strand break is formed. An additional GFP fragment in the cassette (iGFP) can repair the DSB by HR, resulting in full-length, fluorescent GFP that is assessed by fluorescence microscopy (Figure 3.4A).

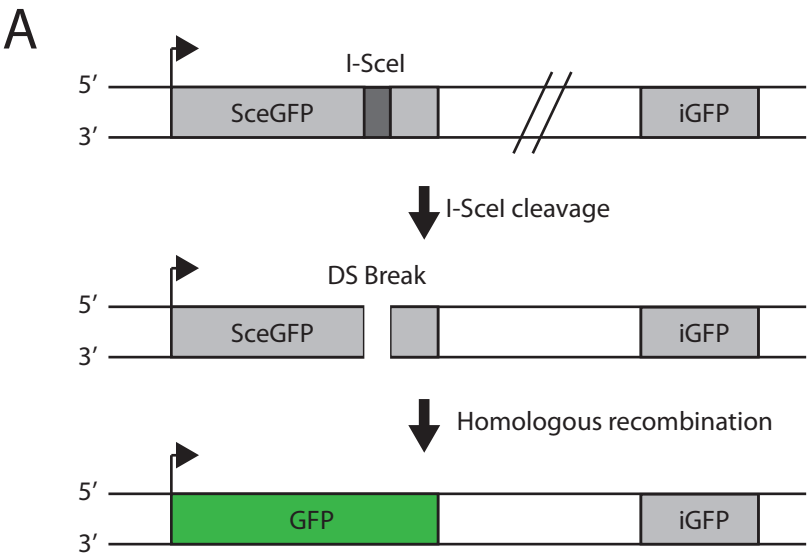
A
I-SceI
5′
3′
SceGFP
iGFP
I-SceI cleavage
DS Break
5′
3′
SceGFP
iGFP
Homologous recombination
5′
3′
GFP
iGFP

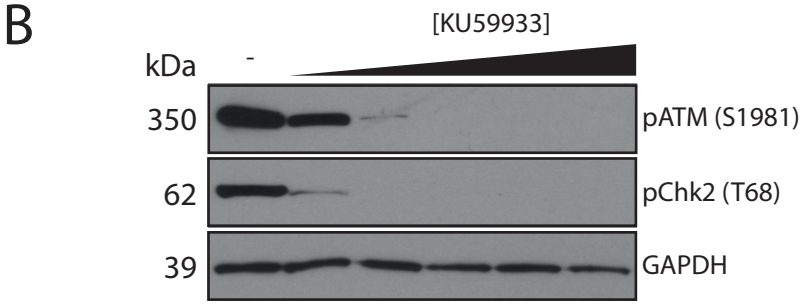
B
[KU59933]
kDa
-
350
pATM (S1981)
62
pChk2 (T68)
39
GAPDH

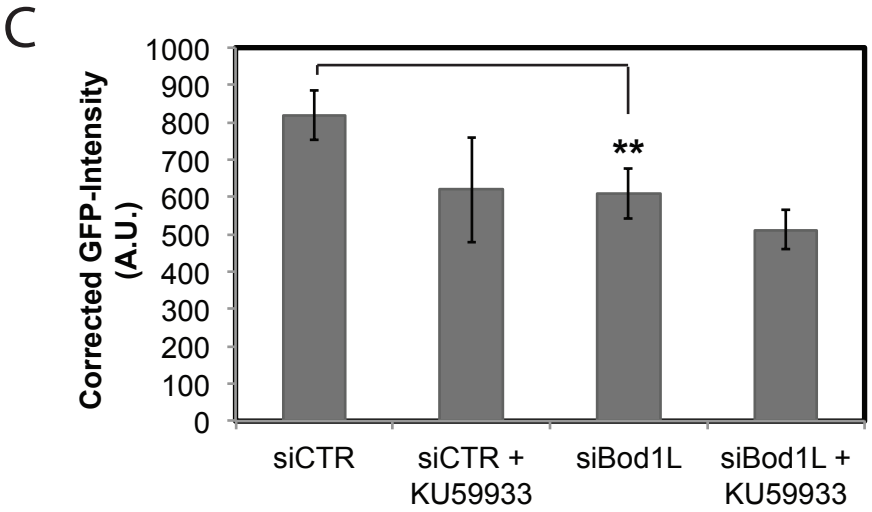
C
Corrected GFP-Intensity (A.U.)
1000
900
800
700
600
500
400
300
200
100
0
**
siCTR
siCTR + KU59933
siBod1L
siBod1L + KU59933

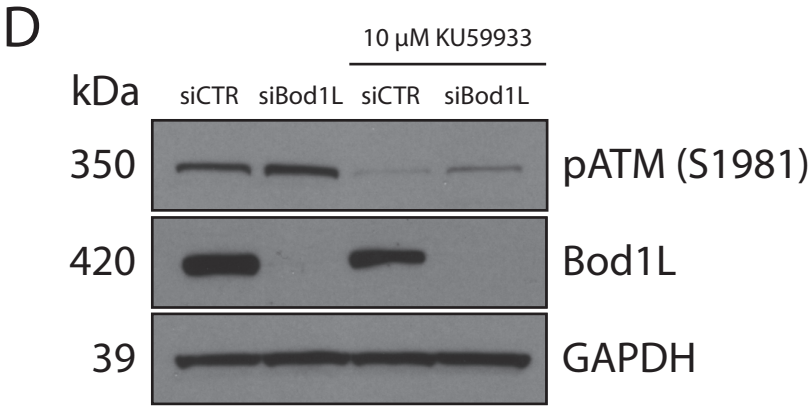
D
10 μM KU59933
kDa
siCTR
siBod1L
siCTR
siBod1L
350
pATM (S1981)
420
Bod1L
39
GAPDH

Figure 3.4: DNA repair by homologous recombination is compromised in the absence of Bod1L

(A) Schematic representation of the DR-GFP homologous recombination (HR) reporter assay. Cassette contains a modified GFP gene (SceGFP) that contains an I-SceI unique restriction site. An additional GFP fragment in the cassette (iGFP) can repair the DSB by HR, resulting in full-length, fluorescent GFP. Adapted from (Schumacher et al., 2012).

(B) Immunoblot of HeLa whole cell lysates treated with a titration of the ATM inhibitor KU59933. DMSO only was used as control. Concentrations of KU59933 used were 1, 5, 10, 20 and 50 μM. Blots were probed with pATM (S1981), pChk2 (T68) and GAPDH.

(C) HeLa DR-GFP cells were transfected with control or Bod1L siRNA. After 48 hours, cells were transfected with a plasmid expressing the I-SceI endonuclease plus DMSO or the ATM kinase inhibitor KU59933. 24 hours later cells were imaged to assess HR dependent GFP expression. Data represented as mean ± 1SD. n=>20 for each condition. **P<0.01.

(D) Immunoblotting of HeLa DR-GFP cell lysates treated as in (G) and probed for pATM (S1981), Bod1L and GAPDH.

The ATM specific inhibitor KU59933 was used as a positive control in the DR-GFP assay. Figure 3.4B shows a titration of KU59933 leading to dose-dependent inhibition of the activating auto-phosphorylation of ATM at S1981, providing a robust read-out of ATM activity. A downstream target of ATM, pChk2 (T68) is also shown to verify the inhibition of the kinase.

Depletion of Bod1L in HeLa cells stably expressing the DR-GFP cassette reduced the efficiency of HR in a manner similar to inhibition of the ATM kinase, indicating a critical role for Bod1L in the HR response to DNA damage (Figure 3.4C). Figure 3.4D confirms the depletion of Bod1L and the KU59933 dependent inhibition of ATM signalling, as determined by western blot of HeLa cell lysates. These data combined with the clonogenic hypersensitivity to DSB inducing agents suggest that Bod1L plays a key role in maintaining a robust cellular response to DNA damage, with loss of the protein leading to genomic instability.

Bod1L depleted cells contain radial chromosomes that are formed independently of FANC complex assembly failure

The micrograph data in figure 3.2B showed multiple nuclear and chromatin aberrations occurring as a direct result of Bod1L knockdown. In addition to the aberrations shown in the figure, Bod1L depletion also led to the formation of radial chromosomes (Figure 3.5A). Although it is well acknowledged that DNA damage associated with high-levels of interstrand cross-linking leads to the formation of radial chromosomes; the precise mechanism of radial formation remains poorly understood (Hanlon Newell et al., 2008). It is known that in the absence of efficient or functional HR-mediated repair, double-strand breaks that

have occurred as a result of DNA cross-links do give rise to radial chromosomes (Huen et al., 2009).

In HeLa cells treated with siBod1L, I observed an increased number of radial chromosomes, even in the absence of genotoxic stress (Figure 3.5A, B). Addition of a high concentration of MMC further increased the number of radials observed, significantly higher than that seen in siCTR treated cells treated with the same dose of MMC. Increased radial chromosome formation is a common cytogenetic marker of Fanconi Anaemia (FA), a condition characterised by a defective interstrand cross-link repair pathway. Given the similarity between the defects caused by Bod1L depletion and FA, I wanted to interrogate the robustness of the FA pathway following Bod1L depletion. The monoubiquitination of FANCD2 upon DNA damage is a critical event in the FA pathway, with the loss of this protein (or ubiquitin-modification) resulting in a compromised pathway (Andreassen et al., 2004). I designed an siRNA to target FANCD2, which significantly depleted protein levels compared with control treated cells (Figure 3.5C). Depletion of FANCD2 led to hypersensitivity to MMC as previously reported, however this sensitivity was significantly less than that seen following Bod1L depletion, suggestive that these two proteins operate in functionally distinct pathways (Figure 3.5D) (Taniguchi et al., 2002). In addition, Figure 3.5E shows that depletion of Bod1L had no effect on the MMC induced monoubiquitination of FANCD2, further suggesting that Bod1L does not function within the Fanconi Anaemia pathway.

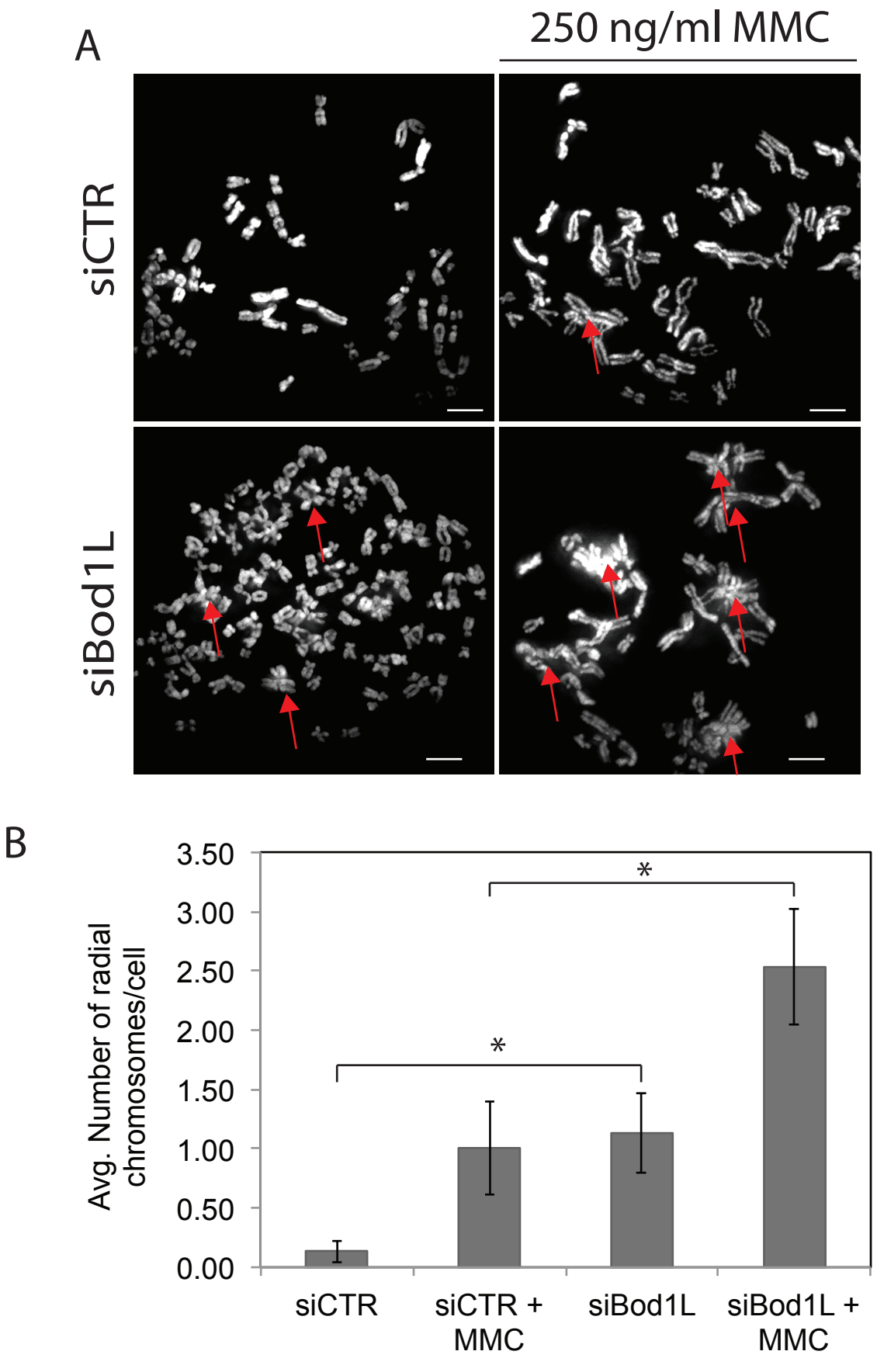
A
250 ng/ml MMC
siCTR
siBod1L
B
Avg. Number of radial chromosomes/cell
3.50
3.00
2.50
2.00
1.50
1.00
0.50
0.00
*
*
siCTR
siCTR + MMC
siBod1L
siBod1L + MMC

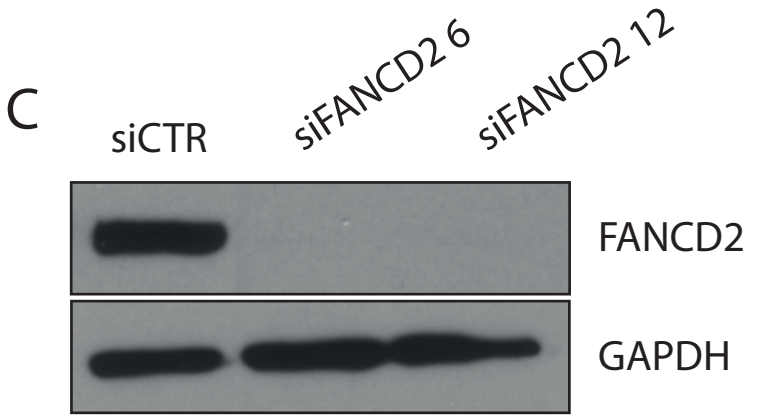
C
siCTR
siFANCD2 6
siFANCD2 12
FANCD2
GAPDH

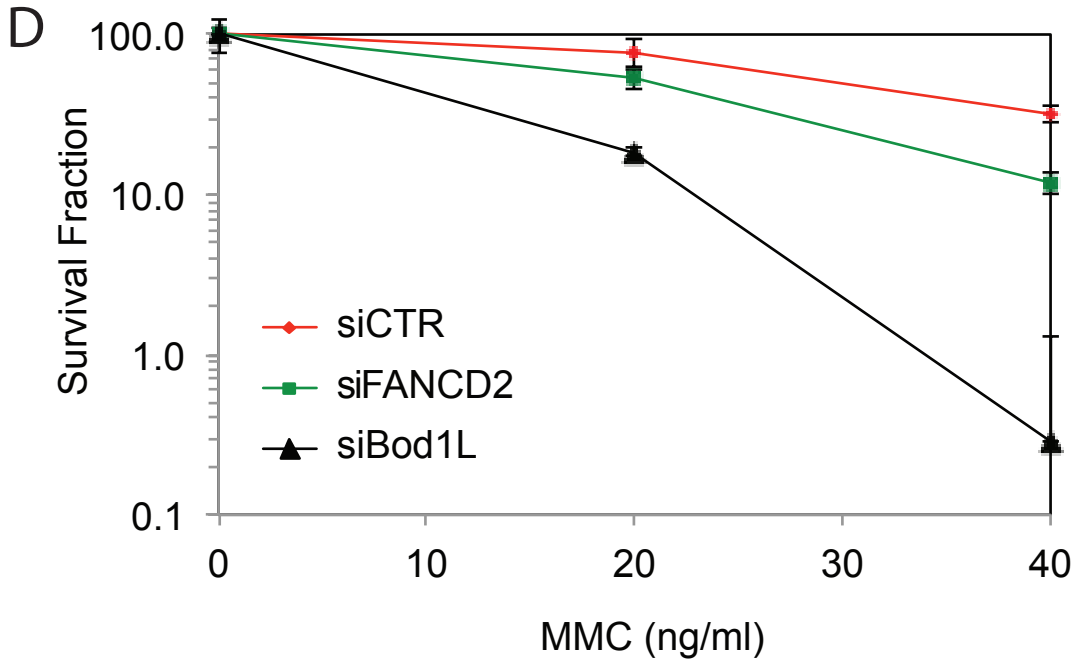
D
100.0
10.0
1.0
0.1
Survival Fraction
siCTR
siFANCD2
siBod1L
0
10
20
30
40
MMC (ng/ml)

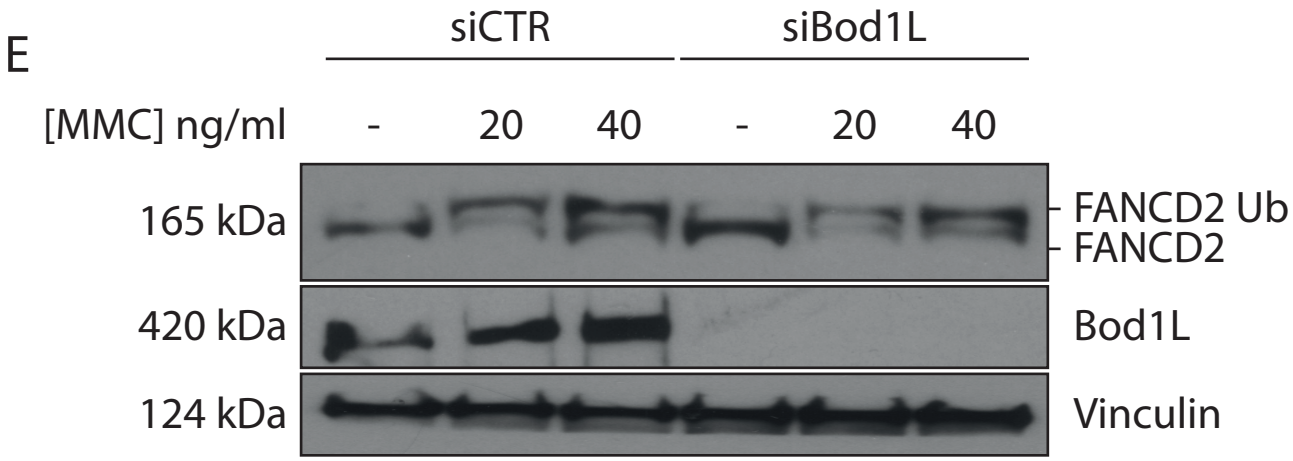
E
siCTR
siBod1L
[MMC] ng/ml
-
20
40
-
20
40
165 kDa
FANCD2 Ub
FANCD2
420 kDa
Bod1L
124 kDa
Vinculin

Figure 3.5: Loss of Bod1L leads to radial chromosome formation, but no change to FANCD2 mono-ubiquitination.

(A) HeLa cells were transfected with either control or Bod1L siRNA. After 24 hours, MMC was added to cells at a final concentration of 250 ng/ml, 3 hours later nocodazole was added to a final concentration of 100 ng/ml and cells were incubated for 16 hours. Chromosome spreads were performed and cells were fixed in PFA and stained with DAPI. Representative maximum intensity projections are shown, arrows indicate radial chromosome.

(B) Quantification of (A). Data represented as mean ± SEM. n=>15 for each condition. *P<0.05.

(C) Immunoblots of HeLa cells treated with either control or FANCD2 siRNA. 6 nM and 12 nM concentration of FANCD2 were used. Immunoblots were probed with antibodies against FANCD2 and GAPDH.

(D) Clonogenic survival assays of U2OS cells transfected with control, Bod1L or FANCD2 siRNA. MMC was added 48 hours after transfection at the indicated concentrations and cells propagated for 10 - 12 days. For each siRNA, cell viability of untreated cells is defined as 100%. 3 repeats/condition, two independent experiments. Data represented as mean ± SEM.

(E) HeLa cells were transfected with either control or Bod1L siRNA. After 24 hours, MMC was added at the concentration indicated for 16 hours and then lysed. Whole cell lysate immunoblots were probed with antibodies against FANCD2, Bod1L and vinculin.

Bod1L is phosphorylated at S1710 by ATM in response to ionising radiation

To examine the recruitment of Bod1L itself to sites of DNA damage, HeLa cells transiently expressing Bod1L-GFP were irradiated and stained for gamma-H2AX to mark sites of damage. Micrograph images and associated quantification (Figure 3.6A, B) detected no recruitment of Bod1L-GFP to IRIF. To explore this further, U2OS cells stably expressing GFP-MDC1 were transfected with cDNA driving the expression of TagRFP-t fused to Bod1L and subjected to our laser micro-irradiation assay. I detected no Bod1L-TagRFP-t at DNA damage sites, despite the strong accumulation of GFP-MDC1 (Figure 3.6C). Switching the location of TagRFP-t to the N-terminus of Bod1L or repeating the experiment using fixed cell immunofluorescence resulted in no detectable concentration of Bod1L to sites of DNA damage.

Whilst the lack of recruitment to damage sites is surprising, given the likely role of Bod1L in the DDR, it is consistent with the behaviour of other chromatin-associated proteins involved in the response to DNA damage. Other immobile proteins involved in the DNA damage response, such as the histone variant H2AX, are instead modified at damage sites, often resulting in complex down-stream signalling cascades (Paull et al., 2000). Previous analysis of global ATM and ATR substrates indicated two major phosphorylation sites on Bod1L at pS1145 and pS1710 (Figure 3.1G) (Matsuoka et al., 2007). Therefore, I immunised sheep with a peptide containing phospho-S1710. The affinity purified anti-pS1710 Bod1L antibody (anti-pBod1L) showed strong specificity to the phosphorylated peptide compared to the unmodified peptide (Figure 3.7A).

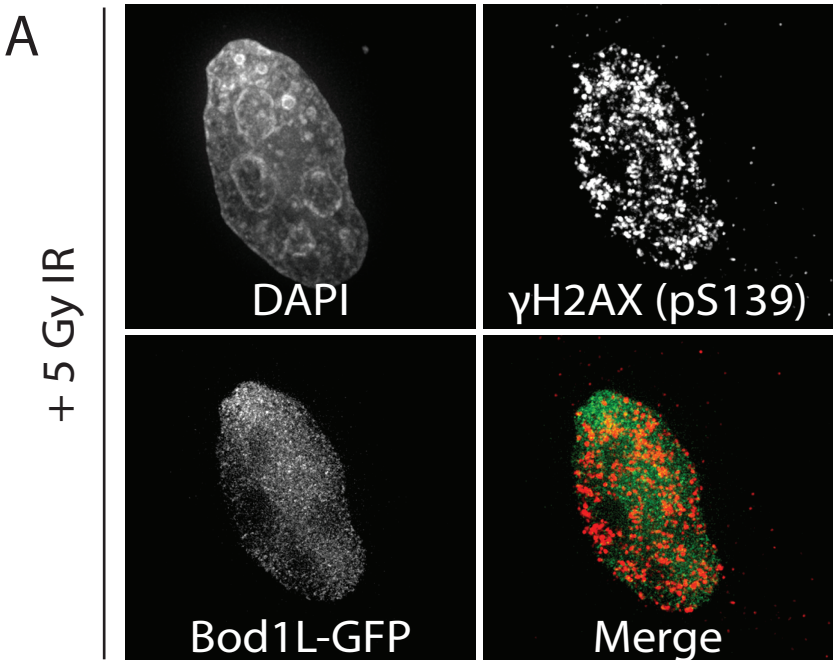
A
+ 5 Gy IR
DAPI
γH2AX (pS139)
Bod1L-GFP
Merge

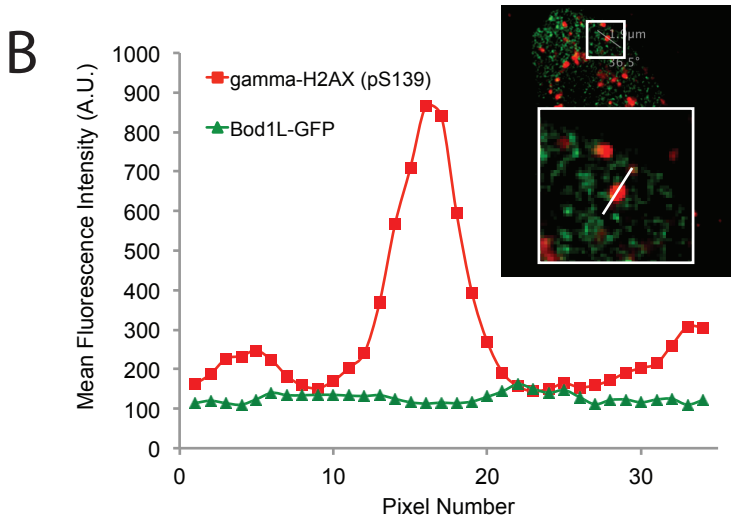
B
gamma-H2AX (pS139)
Bod1L-GFP
Mean Fluorescence Intensity (A.U.)
Pixel Number
0
100
200
300
400
500
600
700
800
900
1000
0
10
20
30

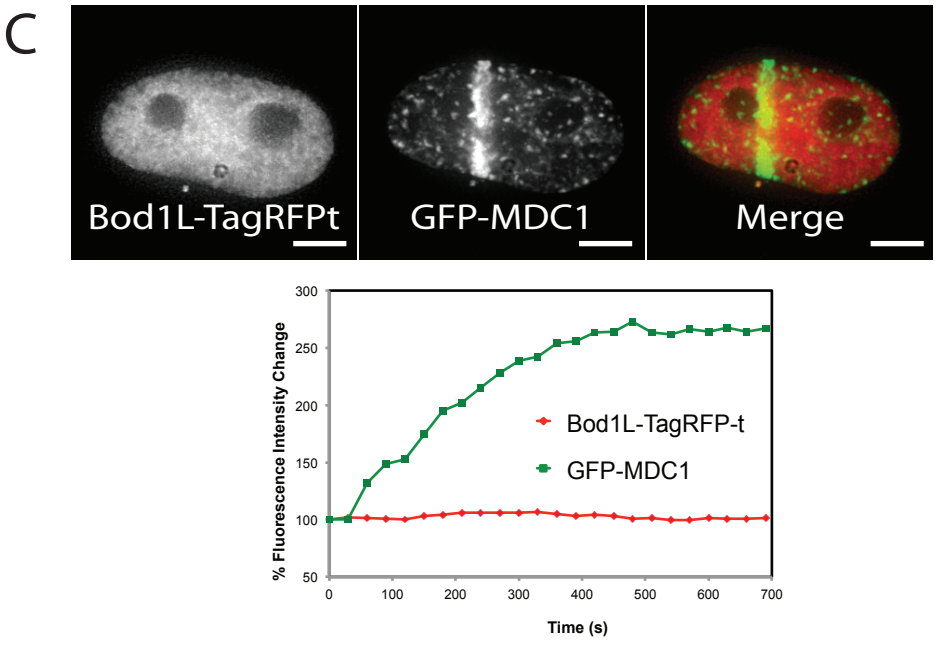
C
Bod1L-TagRFPt
GFP-MDC1
Merge
% Fluorescence Intensity Change
Time (s)
Bod1L-TagRFP-t
GFP-MDC1
50
100
150
200
250
300
0
100
200
300
400
500
600
700

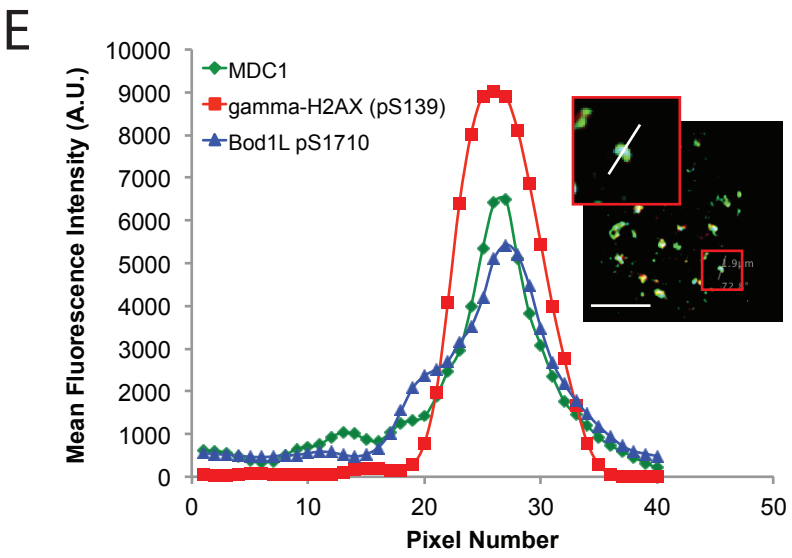
E
Mean Fluorescence Intensity (A.U.)
10000
9000
8000
7000
6000
5000
4000
3000
2000
1000
0
MDC1
gamma-H2AX (pS139)
Bod1L pS1710
0
10
20
30
40
50
Pixel Number

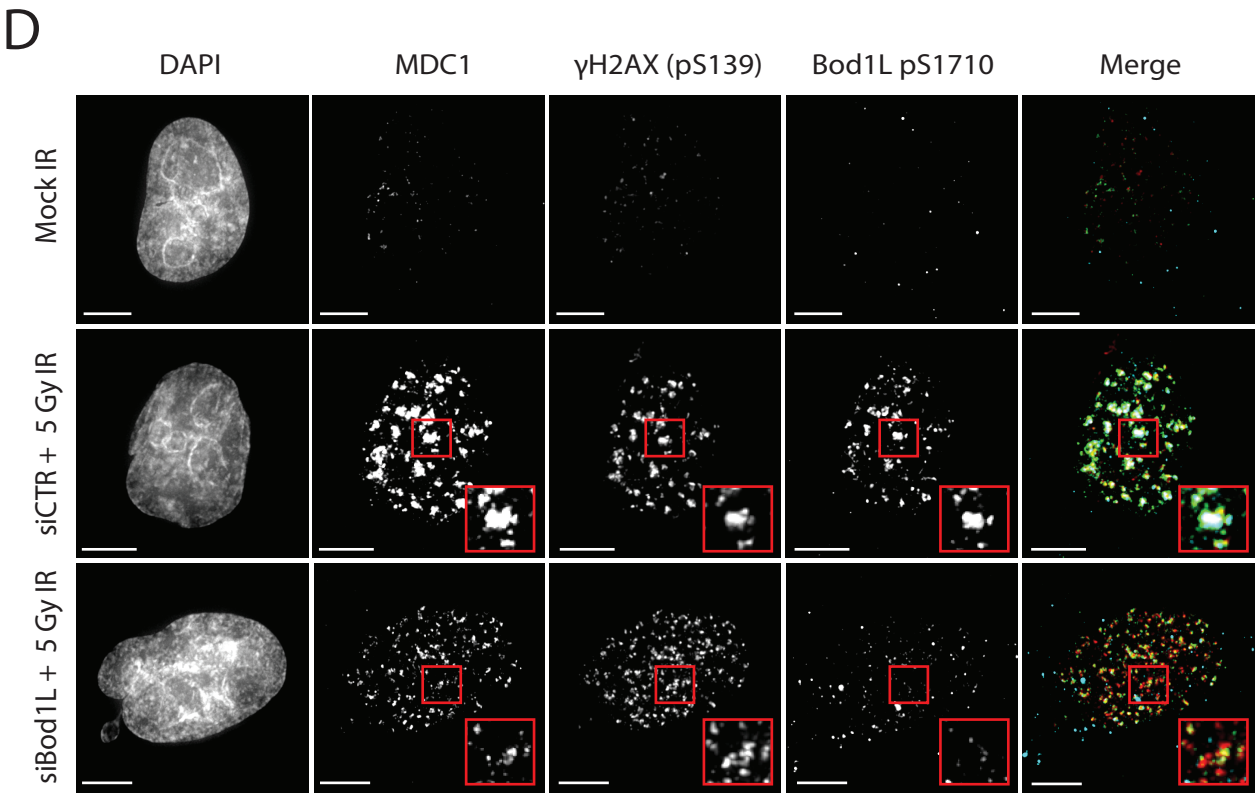
D
DAPI
MDC1
γH2AX (pS139)
Bod1L pS1710
Merge
Mock IR
siCTR + 5 Gy IR
siBod1L + 5 Gy IR

Figure 3.6: Bod1L is not re-localised to sites of damage but is phosphorylated at ionising radiation induced foci (IRIF)

(A) HeLa cells were transfected with Bod1L-GFP. 48 hours late, cells were treated with 5 Gy IR, allowed to recover for 1 hour and immunostained for γH2AX (S139). Projections of representative images are shown.

(B) Protein accumulation at the damage foci from (A) indicated (inset) was determined by quantifying the fluorescent intensity of each channel along the indicated line.

(C) U2OS cells stably expressing GFP-MDC1 (green) were transfected with Bod1LTagRFPt (red). Cells were pretreated with Hoescht and striped with a 405 nm laser. Accumulation of GFP-MDC1 and Bod1L-TagRFPt was quantified along the line of the laser stripe. U2OS cells stably expressing GFP-MDC1 (green) were transfected with Bod1LTagRFPt (red). Cells were pretreated with Hoescht and striped with a 405 nm laser. Accumulation of GFP-MDC1 and Bod1L-TagRFPt was quantified along the line of the laser stripe.

(D) Immunostaining of mock or IR treated HeLa cells transfected with control or Bod1L siRNA. Cells were exposed to 5 Gy IR 48 hours after transfection. Cells were fixed two hours post IR treatment and immuno-stained for MDC1 (green), γH2AX(pS139) (red) or Bod1L (pS1710) (cyan).

(E) HeLa cells were treated with 5 Gy IR and immunostained for MDC1 (green), γH2AX (pS139) (red) or Bod1L (pS1710) (cyan). Protein accumulation at the damage foci indicated (inset) was determined by quantifying the fluorescent intensity of each channel along the indicated line.

In addition, incubation of anti-pBod1L with the phospho-peptide antigen, but not with the non-phospho-peptide, led to a marked reduction in signal (Figure 3.7B, C).

After treatment with IR, anti-pBod1L accumulated at ionising radiation-induced foci (IRIF), co-localising with the phosphorylated H2AX (γH2AX) and endogenous MDC1 (Figure 3.6D). Anti-pBod1L (S1710) staining was largely eliminated when Bod1L expression was ablated by siRNA, confirming the specificity of this antibody (Figure 3.6D, lower row). Quantification of signal intensity at individual foci revealed peak distribution of anti-pBod1L similar to that of γH2AX and MDC1 (Figure 3.6E). To further examine the modification of Bod1L at sites of DNA damage, U2OS cells stably expressing GFP-MDC1 were once again sensitised with Hoechst 33342 and subjected to laser micro-irradiation (Figure 3.8A). Anti-pBod1L (S1710) co-localised with MDC1 and γH2AX along the laser-stripe, which was confirmed by quantification of micrographs (Figure 3.8B).

ATM phosphorylation of H2AX and the subsequent recruitment of MDC1 to sites of DNA damage, is a rapid process, occurring within 1-5 minutes of the initial DNA lesion (Lou et al., 2003; Paull et al., 2000; Stewart et al., 2003). To determine whether the phospho-Bod1L (S1710) modification occurred rapidly following the DNA lesion or whether Bod1L phosphorylation was dependent on recruitment of additional factors to DNA lesions, I performed a time-course immunostaining post-IR (Figure 3.8C). Low levels of anti-pBod1L (S1710) signal were present from the earliest time point measured (5 minutes), and signal intensity increased in line with γH2AX and MDC1 accumulation at damage sites.

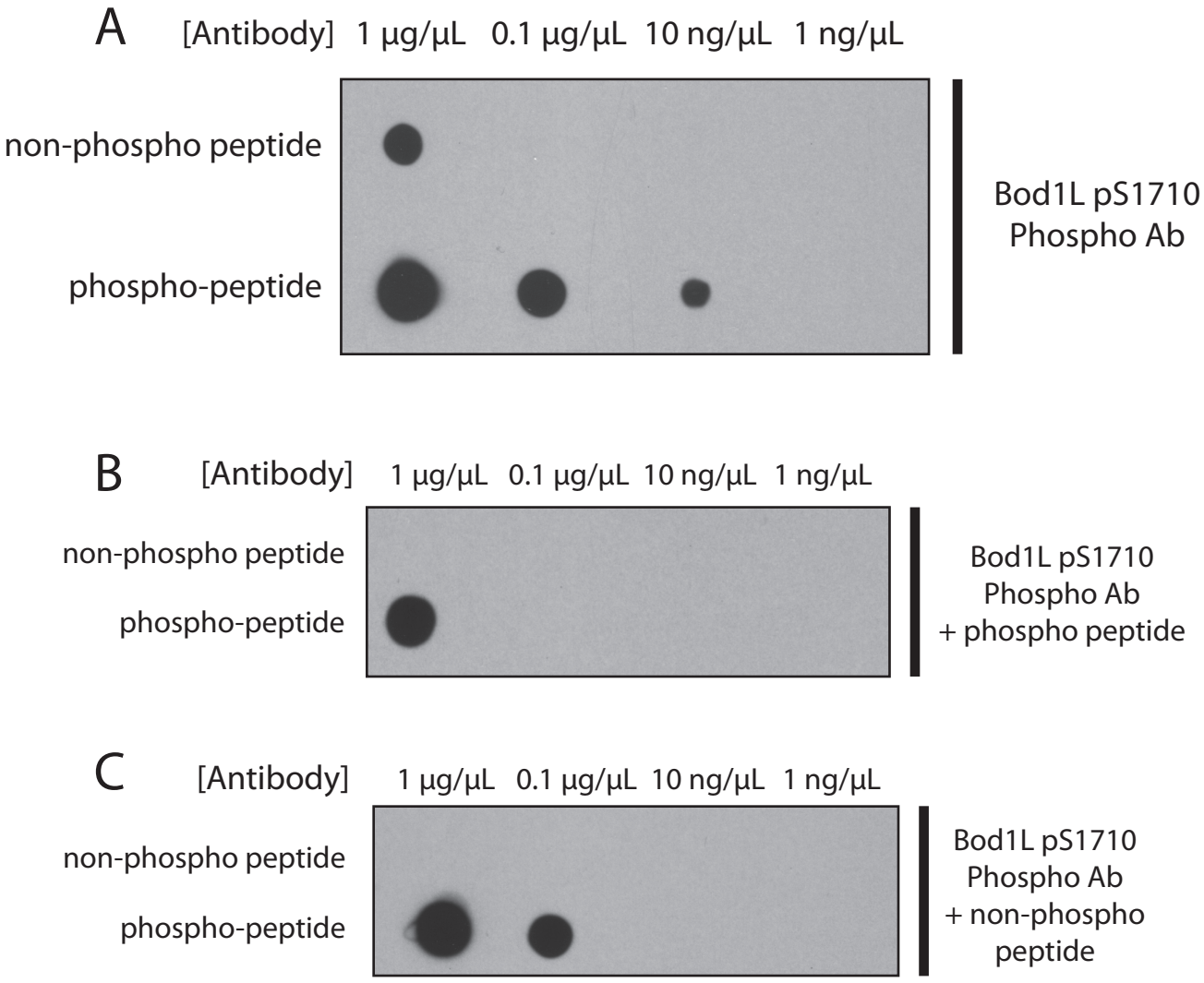
A
[Antibody] 1 µg/µL 0.1 µg/µL 10 ng/µL 1 ng/µL
non-phospho peptide
phospho-peptide
Bod1L pS1710
Phospho Ab
B
[Antibody] 1 µg/µL 0.1 µg/µL 10 ng/µL 1 ng/µL
non-phospho peptide
phospho-peptide
Bod1L pS1710
Phospho Ab
+ phospho peptide
C
[Antibody] 1 µg/µL 0.1 µg/µL 10 ng/µL 1 ng/µL
non-phospho peptide
phospho-peptide
Bod1L pS1710
Phospho Ab
+ non-phospho
peptide

Figure 3.7: Production of a phospho-Bod1L S1710 antibody

(A) Dot blot of pBod1L S1710 antibody with a dilution series of the non-phosphorylated (upper row) and phosphorylated (lower row) antigenic peptide NH_2-CEEVDG[pS]QGNMMR-COOH corresponding to E1705-R1716 of human Bod1L.

(B) pBod1L S1710 antibody was incubated with phosphorylated antigenic peptide at an equimolar ratio of 50:1. A dot blot of the incubated antibody with a dilution series of the non-phosphorylated (upper row) and phosphorylated (lower row) antigenic peptide was performed.

(C) pBod1L S1710 antibody was incubated with non-phosphorylated antigenic peptide at an 1:50 ratio to saturate the antibody. A dot blot of the incubated antibody with a dilution series of the non-phosphorylated (upper row) and phosphorylated (lower row) antigenic peptide was performed. Scale bars, 5 microns.

Indeed, it is clear that γH2AX is phosphorylated initially at 5-15 minutes and is then followed by strong MDC and phospho-Bod1L (S1710) response (Figure 3.8C-D). These data suggest that phospho-Bod1L (S1710) phosphorylation is an early event in the DNA damage-signalling pathway and is unlikely to be reliant on downstream protein recruitment.

Bod1L S1710 conforms to the ATM phosphorylation motif, S/T-Q-X, and as mentioned previously, has been identified in several ATM/ATR substrate specific phospho-proteomic screens (Kim et al., 1999; Matsuoka et al., 2007; Traven and Heierhorst, 2005). Immunoblot analysis of HeLa cell lysates dosed with IR and treated with the ATM inhibitor KU59933 revealed that phospho-Bod1L S1710 signal was lost upon inhibition of ATM (Figure 3.9A). Additional immunofluorescence analysis confirmed that treatment of irradiated cells with KU59933 led to a significant reduction in phospho-Bod1L S1710 signal, in addition to another ATM target, γH2AX (S139), thus preventing the timely recruitment of MDC1 to sites of damage (Figure 3.9B). Treatment of cells with caffeine, a pan-specific ATM/ATR inhibitor also led to a loss in signal, albeit to a slightly lesser extent (Figure 3.9B, lower panels). Although these data suggest that it is highly likely that ATM phosphorylates Bod1L, since pBod1L (1710) signal decreases once total ATM kinase activity is inhibited, it is possible that the loss of phospho-Bod1L S1710 signal could solely be due to loss of γH2AX phosphorylation. As such, if Bod1L phosphorylation were dependent on γH2AX phosphorylation by ATM, this could also explain the loss of phospho-Bod1L S1710 signal.

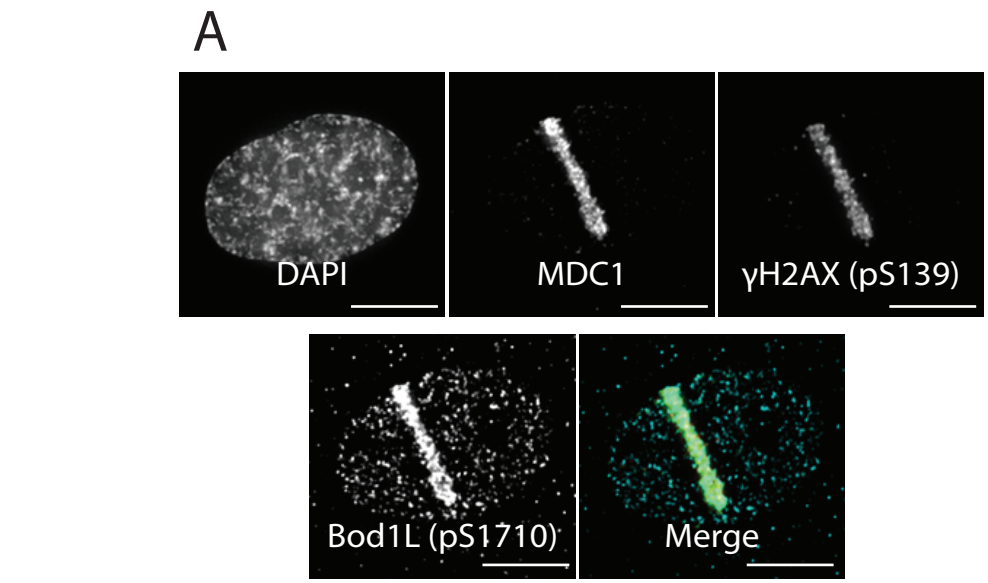
A
DAPI
MDC1
γH2AX (pS139)
Bod1L (pS1710)
Merge

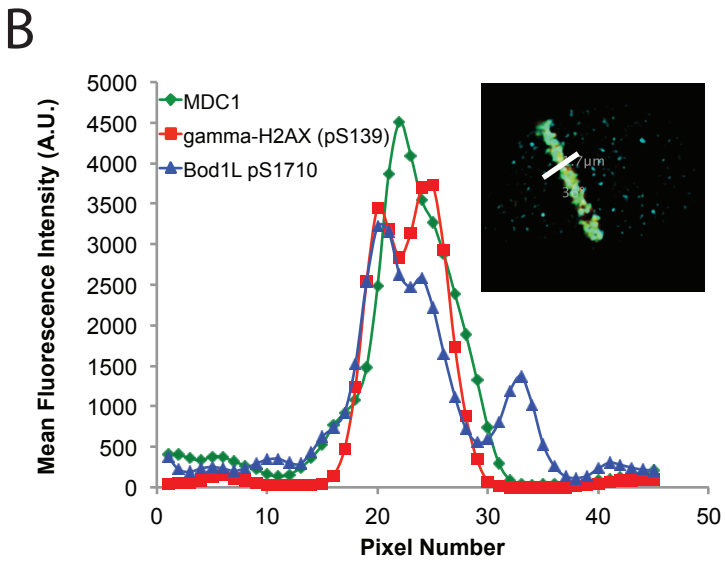
B
MDC1
gamma-H2AX (pS139)
Bod1L pS1710
Mean Fluorescence Intensity (A.U.)
Pixel Number
0
500
1000
1500
2000
2500
3000
3500
4000
4500
5000
0
10
20
30
40
50

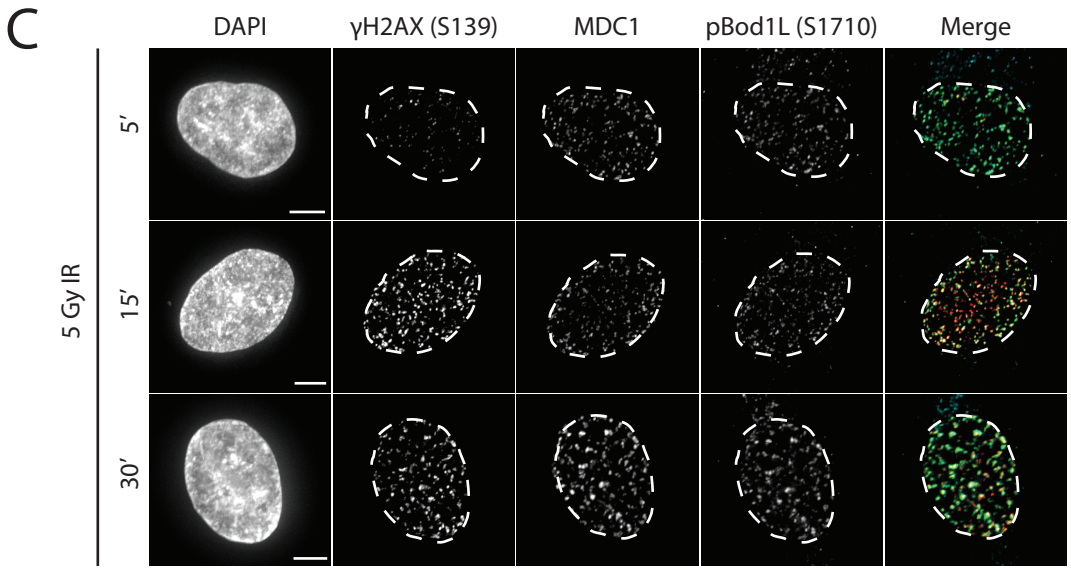
C
DAPI
γH2AX (S139)
MDC1
pBod1L (S1710)
Merge
5 Gy IR
5′
15′
30′

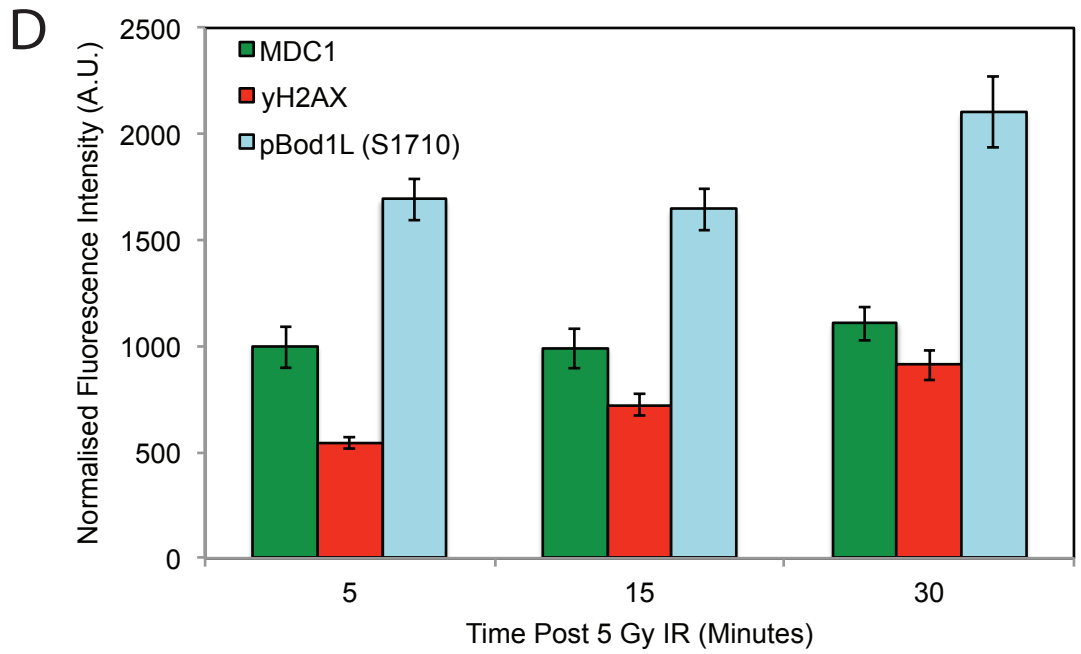

Figure 3.8: Bod1L phosphorylation at IRIF or micro-irradiation stripes occurs rapidly following damage

(A) U2OS cells stably expressing GFP-MDC1 (green) were pre-treated with Hoechst 33342 and striped with a 405 nm laser. Cells were fixed in PFA and stained for MDC1 (green), γH2AX (pS139) (red) or Bod1L (pS1710) (cyan).

(B) Quantification of fluorescence signal (from (A)) for each channel along the indicated line profile.

(C) HeLa cells were treated with 5 Gy IR and allowed to recover for 5, 15 or 30 minutes prior to PFA fixation. Cells were immunostained for MDC1 (green),

γH2AX (pS139) (red) or Bod1L (pS1710) (cyan). Representative maximum intensity projections are shown.

(D) Quantification of (C). >10 cells per condition, Data represented as mean ± SEM.

To test further whether Bod1L is directly phosphorylated by ATM upon DNA damage, we generated a ~160 kDa GST labelled fragment of Bod1L, corresponding to amino acids aa1007 to aa2038 (Bod1L-T), containing the S1710 phosphorylation site (Figure 3.9C)(Fragments generated by Michael Porter, Swedlow group). We utilised recombinant DNA-PK, which shares identical specificity to ATM *in vitro* (Kim et al., 1999; O'Neill et al., 2000), to confirm that phospho-Bod1L S1710 is phosphorylated by ATM in response to DNA damage *in vitro* and most likely *in vivo* (DNA-PK a kind gift from Susan Lees-Miller, Calgary). Mutation of S1710A ablated phosphorylation by DNA-PK at this site, confirming antibody specificity (Figure 3.9D).

I have demonstrated that Bod1L, at one or more sites, is rapidly and specifically phosphorylated at sites of DNA by ATM, however the functional significance of this modification remains unclear. To assess the function of this modification I generated full-length Bod1L constructs containing S1710A phospho-dead mutants and performed clonogenic survival assays, depleting endogenous Bod1L and rescuing with the mutant construct (Figure 3.9E). Bod1L containing S1710A appeared to rescue the MMC hypersensitivity equally as well as wild-type Bod1L, suggesting that upon DNA damage, loss of Bod1L S1710 phosphorylation alone does not affect overall cell survival.

Bod1L is phosphorylated at S1145 in response to ionising radiation

As mentioned previously, analysis of global ATM and ATR substrates, as well as ultradeep phosphoproteome mass-spectrometry, revealed an additional phosphorylation sites on Bod1L at position S1145 (Figure 3.1G) (Matsuoka et al., 2007; Sharma et al., 2014). To determine whether phosphorylation at this

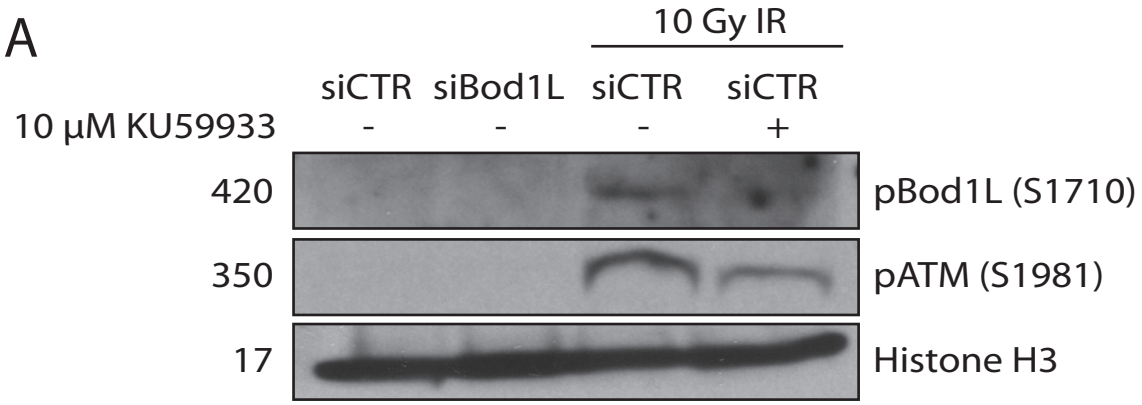
A
10 Gy IR
siCTR
siBod1L
siCTR
siCTR
10 µM KU59933
-
-
-
+
420
pBod1L (S1710)
350
pATM (S1981)
17
Histone H3

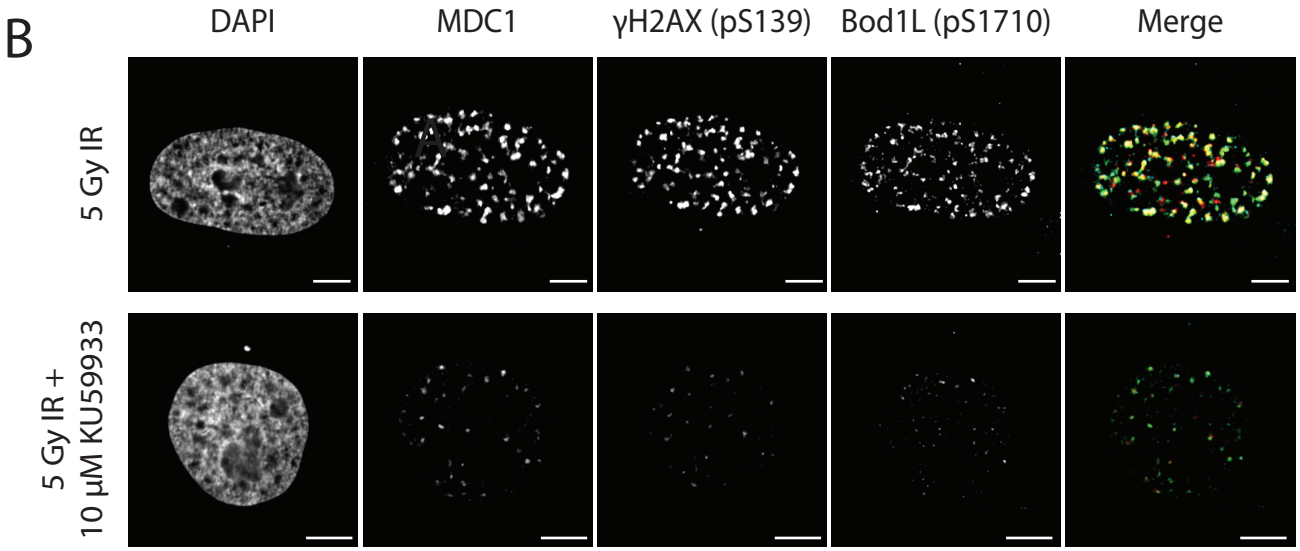
B
DAPI
MDC1
γH2AX (pS139)
Bod1L (pS1710)
Merge
5 Gy IR
5 Gy IR +
10 µM KU59933

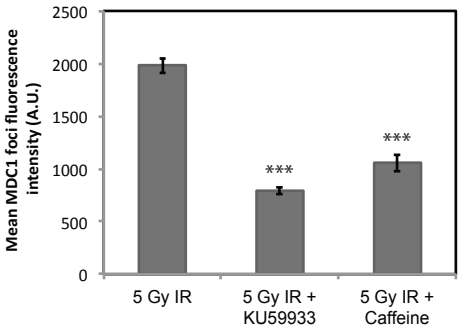
Mean MDC1 foci fluorescence intensity (A.U.)
2500
2000
1500
1000
500
0
***
***
5 Gy IR
5 Gy IR + KU59933
5 Gy IR + Caffeine

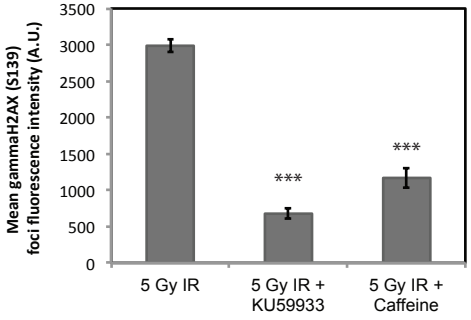
Mean gammaH2AX (S139) foci fluorescence intensity (A.U.)
3500
3000
2500
2000
1500
1000
500
0
***
***
5 Gy IR
5 Gy IR + KU59933
5 Gy IR + Caffeine

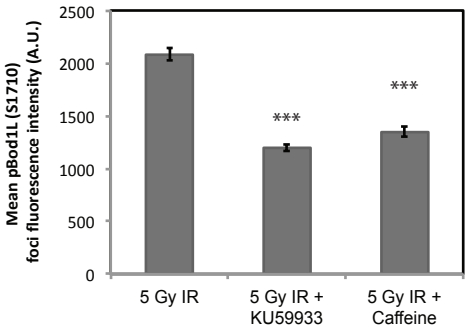
Mean pBod1L (S1710) foci fluorescence intensity (A.U.)
2500
2000
1500
1000
500
0
***
***
5 Gy IR
5 Gy IR + KU59933
5 Gy IR + Caffeine

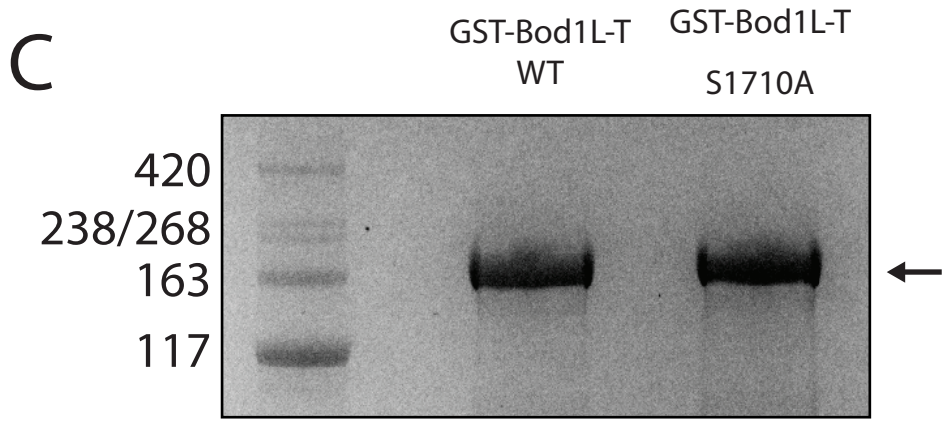
C
GST-Bod1L-T WT
GST-Bod1L-T S1710A
420
238/268
163
117

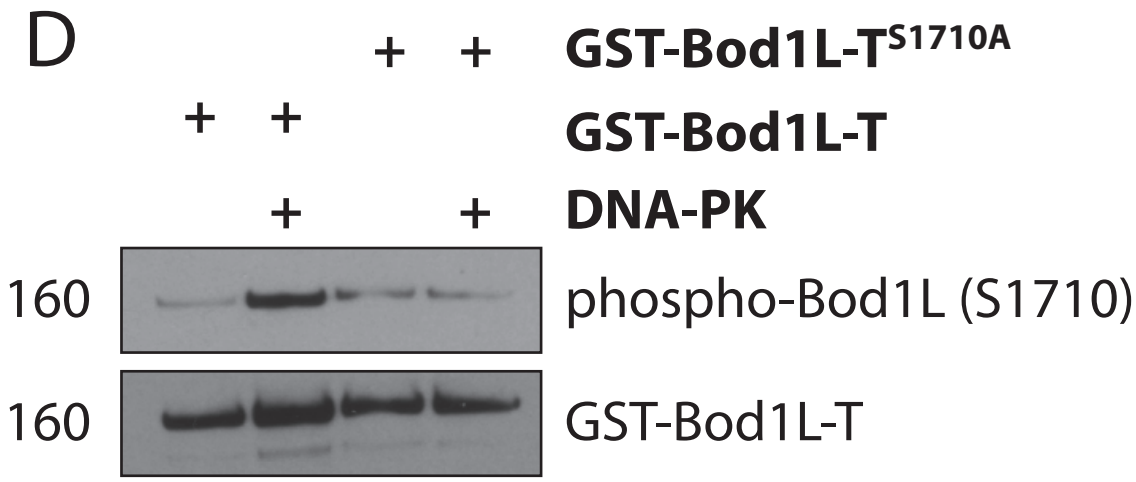
D
+ +
GST-Bod1L-T^{S1710A}
+ +
GST-Bod1L-T
+ +
DNA-PK
160
phospho-Bod1L (S1710)
160
GST-Bod1L-T

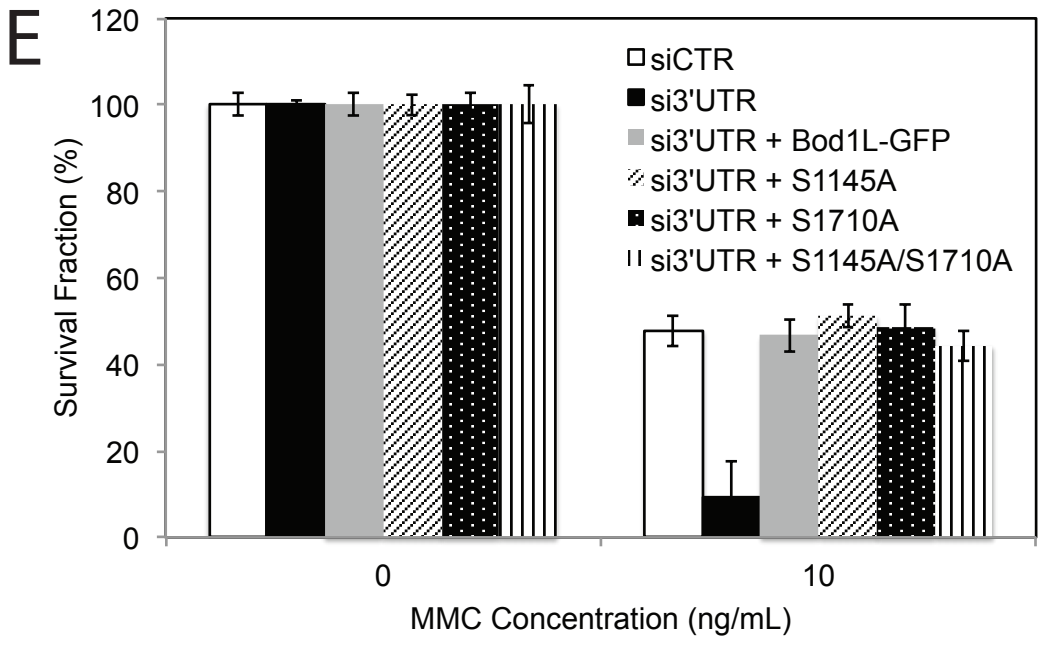
E
120
100
80
60
40
20
0
Survival Fraction (%)
siCTR
si3'UTR
si3'UTR + Bod1L-GFP
si3'UTR + S1145A
si3'UTR + S1710A
si3'UTR + S1145A/S1710A
0
10
MMC Concentration (ng/mL)

Figure 3.9: Bod1L is phosphorylated at S1710 by ATM *in vitro*

(A) HeLa cells were transfected with either control or Bod1L siRNA. After 48 hours, cells were treated with 10 μM KU59933 where indicated, before treatment with 10 Gy IR. Immuno-blots were probed with pBod1L (S1710), pATM (S1981) and histone H3.
(B) HeLa cells were treated with DMSO control, 10 μM KU59933 or 5 mM Caffeine and then treated with 5 Gy IR. Cells were fixed in PFA and stained for endogenous MDC1 (green), γH2AX (pS139) (red) or Bod1L (pS1710) (cyan). Lower panels show quantification of signal for each channel. Data represented as mean ± SEM. n=>20 for each condition. ***P<0.001. Scale bar, 5 microns.
(C) Purified WT or S1710A GST-Bod1L-T were separated by SDS-PAGE and subjected to colloidal Coomassie staining. Purified WT and S1710A protein is indicated by arrow (GST fragments generated by Michael Porter, Swedlow Group).
(D) Purified WT or S1710A GST-Bod1L-T were incubated in a kinase buffer containing recombinant DNA-PK. SDS–polyacrylamide gel electrophoresis-separated proteins were transferred and probed with antibodies against phospho- phospho-Bod1L (S1710) and GST.
(E) HeLa cells were transfected with control or 3'UTR-Bod1L siRNA. To assess rescue of phenotype, cells were then transfected with either Bod1L-GFP, Bod1L-GFP_S1710A, Bod1L-GFP_S1145A or Bod1L-GFP_S1710A/S145A and clonogenic survival assays were carried out with Mitomycin-C. For each treatment, cell viability of untreated cells is defined as 100%.

site was a damage dependent event, I immunised sheep with a peptide containing phospho-S1145. The affinity purified anti-pBod1L (S1145) antibody showed strong specificity to the phosphorylated peptide compared to the unmodified peptide (Figure 3.10A). In a manner analogous to modification of Bod1L at S1710, after treatment with IR, anti-pBod1L (S1145) accumulated at ionising radiation-induced foci (IRIF), co-localising with the phosphorylated H2AX (γH2AX) and endogenous MDC1 (Figure 3.10B). Anti-pBod1L (S1145) staining was largely eliminated when Bod1L expression was ablated by siRNA, once again confirming the specificity of this antibody (Figure 3.10, lower row). Quantification of signal intensity at individual IRIF revealed peak distribution of anti-pBod1L (S1145) similar to that of γH2AX and MDC1 (Figure 3.10C)

Like modification of Bod1L at S1710, phosphorylation of Bod1L at S1145 appears to only occur at DNA lesions. Once again, to determine the function of this modification I generated additional full-length Bod1L constructs containing S1145A phospho-dead mutants as well as double S1145A/S1710A mutants and performed clonogenic survival assays, depleting endogenous Bod1L and rescuing with the mutant construct (Figure 3.9E). Bod1L containing the S1145A appeared to rescue the MMC hypersensitivity equally as well as wild-type Bod1L, suggesting that similar to S1710, loss of Bod1L S1145 phosphorylation alone upon DNA damage does not affect overall cell survival. The double mutant, S1145A/S1710 also appeared to have no affect on the survival of Bod1L depleted cells treated with MMC, suggesting that there are multiple, redundant sites, that are phosphorylated by ATM in the response to damage.

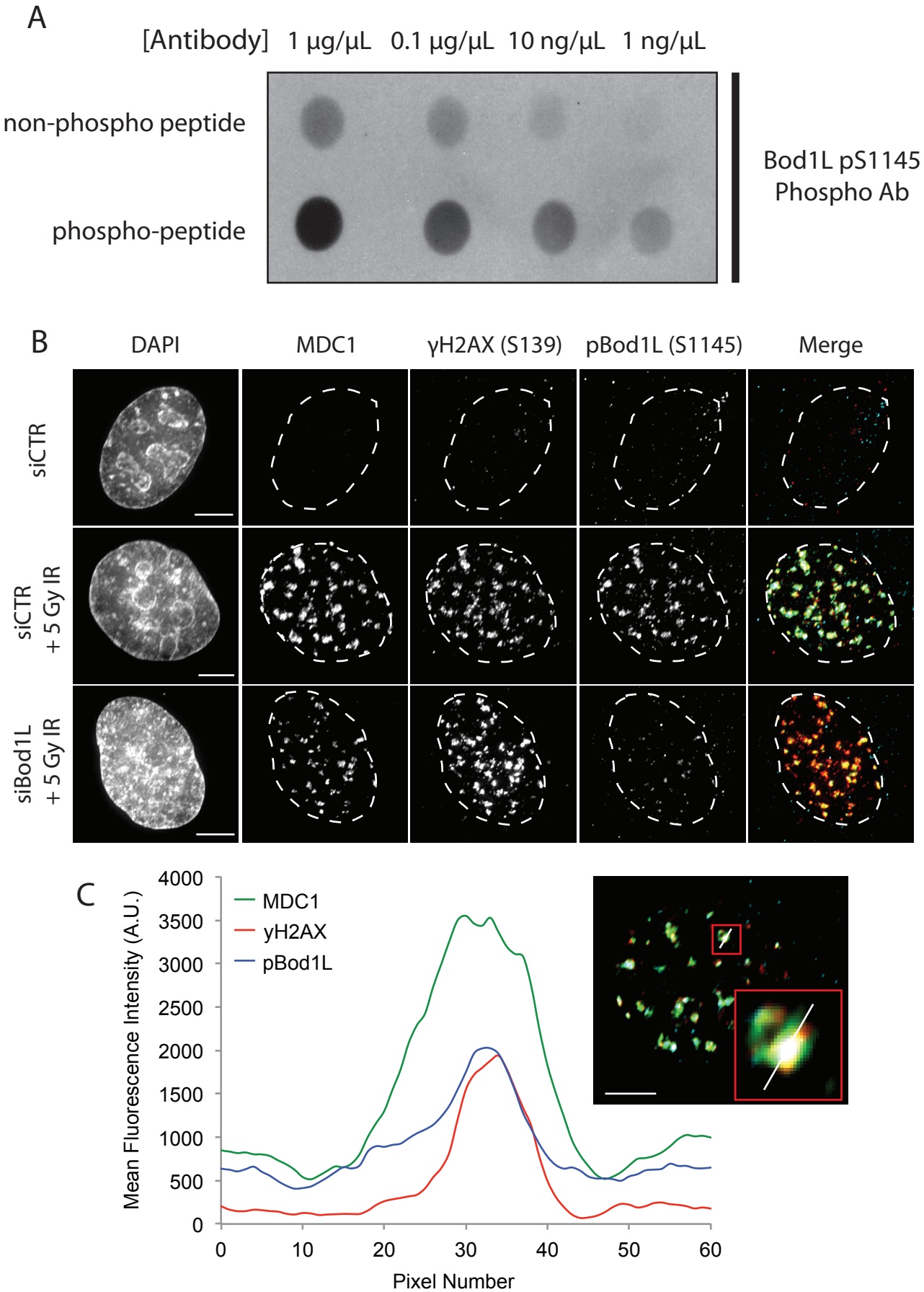
A
[Antibody] 1 µg/µL 0.1 µg/µL 10 ng/µL 1 ng/µL
non-phospho peptide
phospho-peptide
Bod1L pS1145
Phospho Ab
B
DAPI
MDC1
γH2AX (S139)
pBod1L (S1145)
Merge
siCTR
siCTR
+ 5 Gy IR
siBod1L
+ 5 Gy IR
C
MDC1
yH2AX
pBod1L
Mean Fluorescence Intensity (A.U.)
4000
3500
3000
2500
2000
1500
1000
500
0
0
10
20
30
40
50
60
Pixel Number

Figure 3.10: Bod1L is phosphorylated at S1145 at IRIF

(A) Dot blot of pBod1L S1145 antibody with a dilution series of the non-phosphorylated (upper row) and phosphorylated (lower row) antigenic peptide NH_2-CDNRNNN[pS]QQDID-COOH corresponding to D1138-D1150 of human Bod1L.

(B) Immunostaining of mock or IR treated HeLa cells transfected with control or Bod1L siRNA. Cells were exposed to 5 Gy IR 48 hours after transfection. Cells were fixed two hours post IR treatment and immuno-stained for MDC1 (green), γH2AX (pS139) (red) or Bod1L (pS1145) (cyan).

(C) HeLa cells were treated with 5 Gy IR and immunostained for MDC1 (green), γH2AX (pS139) (red) or Bod1L (pS1145) (cyan). Protein accumulation at the damage foci indicated (inset) was determined by quantifying the fluorescent intensity of each channel along the indicated line.

ATM activation and down-stream signalling is unaffected by depletion of Bod1L

The DNA damage kinase ATM has been shown to physically interact with a number of critical DNA damage signalling and effector proteins including Nbs1 (Gatei et al., 2000b), Rad51 (Chen et al., 1999), BRCA1 (Gatei et al., 2000a) and Chk2 (Paz et al., 2010). These interactions have proven to be critical for mediating correct phosphorylation of target proteins and the subsequent down stream signalling and protein recruitment to sites of damage. To assess any potential interaction between ATM and Bod1L, I immunoprecipitated Bod1L from HeLa cells expressing Bod1L-GFP and observed no evidence of active ATM binding in a chromatin cell fraction, above that of control levels (Figure 3.11A).

Although Bod1L and ATM do not interact, the data in figure 3.9 strongly suggests that Bod1L is an ATM target following DNA damage. It has previously been shown that loss of some ATM targets, such as the MRN complex, can lead to changes in ATM activation and activity (Uziel et al., 2003). To determine whether loss of Bod1L from cells had a similar effect on ATM activity, HeLa cells were depleted of Bod1L, treated with a low dose of IR and allowed to recover (Figure 3.11B). No loss of ATM auto-phosphorylation could be detected in the absence of Bod1L, suggesting that sustained ATM activation was unaffected. Moreover, when cells were allowed to fully recover from IR induced DNA lesions, siBod1L treatment did not prevent proper inactivation of ATM following damage resolution (Figure 3.11C). To probe the activation and signalling of ATM following Bod1L depletion further, HeLa cells were depleted

of Bod1L, treated with a titration of the ATM inhibitor KU59933 and then dosed with IR and lysed immediately (Figure 3.11D). Loss of Bod1L from cells once again had no effect on ATM auto-phosphorylation, nor did it affect the phosphorylation of downstream targets of ATM such as Chk2. Bod1L knock-down also had no effect on the potency of KU59933 ATM inhibition. These data from figure 3.9 and figure 3.11 taken together suggest that although Bod1L is a phosphorylation target of ATM, loss of Bod1L from cells has no observable effect on ATM kinase activity following DNA damage.

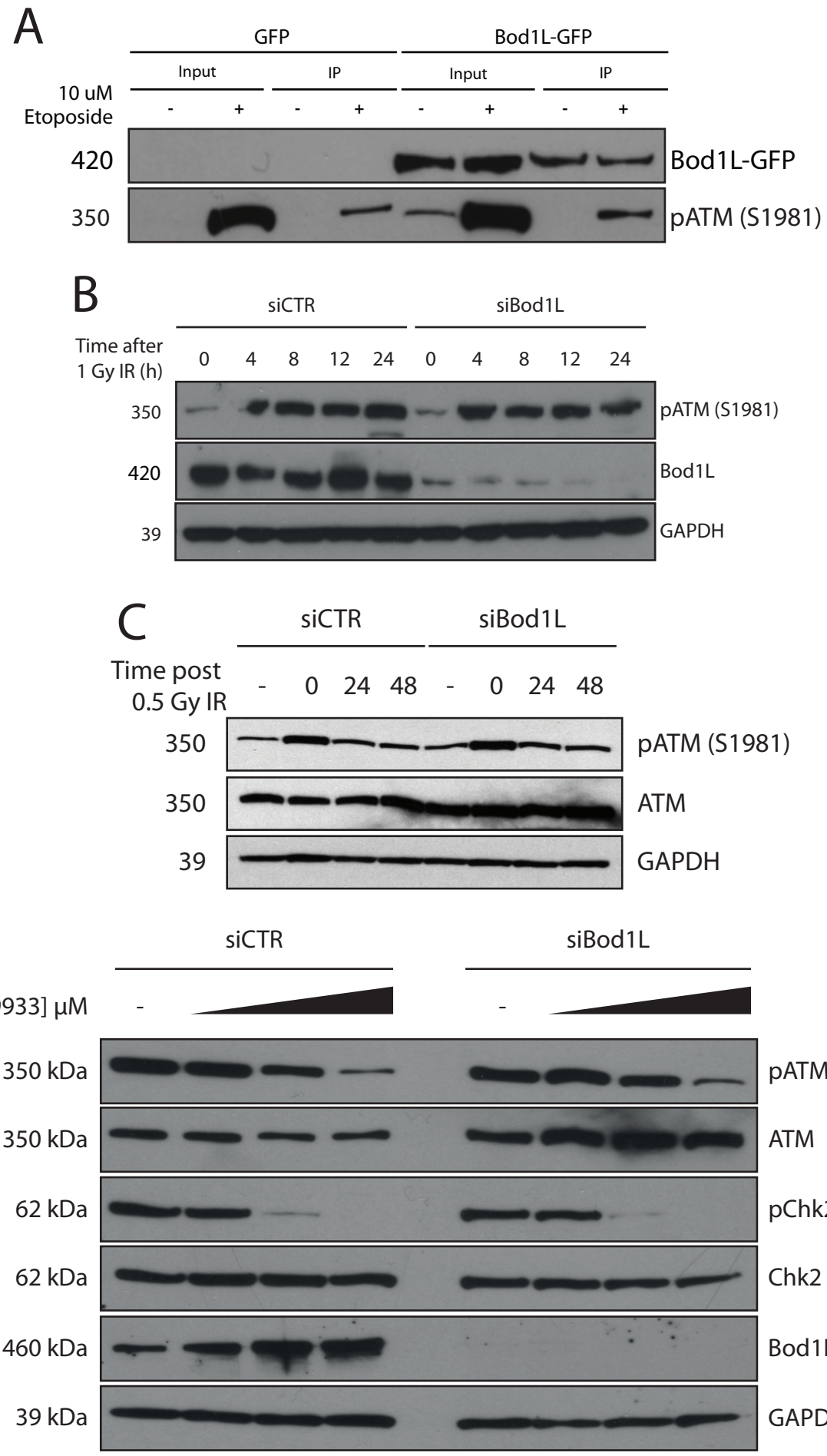
A
GFP
Bod1L-GFP
Input
IP
Input
IP
10 uM Etoposide
- + - + - + - +
420
Bod1L-GFP
350
pATM (S1981)
B
siCTR
siBod1L
Time after 1 Gy IR (h)
0 4 8 12 24 0 4 8 12 24
350
pATM (S1981)
420
Bod1L
39
GAPDH
C
siCTR
siBod1L
Time post 0.5 Gy IR
- 0 24 48 - 0 24 48
350
pATM (S1981)
350
ATM
39
GAPDH
D
siCTR
siBod1L
[KU59933] µM
-
-
350 kDa
pATM (S1981)
350 kDa
ATM
62 kDa
pChk2 (T68)
62 kDa
Chk2
460 kDa
Bod1L
39 kDa
GAPDH

Figure 3.11: Loss of Bod1L does not affect ATM kinase activity

(A) GFP-Trap Immunoprecipitation (IP) of Bod1L-GFP from the chromatin fraction of HeLa cells was performed. Prior to lysis, cells were treated +/- 10 μM Etoposide for 24 hours. IPs were analysed by western blotting using antibodies against GFP and pATM (S1981).

(B) Immunoblots of HeLa cells treated with control or Bod1L siRNA and 1 Gy IR. Cell lysates were collected at the time points indicated and analysed using antibodies against pATM (S1981), Bod1L and GAPDH.

(C) Immunoblots of HeLa cells treated with control or Bod1L siRNA and 0.5 Gy IR. Control cells were mock irradiated. Cell lysates were collected at 0, 24 and 48 hours and analysed using antibodies against pATM (S1981), ATM and GAPDH.

(D) Immunoblots of HeLa cells treated with control or Bod1L siRNA. Prior to treatment with 5 Gy IR, cells were incubated for 1 hour in an increasing concentration of KU59933. Cell lysates were collected after 1 hour and analysed using antibodies against pATM (S1981), ATM, pChk2 (T68), Chk2, Bod1L and GAPDH.

Discussion

The data presented in this chapter reveal Bod1L as a novel component of the DNA damage repair machinery. Bioinformatic analysis reveals Bod1L to contain few annotated regions that would suggest the function of this protein. Whilst not as detrimental as a loss of BRCA2, depletion of Bod1L led to hypersensitivity to a range of DNA lesions and fixed cell immunofluorescence analysis revealed that Bod1L depletion resulted in severe genomic instability. ATM signalling is unaffected in the absence of Bod1L and these two proteins do not physically interact in the presence or absence of DNA damage. Unlike the vast majority of DNA damage repair proteins, I found no evidence that Bod1L is specifically re-localised or recruited in excess to DNA lesions. Instead, phospho-proteomic analysis of ATM/ATR substrates identified Bod1L as an ATM target upon DNA damage, which was confirmed using phospho-specific antibodies raised against these sites (Matsuoka et al., 2007). Bod1L S1710 is rapidly phosphorylated at sites of DNA damage in a manner analogous with the phosphorylation of γH2AX and the γH2AX dependent recruitment of MDC1. Treatment of cells with ATM specific inhibitors, demonstrated that Bod1L is phosphorylated by ATM, which was confirmed by *in vitro* phosphorylation of Bod1L-T at S1710 using recombinant DNA-PK.

Although the phosphorylation of Bod1L by ATM at S1710/S1145 in response to DNA damage is clear, the functional significance of these likely ATM sites on Bod1L remains unclear. Functional rescues of Bod1L depletion revealed that mutation of either site individually, or together, had no effect on the ability of Bod1L-GFP to rescue clonogenic sensitivity to MMC. Recent literature has

highlighted evidence for multiple ATM phosphorylation sites on a key DNA damage repair component, which can display a degree of redundancy (Cheng et al., 2009). These multiple ATM target sites near a key domain of the MDM2 protein, function in a redundant manner to provide robust DNA damage signalling. The additional ATM phosphorylation sites on Bod1L identified from bioinformatic analysis as well as ultradeep phosphoproteome studies (Sharma et al., 2014)(Figure 3.1G), suggest that in the event of single or even double mutations at these key sites, other phosphorylation sites on Bod1L could still elicit a cellular effect. An alternative PIKK kinase, DNA-dependent protein kinase (DNA-PK) is able to phosphorylate key ATM targets, such as H2AX, in cells depleted of ATM (Stiff et al., 2004). Given that ATM and DNA-PK are able to function in a redundant, overlapping manner, it is possible that when key ATM phosphorylation sites are modified on Bod1L, other previously redundant sites are modified via alterative kinases. More detailed phospho-proteomic analysis specifically of Bod1L phosphorylation before and after DNA damage is needed to verify these additional sites.

Bod1L sequence analysis reveals a highly conserved, proline-rich region at the N-terminus of the protein, located prior to the Bod1 homologous region (Figure 3.1A). Such proline-rich repeats have been shown to facilitate a range of protein-protein interactions with a variety of proteins containing SH3, WW and EVH1 domains (Kay et al., 2000). SH3-Proline domain signalling has shown to play an important role in a number of cellular process, such as the response to DNA damage (Shafman et al., 1997), with the crystal structure having been recently solved for the SH3 domain of the phosphoinositide 3-kinases (Chen et al., 2011). Whilst the necessity of this proline-rich region of Bod1L was not

investigated during this study, it presents an interesting future target for modulating the signalling pathways associated with Bod1L.

Assessment of common cancer cell mutations revealed that Bod1L has been identified with over 400 unique mutations in tumour samples analysed (Forbes et al., 2015). A large majority of these mutations (>75%) resulted in missense mutation. Whilst tissue distribution of these mutations appears varied, the presence of so many mutations in cancer tissue reveals an interesting target for future investigation and suggests that mutations in Bod1L may act as drivers for cancer development.

The data presented in figure 3.5 implies that genomic instability associated with Bod1L depletion does not arise due to a failure in the FA pathway. Yet one open question that remains is how depletion of Bod1L leads to the failure of DNA repair by homologous recombination (Figure 3.4). Previous papers have demonstrated that the mislocalisation of the key DNA damage repair proteins BRCA2 and Rad51, via depletion or deletion of interacting proteins, can lead to a failure of DNA repair and subsequent genomic instability (Davies et al., 2001; Moynahan et al., 2001; Saitoh et al., 2002). Given the data in figure 3.11, demonstrating that ATM activation and downstream signalling is unaffected following Bod1L depletion, one hypothesis could be that phosphorylation of Bod1L by ATM controls recruitment or retention of other proteins at DNA lesions. Thus, loss of Bod1L would affect any associated binding of such proteins.

Another consideration of why HR may be compromised in Bod1L depletion cells is that phosphorylation of other ATM or casein kinase 2 (CK2) targets may be affected as a result of Bod1L loss. I have already demonstrated that ATM function is normal following Bod1L depletion, so if phosphorylation of other DNA repair proteins is affected then is this may be due to compromised or uncontrolled phosphatase activity. Figure 1.7 expresses the complexity of Serine/Threonine phosphatase activity associated with DNA damage repair. As such it is highly likely that any factor that altered the careful kinase/phosphatase balance would have a dramatic effect on maintaining robust DNA repair. Indeed, several recent studies have demonstrated that depletion of either a phosphatase directly (PP6) or a controlling/regulatory protein (TIPRL/PP2A, PNUTS/PP1) can lead to hypersensitivity to genotoxic stress, decreased clonogenic survival, changes in protein phosphorylation and protein mislocalisation (Douglas et al., 2010; Landsverk et al., 2010; McConnell et al., 2007). Figure 3.1 showed that Bod1L contains a region of homology with the mitotic PP2A-B56 inhibitor, Bod1. Given the sequence similarity of this region between Bod1 and Bod1L and the high degree of conservation of this site in Bod1L, investigation is needed to understand whether Bod1L also acts as a PP2A interacting protein at sites of DNA damage. The following chapter is dedicated to exploring the role of Bod1L in controlling PP2A activity at DNA lesions.

Chapter 4 - Bod1L controls MDC1 and PP2A-56 recruitment to sites of DNA damage

The data in Chapter 3 revealed Bod1L as a novel component of the DNA damage repair machinery, with loss of Bod1L resulting in compromised damage repair and genomic instability. Unlike other DDR proteins, Bod1L associates with chromatin during all non-mitotic phases of the cell cycle and is not actively recruited to DNA lesions. Instead, I showed that upon DNA damage, ATM rapidly phosphorylates Bod1L at multiple sites, suggesting Bod1L may act as some form of signalling platform.

Whilst I have evidence of ATM phosphorylation of Bod1L occurring specifically at DNA lesions, the functional consequence of such a modification remains unclear. Indeed, the mechanism by which Bod1L plays a role in the normal DNA damage response still remains uncertain. The data and evidence presented in this chapter aims to establish the functional role of Bod1L, both before and after DNA damage has occurred, and attempt to elucidate the mechanism by which Bod1L depletion leads to the observed genomic instability.

Results

Depletion of Bod1L results in changes in the dynamics of DNA repair proteins at sites of DNA damage

Phosphorylation of the histone H2A variant H2AX at Ser139 by ATM establishes a binding site onto which regulators of DNA damage repair are able to accumulate (Burma et al., 2001; Rogakou et al., 1998; Stiff et al., 2004).

MDC1 is recruited via this phospho-epitope and acts as a crucial scaffold for further protein recruitment and signal amplification (Lou et al., 2006; Stewart et al., 2003; Stucki and Jackson, 2006). I assessed the formation of γH2AX foci formation following etoposide treatment (Figure 4.1A), which determined that peak foci intensity was achieved between 16-24 hours of 10 μM etoposide treatment. Incubation with etoposide in excess of 24 hours led to apoptosis and nuclear morphology changes. Following 16 hours of etoposide treatment I observed that phosphorylation of H2AX was unaffected after Bod1L depletion (Figure 4.1B). Whilst I saw no change in γH2AX phosphorylation following Bod1L depletion, MDC1 recruitment to damage sites after etoposide treatment was significantly increased in the absence of Bod1L (Figure 4.1B).

To determine whether the increase in MDC1 accumulation following Bod1L depletion was due to increased DNA damage or failure to repair existing damage, I treated HeLa cells with etoposide, before washout of the drug and assessment of MDC1 accumulation. Under these conditions, no additional etoposide-associated DNA damage could occur following washout. I observed that when siBod1L cells were allowed to recover from DNA damage, MDC1 accumulation on chromatin continued to increase, in contrast to siCTR treated cells where MDC1 chromatin recruitment remained stable or decreased as damage was repaired (Figure 4.1C, D). This result suggests that rather than etoposide exhibiting an increased damaging effect in the absence of Bod1L, MDC1 was hyper-recruited to existing damage sites in the absence of Bod1L.

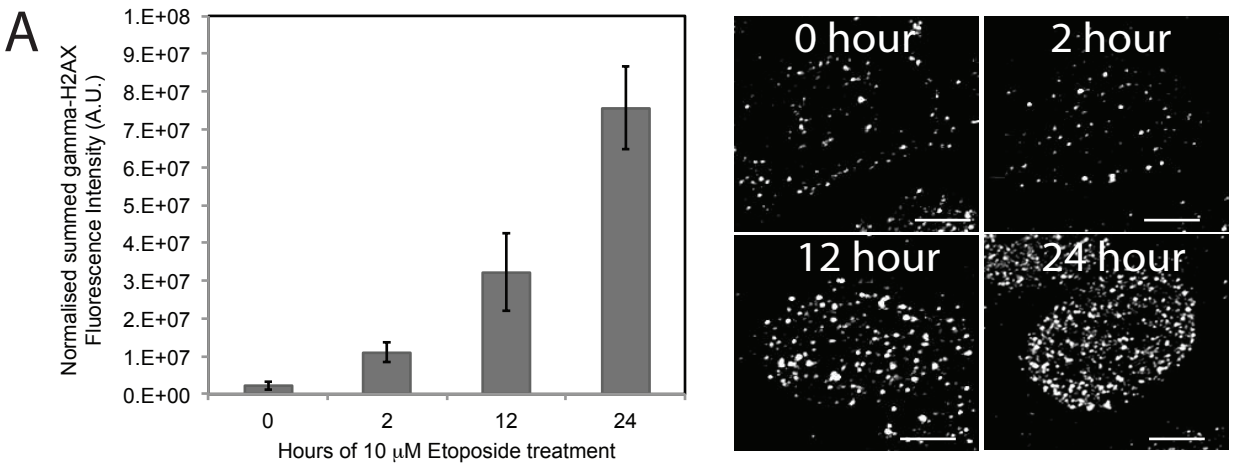
A
Normalised summed gamma-H2AX Fluorescence Intensity (A.U.)
1.E+08
9.E+07
8.E+07
7.E+07
6.E+07
5.E+07
4.E+07
3.E+07
2.E+07
1.E+07
0.E+00
0
2
12
24
Hours of 10 μM Etoposide treatment
0 hour
2 hour
12 hour
24 hour

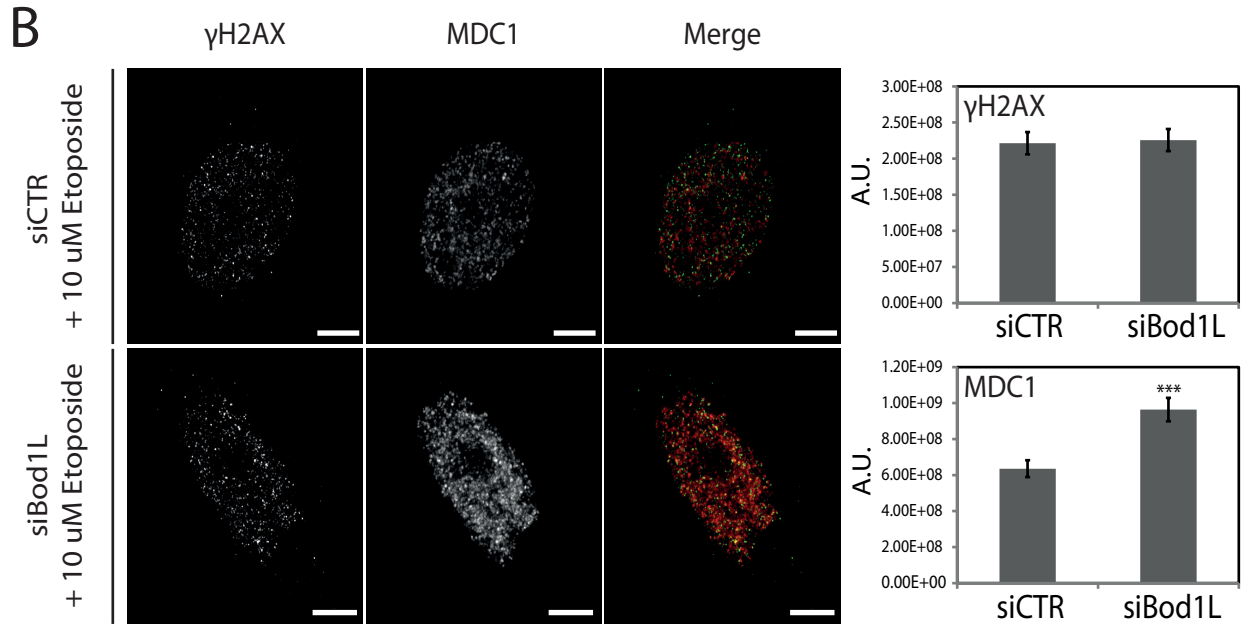
B
γH2AX
MDC1
Merge
siCTR
+ 10 uM Etoposide
siBod1L
+ 10 uM Etoposide
γH2AX
A.U.
3.00E+08
2.50E+08
2.00E+08
1.50E+08
1.00E+08
5.00E+07
0.00E+00
siCTR
siBod1L
MDC1
A.U.
1.20E+09
1.00E+09
8.00E+08
6.00E+08
4.00E+08
2.00E+08
0.00E+00
***
siCTR
siBod1L

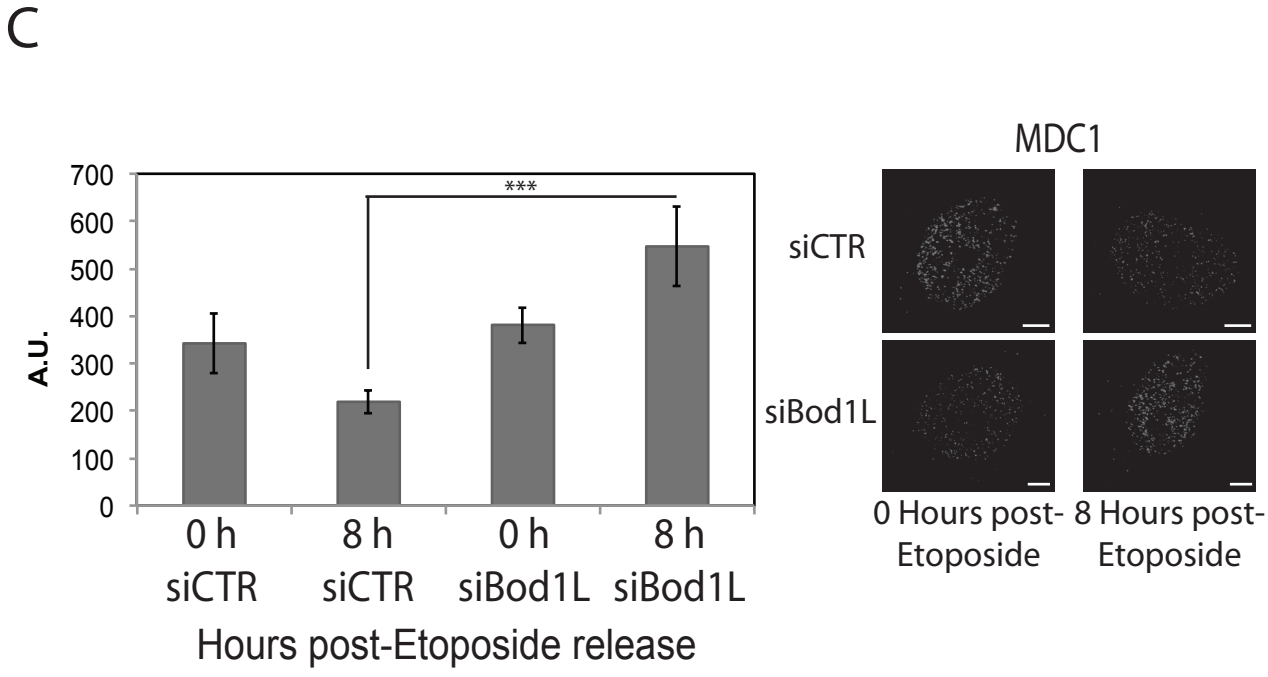
C
A.U.
700
600
500
400
300
200
100
0
***
0 h siCTR
8 h siCTR
0 h siBod1L
8 h siBod1L
Hours post-Etoposide release
MDC1
siCTR
siBod1L
0 Hours post-Etoposide
8 Hours post-Etoposide

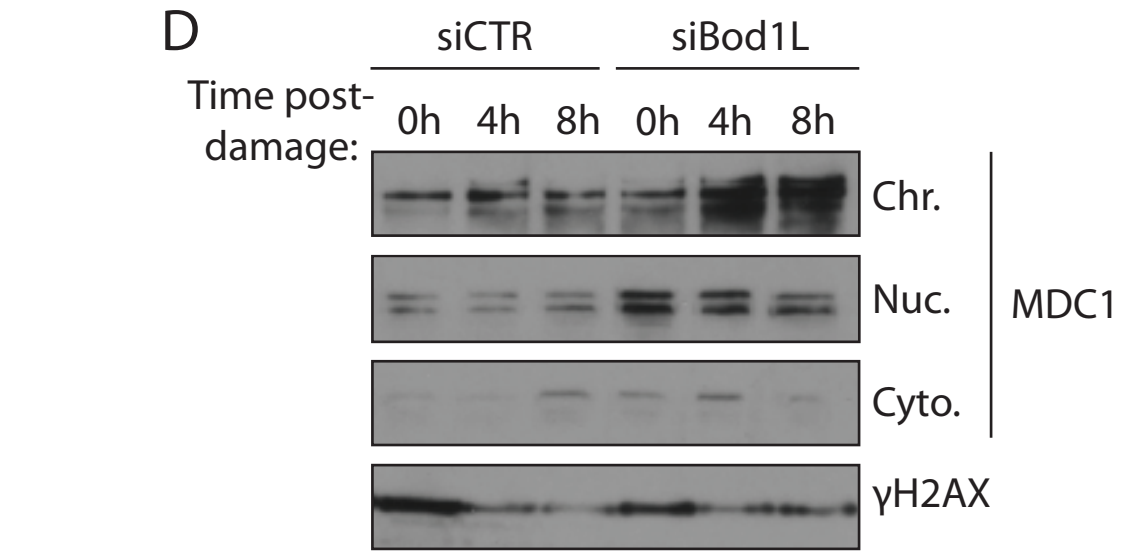
D
siCTR
siBod1L
Time post-damage:
0h 4h 8h 0h 4h 8h
Chr.
Nuc.
Cyto.
MDC1
γH2AX

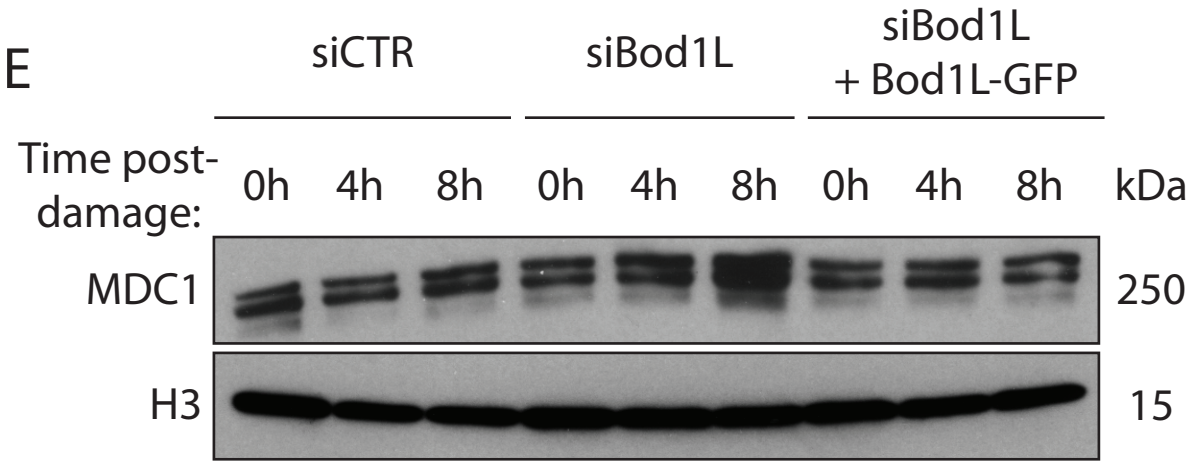
E
siCTR
siBod1L
siBod1L + Bod1L-GFP
Time post-damage:
0h 4h 8h 0h 4h 8h 0h 4h 8h
kDa
MDC1
250
H3
15

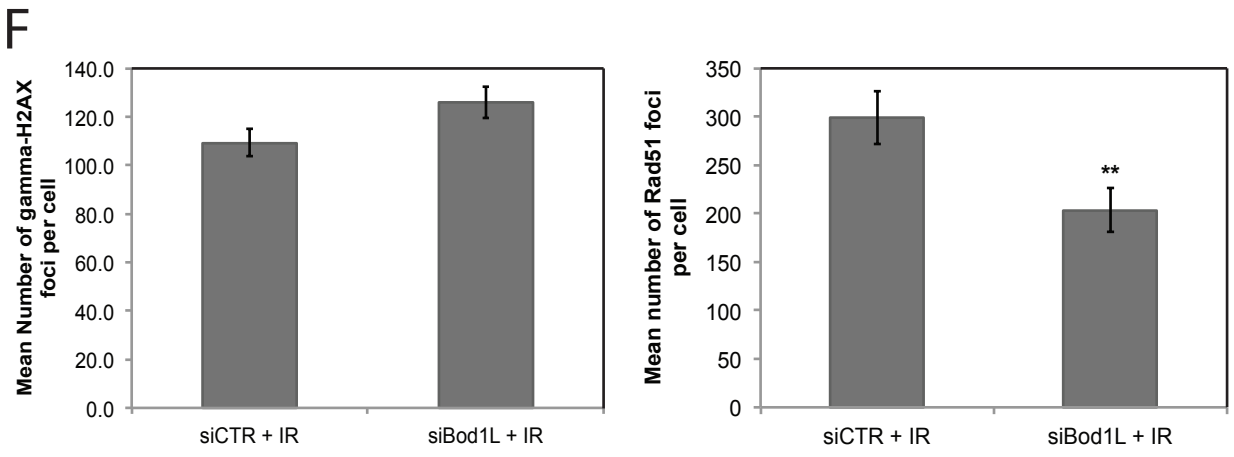
F
Mean Number of gamma-H2AX foci per cell
140.0
120.0
100.0
80.0
60.0
40.0
20.0
0.0
siCTR + IR
siBod1L + IR
Mean number of Rad51 foci per cell
350
300
250
200
150
100
50
0
**
siCTR + IR
siBod1L + IR

G

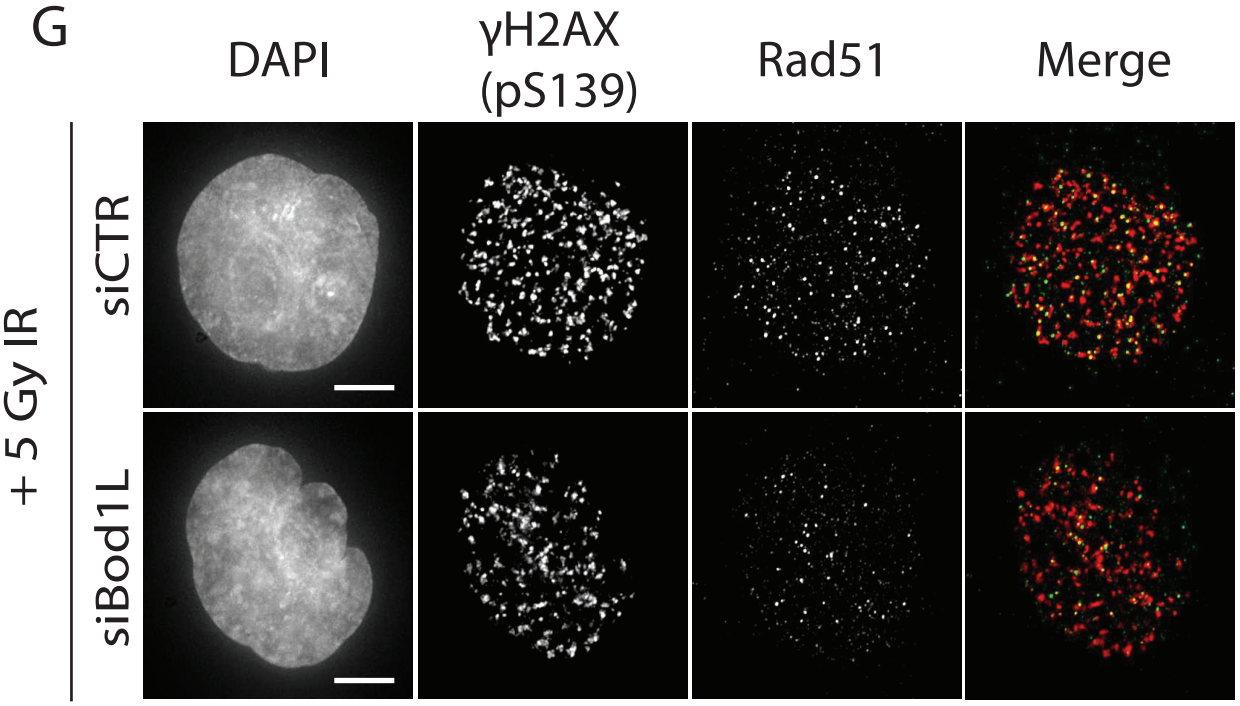
DAPI
γH2AX (pS139)
Rad51
Merge
+ 5 Gy IR
siCTR
siBod1L

H

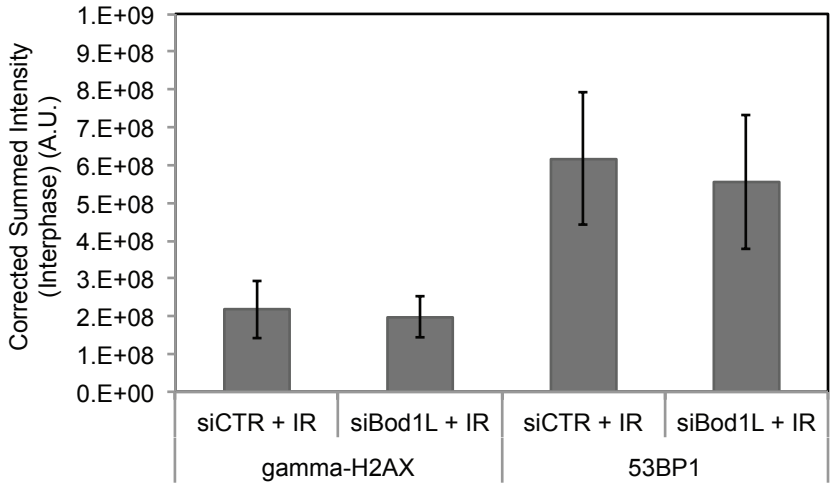
Corrected Summed Intensity (Interphase) (A.U.)
1.E+09
9.E+08
8.E+08
7.E+08
6.E+08
5.E+08
4.E+08
3.E+08
2.E+08
1.E+08
0.E+00
siCTR + IR
siBod1L + IR
siCTR + IR
siBod1L + IR
gamma-H2AX
53BP1

I

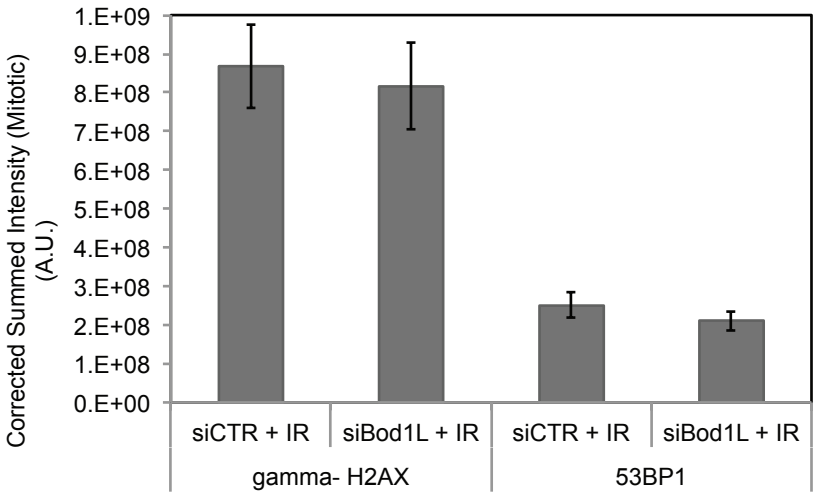
Corrected Summed Intensity (Mitotic) (A.U.)
1.E+09
9.E+08
8.E+08
7.E+08
6.E+08
5.E+08
4.E+08
3.E+08
2.E+08
1.E+08
0.E+00
siCTR + IR
siBod1L + IR
siCTR + IR
siBod1L + IR
gamma- H2AX
53BP1

Figure 4.1: Changes in the dynamics of DNA repair proteins at sites of damage in Bod1L depleted cells

(A) HeLa cells were transfected with control siRNA. After 48 hours cells were treated with 10 μM etoposide for the time indicated then immediately fixed in PFA and stained for γH2AX (pS139). DMSO only was used for 0 μM control. Projections of representative images are shown underneath. Graph shows quantification of fluorescence signal for γH2AX. >10 cells per condition. Data represented as mean ± SEM. Scale bar, 5 microns.

(B) HeLa cells were transfected with control or Bod1L siRNA. After 48 hours cells were treated with 10 μM etoposide for 16 hours then immediately fixed in PFA and stained for MDC1 (red) and γH2AX (pS139)(green). Projections of representative images are shown. Right hand panels show quantification of fluorescence signal for each channel. >10 cells per condition, two independent experiments. Data represented as mean ± SEM. ***P<0.001. Scale bar, 5 microns.

(C) HeLa cells were transfected with control or Bod1L siRNA. 48 hours post transfection cells were treated with 10 μM etoposide for 24 hours before washout and fixation in PFA at 0 and 8 hours post washout. Endogenous MDC1 was immunostained. Upper panel shows representative projections of MDC1 signal. Lower panel shows quantification of MDC1 signal. 20 cells per condition, representative images and quantitation of 2 independent experiments. Data represented as mean ± SEM. ***P<0.001. Scale bar, 5 microns.

(D) HeLa cells transfected with control or Bod1L siRNA were treated with etoposide before wash-out of the drug and subcellular fractionation lysis at 0, 4 and 8 hours post wash-out. Chromatin, nucleoplasmic and cytoplasmic fraction immunoblot of MDC1 is shown along with γH2AX chromatin immunoblot.

(E) HeLa cells transfected with control or Bod1L siRNA were treated with etoposide before wash-out of the drug and subcellular fractionation lysis at 0, 4 and 8 hours post wash-out. Chromatin fraction immunoblot of MDC1 is shown. Rescue experiments were performed by transfecting HeLa cells with Bod1L siRNA targeting the 3'UTR of Bod1L. Cells were then transfected with Bod1L-GF before treatment. Histone H3 was used as a loading control.

(F) HeLa cells were transfected with control or Bod1L siRNA. After 48 hours cells were treated with 5 Gy IR and samples were fixed in PFA after 2 hours. Cells were immuno-stained for and quantified for endogenous γH2AX (S139) and Rad51. Data shows mean number of foci per cell and is represented as mean ± SEM. n=20 for each condition. **P<0.01.

(G) Representative images from (H). Images show maximum intensity projections of cells stained immuno-stained for endogenous γH2AX (S139)(red) and Rad51 (green). Scale bar, 5 microns.

(H, I) HeLa cells were transfected with control or Bod1L siRNA. 48 hours post transfection, cells were dosed with 5 Gy IR, incubated for 1 hour at 37°C before being PFA fixed and stained with antibodies against γH2AX (S139), 53BP1 and ACA. Interphase (H) and mitotic cells (I) were identified by ACA and DAPI staining. 20 cells per condition were imaged, quantitation of 2 independent experiments. Data represented as mean ± SEM.

Figure 4.1D demonstrates that the over-accumulation of MDC1 in the absence of Bod1L occurs only in the chromatin fraction of the cell lysate. To verify that this increased recruitment of MDC1 to sites of DNA damage is a Bod1L specific effect, cells were treated with siRNA targeting the 3'UTR of Bod1L and exogenous Bod1L-GFP was expressed in these cells (Figure 4.1E). Expression of Bod1L-GFP in si3'UTR treated cells rescued the accumulation of MDC1 at damage sites.

As mentioned previously, MDC1 acts as a crucial scaffold whose activity is regulated by phosphorylation. MDC1 controls further protein recruitment and signal amplification in response to DNA damage. Whilst loss of MDC1 is known to lead to genomic instability and compromised DNA repair by HR in both cell lines and knockout mice; very little is understood regarding the effect of MDC1 over accumulation at DNA lesions (Lou et al., 2003; 2006; Stewart et al., 2003; Zhang et al., 2005). To understand the downstream effect of excessive MDC1 accumulation, I assayed the formation of Rad51 foci in the presence and absence of Bod1L (Figure 4.1F, G). Rad51 is a protein recruited to damaged DNA further downstream of MDC1 that plays a major role in the repair of DSBs by HR, a process shown to be affected by Bod1L depletion (Figure 3.4) (Baumann and West, 1998). As the quantification and representative micrographs show, loss of Bod1L led to a small, but reproducible decrease in the number of Rad51 foci in damaged cells, whilst the number of γH2AX foci remained unaffected. This Bod1L knockdown mediated decrease in the critical HR protein, responsible for promoting homologous pairing and strand exchange, could explain the compromised HR repair demonstrated in figure 3.4C.

The importance of timely and regulated recruitment and signalling at DNA lesions was further highlighted in two recent papers, describing the role of 53BP1 in DNA damage repair during interphase and mitosis (Lee et al., 2014; Orthwein et al., 2014). Here the authors describe that the reversal of 53BP1 inactivation during mitosis, allowing 53BP1 recruitment to DNA lesions, is dependent on targeted phosphatase activity. Given the possible phosphatase interaction with Bod1L, I wanted to investigate whether this defined process was functional following Bod1L depletion. siCTR or siBod1L cells were treated with ionising radiation and intensity of γH2AX and 53BP1 signal was measured in an interphase population (Figure 4.1H) and a mitotic population (Figure 4.1I). The data revealed that 53BP1 recruitment to DNA lesions was unaffected by Bod1L depletion during interphase (Figure 4.1H) and that 53BP1 recruitment was inhibited correctly during mitosis (Figure 4.1I), suggesting no role for Bod1L in this pathway.

Depletion of Bod1L leads to changes in MDC1 localisation and dynamics at sites of DNA damage

Data from figure 4.1 suggested that loss of Bod1L led to a failure in correctly localising MDC1 to sites of DNA damage. This data generally assessed the increase of MDC1 at chromatin on a population-basis. To assess recruitment of MDC1 to sites of damage on a single-cell basis, I performed a live cell GFP-

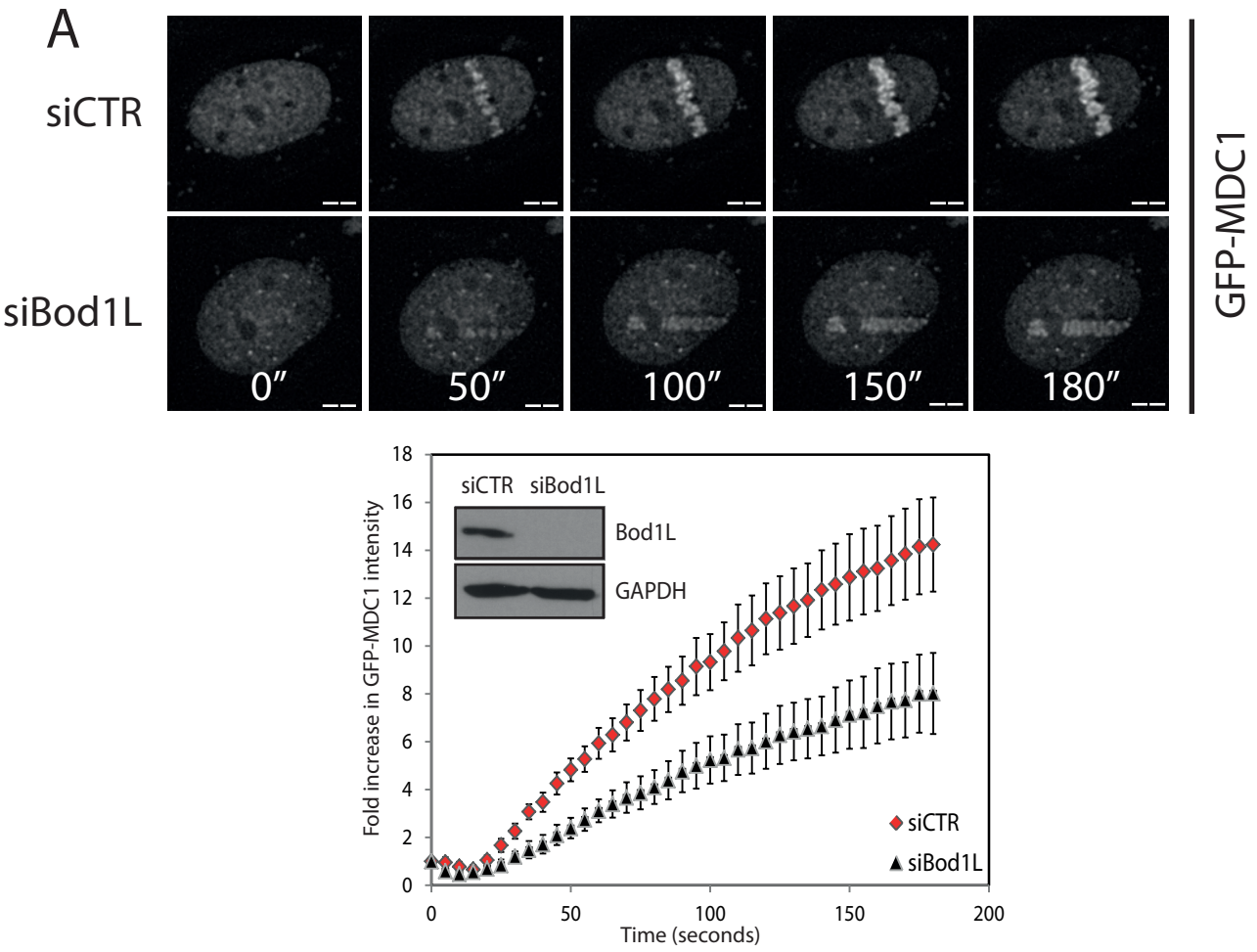
A
siCTR
siBod1L
0″
50″
100″
150″
180″
GFP-MDC1
siCTR siBod1L
Bod1L
GAPDH
Fold increase in GFP-MDC1 intensity
Time (seconds)
siCTR
siBod1L

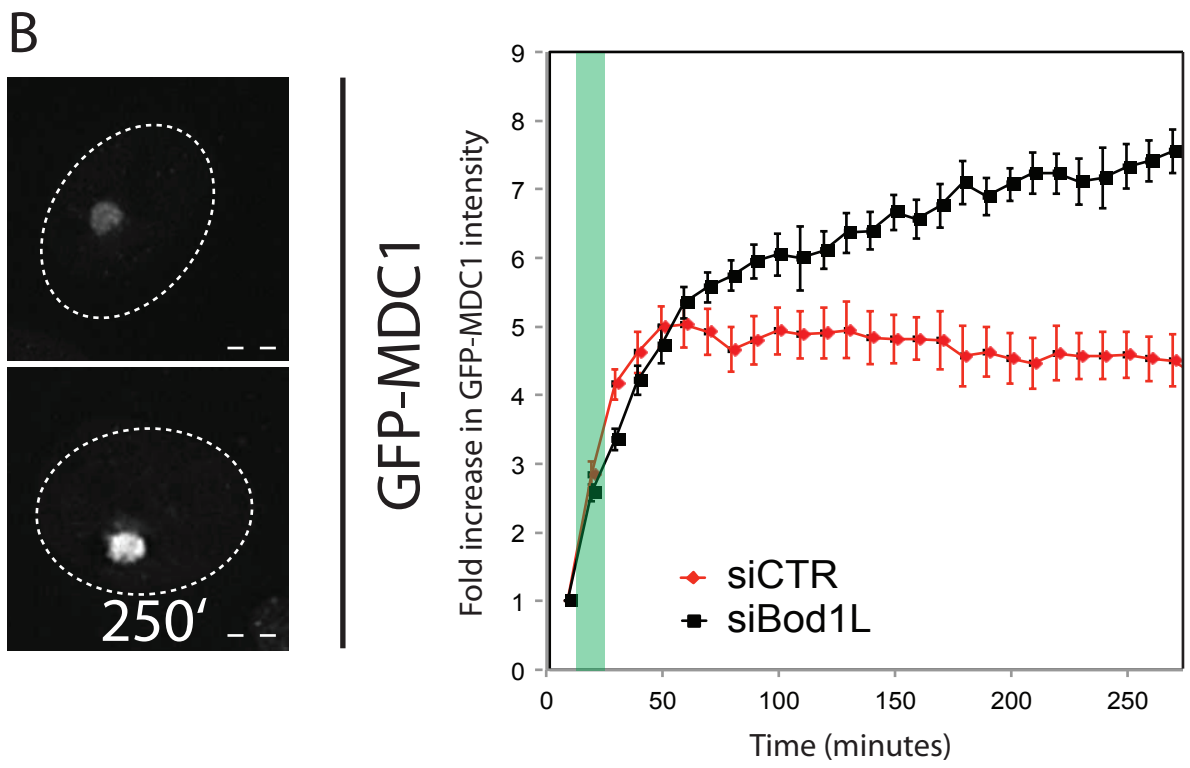
B
250′
GFP-MDC1
Fold increase in GFP-MDC1 intensity
Time (minutes)
siCTR
siBod1L

C

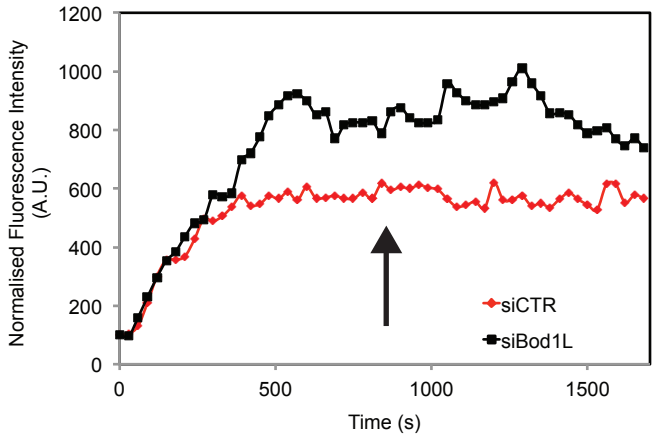
Normalised Fluorescence Intensity (A.U.)
1200
1000
800
600
400
200
0
0
500
1000
1500
Time (s)
siCTR
siBod1L

D

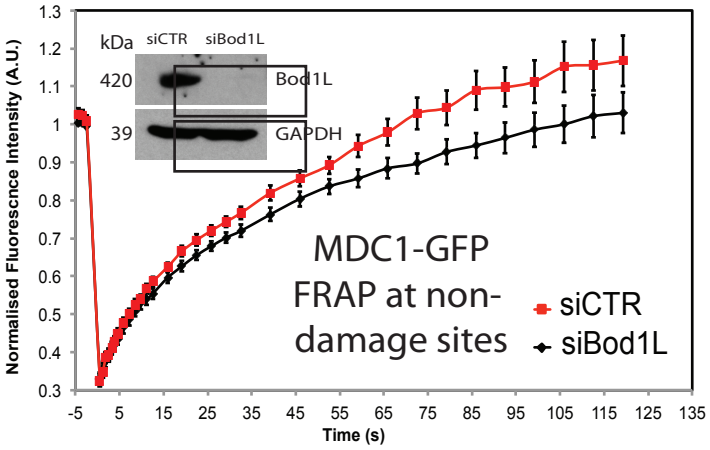
Normalised Fluorescnce Intensity (A.U.)
1.3
1.2
1.1
1
0.9
0.8
0.7
0.6
0.5
0.4
0.3
kDa
siCTR
siBod1L
420
Bod1L
39
GAPDH
MDC1-GFP
FRAP at non-
damage sites
siCTR
siBod1L
-5
5
15
25
35
45
55
65
75
85
95
105
115
125
135
Time (s)

E

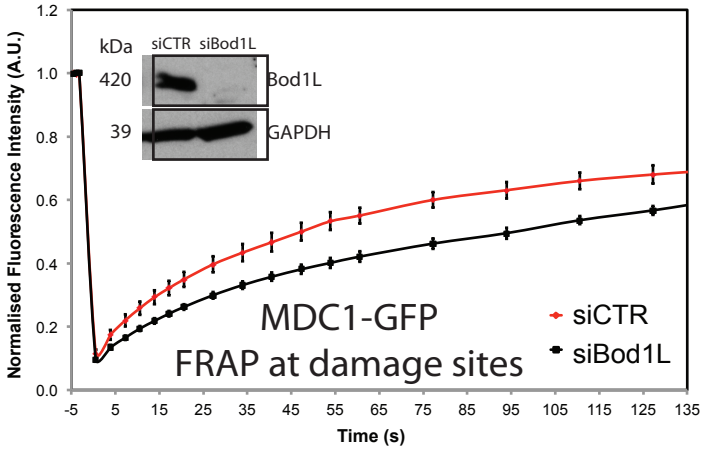
Normalised Fluorescence Intensity (A.U.)
1.2
1.0
0.8
0.6
0.4
0.2
0.0
kDa
siCTR
siBod1L
420
Bod1L
39
GAPDH
MDC1-GFP
FRAP at damage sites
siCTR
siBod1L
-5
5
15
25
35
45
55
65
75
85
95
105
115
125
135
Time (s)

F

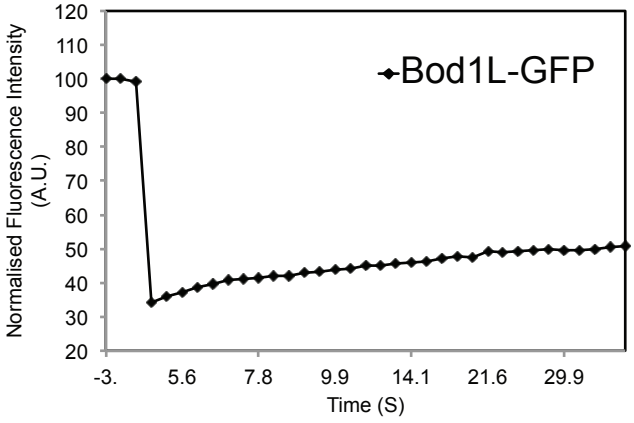
Normalised Fluorescence Intensity (A.U.)
120
110
100
90
80
70
60
50
40
30
20
Bod1L-GFP
-3.
5.6
7.8
9.9
14.1
21.6
29.9
Time (S)

Figure 4.2: Depletion of Bod1L leads to changes in MDC1 localisation to sites of DNA damage

(A) U2OS cells stably expressing GFP-MDC1 were transfected with control siRNA or Bod1L siRNA and pre-treated with Hoechst 33342. Cells were striped or spotted with 405 nm laser and GFP-MDC1 fluorescent intensity accumulation was measured within a narrow temporal window. Upper panel shows representative images for each time-point. Bod1L depletion was assessed by immunoblotting (inset), GAPDH was used as loading control. Time from onset of laser stripe is shown underneath. Data represented as mean ± SEM. n=>20 for each condition. Scale bars, 5 microns.

(B) U2OS cells stably expressing GFP-MDC1 were transfected with control siRNA or Bod1L siRNA and pre-treated with Hoechst 33342. Cells were striped or spotted with 405 nm laser and GFP-MDC1 fluorescent intensity accumulation was measured over a longer period of time. Green box represents time-period of (A). Left hand panel shows representative images for selected time-points. Bod1L depletion was assessed by immunoblotting (inset), GAPDH was used as loading control. Data represented as mean ± SEM. n=>20 for each condition. Scale bars, 5 microns.

(C) U2OS cells stably expressing GFP-MDC1 were transfected with control siRNA or Bod1L siRNA. DNA Damage was generated by pre-treating cells with Hoechst 33342 and 405 nm laser striping. GFP-MDC1 fluorescence at the damage stripe was assessed, with the plateau of re-localisation indicated by the arrow

(D) U2OS cells stably expressing GFP-MDC1 were transfected with control siRNA or Bod1L siRNA and FRAP was performed at sites of non-damage sites. Bod1L depletion was assessed by immunoblotting (inset). GAPDH was used as a loading control.

(E) U2OS cells stably expressing GFP-MDC1 were transfected with control siRNA or Bod1L siRNA and FRAP was performed at sites of damage. Damage was generated by pre-treating with Hoechst 33342 and 405 nm laser striping. FRAP was performed once GFP-MDC1 levels had plateaued (Indicated by arrow in (B)). Bod1L depletion was assessed by immunoblotting (inset). GAPDH was used as a loading control.

(F) HeLa cells were transfected with Bod1L-GFP. After 48 hours, FRAP was performed at a non-damaged nuclear site and recovery was assessed over time period indicated.

MDC1 recruitment assay (Figure 4.2A and 4.2B). U2OS cells stably expressing GFP-MDC1 were sensitised with Hoechst 33342 and subjected to laser micro-irradiation (Dinant et al., 2007; Luijsterburg et al., 2009). The increase of GFP-MDC1 associated fluorescence became discernable after 10-20 seconds, after which a rapid accumulation occurred at the damage site in line with previous observation (Lukas et al., 2004a). Loss of Bod1L appeared to impede the initial rapid recruitment of MDC1 to damage sites, yet over a longer period of time post-damage, Bod1L depletion led to a continued accumulation of GFP-MDC1 at laser spots, complementing data from Figure 4.1B and E.

To confirm these results, I measured the binding of MDC1 to sites of DNA damage in live cells stably expressing GFP-MDC1 in a fluorescence recovery after photobleaching (FRAP) assay. GFP-MDC1 is actively recruited to sites of DNA damage, reaching a plateau level after approximately 10 minutes. To ensure that GFP-MDC1 localisation to damage foci had stabilised prior to FRAP, I performed laser micro-irradiation and measured the accumulation of GFP-MDC1 to damage sites (Figure 4.2C). Failure to allow for plateau to be reached could result in a skewed FRAP measurement, occurring due to the additive effect of damage-dependent accumulation of MDC1, in addition to fluorescence recovery at the FRAP spot. I also confirmed that the FRAP 488nm laser did not generate DNA damage within the cell. FRAP assays were performed at the time point indicated by the arrow once GFP-MDC1 fluorescence had plateaued. At sites of DNA damage, following Bod1L depletion, I observed a delayed initial recovery of GFP-MDC1 ($t^{1/2}$: siCTR=50.3s ± 3.2s; siBod1L=76.6s ± 5.4s), suggesting impairment in MDC1 recruitment (Figure 4.2E). I also detected a smaller impairment in MDC1 recruitment to non-

damaged sites ($t^{1/2}$: siCTR=22.9s ± 2.3s; siBod1L=26.4s ± 3.0s) (Figure 4.2D), suggesting that Bod1L may also affect association of MDC1 at undamaged DNA and chromatin. FRAP of GFP labelled Bod1L revealed a very slow turnover of the protein, indicative of robust chromatin binding as revealed in figure 3.1E. Together these data suggest that Bod1L is associated with chromatin throughout the nucleus and provides a binding platform for MDC1. In the absence of Bod1L, MDC1 turnover and recovery is slower, both at non-damage and damage sites, possibly as this recovery is now more reliant upon passive diffusion.

The C-terminal fragment of Bod1L interacts in vivo with components of the DNA damage machinery

Figures 4.1 and 4.2 demonstrated a clear functional link between the unknown function of Bod1L, and the correct localisation of key DNA damage repair components, particularly the phospho-scaffold MDC1. Given this functional relationship between Bod1L and normal MDC1 function, I wanted to investigate whether these two proteins shared a physical interaction. Immunoprecipitation of GFP-MDC1 stably expressed in U2OS cells revealed that GFP-MDC1 and Bod1L bind both in the presence and absence of DNA damage, primarily at chromatin (Figure 4.3A). Bod1L immunoprecipitated from HeLa cells expressing Bod1L-GFP confirmed this interaction, demonstrating damage-independent binding to MDC1 in a chromatin cell fraction (Figure 4.3B). NBS1, a component of the MRN complex known to interact with MDC1 at sites of damage (Chapman and Jackson, 2008; Lou et al., 2003; Wu et al., 2008), also co-immunoprecipitated with Bod1L (Figure 4.3C). In both the Bod1L-MDC1 IPs as

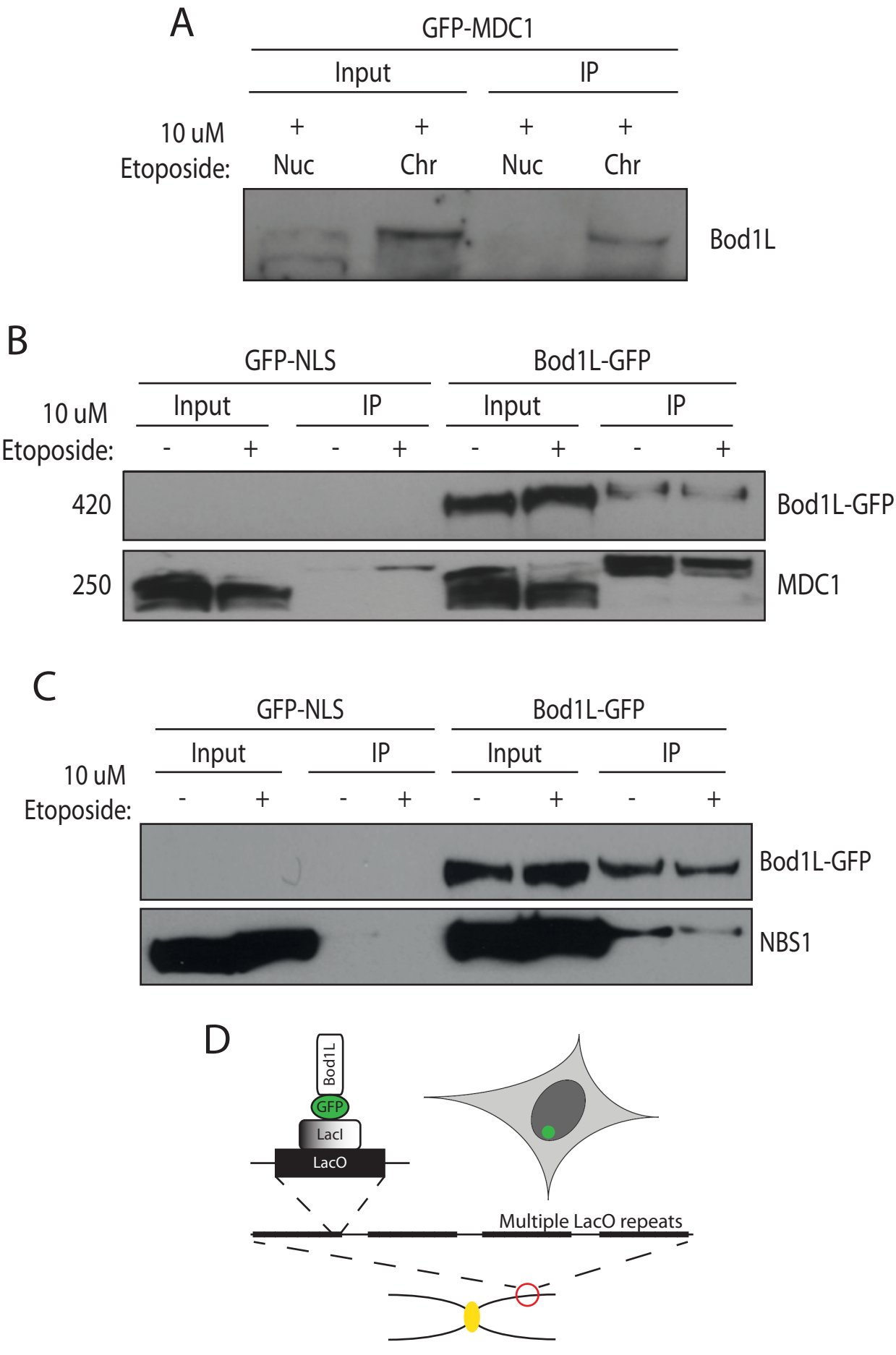
A
GFP-MDC1
Input
IP
10 uM
Etoposide:
+
+
+
+
Nuc
Chr
Nuc
Chr
Bod1L
B
GFP-NLS
Bod1L-GFP
10 uM
Etoposide:
Input
IP
Input
IP
-
+
-
+
-
+
-
+
420
250
Bod1L-GFP
MDC1
C
GFP-NLS
Bod1L-GFP
10 uM
Etoposide:
Input
IP
Input
IP
-
+
-
+
-
+
-
+
Bod1L-GFP
NBS1
D
Bod1L
GFP
LacI
LacO
Multiple LacO repeats

E

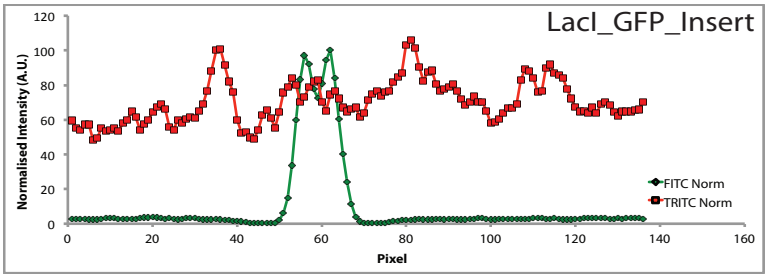
LacI_GFP_Insert
Normalised Intensity (A.U.)
Pixel
FITC Norm
TRITC Norm

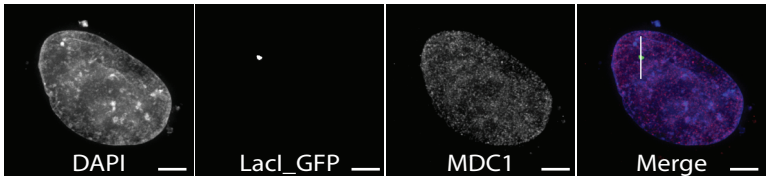
DAPI
LacI_GFP
MDC1
Merge

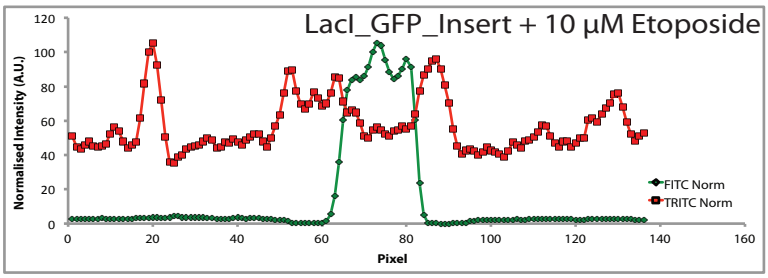
LacI_GFP_Insert + 10 µM Etoposide
Normalised Intensity (A.U.)
Pixel
FITC Norm
TRITC Norm

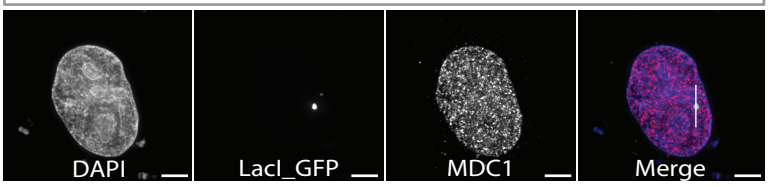
DAPI
LacI_GFP
MDC1
Merge

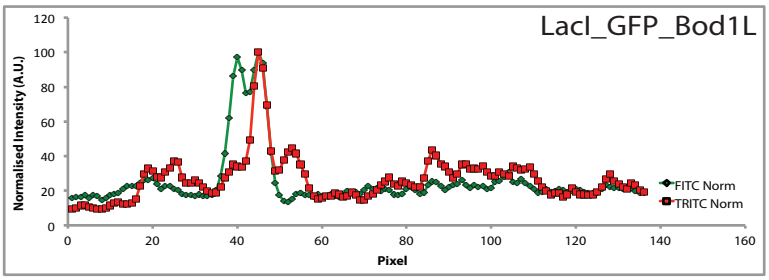
LacI_GFP_Bod1L
Normalised Intensity (A.U.)
Pixel
FITC Norm
TRITC Norm

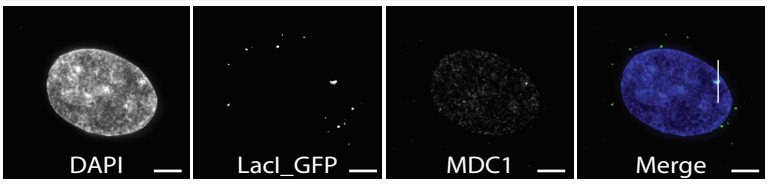
DAPI
LacI_GFP
MDC1
Merge

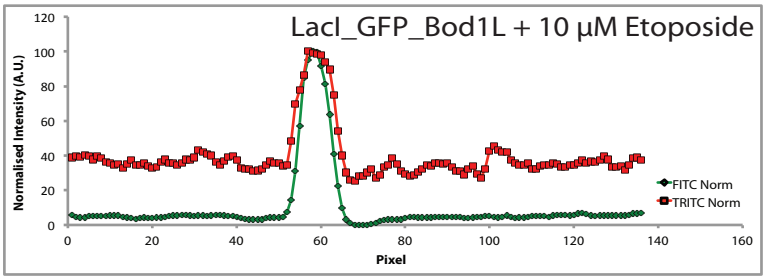
LacI_GFP_Bod1L + 10 µM Etoposide
Normalised Intensity (A.U.)
Pixel
FITC Norm
TRITC Norm

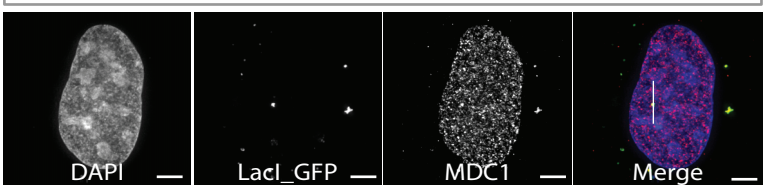
DAPI
LacI_GFP
MDC1
Merge

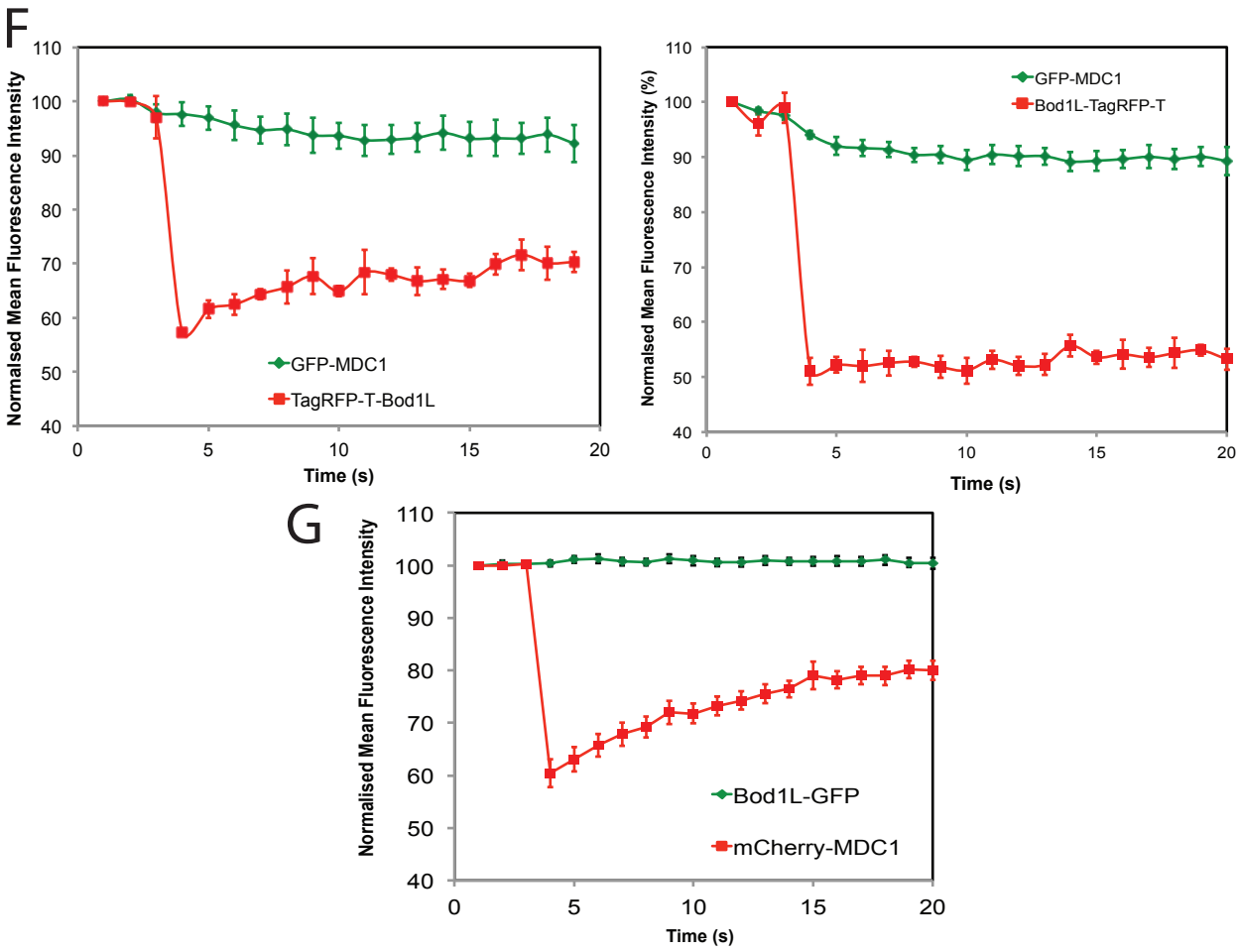
F
Normalised Mean Fluorescence Intensity
Time (s)
GFP-MDC1
TagRFP-T-Bod1L
Normalised Mean Fluorescence Intensity (%)
GFP-MDC1
Bod1L-TagRFP-T
G
Normalised Mean Fluorescence Intensity
Bod1L-GFP
mCherry-MDC1

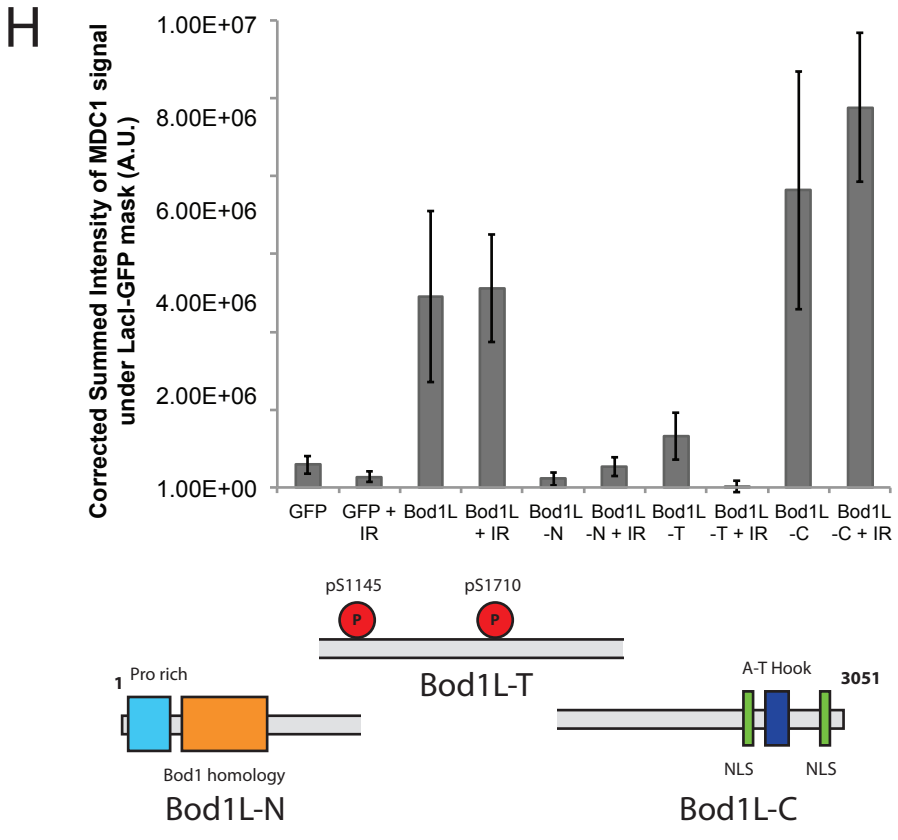
H
Corrected Summed Intensity of MDC1 signal under LacI-GFP mask (A.U.)
GFP
GFP + IR
Bod1L
Bod1L + IR
Bod1L -N
Bod1L -N + IR
Bod1L -T
Bod1L -T + IR
Bod1L -C
Bod1L -C + IR
pS1145
pS1710
Bod1L-T
Pro rich
Bod1 homology
Bod1L-N
A-T Hook
3051
NLS
NLS
Bod1L-C

Figure 4.3: Bod1L interacts *in vivo* with components of the DNA damage repair machinery

(A) GFP-Trap Immunoprecipitation (IP) of GFP-MDC1 from the nucleoplasmic and chromatin fraction of U2OS cells stably expressing GFP-MDC1 and treated with 10 μM etoposide. IPs were analysed by western blotting using antibodies against Bod1L.
(B) GFP-Trap Immunoprecipitation (IP) of Bod1L-GFP from the chromatin fraction of HeLa cells transiently expressing Bod1L-GFP. IPs were analysed by western blotting using antibodies against GFP and MDC1.
(C) GFP-Trap Immunoprecipitation (IP) of Bod1L-GFP from the chromatin fraction of HeLa cells transiently expressing Bod1L-GFP. IPs were analysed by western blotting using antibodies against GFP and NBS1.
(D) Schematic representation of the LacO single cell interaction assay. A construct containing LacI sequence fused to GFP and full length Bod1L is transiently expressed in a U2OS cell line stably expressing a LacO tandem repeat on a chromosome arm. This local cluster of fluorescently tagged Bod1L is visualised as a single nuclear focus.
(E) U2OS cells containing a stably integrated lacO tandem repeat were transfected with either LacI-GFP or LacI-Bod1L-GFP fusion and treated with 10 μM Etoposide for 24 hours. Protein accumulation at the Lac foci was determined by quantifying the fluorescent intensity of each channel along the indicated line. Scale bar, 5 microns.
(F) U2OS cells stably expressing GFP-MDC1 were transfected with either TagRFP-t-Bod1L (left panel) or Bod1L-TagRFP-t (right panel). After 48 hours, acceptor photobleaching was performed at a non-damaged nuclear site. 10 cells per condition, 2 independent experiments. Data represented as mean ± SEM.
(G) HeLa cells were transfected with mCherry-MDC1 and Bod1L-GFP. After 48 hours, acceptor photobleaching was performed at a non-damaged nuclear site. 10 cells per condition, 2 independent experiments. Data represented as mean ± SEM.
(H) Upper panel: U2OS cells containing a stably integrated lacO tandem repeat were transfected with the various LacI-Bod1L-GFP fusions indicated. The recruitment of MDC1 to LacI-GFP foci was determined for each of the Bod1L fusions. 10 cells per condition, representative images and quantitation of 2 independent experiments. Data represented as mean ± SEM. Lower panel shows graphic representation of Bod1L-GFP labelled fragments, containing Bod1L NLS sequence. Bod1L-N corresponds to aa1 to aa1009. Bod1L-T corresponds to aa1007 to aa2038. Bod1L-C corresponds to aa2002 to aa3051. Scale bar, 5 microns.

well as the Bod1L-NBS1 IPs, I detected a small, but reproducible, decrease in binding between Bod1L and both MDC1 and NBS1 after treatment with etoposide (Figure 4.3A, B and C). This small decrease in binding suggests that a small population of Bod1L/MDC1/NBS1 dissociates upon DNA damage, whilst the majority of the cellular pool of Bod1L/MDC1/NBS1 remain associated in complex.

To investigate the interaction between Bod1L and MDC1 further, single-cell binding assays were performed utilising the LacO-LacI system (Janicki et al., 2004)(Figure 4.3D). Full-length Bod1L was fused to a LacI repressor and coupled with GFP. This construct was transiently expressed in a U2OS cell line stably expressing a LacO tandem repeat in a euchromatic region of chromosome 1p36 (Janicki et al., 2004). This local cluster of fluorescently tagged Bod1L was visualised as a single nuclear focus. Immunofluorescent staining of cells with anti-MDC1 antibodies confirmed the damage-independent interaction between Bod1L and MDC1, with no recruitment of MDC1 to the GFP-only focus (Figure 4.3E).

To further explore the *in vivo* interaction between Bod1L and MDC1, a FRET-based approach was employed to interrogate whether interaction between Bod1L and MDC1, labelled with fluorescent tags, could be detected. Using either GFP-MDC1 and TagRFP-T-Bod1L/Bod1L-TagRFP-T (Figure 4.3F) or Bod1L-GFP and mCherry-MDC1 (Figure 4.3G), FRET could not be detected between these two proteins.

Finally, I sought to further interrogate the specific domain or region of Bod1L that interacted with MDC1. I expressed either full-length LacI-Bod1L-GFP or fragments of LacI-Bod1L-GFP and assessed recruitment of MDC1 when targeted to a non-damaged nuclear focus. These LacI constructs (Figure 4.3H, lower panel) were targeted to a LacO array to assess MDC1 co-localisation. Targeting of either full-length Bod1L or the C-terminal fragment (Bod1L-C) to the *lacO* array caused recruitment of endogenous MDC1 (Figure 4.3H, upper panel). Taken together with the complementary results in this section, these data suggest that Bod1L and MDC1 interact directly or indirectly through the C-terminal domain of Bod1L at chromatin. It appears that this interaction is constitutive throughout the nucleus and not damage-dependent.

Phosphorylation of MDC1 by ATM in response to DNA damage is increased in the absence of Bod1L

The function of MDC1 as a scaffold at sites of damage is dependent on its dimerisation/oligomerisation (Jungmichel et al., 2012). Phosphorylation of the MDC1 FHA domain at T4, primarily by ATM, stimulates the dimerisation of MDC1 and accumulation of downstream DDR factors at sites of DNA damage (Jungmichel et al., 2012; Liu et al., 2012; Luo et al., 2011). In addition, increased local density of MDC1 at DNA lesions promotes accumulation of activated ATM at sites flanking DNA damage, further facilitating ATM-dependent phosphorylation of H2AX and the amplification of DNA damage signals (Lou et al., 2006). I used ATM immunoprecipitated from damaged cells to phosphorylate GFP-MDC1 pulled down from undamaged cells (Figure 4.4A-B). GFP-MDC1 pulled down from cells incubated in kinase buffer alone showed little to no phosphorylation at T4. GFP-MDC1 incubated with active ATM

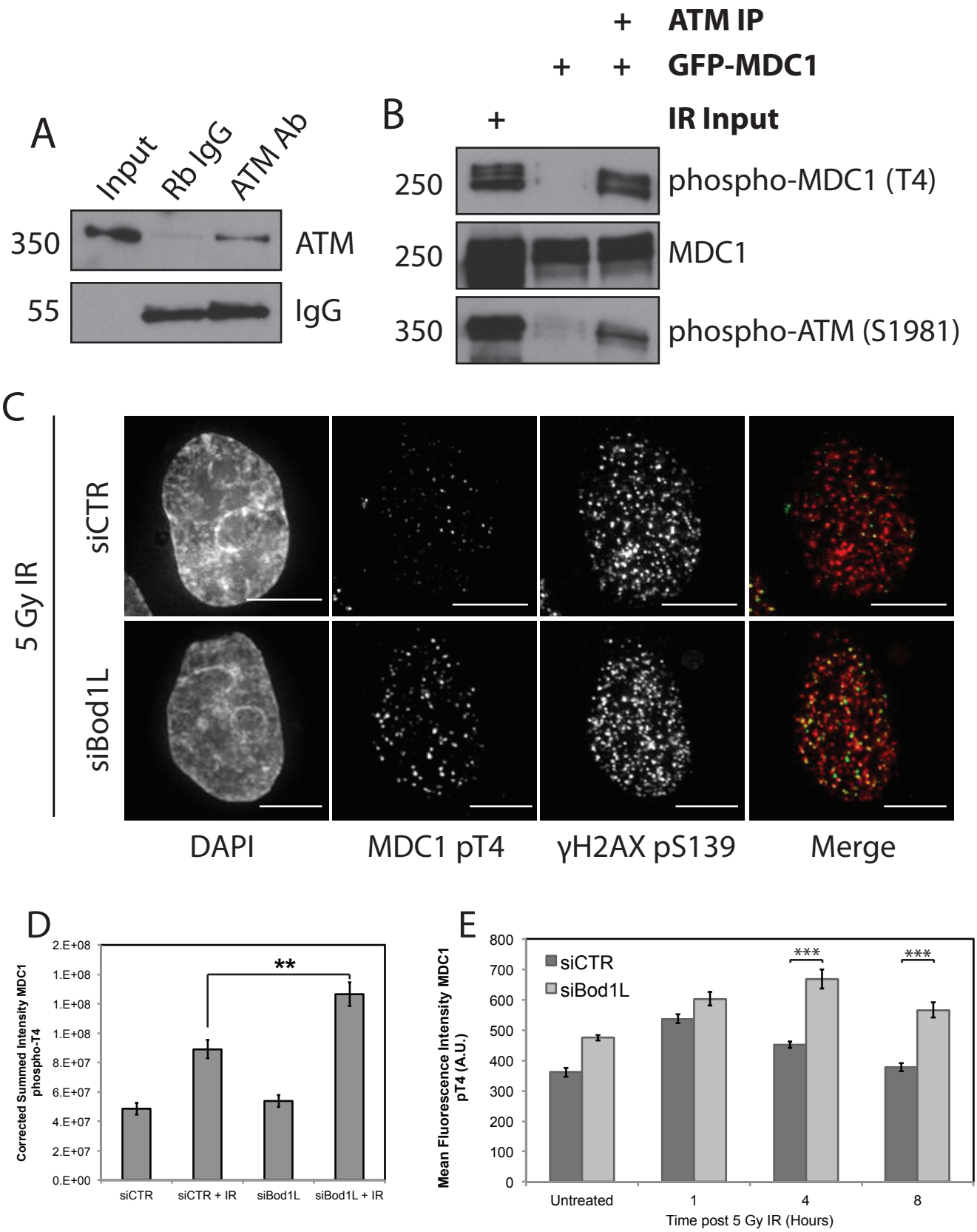
A
Input
Rb IgG
ATM Ab
350
ATM
55
IgG
B
+
ATM IP
+ +
GFP-MDC1
+
IR Input
250
phospho-MDC1 (T4)
250
MDC1
350
phospho-ATM (S1981)
C
5 Gy IR
siCTR
siBod1L
DAPI
MDC1 pT4
γH2AX pS139
Merge
D
Corrected Summed Intensity MDC1 phospho-T4
2.E+08
1.E+08
1.E+08
1.E+08
8.E+07
6.E+07
4.E+07
2.E+07
0.E+00
**
siCTR
siCTR + IR
siBod1L
siBod1L + IR
E
Mean Fluorescence Intensity MDC1 pT4 (A.U.)
800
700
600
500
400
300
200
100
0
siCTR
siBod1L
***
***
Untreated
1
4
8
Time post 5 Gy IR (Hours)

Figure 4.4: Phospho-MDC1 T4 phosphorylation is increased following Bod1L depletion

(A) Immunoprecipitation (IP) of ATM or rabbit IgG from HeLa cells was performed. Prior to lysis, cells were treated with 5 Gy IR and allowed to recover for 60 minutes. IPs were analysed by western blotting using antibodies against ATM.

(B) GFP-trap purified GFP-MDC1 was incubated in a kinase buffer containing ATM precipitated from cells dosed with 5 Gy IR. SDS–polyacrylamide gel electrophoresis-separated proteins were transferred and probed with antibodies against phospho-ATM (S1981), phospho-MDC1 (T4) or MDC1.

(C) HeLa cells were transfected with either control or Bod1L siRNA. After 24 hours, cells were treated with 10 μM etoposide for 16 hours. Cells were lysed by fractionation. Immunoblot was probed with antibodies against pMDC1 T4, MDC1, Bod1L, GAPDH and H3.

(D) HeLa cells were transfected with control or Bod1L siRNA. After 48 hours cells were treated with 5 Gy IR to generate IRIF. Cells were fixed in PFA after 2 hours and stained for endogenous MDC1 (pT4) (green) or γH2AX (pS139) (red). Scale bar, 5 microns.

(E) Quantification of MDC1 (pT4) signal (B). >50 cells per condition, representative images and quantitation of 3 independent experiments.

(F) HeLa cells were transfected with control or Bod1L siRNA. After 48 hours cells were treated with 5 Gy IR and samples were fixed in PFA at 1, 4 and 8 hours. Cells were immuno-stained for endogenous MDC1 (pT4) and quantified for MDC1 (pT4) signal. Data represented as mean ± SEM. ***P<0.001.

showed strong phosphorylation at T4, confirming that MDC1 is phosphorylated at this site by ATM following activation of the kinase (Figure 4.4B).

In figure 4.1B I observed that depletion of Bod1L resulted in increased MDC1 at DNA lesions that was independent of additional DNA damage. As such, I hypothesised that this increase of MDC1 at sites of damage could be as a result of increased dimerisation/oligomerisation. Following depletion of Bod1L and treatment with IR, I assessed the phosphorylation of phospho-MDC1 T4, using an antibody specific for this modification. I depleted Bod1L from HeLa cells and assessed phospho-MDC1 T4 signal by immunofluorescence observing that loss of Bod1L led to a significant increase in the ratio of phospho-MDC1 T4/total MDC1 (Figure 4.4C, D). Furthermore, phospho-MDC1 T4 in Bod1L-depleted cells remained elevated relative to control cells for several hours after damage (Figure 4.4E). This result is in agreement with the data showing increased MDC1 recruitment to DNA lesions at these time points (Figure 4.1C-E). As demonstrated previously, I detected no specific interaction between ATM and Bod1L above GFP-only control levels, with activation of ATM following DNA damage appearing normal (Figure 3.11A-C). Immediate phosphorylation of downstream targets of ATM such as the checkpoint kinase Chk2 (Ahn et al., 2000) also appeared normally phosphorylated after Bod1L depletion (Figure 3.11D).

Additional MDC1 phosphorylation sites are affected by loss of Bod1L, leading to loss of critical DNA damage repair interactions

MDC1 functions as a phospho-scaffold required for recruitment of downstream effectors to sites of damage (Lou et al., 2003; Stewart et al., 2003). One such

interaction, with the NBS1-containing MRN complex, is dependent on phosphorylation of the SDT-rich N-terminus of MDC1 by casein kinase 2 (CK2) (Chapman and Jackson, 2008; Melander et al., 2008; Spycher et al., 2008). Upon DNA damage, the CK2-phosphorylated modification of MDC1 is stabilised relative to the total MDC1 pool. I used an MDC1 pSDpTD antibody (phospho-S329/T331-MDC1)(a kind gift from Jackson group, Cambridge) to determine the role of Bod1L in control of this modification. Depletion of Bod1L from HeLa cells treated with etoposide led to a damage-independent decrease in the phospho-S329/T331-MDC1 signal (Figure 4.5A). In cells treated with a moderate dose of IR and then fixed and immunostained for phospho-S329/T331-MDC1, Bod1L depletion led to a significant reduction in the presence of this modification following IR (Figure 4.5B). Quantification of this data revealed that Bod1L depletion reduced the presence of this modification only in the presence of DNA damage, with no reduction seen in undamaged cells (Figure 4.5C).

As mentioned above, sustained phosphorylation of MDC1 at this cluster of SDTD repeats (highlighted in figure 1.5B) is critical for establishing MDC1 interaction with NBS1 and the MRN complex. Failure to maintain this key interaction at DNA lesions abrogates the accumulation of the MRN complex at such lesions and leads to compromised damaged repair and checkpoint signalling (Spycher et al., 2008). To examine whether the decrease in phospho-S329/T331-MDC1 signal led to a functional consequence, I depleted Bod1L and immunoprecipitated MDC1 from U2OS cells stably expressing GFP-MDC1, observing damage dependent decrease in MDC1 binding to NBS1 in the absence of Bod1L (Figure 4.5D).

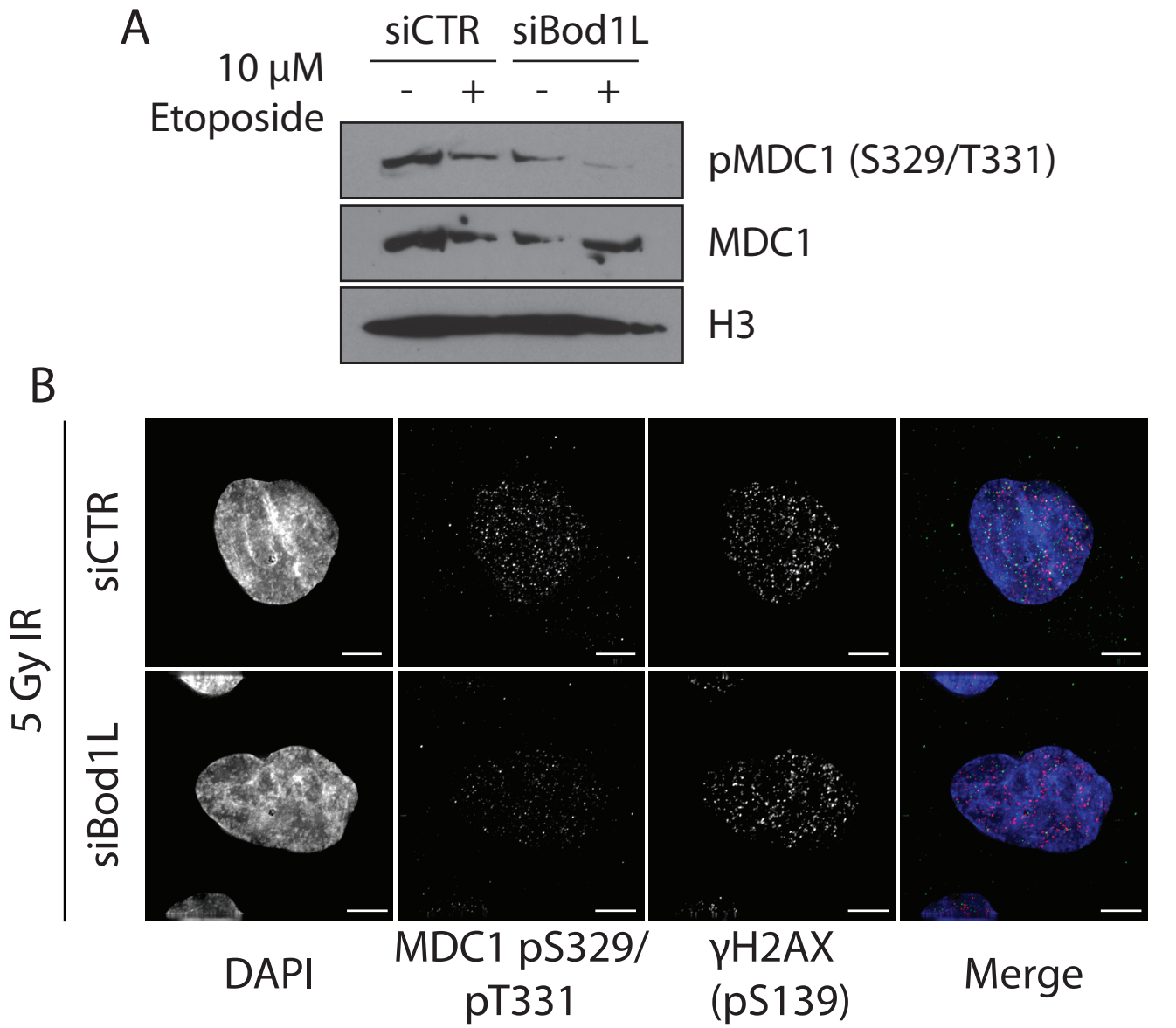
A
siCTR
siBod1L
10 μM
Etoposide
- + - +
pMDC1 (S329/T331)
MDC1
H3
B
5 Gy IR
siCTR
siBod1L
DAPI
MDC1 pS329/
pT331
γH2AX
(pS139)
Merge

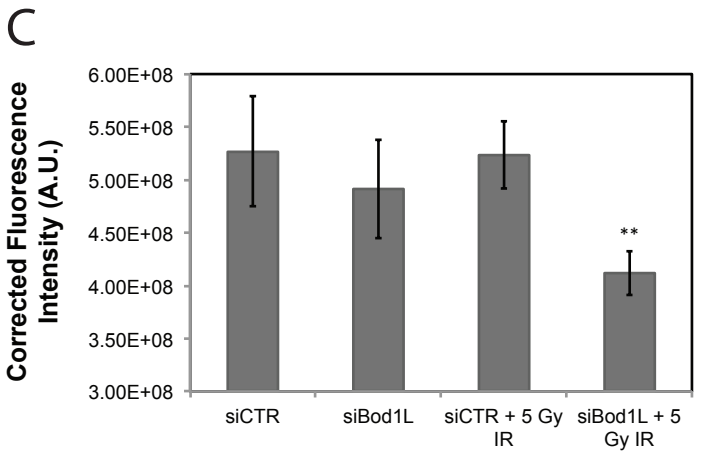
C
Corrected Fluorescence Intensity (A.U.)
6.00E+08
5.50E+08
5.00E+08
4.50E+08
4.00E+08
3.50E+08
3.00E+08
**
siCTR
siBod1L
siCTR + 5 Gy IR
siBod1L + 5 Gy IR

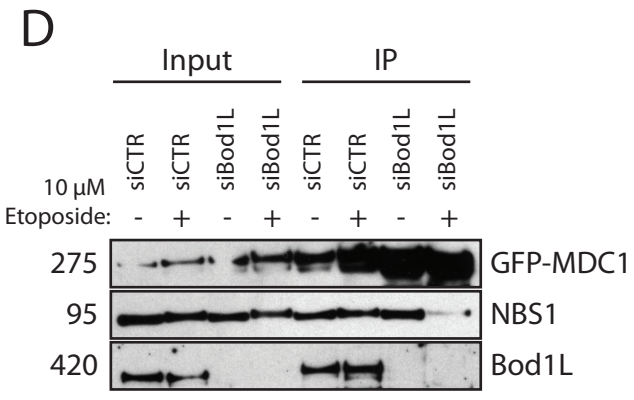
D
Input
IP
siCTR
siCTR
siBod1L
siBod1L
siCTR
siCTR
siBod1L
siBod1L
10 μM
Etoposide: - + - + - + - +
275
95
420
GFP-MDC1
NBS1
Bod1L

Figure 4.5: Phospho-MDC1 S329/T331 signalling is reduced following Bod1L depletion leading to a loss of MDC1-NBS1 binding

(A) HeLa cells were transfected with either control or Bod1L siRNA. After 24 hours, cells were treated with 10 μM etoposide for 16 hours. Immunoblots were probed with antibodies against pMDC1 (S329/T331), MDC1 and H3.

(B) HeLa cells were transfected with control or Bod1L siRNA. After 48 hours cells were treated with 5 Gy IR to generate IRIF. After 2 hours, cells were fixed in PFA and stained for endogenous MDC1 (pS329/pT331) (green) or γH2AX (pS139) (red). Representative maximum intensity projections shown. Scale bar, 5 microns

(C) Panel shows quantification of MDC1 (pS329/pT331) signal. Data shows background corrected mean signal intensity per cell and is represented as mean ± SEM. n=10 for each condition. **P<0.01.

(D) GFP-Trap Immunoprecipitation (IP) of GFP-MDC1 from the chromatin fraction of U2OS cells transfected with control or Bod1L siRNA for 48 hours. Prior to lysis, cells were treated +/- 10 μM Etoposide for 24 hours. Immunoblots were analysed by western blotting using antibodies against GFP, NBS1 and Bod1L.

Together with the results from figure 4.4, these data suggest that Bod1L depletion leads to a significant change in the phosphorylation dynamics of MDC1 sites of DNA damage, resulting in an overall increase of MDC1 at damaged DNA and a decrease in binding to known interaction partners. Increased phospho-MDC1 T4 should increase the MDC1 accumulation, exactly as observed in biochemical and live cell analyses (Figure 4.1B-E, Figure 4.2A-B). I hypothesise that this uncontrolled dimerisation/oligomerisation causes steric hindrance, which could explain the loss of phosphorylation within the SDT domain and thus interaction with key down-stream protein complexes, such as the MRN complex.

Bod1L and the B56 regulatory subunit of PP2A interact in vivo

As described above, I had observed changes in multiple phosphorylation sites on MDC1 in Bod1L-depleted cells, but had not detected any change in ATM activity (Figure 3.11). I therefore focused on determining whether changes to antagonising phosphatases were the cause of the Bod1L-depletion phenotype. Several groups of Ser/Thr phosphatases have been implicated in the control of the DNA damage response (Heideker et al., 2014), including PP2A (Chowdhury et al., 2005; Li et al., 2007; 2015; Shouse et al., 2011) and PP4 (Chowdhury et al., 2008; Nakada et al., 2008). As described in figure 3.1, Bod1L contains a region of highly conserved homology with Bod1, which has been shown to functionally interact with the regulatory B56 subunit of the PP2A holocomplex (Porter et al., 2013). I immunoprecipitated Bod1L-GFP from HeLa cells transiently expressing Bod1L-GFP and observed specific binding of the B56 regulatory subunit upon DNA damage (Figure 4.6A). No specific interaction could be detected between Bod1L and the α-subunit of the PP2A catalytic

subunit, most likely due to the very high expression of this subunit and the associated promiscuous binding in immunoprecipitation assays. I also immunoprecipitated stably expressed PP2A-B56-GFP and observed a chromatin specific co-immunoprecipitation of endogenous Bod1L (Figure 4.6B).

Depletion of the B56 regulatory subunit of the PP2A holocomplex phenocopies Bod1L depletion

To assess whether the interaction between Bod1L and PP2A-B56 had a functional effect on maintaining a robust response to DNA damage, I sought to evaluate the effect of B56 depletion on DNA repair. To test this, I depleted all five PP2A-B56 isoforms from HeLa cells and carried out clonogenic survival assays using MMC (Figure 4.6C). Whilst depletion of the B56 pool led to a degree of mitotic arrest, a shorter siRNA incubation (24 hours) allowed the large majority of cells to continue to cycle for the duration of the assay. Loss of Bod1L led to severe hypersensitivity to MMC as described previously (Figure 3.3E). Depletion of B56 from cells led to an equally pronounced sensitivity to MMC, whilst co-depletion of both Bod1L and PP2A led to no additional sensitivity to MMC. These data suggest that Bod1L and PP2A-B56 function in a non-epistatic manner and likely function in the same pathway.

I demonstrated previously that depletion of Bod1L led to slower accumulation of GFP-MDC1 at sites of DNA damage (Figure 4.2A). Assessment of GFP-MDC1 localisation following B56 depletion revealed that loss of the PP2A regulatory subunit phenocopied this effect (Figure 4.6D). Since depletion of Bod1L led to

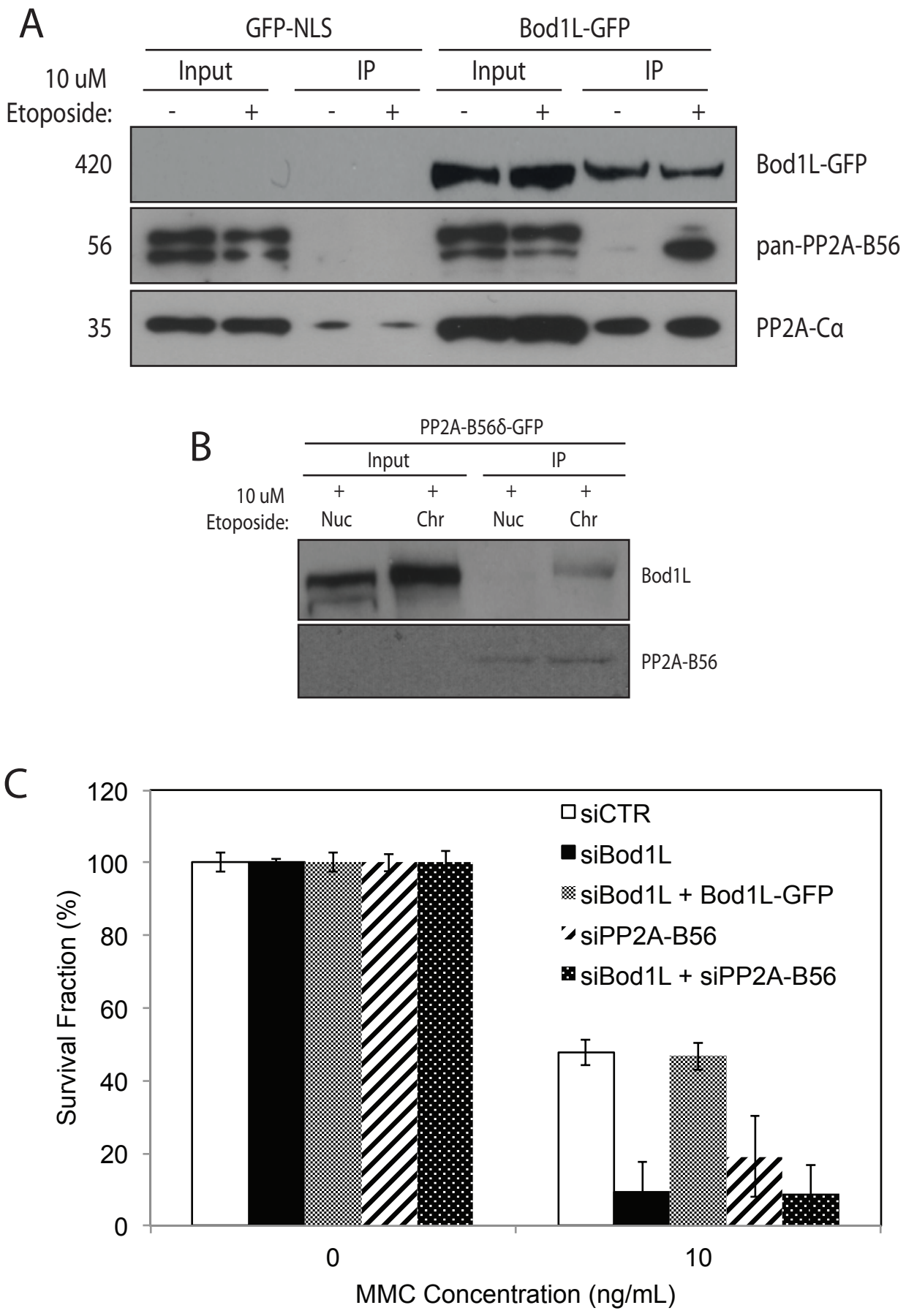
A
GFP-NLS
Bod1L-GFP
10 uM
Etoposide:
Input
IP
Input
IP
- + - + - + - +
420
56
35
Bod1L-GFP
pan-PP2A-B56
PP2A-Cα
B
PP2A-B56δ-GFP
Input
IP
10 uM
Etoposide:
+ + + +
Nuc Chr Nuc Chr
Bod1L
PP2A-B56
C
Survival Fraction (%)
120
100
80
60
40
20
0
siCTR
siBod1L
siBod1L + Bod1L-GFP
siPP2A-B56
siBod1L + siPP2A-B56
0
10
MMC Concentration (ng/mL)

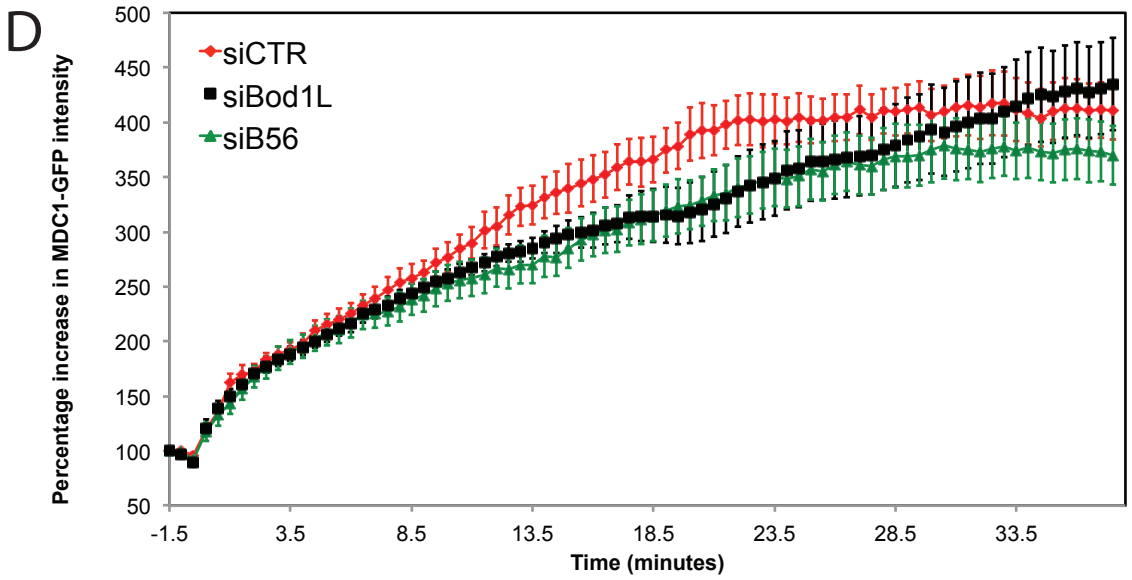
D
Percentage increase in MDC1-GFP intensity
siCTR
siBod1L
siB56
500
450
400
350
300
250
200
150
100
50
-1.5
3.5
8.5
13.5
18.5
23.5
28.5
33.5
Time (minutes)

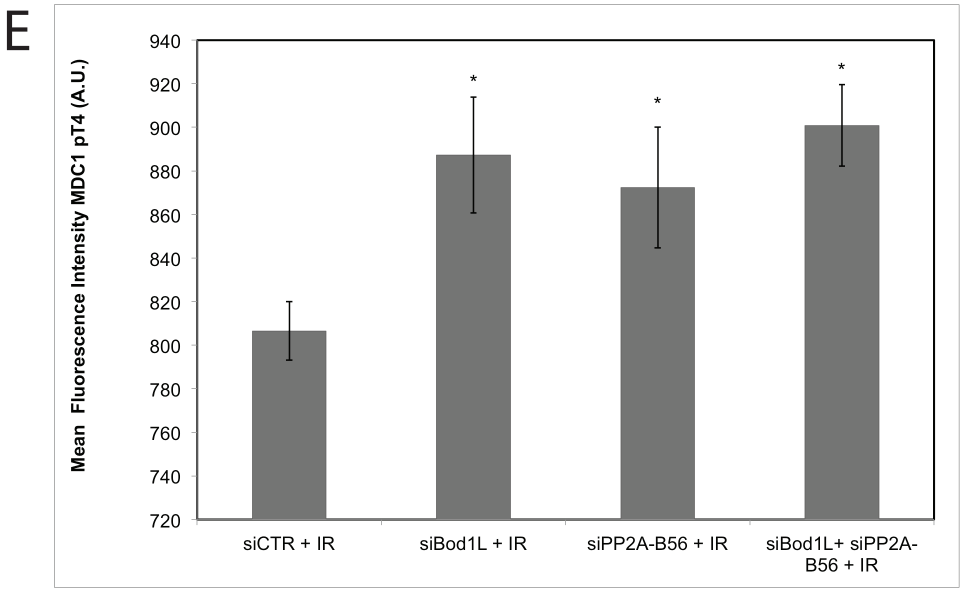
E
Mean Fluorescence Intensity MDC1 pT4 (A.U.)
940
920
900
880
860
840
820
800
780
760
740
720
*
*
*
siCTR + IR
siBod1L + IR
siPP2A-B56 + IR
siBod1L+ siPP2A-B56 + IR

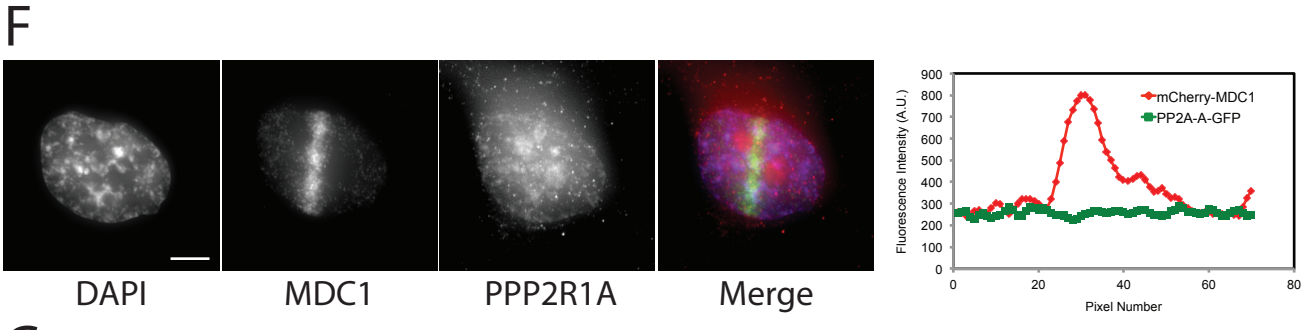
F
DAPI
MDC1
PPP2R1A
Merge
Fluorescence Intensity (A.U.)
mCherry-MDC1
PP2A-A-GFP
Pixel Number

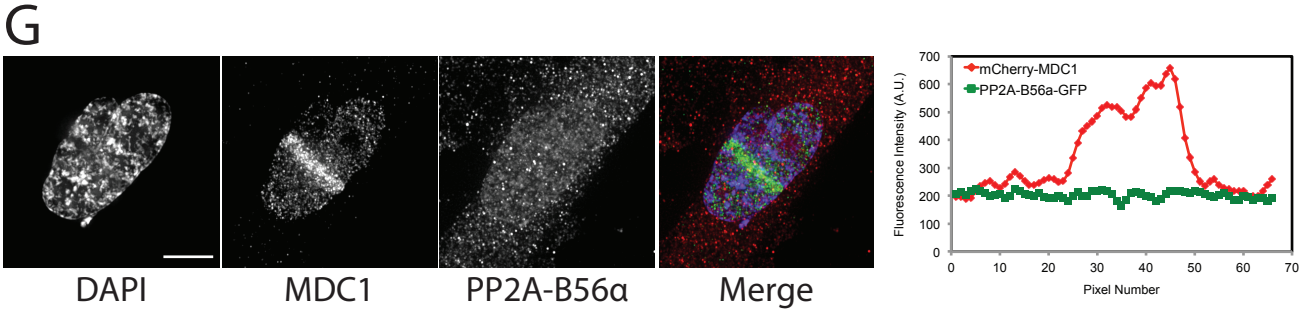
G
DAPI
MDC1
PP2A-B56α
Merge
Fluorescence Intensity (A.U.)
mCherry-MDC1
PP2A-B56a-GFP
Pixel Number

Figure 4.6: Bod1L interacts in vivo with PP2A-B56 with PP2A-B56 depletion phenocopying loss of Bod1L

(A) GFP-Trap immunoprecipitation of Bod1L-GFP from chromatin fraction of HeLa cells transiently expressing Bod1L-GFP and mock treated or treated with 10 μM etoposide for 24 hours. IPs were analysed by immuno-blotting using antibodies against GFP, PP2A-B56 (pan-specific) and PP2A-Cα. Upper band of PP2A-B56 blot shows PP2A-B56δ, lower band is all other PP2A-B56 isoforms.

(B) Immunoprecipitation (IP) of PP2A-B56-GFP from the nucleoplasmic and chromatin fraction of HeLa cells stably expressing PP2A-B56-GFP and treated with 10 μM etoposide. IPs were analysed by western blotting using antibodies against Bod1L and GFP.

(C) HeLa cells were transfected with control, Bod1L, or B56 pool siRNA or combinations as indicated. Clonogenic survival assays were carried out with MMC. For each siRNA, cell viability of untreated cells is defined as 100%. To assess rescue of phenotype, HeLa cells were transfected with Bod1L siRNA targeting the 3'UTR repeat of Bod1L. Cells were then transfected with Bod1L GFP and clonogenic survival assays were carried out with Mitomycin-C.

(D) Accumulation of GFP-MDC1 at sites of DNA damage. U2OS cells stably expressing GFP-MDC1 were transfected with control siRNA, Bod1L siRNA or siRNA targeting the B56 pool of PP2A and pre-treated with Hoechst 33342. Cells were striped with 405 nm laser and GFP-MDC1 fluorescent intensity accumulation was measured. Time from onset of laser stripe is shown underneath. Data represented as mean ± SEM. n=10 for each condition.

(E) HeLa cells were transfected with control siRNA, Bod1L siRNA or siRNA targeting the B56 pool of PP2A. After 24/48 hours cells were treated with 5 Gy IR to generate IRIF. Cells were fixed in PFA after 2 hours and stained for endogenous MDC1 (pT4) (green). Quantification of MDC1 (pT4) fluorescence signal is shown.

(F, G) HeLa cells stably expressing PP2A-A-GFP (F) or PP2A-B56α-GFP (G) were transfected with mCherry-MDC1. Cells were pre-treated with Hoescht and striped with a 405 nm laser. Accumulation of GFP-MDC1 and PP2A were quantified along the line of the laser stripe (right-hand panel).

no change in the activation or activity of ATM (Figure 3.11), I hypothesised that Bod1L may bind PP2A-B56 specifically at sites of DNA damage and subsequently control the modification of phospho-MDC1 T4. If this hypothesis was correct, then a deletion of PP2A-B56 in the presence of Bod1L should mimic the Bod1L phenotype. To test this, I depleted all five PP2A-B56 isoforms from HeLa cells and assessed phospho-MDC1 T4 after treatment with IR (Figure 4.6E). As predicted, loss of PP2A-B56 led to an increase in phospho-MDC1 T4 signal, even in the presence of Bod1L. Once again, depletion of either PP2A-B56 alone, or co-depletion of Bod1L and PP2A-B56, phenocopied this increase in phospho-MDC1 T4 signal at DNA lesions. Taken together these data suggest that PP2A-B56 is required in the same functional pathway as Bod1L.

Localisation of PP2A-B56γ1 to sites of damage is lost upon Bod1L depletion

I have demonstrated so far that loss of either Bod1L or the B56 regulatory subunit of PP2A leads to hypersensitivity to MMC and changes in the localisation and control of MDC1 at sites of DNA damage (Figure 4.6). Evidence from figure 4.6C and E suggest that PP2A-B56 and Bod1L act in a non-epistatic manner, most likely functioning in the same pathway upon DNA damage. I demonstrated that although Bod1L is not re-localised to DNA lesions, ATM phosphorylates Bod1L at sites of DNA damage (Figure 3.7-9). Using either GFP labelled PP2A structural 'Aα' subunit, or GFP labelled B56α I detected no localisation of PP2A to sites of laser micro-irradiation DNA damage (Figure 4.6 F, G), despite strong mCherry-MDC1 accumulation at these stripes.

It has previously been reported that the catalytic (C) PP2A subunit, co-localised and co-immunoprecipitated with γH2AX; an interaction important for the dephosphorylation of γH2AX upon resolution of DNA damage (Chowdhury et al., 2005). More recent studies have identified an additional DNA damage role for the specific B56-gamma subunit, identifying functional association of p53 and PP2A-B56γ at sites of DNA damage (Li et al., 2007; Shouse et al., 2011). To assess and determine whether Bod1L specifically regulates this DNA damage specific PP2A-B56γ function, I applied the laser damage assay to a HeLa cell line stably expressing PP2A-B56γ1-YFP and observed PP2A-B56 rapidly localising to sites of laser damage (Figure 4.7A). To verify the localisation of PP2A-B56 in damaged cells, I transfected PP2A-B56γ1-YFP cells with mCherry-MDC1 and detected co-localisation of YFP and mCherry fluorescence at laser stripes (Figure 4.7A). PP2A-B56γ1-YFP fluorescence could be detected and quantified at the laser stripe track as early as 5 minutes post-irradiation (Figure 4.7B). This rapid recruitment to DNA lesions is on a similar timescale to the phosphorylation of Bod1L at damage sites (Figure 3.8D). Depletion of Bod1L prevented any detectable accumulation of PP2A-B56γ1-YFP at damage sites (Figure 4.7C).

Given that depletion of PP2A-B56 phenocopied Bod1L depletion (Figure 4.6C-E), I hypothesised that Bod1L may control the delivery of MDC1 to sites of DNA damage, buffering the ATM-mediated oligomerisation of MDC1 through recruitment of PP2A-B56 to sites of DNA damage. To test this hypothesis, I employed *In vitro* phosphatase assays consisting of GFP-MDC1 and PP2A-B56δ-

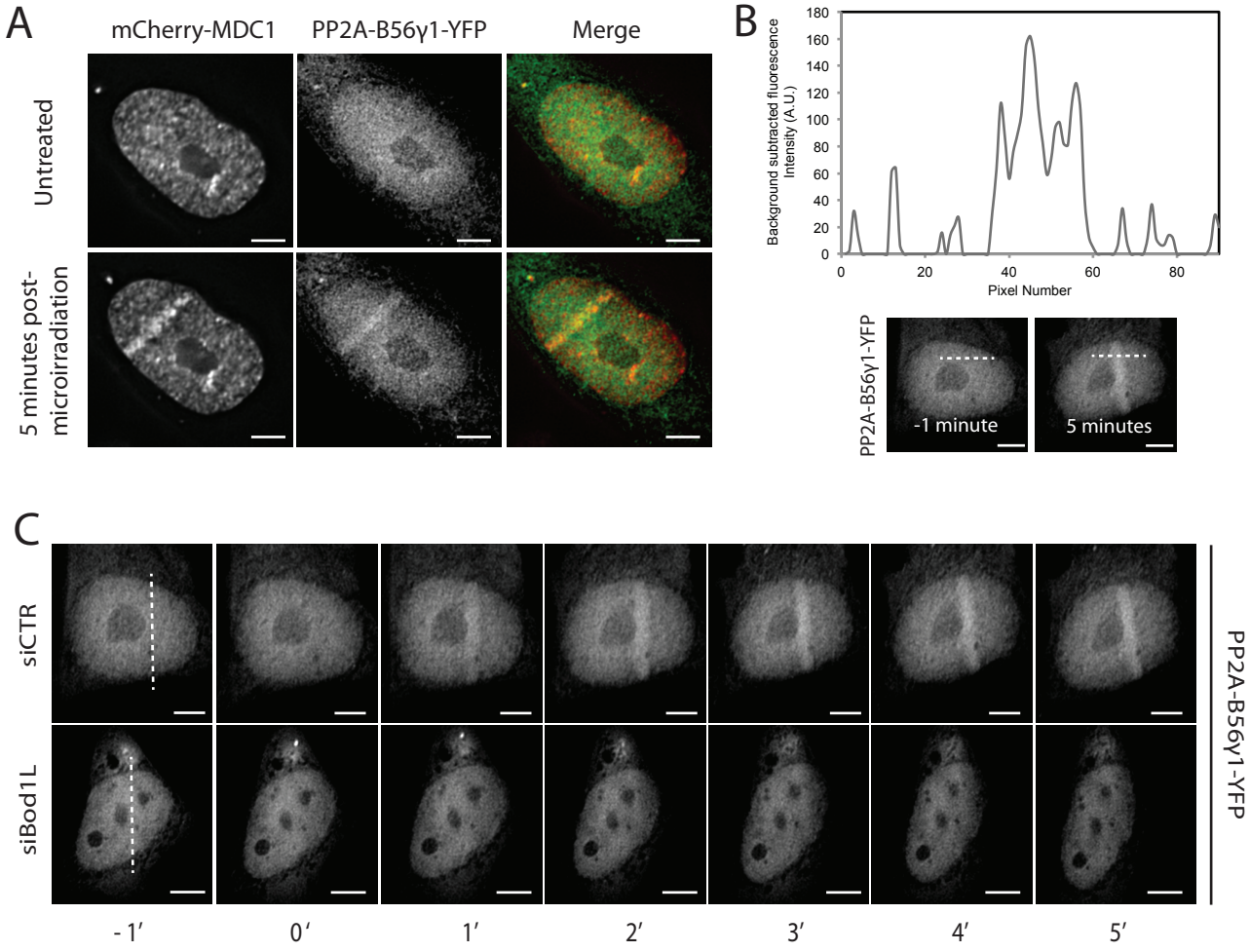
A
mCherry-MDC1
PP2A-B56γ1-YFP
Merge
Untreated
5 minutes post-microirradiation
B
Background subtracted fluorescence Intensity (A.U.)
Pixel Number
PP2A-B56γ1-YFP
-1 minute
5 minutes
C
siCTR
siBod1L
PP2A-B56γ1-YFP
- 1′
0′
1′
2′
3′
4′
5′
D
2nM OA
PP2A-B56δ
MDC1
250
MDC1 pT4
250
MDC1-GFP
56
B56δ-GFP
36
PP2A-C

Figure 4.7: PP2A-B56γ1-YFP localisation to sites of laser DNA damage is ablated upon Bod1L depletion and mediates phospho-MDC1 T4 dephosphorylation

(A) Inducible HeLa cells stably expressing PP2A-B56γ1-YFP were transfected with mCherry-MDC1. After 24 hours cells were induced with 1 μg/ml doxycycline for 16 hours. Cells were pre-treated with Hoescht and striped with a 405 nm laser. Representative maximum intensity projections are shown. Data represented as mean ± SEM. n=>20 for each condition. *P<0.05, **P<0.01, ***P<0.001. Scale bar, 5 microns.

(B) Quantification of PP2A-B56γ1-YFP signal along the 10 μm (90 pixel) indicated line profile. Fluorescence values subtracted against background signal.

(C) Inducible HeLa cells stably expressing PP2A-B56γ1-YFP were transfected with control or Bod1L siRNA. After 24 hours cells were induced with 1 μg/ml doxycycline for 16 hours. Cells were pre-treated with Hoescht and striped with a 405 nm laser. Images were acquired every 1 minute.

(D) GFP-MDC1 was pulled down using GFP-Trap, from stably expressing U2OS cells treated with 10 μM etoposide. PP2A-B56δ-GFP was pulled down from stably expressing RPE1 cells. *In vitro* phosphatase assay was performed in the presence or absence of 2 nM Okadaic acid. Immunoblots were stained for phospho-MDC1 T4, GFP and PP2A-C (Experiment performed by Iain Porter, Swedlow Group).

GFP pulled down from damaged cell lysates, which revealed that PP2A-B56δ-GFP could dephosphorylate phospho-MDC1 T4 *in vitro*. This specific dephosphorylation event was inhibited following a dose of Okadaic acid that only targets PP2A (Figure 4.7D).

Bod1L does not interact with the Ser/Thr phosphatase PP4 in vivo

As shown in figure 1.7, multiple Ser/Thr phosphatases have been shown to play a role in regulation of DNA damage repair. One of the better studied Ser/Thr phosphatases in the response to DNA damage is PP4, which has been shown to dephosphorylate γH2AX following resolution of DNA damage, allowing recovery from the G2/M checkpoint arrest as a result of replication stress (Chowdhury et al., 2008; Nakada et al., 2008). In addition, PP4 has been shown to dephosphorylate replication protein A (RPA) subunit RPA2 at DNA lesions, promoting efficient loading of the essential HR factor RAD51 (Lee et al., 2010). I demonstrated above that PP2A-B56 is involved in controlling the phosphorylation of MDC1 following DNA damage. Given the multiple roles previously described for PP4 in maintaining robust HR mediated repair, I wanted to establish whether Bod1L and PP4C also functionally interact during DNA repair.

I used siRNA to target the catalytic subunit of PP4 (PP4C) (Chowdhury et al., 2008) and probed depleted lysates with an antibody specific for the PP4C subunit. This siRNA significantly depleted PP4C protein levels compared with control treatment, and had no effect on Bod1L expression (Figure 4.8A). Fractionation of HeLa cell lysates revealed PP4C expression almost exclusively in the nucleoplasm, with a small amount associated with chromatin as reported

in the literature (Shimada and Nakanishi, 2013)(Figure 4.8B). Depletion of PP4C from HeLa cells led to hypersensitivity to MMC in a manner similar to loss of Bod1L (Figure 4.8C), which is unsurprising given the literature describing the role of PP4C in HR-mediated repair (Lee et al., 2010). To assess any interaction of Bod1L with PP4C, I generated a full-length GFP labelled PP4C construct, which was transiently expressed in HeLa cells. Immunoprecipitation of PP4C-GFP from HeLa cells expressing the construct revealed that PP4C-GFP and Bod1L did not bind either in the presence or absence of DNA damage in the nucleoplasmic fraction of cell lysates (Figure 4.8D). Reciprocal experiments performed using HeLa cells transiently expressing Bod1L-GFP also failed to immunoprecipitate PP4C suggesting that it is unlikely that these two proteins interact in the nucleus *in vivo*. Using the PP4C-GFP construct, I could detect PP4C signal in the nucleus which was unaffected by depletion of Bod1L or the induction of DNA lesions by gamma-irradiation (Figure 4.8E).

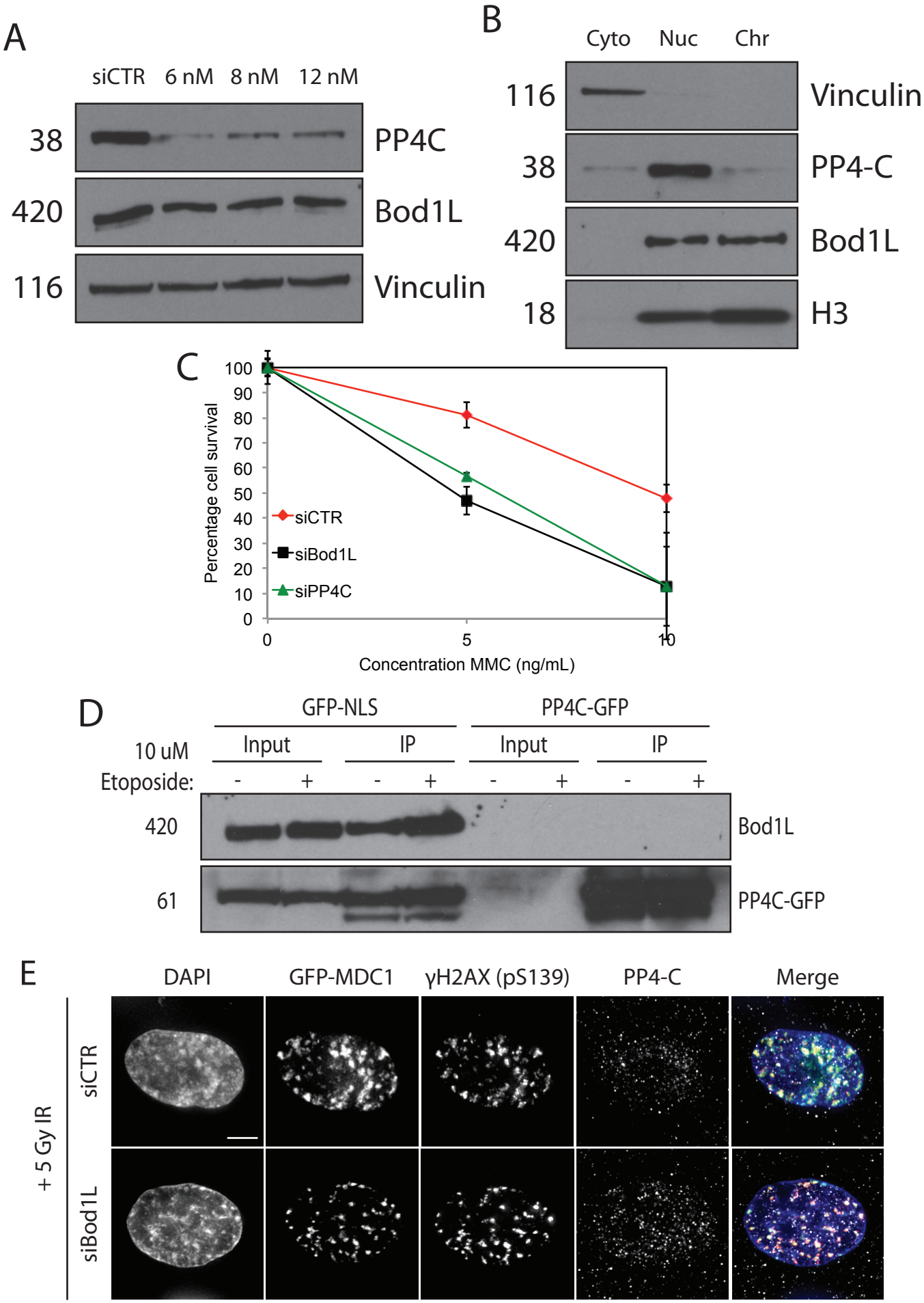
A
siCTR
6 nM
8 nM
12 nM
38
PP4C
420
Bod1L
116
Vinculin
B
Cyto
Nuc
Chr
116
Vinculin
38
PP4-C
420
Bod1L
18
H3
C
Percentage cell survival
100
90
80
70
60
50
40
30
20
10
0
siCTR
siBod1L
siPP4C
0
5
10
Concentration MMC (ng/mL)
D
GFP-NLS
PP4C-GFP
10 uM
Input
IP
Input
IP
Etoposide:
- + - + - + - +
420
Bod1L
61
PP4C-GFP
E
DAPI
GFP-MDC1
γH2AX (pS139)
PP4-C
Merge
+ 5 Gy IR
siCTR
siBod1L

Figure 4.8: Bod1L does not interact in vivo with PP4C

(A) Immunoblots of HeLa cells treated with either control or PP4C siRNA. 6, 8 and 12 nM concentration of siPP4C were used. Immunoblots were probed with antibodies against PP4C, Bod1L and GAPDH

(B) Subcellular fractionation of HeLa cell lysate. Immunoblots were probed with antibodies against vinculin, PP4C, Bod1L and H3.

(C) Clonogenic survival assays of HeLa cells transfected with control, Bod1L or PP4C siRNA. MMC was added 48 hours after transfection at the indicated concentrations and cells propagated for 10 - 12 days. For each siRNA, cell viability of untreated cells is defined as 100%. 3 repeats/condition, two independent experiments. Data represented as mean ± SEM.

(D) Immunoprecipitation (IP) of PP4C-GFP using GFP-Trap from the chromatin fraction of HeLa cells transiently expressing PP4C-GFP. IPs were analysed by western blotting using antibodies against GFP and Bod1L.

(E) U2OS cells stably expressing MDC1-GFP (green) were transfected with control or Bod1L siRNA. After 48 hours cells were treated with 5 Gy IR to generate IRIF. Cells were allowed to recover for 1 hour, fixed in PFA and stained for endogenous γH2AX (pS139) (red) and PP4C (cyan). Representative maximum intensity projections shown. Scale bar, 5 microns.

Discussion

I have shown in the previous chapter that Bod1L acts as a chromatin-bound component of the repair machinery. Bod1L localises throughout the nucleus but is specifically phosphorylated at damage sites by ATM, with phosphorylated Bod1L co-localizing with γH2AX and MDC1. Here I expand my previous findings and show that Bod1L makes two critical contributions to the DNA damage response: it promotes the initial targeting of MDC1 to sites of DNA damage and limits MDC1 accumulation by targeting PP2A-B56 to dephosphorylate ATM phosphorylated MDC1-T4.

I demonstrate that the depletion of Bod1L results in two defects that occur at different timescales; first, the delivery of MDC1 to sites of DNA damage is impaired in the first few minutes after damage, which also compromises the targeting of downstream repair factors (Figure 4.5D). Secondly at longer timescales, control of MDC1 accumulation is lost, leading to MDC1 over-recruitment which results in deficient repair at sites of DNA damage. Previous literature has demonstrated using a budding-yeast system that over-recruitment of DNA damage factors to sites, sequesters HR proteins and can prevent proper repair at *bona fide* DSB (Lin et al., 2009). In human cells, other studies investigating the functional dependence of key HR components, observe that suppression of 53BP1 expression led to increased recruitment of NFBD1/MDC1 and Nbs1 to sites of DNA DSBs (Mochan et al., 2003). Given this precedent of improper protein recruitment resulting in repair defects, the Bod1L mediated control of MDC1 levels is very credible.

I have shown that Bod1L binds to MDC1 both in the presence and absence of DNA damage, with a small but reproducible decrease in binding between the proteins observed upon damage. Despite clear evidence of interaction between Bod1L and MDC1, no FRET could be detected between the two proteins (Figure 4.3F-G). Given the large size of the protein pair, achieving Förster distance between C- or N-terminally tagged fluorophores is challenging. As figure 4.3H showed that only the C-terminal fragment of Bod1L is necessary for MDC1 binding, repeating these FRET assays with a smaller Bod1L fragment may increase the chance of achieving the Förster distance between the two fluorophores and thus detecting FRET.

In addition to strong evidence of an interaction with MDC1, I show that Bod1L interacts with the MRN complex via NBS1. Given that this interaction is only detectable using immunoprecipitation from fractionated HeLa cell lysate, and not using the single-cell binding LacO-LacI system, I suggest that the interaction between Bod1L and NBS1 is likely mediated through MDC1 (Figure 4.3C). I also observe that the interactions between Bod1L and MDC1/NBS1 are constitutive but are slightly, although reproducibly reduced, after damage (Figure 4.3A, B and C). Given that these immunoprecipitation reactions pull-down total cellular Bod1L, I hypothesise that whilst most cellular Bod1L interacts with MDC1/NBS1 in the absence of damage, this interaction is lost at DNA lesions, explaining the small, but reproducible, reduction in interaction after damage.

I also show that Bod1L binds PP2A-B56 exclusively in damaged cells and together these factors moderate the proper level of MDC1 phosphorylation.

Previous studies have highlighted the role of the Bod1L family member, Bod1, as a PP2A-B56 inhibitor during mammalian cell mitosis. Although Bod1L and Bod1 share a strong degree of homology, key residues identified within Bod1 which are critical for PP2A-B56 inhibition, are not conserved in Bod1L (Porter et al., 2013). This evidence, coupled with the loss of PP2A-B56 localisation to DNA lesions upon Bod1L depletion, leads us to hypothesise that the Bod1L-PP2A-B56 interaction mediates localisation of the phosphatase holocomplex rather than its inhibition. The data suggest that only specific PP2A holocomplexes are associated with DNA lesions, the specifics of which are unclear. I observed PP2A-B56γ1 localising to laser stripes, however I saw no evidence of the B56α subunit also localising to such stripes, consistent with the recruitment of specific B56 holocomplexes (Figure 4.6G). Given the hypothesis that Bod1L recruits PP2A-B56 holocomplexes to sites of DNA damage, it is surprising that I could not detect localisation of the PP2A-Aα scaffold subunit to micro-irradiation stripes (Figure 4.6F). Whilst this could be due to the high-fluorescence background caused by reagent choice and experimental design, it could be that Bod1L recruited complexes contain the PP2A-Aβ isoform instead of the PP2A-Aα isoform. More investigation is needed to explore the subunit composition of PP2A-B56 complexes recruited to damage sites by Bod1L. Previous studies have detected the catalytic subunit of PP2A at IRIF, however I was unable to reproduce this observation (Chowdhury et al., 2005). Once again, it is possible that different PP2A holocomplexes localise to DNA lesions under differing temporal conditions; perhaps related to their function, hence the differences in localisation observed.

I have demonstrated that a loss of Bod1L prevents the proper recruitment of PP2A-B56 to sites of damage, affecting the delicate balance of kinase and phosphatase at DNA lesions. This data suggests that the resulting unbalanced hyper-phosphorylation of MDC1 results in the excessive accumulation of MDC1. Literature data suggests that this excessive accumulation may be mediated through the unregulated oligomerisation of this critical DNA repair scaffold (Jungmichel et al., 2012; Liu et al., 2012; Luo et al., 2011). I hypothesise that in the absence of Bod1L, the resulting high phospho-MDC1 T4, which persists even 8 hours after damage compared with control, could explain the continued accumulation of MDC1 at sites of damage even in the absence of the damaging agent. The hyper-phosphorylation leads to further oligomerisation thus increasing local concentrations of MDC1 at these sites as seen in figure 4.1B-E. The data are in agreement with studies showing that disruption of MDC1 dimerisation/oligomerisation at DSBs can lead to disruption of proper DDR (Jungmichel et al., 2012; Liu et al., 2012; Luo et al., 2011). I show that in the absence of Bod1L, PP2A-B56 function at sites of damage is perturbed, leading to hyper-phosphorylation of MDC1 T4. The resulting uncontrolled increase of MDC1 at damaged sites possibly sterically hinders CKII phosphorylation of MDC1 (Figure 4.5B, C), preventing interaction with NBS1, which is critical for downstream break processing (Chapman and Jackson, 2008; Melander et al., 2008; Spycher et al., 2008).

The role of kinases such as ATM and ATR have long been established as critical for repair (Sancar et al., 2004), however the role of antagonising phosphatases is poorly understood, especially during early DNA damage protein complex formation. This study reveals Bod1L as a key modulator of

early phosphatase activity at sites of DNA damage and begins to shed light on the complex role of phosphatases in the control of DDR. Here I show an important role for the direct recruitment of PP2A to the sites of DNA damage, early in the repair process, an observation previously unreported. The data presented here are complementary to recent studies which highlight the function of phosphatase activity earlier in the repair process both in activating cell cycle checkpoints in response to damage (Yan et al., 2010) and in preventing incorrect DDR complex formation at specific cell cycle stages (Lee et al., 2014; Orthwein et al., 2014).

Despite emerging evidence for the important role of phosphatases in the damage response, several questions remain to be investigated (Shimada and Nakanishi, 2013). Primarily, it is not clear how the activity of each phosphatase is regulated to induce dynamic dephosphorylation events following DNA damage, as outlined in figure 1.7. In the case of PP1, DNA damage triggers dissociation of PP1 from its inhibitory subunits which results in its activation (Tang et al., 2008). Yet, the role of cellular PP2A inhibitory proteins in DNA damage repair, shown to be crucially important during other cellular processes, remains poorly understood (Haesen et al., 2014). One inhibitor identified to be involved in damage repair, TIPRL, has been shown to interact with both PP2A and PP4C to inhibit ATM/ATR signalling, with loss of the protein leading to cisplatin sensitivity (Gingras et al., 2005; McConnell et al., 2007). Indeed, multiple PP2A inhibitors in phase I clinical trials have been shown to hypersensitise tumour cells to DNA damaging agents, identifying this pathway as a promising combination therapy in cancer treatment (Chang et al., 2015; Lv et al., 2014; Wei et al., 2013). The function of chromatin associated proteins

such as Bod1L, located and modified close to DNA lesions, may be key in maintaining the correct localisation and activity of these dynamically regulated protein phosphatases.

Chapter 5 - The role of Bod1L in control of DNA damage checkpoints

In the previous two chapters, I have established that Bod1L is a critical player in the maintenance of genomic stability. Whilst it is likely that Bod1L plays many roles in the repair process, I have specifically shown that Bod1L functionally interacts with the B56 regulatory subunit of PP2A to regulate the phosphorylation of the critical phospho-scaffold MDC1. Depletion of Bod1L initially results in a loss of rapid MDC1 recruitment to DNA lesions. In addition to this, Bod1L depletion leads to a loss of PP2A-B56 recruitment to sites of damage, resulting in a failure of cells to control further MDC1 localisation to DNA lesions, eventually culminating in defective HR repair.

As outlined in figure 1.2, Chk2 is a cell-cycle specific kinase that is necessary in activating cell-cycle checkpoints upon genotoxic stress (Ahn et al., 2004). Chk2 phosphorylates a number of downstream targets that results in the arrest of the cell cycle at various different stages (Figure 1.6). Chk2 has been shown to physically interact with a number of critical DNA damage repair components including the phospho-scaffold MDC1 (Lou et al., 2003). Upon DNA damage, the FHA domain of MDC1 is able to bind to the phospho-T68 Chk2 protein (Wu et al., 2012). Interestingly, Chk2 does not co-localise with MDC1 at DNA lesions, instead remaining diffusely localised in the nucleus, implying a transient interaction between the two proteins (Jungmichel and Stucki, 2010). Furthermore, forced localisation of Chk2 to MDC1 containing IRIF, impaired the downstream signal transduction associated with the kinase, suggesting that

although the interaction with MDC1 is important, the dynamic mobilisation of Chk2 is critical for proper kinase function (Lukas et al., 2003).

In addition to interacting with core components of the DNA repair machinery, Chk2 has also been shown to physically interact with the Ser/Thr phosphatase PP2A-B56 (Dozier et al., 2004; Freeman et al., 2010). Studies have demonstrated a damage-dependent, direct interaction with both the B56γ and B56α subunits of the PP2A holocomplex. Although the precise functional consequence of such interactions remains unclear, subsequent studies have hypothesised that PP2A-B56 (in association with other phosphatases) counteracts the low basal kinase activity of ATM in the absence of DNA damage (Figure 1.7). Activation of ATM in response to genotoxic stress deactivates this negative feedback loop allowing the phosphorylation of Chk2 by ATM and subsequent downstream signalling (Carlessi et al., 2010). Inhibition of PP2A with Okadaic acid (OA) or depletion by siRNA, induced accumulation of phospho-T68 Chk2 (as well as auto- and trans-phosphorylations involved in its full activation), highlighting the importance of the phosphatases in the Chk2 pathway.

Given that I have demonstrated a damage dependent interaction of Bod1L with PP2A-B56γ, I wanted to investigate whether Bod1L was involved in the ATM-Chk2-CDC25A pathway. The following chapter outlines the findings showing that loss of Bod1L leads to compromised T68 phosphorylation of Chk2 following DNA damage, resulting in defective checkpoint control.

Results

The activation and role of the checkpoint kinase Chk2 in response to DNA damage

DNA damage dependent activation of the critical checkpoint kinase Chk2, is a complex but well understood process (Figure 5.1A) (Cai et al., 2009). In undamaged cells, Chk2 exists as an inactive monomer, predominantly localised in the nucleus during interphase (Chouinard et al., 2013). Upon activation of ATM occurring at DNA lesions, the inactive Chk2 monomer is phosphorylated at the SQ/TQ cluster domain, specifically at T68 (Ahn et al., 2000; Matsuoka et al., 2000), with mutation of T68 resulting in failure to activate the kinase. The phosphorylated Chk2 monomer then binds to another inactive phospho-Chk2 monomer via the FHA domain, forming an inactive dimer (Ahn et al., 2002). The kinase domain of Chk2 is then activated via a series of auto- and trans-phosphorylations through the kinase activation loop (Schwarz et al., 2003). Once activated, the kinase exists as an active dimer or monomer, with the T68 modification no longer required for sustained activation of the kinase (Ahn and Prives, 2002).

The activated Chk2 kinase plays many roles in response to DNA damage, including signal propagation, cell-cycle arrest and apoptosis (Figure 5.1B) (Ahn et al., 2004). The first characterised, and arguably best validated, Chk2 substrates are the CDC25 phosphatase family, consisting of CDC25A and CDC25C. The primary role of these two phosphatases is promoting cell-cycle progression via activation of CDK1/2 through the dephosphorylation of inhibitory phosphorylation at T14/15 (Falck et al., 2001). Chk2 phosphorylation of

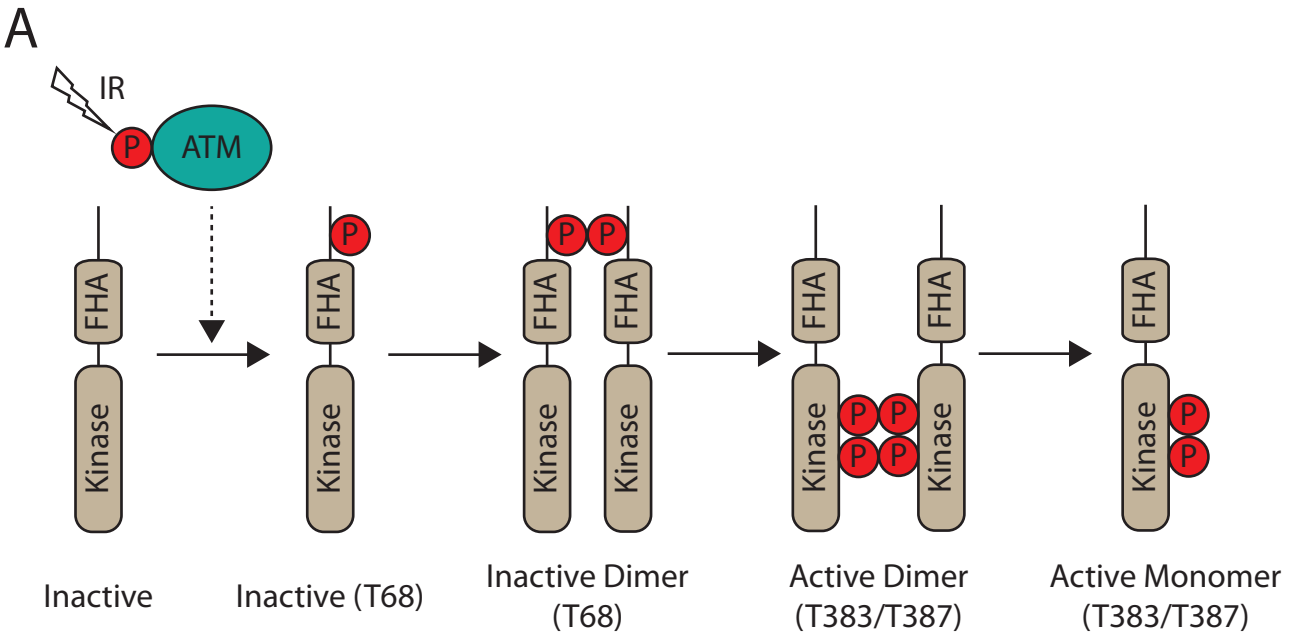
A
IR
P
ATM
FHA
Kinase
Inactive
Inactive (T68)
Inactive Dimer
(T68)
Active Dimer
(T383/T387)
Active Monomer
(T383/T387)

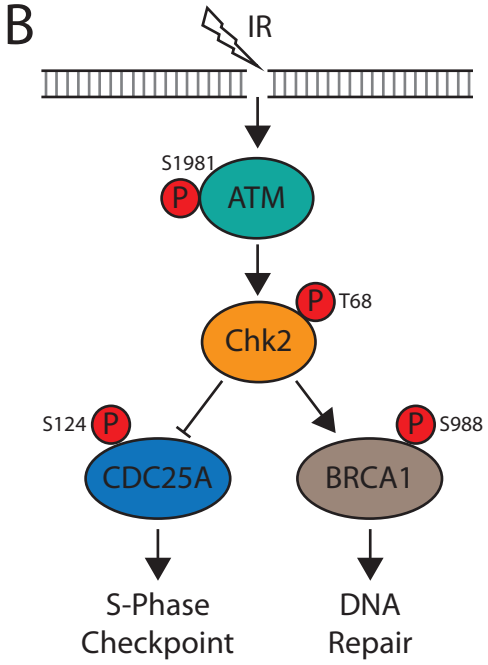
B
IR
S1981
P
ATM
P
T68
Chk2
S124
P
CDC25A
P
S988
BRCA1
S-Phase
Checkpoint
DNA
Repair

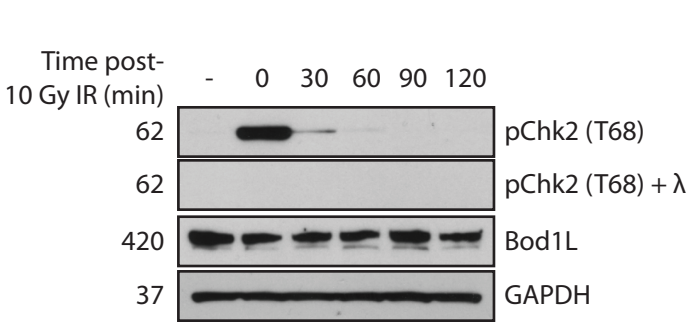
C
Time post-
10 Gy IR (min)
-
0
30
60
90
120
62
pChk2 (T68)
62
pChk2 (T68) + λ
420
Bod1L
37
GAPDH

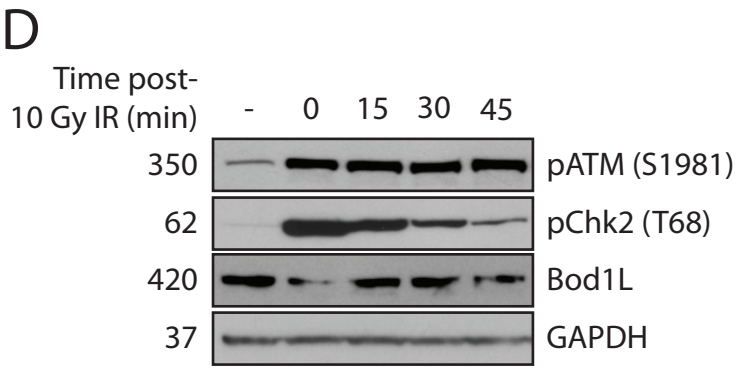
D
Time post-
10 Gy IR (min)
-
0
15
30
45
350
pATM (S1981)
62
pChk2 (T68)
420
Bod1L
37
GAPDH

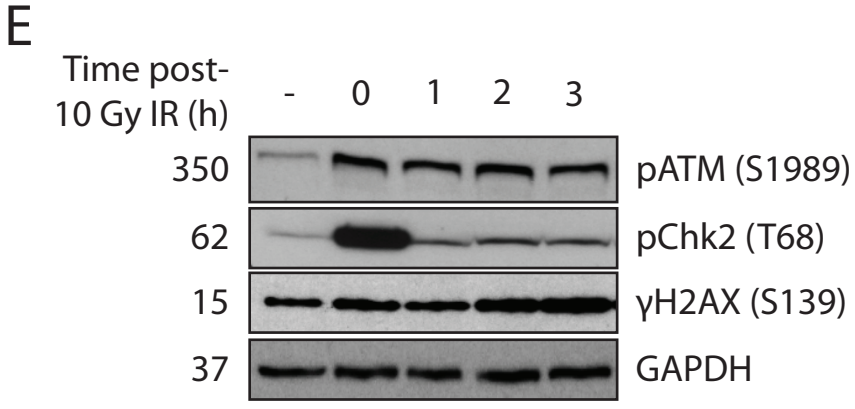
E
Time post-
10 Gy IR (h)
-
0
1
2
3
350
pATM (S1989)
62
pChk2 (T68)
15
γH2AX (S139)
37
GAPDH

Figure 5.1: The role of Chk2 kinase in DNA damage repair

(A) Schematic representation of Chk2 activation upon DNA damage. Active ATM phosphorylates Chk2 at T68 resulting in dimerisation. Trans- and auto-phosphorylation at T383 and T387 results in the formation of an active dimer which splits to form an active monomeric kinase. Adapted from (Ahn et al., 2004).

(B) Schematic representation of the role of Chk2 during the DNA damage response. Activated ATM phosphorylates and activates Chk2 as described (A). Chk2 can then phosphorylate CDC25A resulting in proteosomal degradation of the phosphatase. Active Chk2 can also phosphorylate BRCA1 at S988, promoting repair by HR. Adapted from (Zhou and Bartek, 2004).

(C) HeLa cells were dosed with 10 Gy IR and lysed at time-points indicated. Immunoblots were probed with antibodies targeting pChk2 (T68), Bod1L and GAPDH. To determine phospho-specificity of antibody, lambda phosphatase (λ) was included as a control.

(D) HeLa cells were dosed with 10 Gy IR and lysed at time-points indicated. Immunoblots were probed with antibodies targeting pATM (1981), pChk2 (T68), Bod1L and GAPDH.

(E) HeLa cells were dosed with 10 Gy IR and lysed at time-points indicated. Immunoblots were probed with antibodies targeting pATM (1981), pChk2 (T68), γH2AX (S139) and GAPDH.

CDC25A at S124 leads to proteosomal degradation of the phosphatase, thus maintaining the inhibition of CDK2 and preventing cell cycle progression (Bartek and Lukas, 2001). Chk2 phosphorylation of CDC25C leads to interaction of the phosphatase with 14-3-3 scaffold proteins, inhibiting interaction with CDK1, thus halting cell-cycle progression (Peng et al., 1997). In addition to a role in regulating cell-cycle progression upon damage, Chk2 also mediates DNA repair through the phosphorylation of Breast cancer type 1 susceptibility protein (BRCA1) (Zhang et al., 2004). Chk2 mediated phosphorylation of BRCA1 at S988 promotes repair via HR, thus inhibiting the more error-prone NHEJ (Zannini et al., 2014). Knock-in of an equivalent S988 mutation in mice revealed that the BRCA1$^{S971A/S971A}$ mice displayed increased instance of spontaneous tumour formation and were hypersensitive to DNA damaging agents (Kim et al., 2004), indicating the importance of Chk2 phosphorylation of BRCA1 in maintaining robust DNA repair.

I observed that HeLa cells treated with 10 Gy IR displayed a rapid induction of phospho-T68 Chk2, with phosphorylation peaking immediately after damage and rapidly decreasing after 30 minutes (Figure 5.1C). Treatment of cellular lysates, damaged with IR, with lambda phosphatase revealed that the antibody was specific for the phosphorylated form of the kinase. Assessing a much narrower window post-IR treatment revealed that phospho-T68 Chk2 levels decrease as soon as 15 minutes post damage, returning to almost basal levels after 60 minutes (Figure 5.1D, E). The increase in phospho-T68 Chk2 phosphorylation directly correlates with ATM activation, with ATM remaining active throughout the time course examined (Ward et al., 2001; Zhao et al., 2008). I detected γH2AX phosphorylation at later time-points compared with

Chk2 (Figure 5.1E), suggesting that these two components of the damage repair machinery act in separate pathways.

Sustained IR-induced phospho-T68 Chk2 phosphorylation is lost following Bod1L depletion

The rapid and transient nature of the phospho-T68 Chk2 modification is clearly important in establishing an active Chk2 kinase, which is then able to phosphorylate a number of downstream substrates. Given that I have shown that Bod1L interacts with a number of proteins that have also been shown to interact with Chk2, such as MDC1 and PP2A-B56 (Dozier et al., 2004; Liang et al., 2006; Lou et al., 2003), I wanted to understand whether loss of Bod1L led to a change in Chk2 activation or normal activity upon DNA damage. I depleted Bod1L from HeLa cells and dosed with 10 Gy IR. 30 minutes after IR treatment I lysed the cells and probed the immunoblots for phospho-T68 Chk2. Upon Bod1L depletion, Chk2 is not phosphorylated at T68, despite active ATM as denoted by phospho-S1981 (Figure 5.2A).

Failure of Chk2 phosphorylation at phospho-T68 would result in the kinase remaining inactive, as previously described (Ahn et al., 2000). To assess whether Chk2 kinase was active in the absence of Bod1L, I treated HeLa cells with siBod1L and 10 Gy IR before probing immunoblots with antibodies against phospho-S124 CDC25A. In the absence of Bod1L, initial phosphorylation of phospho-T68 Chk2 was normal but this phosphorylation was not maintained compared with control (Figure 5.1C). The lack of sustained phosphorylation of Chk2 led to a decrease in the phosphorylation of CDC25A, a major downstream

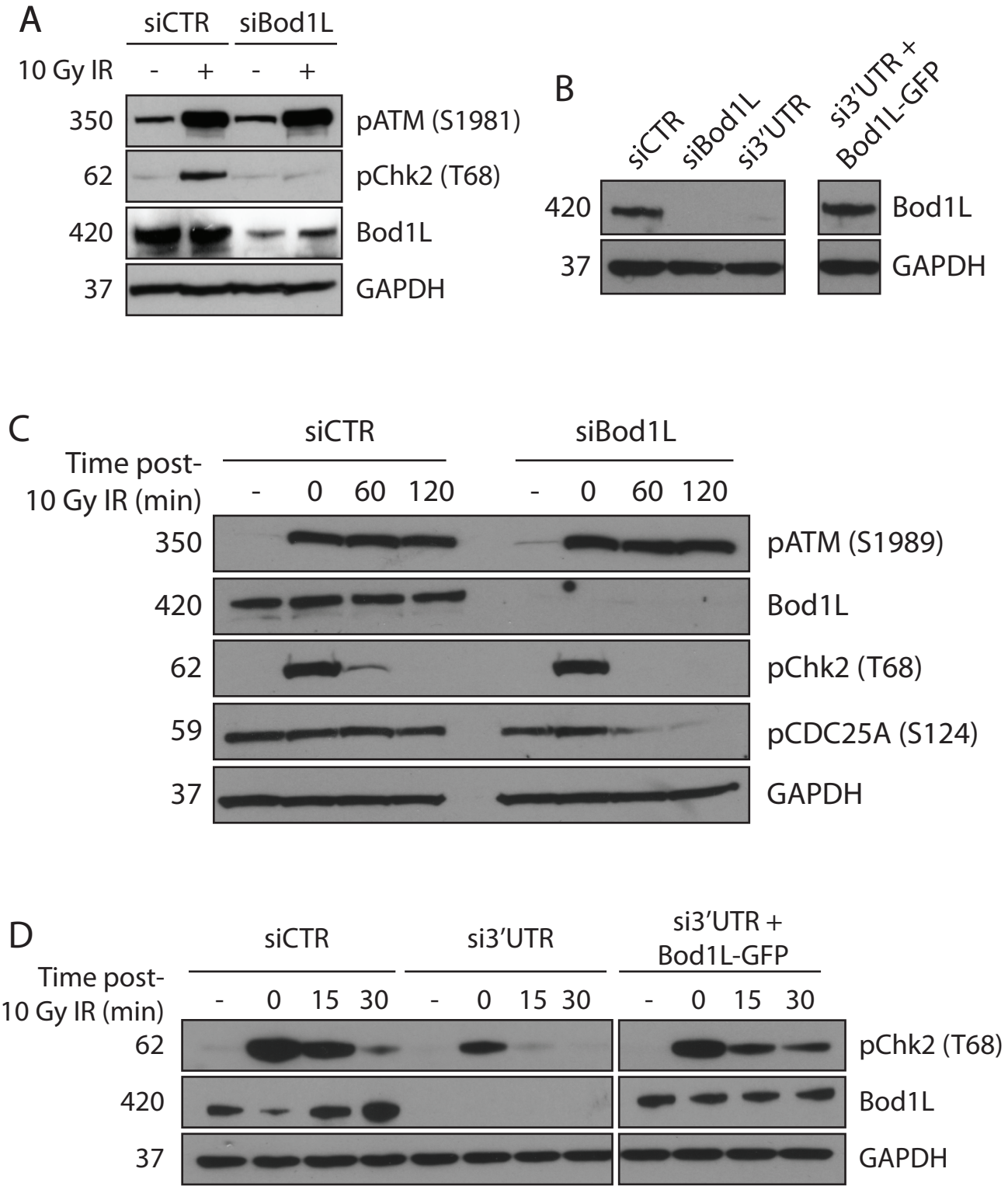
A
siCTR
siBod1L
10 Gy IR
-
+
-
+
350
pATM (S1981)
62
pChk2 (T68)
420
Bod1L
37
GAPDH
B
siCTR
siBod1L
si3'UTR
si3'UTR + Bod1L-GFP
420
Bod1L
37
GAPDH
C
siCTR
siBod1L
Time post-10 Gy IR (min)
-
0
60
120
-
0
60
120
350
pATM (S1989)
420
Bod1L
62
pChk2 (T68)
59
pCDC25A (S124)
37
GAPDH
D
siCTR
si3'UTR
si3'UTR + Bod1L-GFP
Time post-10 Gy IR (min)
-
0
15
30
-
0
15
30
-
0
15
30
62
pChk2 (T68)
420
Bod1L
37
GAPDH

Figure 5.2: Sustained Chk2 phosphorylation post-damage is lost in the absence of Bod1L

(A) HeLa cells were transfected with either control or Bod1L siRNA. After 48 hours, cells were dosed with 10 Gy IR or mock irradiated and lysed immediately. Immunoblots were probed with antibodies targeting pATM (S1981), pChk2 (T68), Bod1L and GAPDH.

(B) HeLa cells were transfected with control, Bod1L or 3'UTR-Bod1L siRNA. After 24 hours, 3'UTR-Bod1L treated cells were transfected with Bod1L-GFP. Immunoblots were probed with antibodies against Bod1L and GAPDH.

(C) HeLa cells were transfected with either control or Bod1L siRNA. After 48 hours, cells were dosed with 10 Gy IR or mock irradiated and lysed at the time point indicated. Immunoblots were probed with antibodies targeting pATM (S1981), Bod1L, pChk2 (T68), pCDC25A (S124) and GAPDH.

(D) HeLa cells were transfected with control, Bod1L or 3'UTR-Bod1L siRNA. After 24 hours, 3'UTR-Bod1L treated cells were transfected with Bod1L-GFP (>70% expression). After 24 hours, cells were dosed with 10 Gy IR or mock irradiated and lysed at the time point indicated. Immunoblots were probed with antibodies against pChk2 (T68) Bod1L and GAPDH.

target of Chk2. This suggests that loss of Bod1L leads to less robust activation of Chk2 and a subsequent reduction in the down stream phosphorylation of Chk2 substrates.

To further explore the loss of sustained phosphorylation of phospho-T68 Chk2 further, I performed repeat experiments utilising a much narrower temporal window. In addition I incorporated a rescue experiment to determine whether depletion of Bod1L was the cause of the changes in Chk2 phosphorylation (Figure 5.2D). Figure 5.2B demonstrates that using a siRNA targeting the 3'UTR of Bod1L whist transiently expressing Bod1L-GFP, I was able to re-express Bod1L to endogenous protein levels. Using this system, I observed that Bod1L depletion has two main effects on phospho-T68 Chk2: firstly initial phosphorylation immediately after damage is slightly lower than control and secondly, this reduced phosphorylation is not sustained for the same duration at siCTR treated cells (Figure 5.1D). Exogenous expression of siRNA resistant Bod1L in such treated cells recovers to phospho-T68 phosphorylation to levels comparable with control treated cells.

Depletion of PP2A-B56 also leads to the loss of sustained phospho-T68 Chk2

Chk2 physically interacts with MDC1 in the presence of DNA damage, an interaction mediated via the MDC1 FHA domain and phosphorylated-T68 of Chk2 (Lou et al., 2003). This interaction has been shown to be critical for the maintenance of Chk2-mediated DNA damage responses. Chk2 also interacts with the B56-gamma regulatory subunit of PP2A (Dozier et al., 2004; Liang et al., 2006). Although the functional impact of this interaction remains unclear, it

appears that the Chk2-PP2A interaction may control the activity of the kinase at sites of DNA damage. Given the evidence that Chk2 and Bod1L share key functional interactions upon DNA damage, I wanted to determine whether Bod1L and Chk2 physically interact in the presence or absence of genotoxic stress. I immunoprecipitated Bod1L-GFP from HeLa cells stably expressing Bod1L-GFP but observed no specific binding of Chk2 in the presence or absence of DNA damage (Figure 5.3A).

I demonstrated in figure 5.1D that initial phosphorylation of Chk2 immediately after damage is marginally lower than in control treated cells and secondly, that this reduced phosphorylation is not sustained for the same duration compared with control. Co-depletion of Bod1L and the B56 regulatory subunit of PP2A phenocopied this effect (Figure 5.3B). Depletion of Bod1L or PP2A-B56 had no effect on Chk2 protein expression as demonstrated by immunoblotting unmodified Chk2. Assessment of phospho-T68 Chk2 modification on a more narrow temporal window reveals that the loss of phosphorylation upon DNA damage is more severe upon PP2A-B56 depletion than Bod1L (Figure 5.3C), suggestive that these two proteins may be possibly acting in an epistatic manner.

Loss of either Bod1L or PP2A-B56 results in compromised intra-S-phase checkpoint control

To help preserve genomic integrity, cells exposed to DNA damage activate the ATM kinase which results in a complex signalling pathway, leading to S-phase checkpoint arrests, thus delaying DNA replication (Falck et al., 2002). Defects in any components of this pathway, such as phospho-T68 Chk2 modification or

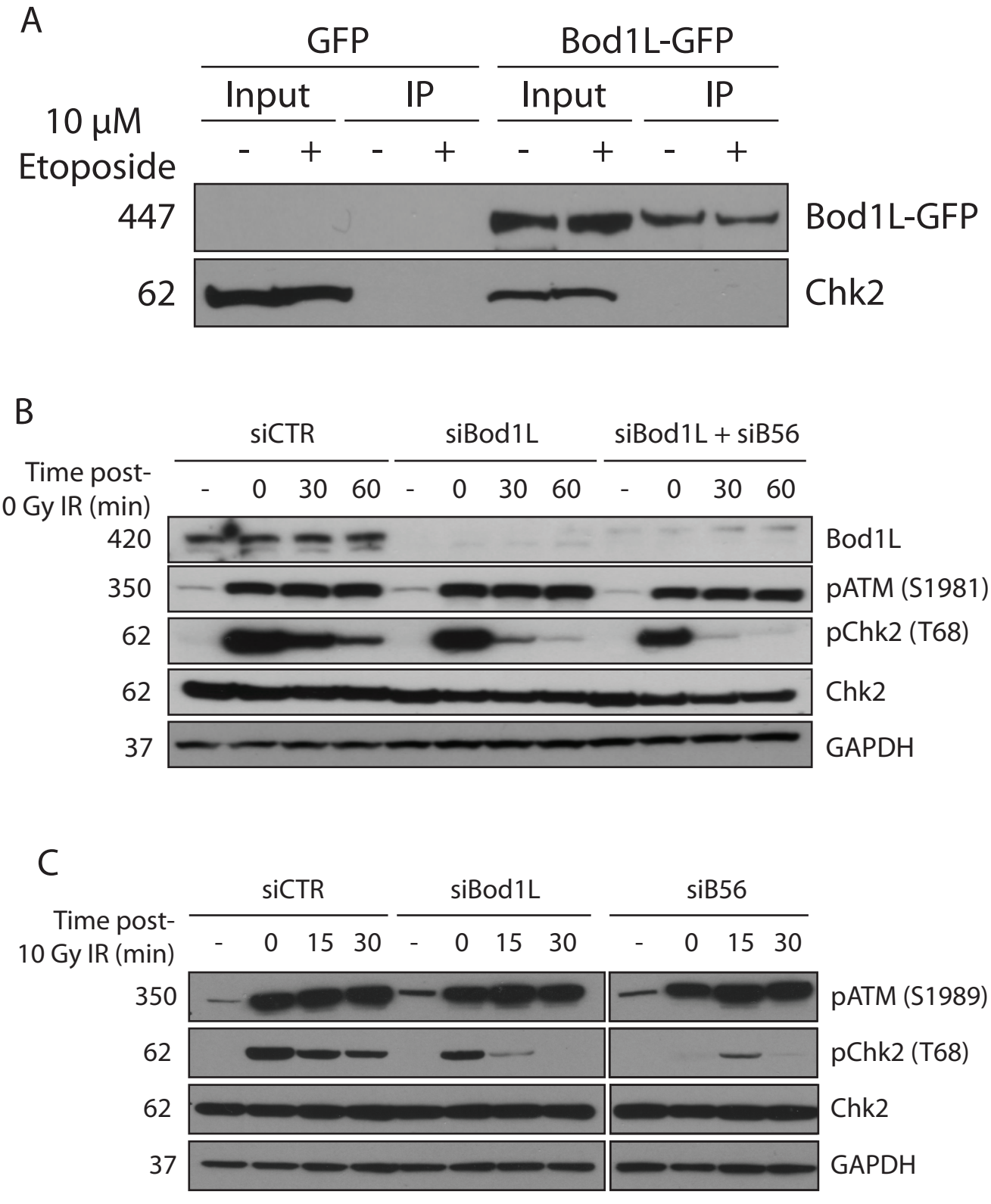
A
GFP
Bod1L-GFP
Input
IP
Input
IP
10 μM Etoposide
- + - + - + - +
447
Bod1L-GFP
62
Chk2
B
siCTR
siBod1L
siBod1L + siB56
Time post-10 Gy IR (min)
- 0 30 60 - 0 30 60 - 0 30 60
420
Bod1L
350
pATM (S1981)
62
pChk2 (T68)
62
Chk2
37
GAPDH
C
siCTR
siBod1L
siB56
Time post-10 Gy IR (min)
- 0 15 30 - 0 15 30 - 0 15 30
350
pATM (S1989)
62
pChk2 (T68)
62
Chk2
37
GAPDH

Figure 5.3: Depletion of PP2A-B56 also results in the loss of Chk2 T68 phosphorylation post-damage

(A) GFP-Trap Immunoprecipitation (IP) of Bod1L-GFP from the chromatin and nuclear fraction of HeLa cells transiently expressing Bod1L-GFP. IPs were analysed by western blotting using antibodies against GFP and Chk2.

(B) HeLa cells were transfected with control, Bod1L or Bod1L + PP2A-B56 siRNA. After 48 hours, cells were dosed with 10 Gy IR or mock irradiated and lysed at the time point indicated. Immunoblots were probed with antibodies targeting Bod1L, pATM (S1981), pChk2 (T68), Chk2 or GAPDH.

(C) HeLa cells were transfected with control, Bod1L or PP2A-B56 siRNA. After 48 hours, cells were dosed with 10 Gy IR or mock irradiated and lysed at the time point indicated. Immunoblots were probed with antibodies targeting pATM (S1981), pChk2 (T68), Chk2 or GAPDH.

ATM inhibition, lead to radio-resistant DNA synthesis (RDS) (Falck et al., 2001). This inability of a cell to reduce the rate or inhibit DNA replication post-DNA damage, leads to replication stress ultimately resulting in mutagenesis or cell death.

Figure 5.4A shows a schematic representation of the ATM-Chk2-CDC25A signalling pathway that acts to protect against such DNA synthesis post-damage. At DNA lesions ATM is activated which leads to the phosphorylation and activation of Chk2 demonstrated in figure 5.1A. Activated Chk2 is then able to phosphorylate CDC25A, resulting in proteolytic degradation of the protein. The loss of CDC25A phosphatase prevents the dephosphorylation of the CDK2/CyclinE complex, thus locking this S-phase promoting complex in the inactive state, preventing Cdc45 loading at replication origins (Bartek and Lukas, 2001). I have already demonstrated that loss of Bod1L, or the B56 regulatory subunit of PP2A, leads to a decrease in the phosphorylation of Chk2, resulting in a loss of downstream CDC25A phosphorylation (Figure 5.1C). The model for S-phase checkpoint inhibition would predict that this loss of CDC25A phosphorylation would result in an activated CDK2/CyclinE complex, leading to radio-resistant DNA synthesis. To test this prediction, I performed an intra s-phase checkpoint assay, using DNA labelled with BrdU to assess for any DNA replication following ionising radiation. I observed that depletion of either Bod1L or PP2A-B56 alone led to a significant amount of RDS at 5 Gy IR compared with control treated cells (Figure 5.4B). Co-depletion of these two proteins interestingly did not lead to RDS, despite knockdown of PP2A-B56 almost completely ablating Chk2 phosphorylation (Figure 5.3C). At higher doses of IR, only Bod1L depletion sustained this significant RDS.

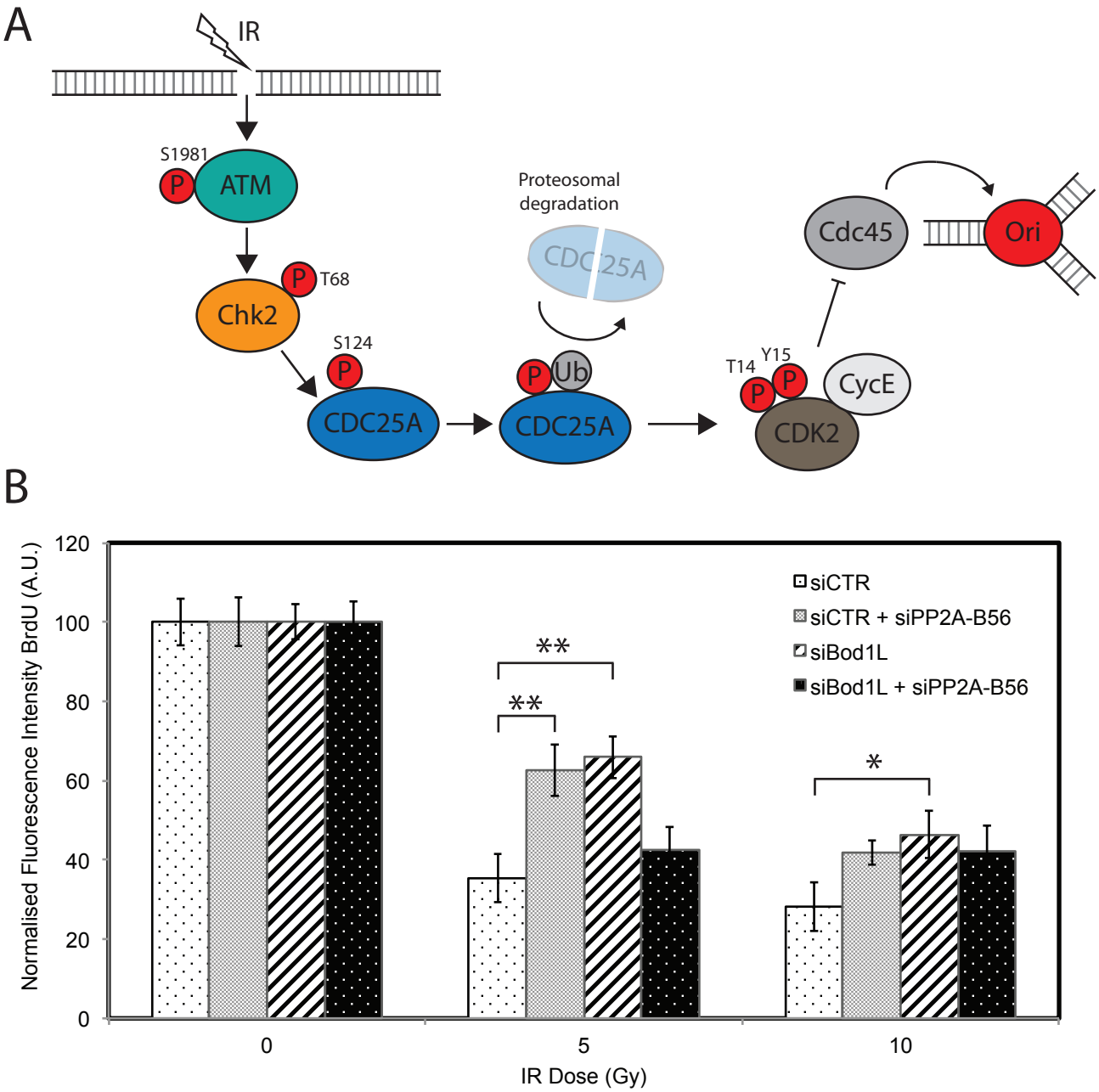

Figure 5.4: Loss of Bod1L or PP2A-B56 leads to a compromised intra-S-phase checkpoint

(A) Schematic representation of the intra-S-phase checkpoint in response to DNA damage during S-phase. Active Chk2 phosphorylates CDC25A resultingtargetting the phosphatase for proteosomal degradation. CDK2/CycE remains phosphorylated at T14/Y15 which prevents CDC45 loading at replication origins. Adapted from (Bartek and Lukas, 2001)

(B) HeLa cells were transfected with control, PP2A-B56, Bod1L or PP2A-B56 + Bod1L siRNA. After 48 hours, cells were irradiated with 0, 5 or 10 Gy and left to recover for 1 hour 37°C. BrdU was added incubated for a further 1 hour. Cells were fixed and BrdU intensity was determined by microscopy. Data represented as mean ± SEM. n=>20 for each condition. *P<0.05, **P<0.01.

Discussion

I have demonstrated that loss of either Bod1L or PP2A-B56 prevents the sustained phosphorylation of phospho-T68 Chk2 in response to DNA damage. The initial phosphorylation of Chk2 immediately upon DNA damage seems only marginally affected by Bod1L depletion, compared with the rapid decrease in phosphorylation at later time points. This data, coupled with evidence from figure 3.11B-D which suggests that ATM kinase activity is unaffected by Bod1L depletion, highlight the probable involvement of phosphatases in this process.

I demonstrate in figure 4.6A-B that Bod1L interacts with PP2A-B56 specifically in the presence of DNA damage, with this interaction critical for proper PP2A-B56γ localisation to DNA lesions (Figure 4.7). I mentioned previously that activation of ATM in response to genotoxic stress deactivates the PP2A-B56/Chk2 negative feedback loop, allowing the phosphorylation of Chk2 by ATM and subsequent downstream signalling (Carlessi et al., 2010). The data presented in this chapter, suggests that Bod1L could possibly act as an additional level of control over this step, acting to release Chk2 from this inhibitory phosphatase complex upon DNA damage, thus allowing it to phosphorylate downstream substrates. Based on the evidence presented in figures 5.1-3, I hypothesise that loss of Bod1L from cells leads to 'uncontrolled' PP2A-B56 that is able to promiscuously dephosphorylate Chk2 irrespective of the presence or absence of DNA damage. The data showed that depletion of PP2A-B56 also led to a loss of sustained phosphorylation of Chk2 following DNA damage. This suggests that an additional phosphatase must also be able to promiscuously dephosphorylate phospho-Chk2 T68 in the absence of PP2A-B56 activity (Figure 6.2). Wip1 is known to target T68 phosphorylation (Oliva-

Trastoy et al., 2006), therefore it would be interesting to investigate the effect of Bod1L and/or PP2A-B56 depletion on the activity of this potentially unregulated phosphatase.

The activation process of the Chk2 kinase is well documented, with the reliance on sustained T68 phosphorylation demonstrated as being important during the early activation phase, but not once the kinase is active (Ahn and Prives, 2002). The hypothesis suggests that the failure to maintain phospho-T68 Chk2 during the initial activation of the kinase renders the downstream signalling compromised as a result of an inactive, or partially inactive, kinase. Further investigation using phosphorylation specific mass-spectrometry, or use of phospho-specific antibodies, is needed to determine whether the auto- and trans-phosphorylations associated with active Chk2 are present in the absence of Bod1L. A reduction in the presence of these 'activating' phosphorylations would verify my hypothesis that Chk2 is less active in the absence of Bod1L.

In chapter 4, I demonstrated that co-depletion of Bod1L and PP2A-B56 phenocopied the Bod1L knockdown with regard to elevated phosphorylation of phospho-T4 MDC1 and the subsequent hypersensitivity to genotoxic stress. Here I show that depletion of Bod1L and PP2A-B56 appears to generate an additive effect in loss of phospho-T68 Chk2 phosphorylation, suggesting that these proteins are acting in epistatic pathways. Alternatively, loss of PP2A-B56 is affecting additional pathways involved in checkpoint arrest, which is resulting in this additive effect. Indeed, I observe that co-depletion of Bod1L and PP2A-B56 rescue RDS at low doses of IR, further suggesting that knockdown of both genes simultaneously, may affect more than one pathway (Figure 5.4B). One

such additional pathway that may be affected by Bod1L depletion with regard to checkpoint control, is ATM mediated phosphorylation of phospho-S343 NBS1 and subsequent MRN complex formation (Falck et al., 2002). I have already shown that Bod1L depletion can alter the MDC1-MRN interaction (Figure 4.5D), so there is precedent for Bod1L depletion to further affect this critical complex. Precisely how the MRN complex affects DNA synthesis is unknown, however recent studies have demonstrated that NBS1 binds to the E2F1 transcription factor, an interaction that directly influences S-phase progression. The significance of this interaction is further strengthened with the evidence that E2F1-NBS1 binding is almost completely lost in NBS and A-TLD cells (Ahn et al., 2004; Maser et al., 2001).

I discussed previously how Chk2 mediated phosphorylation of BRCA1 at S988 promotes repair via HR, inhibiting the more error-prone NHEJ (Lou et al., 2003; Zhang et al., 2004). Literature evidence showed that knock-in of an equivalent S988 mutation in mice revealed that the BRCA1$^{S971A/S971A}$ mice displayed increased instance of spontaneous tumour formation and were hypersensitive to DNA damaging agents (Kim et al., 2004; Wu et al., 2012). Given that I have shown that Bod1L depletion leads not only to defective HR repair, but also compromised Chk2 activation, future investigation is needed into assessing the phosphorylation of BRCA1 following DNA damage. A Bod1L-dependent loss of phospho-S988 BRCA1 phosphorylation could explain the defective HR phenotype I observe, occurring as a result of defective Chk2 activation.

Chapter 6 - Discussion and Future Directions

Bod1L is a novel DNA damage response protein, required for robust DNA repair

The data presented in this thesis, combined with recently published work from the Stewart group, reveal Bod1L as a novel component of the DNA damage repair machinery (Higgs et al., 2015). I identified Bod1L as a novel chromatin bound protein, with a C-terminal cluster of multiple NLS and a single A-T hook that is necessary for nuclear localisation (Figure 3.1). ATM/ATR substrate specific phospho-proteomics studies, in addition to ultradeep phospho-proteomics, revealed that Bod1L was highly modified, with a number of phosphorylation events occurring in response to DNA damage (Matsuoka et al., 2007; Sharma et al., 2014). I confirmed two of these phosphorylation sites, S1145 and S1710, were phosphorylated at sites of DNA damage, with S1710 phosphorylated by DNA-PK *in vitro*.

Depletion of Bod1L from multiple cell types resulted in phenotypes associated with a failure of DNA damage repair, including fragmented, acentric chromatin and nuclear morphology changes (Constantinescu et al., 2010; Terradas et al., 2009)(Figure 3.2). In addition, treatment of Bod1L depleted cells with genotoxic stresses led to severe hypersensitivity, consistent with compromised DNA repair. Indeed, assessment of DNA repair by HR revealed that depletion of Bod1L reduced HR efficiency in a manner similar to ATM inhibition (Figures 3.3 and 3.4).

As mentioned previously, phospho-proteomic analysis of ATM/ATR substrates in response to DNA damage identified two Bod1L phosphorylation sites, S1145 and S1710, which were confirmed using phospho-specific antibodies raised against these sites (Figures 3.6 and 3.10) (Matsuoka et al., 2007). Bod1L S1710 is rapidly phosphorylated at sites of DNA damage in a manner analogous with the phosphorylation of γH2AX and the γH2AX dependent recruitment of MDC1. I utilised recombinant DNA-PK, which shares identical specificity to ATM *in vitro* (Kim et al., 1999; O'Neill et al., 2000), to confirm that phospho-Bod1L S1710 is likely phosphorylated by ATM in response to DNA damage. Investigation into the phosphorylation of phospho-Bod1L S1145 by ATM remains on going. Whilst the data clearly shows damage dependent phosphorylation of Bod1L at DNA lesions, the functional significance of this modification remains unclear. Preliminary functional rescues of Bod1L depletion revealed that mutation of either site individually, or together, had no effect on the ability of Bod1L-GFP to rescue clonogenic sensitivity to MMC. As such, investigation is needed to understand the mechanistic implication of this modification. As Bod1L is bound constitutively to chromatin and other protein-interactors, one could hypothesise that ATM phosphorylation could regulate such interactions, perhaps driving the release of proteins bound to Bod1L. Use of the phospho-mutant and phospho-mimic Bod1L mutants will be vital in understanding this mechanistic step.

Work from the Stewart group identified Bod1L as a component of a pathway that safeguards genome stability following replication stress (Higgs et al., 2015), with loss of Bod1L resulting in sensitivity to replication stress and catastrophic genome instability. They elegantly demonstrated that Bod1L functions

downstream of BRCA2 to stabilise Rad51 nucleofilaments at damaged replication forks, protecting such damaged forks and preventing resection of nascent DNA strands by DNA2. Rad51 localisation to forks was unaffected following Bod1L depletion, suggesting that Bod1L acts to stabilise these nucleofilaments once formed. Whilst this study reveals an additional functional consequence of Bod1L depletion not explored in this thesis, little mechanistic detail is discussed regarding the position and function of Bod1L in this complex pathway. Unlike the data presented in this thesis, no replication defects or phenotype could be detected in cells solely depleted of Bod1L, with all phenotypic observation dependent upon the use of MMC to induce replication stress. Whilst the use of such agents is practical in exacerbating subtle phenotypes, if the principle function of Bod1L was to safeguard genome stability following replication stress, one would expect a more pronounced phenotype occurring as a result of any endogenous replication stress. In addition to this, the data consistently revealed the presence of fragmented and acentric chromatin visible during mitosis, in addition to abnormal nuclear morphology; established indicators of unrepaired DNA DSBs (Constantinescu et al., 2010; Fan et al., 2004; Kumareswaran et al., 2012; Terradas et al., 2009). Whilst the precise molecular mechanism for Rad51 nucleofilament stabilisation by Bod1L remains unclear, the authors did demonstrate that Bod1L interacts with a number of key components of the DDR, including Mre11 and BRCA2. Combining this information, along with the extensive phenotypic data from this thesis and the evidence of unrepaired DSBs in the absence of Bod1L, it is highly likely that Bod1L plays a dual role in both the repair of DSBs as well as Rad51 nucleofilament protection during replication stress.

Initial Bod1L sequence analysis revealed a highly conserved, proline-rich region at the N-terminus of the protein, located prior to the COMPASS homology domain. Proline-rich repeats have been shown to facilitate a range of protein-protein interactions with a variety of proteins containing SH3, WW and EVH1 domains (Kay et al., 2000), in addition to playing an important role in a number of cellular process, such as the response to DNA damage (Shafman et al., 1997). The necessity of this proline-rich region of Bod1L was not investigated during this study, yet given the proximity of this region to the COMPASS/Bod1 homology domain of Bod1L, it presents an interesting avenue of investigation for future work.

As mentioned previously, methylation of H3K4 has been shown to be involved in the DNA damage response in both yeast and mammalian cells (Nakamura et al., 2011). Unlike damage-dependent PTMs, histone methylation appears to occur constitutively, with damage-induced changes in histone methylation correlating with DDR progression (Seiler et al., 2011). Studies in yeast have revealed that cells with a Δ*set1* mutation preventing H3K4 methylation, are defective in NHEJ repair and show compromised S-phase progression in the presence of replication stress (Faucher and Wellinger, 2010). These examples, in addition to other work, highlight the function of H3K4 modification in altering chromatin structure and directing signalling at sites of DNA damage to allow for robust repair. Contained within the Bod1-homology domain of Bod1L is a region of homology with the Complex proteins associated with SET1 protein (COMPASS) component Shg1. Recent data has shown that Bod1L interacts with a key accessory subunit of the COMPASS complex, Ash2L, suggestive of Bod1L being part of the Ash2L containing H3K4 methyltransferase complex.

The study found that H3K4 methyltransferase complexes bind to the Bod1L promoter, suggesting that regulation of chromatin structure at Bod1L locus may be important in regulating cellular H3K4 di- and tri-methylation (Ciotta, 2011). Subsequent work has also identified Bod1L as an interacting partner of the Dpy30 (WRAD) complexes, with Bod1L exclusively present in Set1A/Set1B methyltransferase complexes (van Nuland et al., 2013). These observations, combined with our preliminary data that suggests H3K4 methylation may be decreased in the absence of Bod1L, provide a tantalizing insight into an additional role of Bod1L in the regulation of cellular H3 methylation, possibly in response to DNA damage. This potentially PP2A-independent role of Bod1L certainly warrants investigation in the future.

Bod1L controls MDC1 and PP2A-B56 recruitment at sites of DNA damage

I have shown that Bod1L acts as a chromatin-bound scaffold that facilitates the delivery of MDC1 to sites of DNA damage and regulates multiple phospho-epitopes within MDC1. Depletion of Bod1L results in two defects that occur at different timescales; first, the delivery of MDC1 to sites of DNA damage is impaired in the first few minutes after damage, which also compromises the targeting of downstream repair factors (Figure 4.1). At longer timescales, control of MDC1 accumulation is lost, and this interferes with repair at sites of DNA damage. Bod1L binds MDC1, and possibly through this interaction to NBS1; these interactions are constitutive and are partially reduced after damage (Figure 4.3). Bod1L binds PP2A-B56 exclusively in damaged cells and together these factors moderate the proper level of MDC1 phosphorylation. The data suggest that unbalanced hyperphosphorylation of MDC1, caused by loss of the dephosphorylation of phospho-MDC1 T4 by PP2A-B56, results in the excessive accumulation of MDC1,

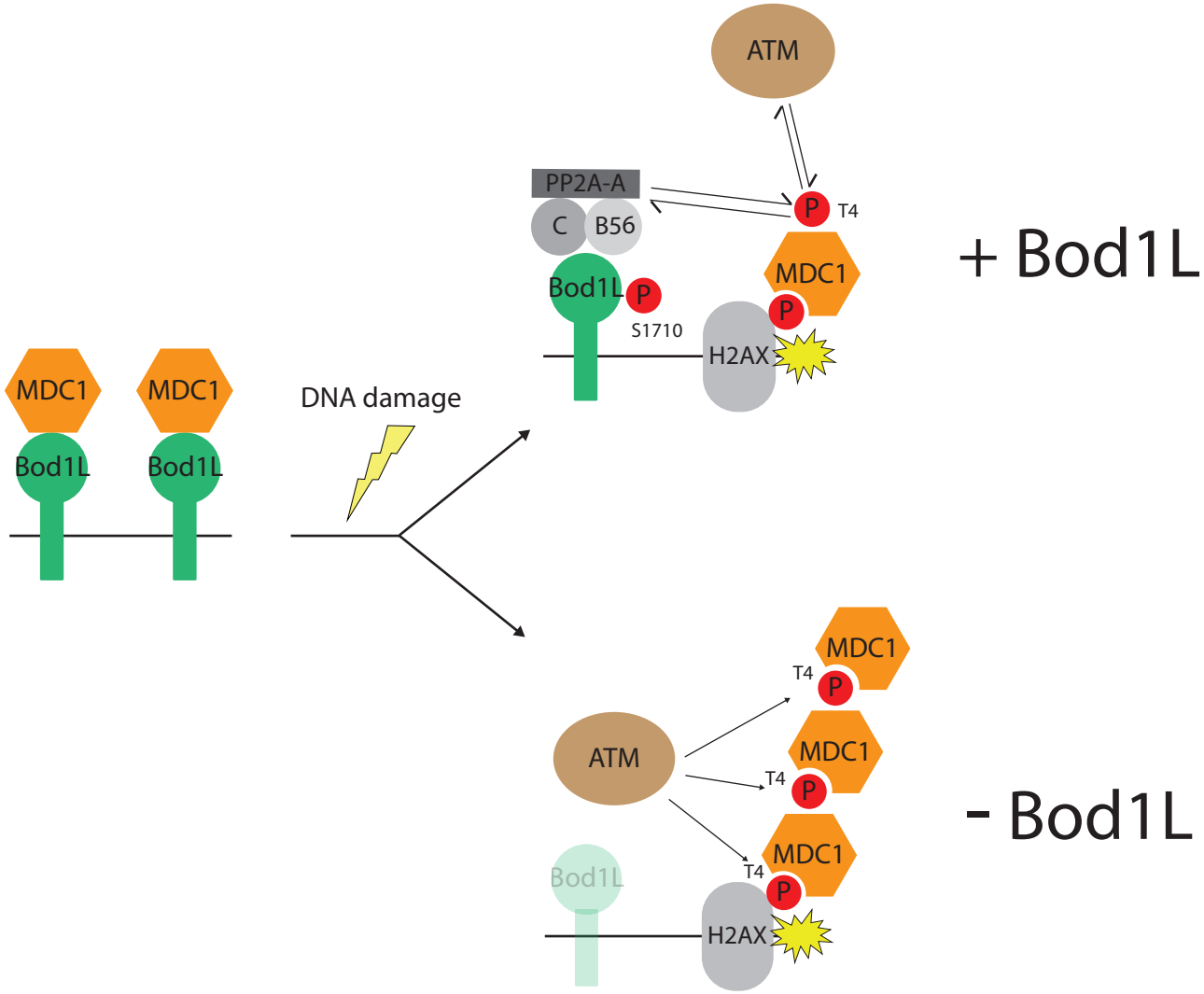

Figure 6.1: Bod1L regulates the recruitment of MDC1 and PP2A-B56 to sites of DNA damage

In the absence of DNA damage, Bod1L and MDC1 are constitutively bound on chromatin. Following recognition of a DNA double-strand break (DSB) and the subsequent activation of ATM, Bod1L is phosphorylated in an ATM dependant manner, allowing MDC1 to bind to γH2AX (pS139). Bod1L binds the PP2A-B56 holo-complex, which acts to 'buffer' the phosphorylation of MDC1 by ATM, controlling the localisation of MDC1 to sites of DSB. In the absence of Bod1L, MDC1 accumulation at sites of DNA damage is slowed, and PP2A-B56 fails to localise leading to increased MDC1 pT4 phosphorylation and uncontrolled oligomerisation at sites of damage.

possibly through unregulated dimerisation/oligomerisation of this critical DNA repair scaffold.

The data suggests there is a defined order of events for MDC1 targeting to sites of DNA damage (Figure 6.1). Bod1L constitutively binds a fraction of MDC1 and following damage; activated ATM phosphorylates H2AX, MDC1 and Bod1L. Whilst the exact order of these events is not yet known, Bod1L phosphorylation occurs relatively early in the DDR process, as I detected phospho-Bod1L S1710 staining by IF as soon as 5 minutes after damage (Figure 3.8). Based on the evidence presented in this thesis, I hypothesise that these modifications decrease the affinity of Bod1L for MDC1, allowing MDC1 to bind to γH2AX and provide a platform for further protein recruitment and signal amplification (Lou et al., 2006). Bod1L binds to the regulatory subunit of PP2A-B56 exclusively in the presence of DNA damage, resulting in accumulation of the phosphatase at sites of DNA damage (Figure 4.7). This recruitment is consistent with a previous study which reports a novel function of DNA-PKcs in recruiting PP6 to sites of DNA damage to facilitate dephosphorylation of γH2AX (Douglas et al., 2010). I have demonstrated that PP2A-B56 dephosphorylates phospho-MDC1 T4, thus ensuring that accumulation of MDC1 is controlled and limited. The balance of ATM and PP2A-B56 activities at DNA lesions then controls the accumulation of MDC1 and the proper repair of DNA damage (Figure 6.1). In the absence of Bod1L, MDC1 is slower to accumulate at sites of DNA damage due to loss of interaction with Bod1L and associated “priming” mechanism. The loss of PP2A-B56 localisation at DNA lesions as a result of Bod1L depletion leads to increased MDC1 pT4 phosphorylation and uncontrolled oligomerisation of MDC1.

The data are in agreement with studies showing that disruption of MDC1 dimerisation/oligomerisation at DSBs can lead to disruption of proper DDR (Jungmichel et al., 2012; Liu et al., 2012; Luo et al., 2011; 2015). Dimerisation through the FHA domain of MDC1 is evolutionarily conserved (*Drosophila melanogaster* and *Schizosaccharomyces pombe*), suggesting the importance of this activity (Luo and Ye, 2012). Indeed, it is only the dimerisation capacity and not Chk2/ATM phospho-dependent binding by MDC1 that is conserved, further strengthening the importance of the dimerisation process. Relatively few studies have explored the functional consequence of increased dimerisation/oligomerisation of MDC1 during the DDR, with the data in this thesis hitherto unreported. This is unsurprising given the lack of data regarding phosphatase involvement during the early DNA damage response. A very recent study revealed a previously unrecognised FHA domain in the fission yeast *Schizosaccharomyces pombe* MDC1 homologue, Mdb1, which mediates functionally important homodimerisation. Similar to the drosophila MDC1 homologue, Mdb1-FHA lacks all of the conserved phospho-binding residues, yet it forms a stable homodimer upon DNA damage. Disruption of this homodimer disrupts DNA damage-induced Mdb1 focus formation and *in vitro* binding of γH2A by Mdb1, leading to defective DNA repair (Luo et al., 2015). The investigation of MDC1 and other DDR protein dimerisation in response to DNA damage represents an exciting future direction for this study.

I show that in the absence of Bod1L, PP2A-B56 is not recruited to sites of DNA damage (Figure 4.7), therefore PP2A-B56 function at these sites is perturbed, resulting in hyperphosphorylation of phospho-MDC1 T4. Whilst I have shown that PP2A-B56 can directly dephosphorylate phospho-MDC1 T4 *in vitro*, it is likely that

the phosphatase is responsible for the dephosphorylation of other DDR proteins during early focus assembly. This presents an exciting opportunity for future investigation as loss of the Bod1L-PP2A association at DNA lesions may have effects on additional phospho-dependent processes. I hypothesise that the resulting uncontrolled increase of MDC1 at damaged sites as a result of increased phospho-MDC1-T4, sterically hinders CK2 phosphorylation of phospho-MDC1 S329/T331 (Figure 4.5), preventing interaction with NBS1, which is critical for downstream break processing (Chapman and Jackson, 2008; Melander et al., 2008; Spycher et al., 2008).

Whilst I have defined an elegant molecular mechanism for the compromised DDR associated with Bod1L depletion, I have only briefly looked into downstream consequence of loss of MDC1 regulation with regard to DDR protein recruitment. I detected significantly fewer Rad51 foci upon DNA damage induction, which was a likely explanation for the reduction in HR efficiency detected with the DR-GFP assay (Figures 3.4 and 4.1). More work is needed to investigate the full affect of Bod1L depletion on downstream DDR protein recruitment to understand and explore the full mechanistic detail into how MDC1 over-accumulation leads to compromised HR repair.

Several studies have identified many crucial phosphatase roles in the reversal of post-translational modifications upon resolution of DNA damage, particularly the dephosphorylation of γH2AX and p53 (Li et al., 2015; Lu et al., 2014). Whilst the data presented in this thesis establishes a role for Bod1L in the regulation of PP2A-B56 during the initial DDR, an unanswered question is whether Bod1L also plays a key role in the dissolution of DNA damage foci following damage

repair, through the regulation of PP2A-B56. This also leads onto investigation into the biochemistry of the interaction between Bod1L and the B56 regulatory subunit of PP2A. Previous studies have shown that the Bod1/PP2A-B56 interaction is dependent upon a putative CDK phosphorylation site and downstream aspartate residue (Porter et al., 2013). Interestingly, these residues are not conserved in Bod1L, suggesting that the interaction between Bod1L and PP2A-B56 is via an entirely different domain. This also perhaps explains why interaction between Bod1L and PP2A-B56, unlike Bod1/PP2A-B56 interaction, does not lead to inhibition of the phosphatase activity.

Cells depleted of Bod1L display defective cell-cycle arrest in response to DNA damage due to loss of Chk2 phosphorylation

Under basal physiological conditions, Chk2 is held in a dephosphorylated state via an interaction with a number of phosphatases, including PP2A-B56, which prevents the phosphorylation-dependent activation of the kinase (Figure 6.2A). Activation of ATM in response to genotoxic stress deactivates this Chk2/PP2A-B56 negative feedback loop, promoting the phosphorylation of Chk2 by ATM at T68 and subsequent activation and downstream Chk2 signalling (Carlessi et al., 2010; Freeman et al., 2010). The presence of sustained T68 phosphorylation has been demonstrated as being central during the early activation phase, to promote full activation of the kinase (Ahn and Prives, 2002).

The data presented in this thesis present strong evidence for an interaction between PP2A-B56 and Bod1L, yet show no interaction directly between Bod1L and Chk2. Given that loss of Bod1L profoundly affects sustained phospho-Chk2 T68 phosphorylation, I hypothesise that Bod1L acts as an additional regulator of

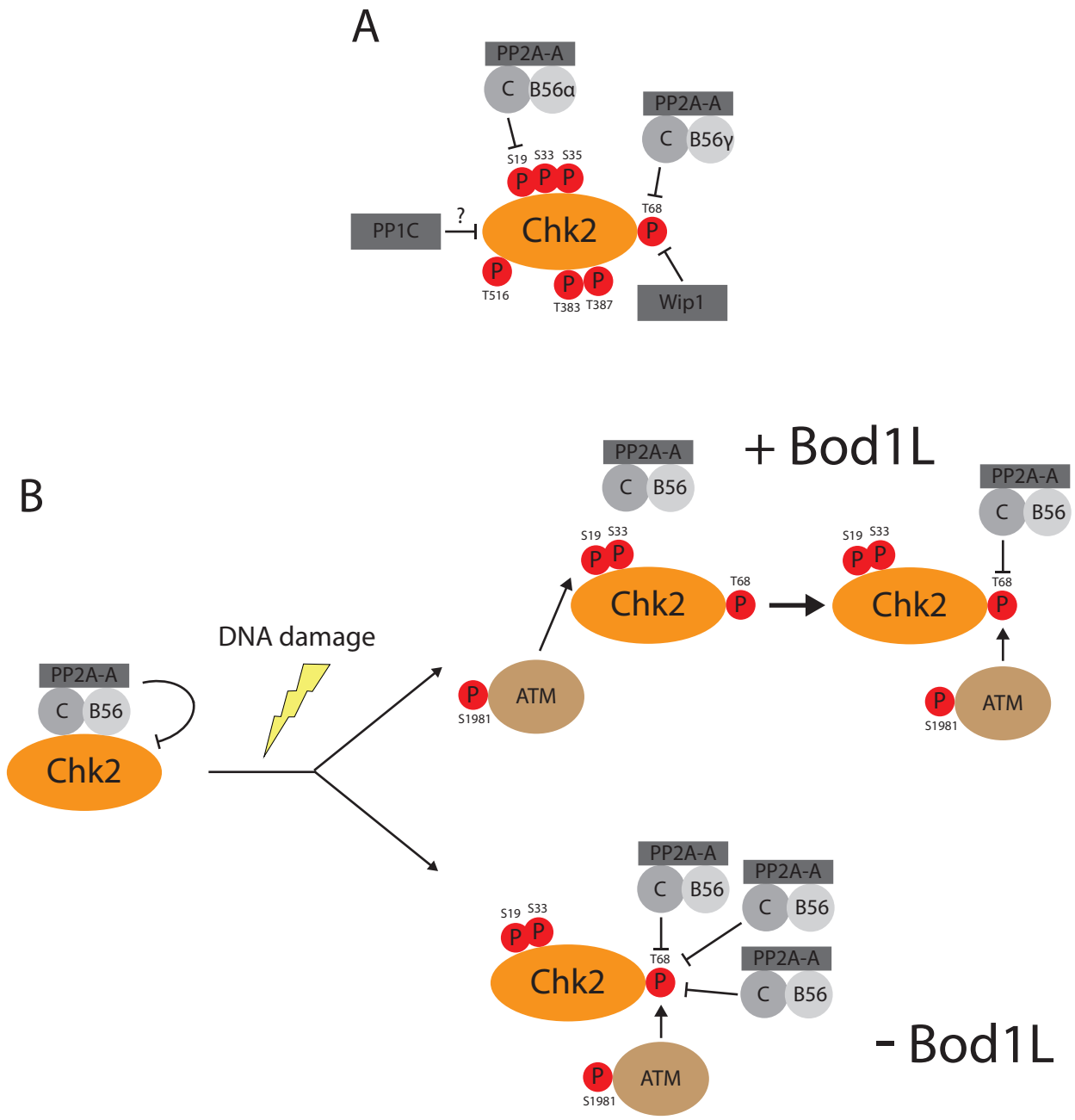

Figure 6.2: Working model for role of Bod1L and PP2A in the activation and activity of Chk2

(A) Schematic representation of the phosphatase regulation of Chk2. Adapted from (Peng and Maller, 2010).

(B) Schematic representation of Chk2 phosphorylation and dephosphorylation following DNA damage. Chk2 and PP2A-B56 interact under physiological conditions (A). ATM activation bought about from DNA damage dissociates the complex. Activation of Chk2 is then regulated by antagonistic kinase and phosphatase activity in the presence of Bod1L. In the absence of Bod1L, normal PP2A-B56 function is perturbed and as such the kinase:phosphatase dependent phosphorylation of Chk2 is disrupted resulting in a loss of phospho-Chk2 T68 and associated down-stream signalling. Depletion of PP2A-B56 perturbs proper ATM activation, preventing phosphorylation of Chk2 at T68.

Chk2 activation, possibly acting to release Chk2 from the inhibitory Chk2/PP2A-B56 phosphatase complex upon DNA damage, thus allowing the kinase to phosphorylate downstream substrates. Based on the evidence presented in figures 5.1-3, I theorise that loss of Bod1L leads to unregulated PP2A-B56 that is able to promiscuously dephosphorylate Chk2, disrupting the normal physiological inhibition of phosphatase activity (Figure 6.2B). The initial, rapid phosphorylation of phospho-Chk2 T68 seems largely unaffected by Bod1L depletion, which is consistent with the data that shows that ATM activity is unaffected under these conditions. The loss of *sustained* phosphorylation is highly indicative of hyperactive phosphatase activity. Consistent with these observations, inhibition of PP2A during DDR with LB100 induced constitutive hyperphosphorylation Chk2, suggesting that a fine phosphorylation balance of Chk2 is needed for robust DDR signalling (Chang et al., 2015).

The data from this thesis suggest that the failure to maintain the phospho-Chk2 T68 modification during initial activation of the kinase renders the downstream signalling compromised as a result of an inactive, or partially inactive, kinase. Further investigation using phosphorylation specific mass-spectrometry, or use of phospho-specific antibodies, is required to determine whether the auto- and trans-phosphorylations associated with active Chk2 are present in the absence of Bod1L (Zannini et al., 2014). A reduction in the presence of these 'activating' phosphorylations would verify the hypothesis that Chk2 is less active in the absence of Bod1L. Another open question that remains is how Bod1L fits into this pathway. It has been previously reported that whilst Chk2 and MDC1 may interact upon DNA damage, Chk2 undergoes only a transient interaction with DSBs, from where it rapidly spreads throughout the nucleus (Lukas et al.,

2003). One hypothesis, which is supported by the data in this thesis, describes Bod1L associating with and “tethering” PP2A-B56 at sites of DNA damage, thus preventing free PP2A-B56 from interacting with free nuclear phosphorylated Chk2. This would act to essentially release Chk2 from the inhibitory Chk2/PP2A-B56 phosphatase complex. Although this would present a rather elegant working model, more work is needed to determine whether in the absence of Bod1L, more Chk2 can be detected in the inhibitory Chk2/PP2A-B56 phosphatase complex, which would help strengthen this model.

Closing Remarks

The data presented in this thesis offers strong evidence for the role of Bod1L as a critical mediator in regulating the DNA damage response. These data strongly suggest that regulation, as opposed to simple inhibition, of serine/threonine protein phosphatases at DNA lesions is critical in the DDR, with Bod1L central in this process. Whilst the action and importance of the PI3K kinase family have been studied in great depth during this process, research into the activity of the antagonistic phosphatases remains is in its infancy. The scope for the importance of these dephosphorylation events is huge, with one key quantitative mass spectrometry-based study identifying a considerable number of sites that undergo DNA damage-induced dephosphorylation (Bennetzen et al., 2010). This growing body of evidence suggests that phosphatases play a more important part early in the DDR than hitherto reported.

References

Ahn, J., and Prives, C. (2002). Checkpoint Kinase 2 (Chk2) Monomers or Dimers Phosphorylate Cdc25C after DNA Damage Regardless of Threonine 68 Phosphorylation. Journal of Biological Chemistry *277*, 48418–48426.

Ahn, J.Y., Schwarz, J.K., Piwnica-Worms, H., and Canman, C.E. (2000). Threonine 68 phosphorylation by ataxia telangiectasia mutated is required for efficient activation of Chk2 in response to ionizing radiation. Cancer Research *60*, 5934–5936.

Ahn, J.Y., Xianghong, L., Davis, H.L., and Canman, C.E. (2002). Phosphorylation of Threonine 68 Promotes Oligomerization and Autophosphorylation of the Chk2 Protein Kinase via the Forkhead-associated Domain. Journal of Biological Chemistry *277*, 19389–19395.

Ahn, J., Urist, M., and Prives, C. (2004). The Chk2 protein kinase. DNA Repair *3*, 1039–1047.

Ahnesorg, P., Smith, P., and Jackson, S.P. (2006). XLF Interacts with the XRCC4-DNA Ligase IV Complex to Promote DNA Nonhomologous End-Joining. Cell *124*, 301–313.

Alexeev, A., Mazin, A., and Kowalczykowski, S.C. (2003). Rad54 protein possesses chromatin-remodeling activity stimulated by the Rad51–ssDNA nucleoprotein filament. Nat Struct Biol *10*, 182–186.

Ali, A., Zhang, J., Bao, S., Liu, I., Otterness, D., Dean, N.M., Abraham, R.T., and Wang, X.-F. (2004). Requirement of protein phosphatase 5 in DNA-damage-induced ATM activation. Genes & Development *18*, 249–254.

Allan, C., Burel, J.-M., Moore, J., Blackburn, C., Linkert, M., Loynton, S., MacDonald, D., Moore, W.J., Neves, C., Patterson, A., et al. (2012). OMERO: flexible, model-driven data management for experimental biology. Nat Meth *9*, 245–253.

Allen, P.B., Kwon, Y.G., Nairn, A.C., and Greengard, P. (1998). Isolation and characterization of PNUTS, a putative protein phosphatase 1 nuclear targeting subunit. J. Biol. Chem. *273*, 4089–4095.

Andreassen, P.R., Lacroix, F.B., Villa-Moruzzi, E., and Margolis, R.L. (1998). Differential subcellular localization of protein phosphatase-1 alpha, gamma1, and delta isoforms during both interphase and mitosis in mammalian cells. The Journal of Cell Biology *141*, 1207–1215.

Andreassen, P.R., D'Andrea, A.D., and Taniguchi, T. (2004). ATR couples FANCD2 monoubiquitination to the DNA-damage response. Genes &

Development *18*, 1958–1963.

Aparicio, T., Baer, R., and Gautier, J. (2014). DNA double-strand break repair pathway choice and cancer. DNA Repair *19*, 169–175.

Aravind, L., and Landsman, D. (1998). AT-hook motifs identified in a wide variety of DNA-binding proteins. Nucleic Acids Research *26*, 4413–4421.

Baharians, Z., and Schönthal, A.H. (1998). Autoregulation of protein phosphatase type 2A expression. J. Biol. Chem. *273*, 19019–19024.

Bahassi, E.M., Ovesen, J.L., Riesenberg, A.L., Bernstein, W.Z., Hasty, P.E., and Stambrook, P.J. (2008). The checkpoint kinases Chk1 and Chk2 regulate the functional associations between hBRCA2 and Rad51 in response to DNA damage. Oncogene *27*, 3977–3985.

Bakkenist, C.J., and Kastan, M.B. (2003). DNA damage activates ATM through intermolecular autophosphorylation and dimer dissociation. Nature *421*, 499–506.

Barber, L.J., Youds, J.L., Ward, J.D., McIlwraith, M.J., O'Neil, N.J., Petalcorin, M.I.R., Martin, J.S., Collis, S.J., Cantor, S.B., Auclair, M., et al. (2008). RTEL1 Maintains Genomic Stability by Suppressing Homologous Recombination. Cell *135*, 261–271.

Bartek, J., and Lukas, J. (2001). Mammalian G1- and S-phase checkpoints in response to DNA damage. Curr. Opin. Cell Biol. *13*, 738–747.

Bartek, J., Bartkova, J., and Lukas, J. (2007). DNA damage signalling guards against activated oncogenes and tumour progression. Oncogene *26*, 7773–7779.

Bartek, J., and Lukas, J. (2007). DNA damage checkpoints: from initiation to recovery or adaptation. Curr. Opin. Cell Biol. *19*, 238–245.

Bartkova, J., Horejsí, Z., Koed, K., Krämer, A., Tort, F., Zieger, K., Guldberg, P., Sehested, M., Nesland, J.M., Lukas, C., et al. (2005). DNA damage response as a candidate anti-cancer barrier in early human tumorigenesis. Nature *434*, 864–870.

Baumann, P., and West, S.C. (1998). Role of the human RAD51 protein in homologous recombination and double-stranded-break repair. Trends in Biochemical Sciences *23*, 247–251.

Bekker-Jensen, S. (2005). Dynamic assembly and sustained retention of 53BP1 at the sites of DNA damage are controlled by Mdc1/NFBD1. The Journal of Cell Biology *170*, 201–211.

Bekker-Jensen, S., and Mailand, N. (2010). Assembly and function of DNA double-strand break repair foci in mammalian cells. DNA Repair *9*, 1219–1228.

Bekker-Jensen, S., Danielsen, J.R., Fugger, K., Gromova, I., Nerstedt, A., Bartek, J., Lukas, J., and Mailand, N. (2009). HERC2 coordinates ubiquitin-dependent assembly of DNA repair factors on damaged chromosomes. Nature Cell Biology *12*, 80–86.

Bell, S.P., and Dutta, A. (2002). DNA REPLICATION IN EUKARYOTIC CELLS. Annu. Rev. Biochem. *71*, 333–374.

Bennardo, N., Cheng, A., Huang, N., and Stark, J.M. (2008). Alternative-NHEJ Is a Mechanistically Distinct Pathway of Mammalian Chromosome Break Repair. PLoS Genet *4*, e1000110.

Bennetzen, M.V., Larsen, D.H., Bunkenborg, J., Bartek, J., Lukas, J., and Andersen, J.S. (2010). Site-specific phosphorylation dynamics of the nuclear proteome during the DNA damage response. Mol. Cell Proteomics *9*, 1314–1323.

Blow, J.J., and Dutta, A. (2005). Preventing re-replication of chromosomal DNA. Nature Publishing Group *6*, 476–486.

Bohgaki, M., Bohgaki, T., Ghamrasni, El, S., Srikumar, T., Maire, G., Panier, S., Fradet-Turcotte, A., Stewart, G.S., Raught, B., and Hakem, A. (2013). RNF168 ubiquitylates 53BP1 and controls its response to DNA double-strand breaks. Proc. Natl. Acad. Sci. U.S.a. *110*, 20982–20987.

Bohgaki, T., Bohgaki, M., and Hakem, R. (2010). DNA double-strand break signaling and human disorders. Genome Integrity *1*, 15.

Bollen, M., Peti, W., Ragusa, M.J., and Beullens, M. (2010). The extended PP1 toolkit: designed to create specificity. Trends in Biochemical Sciences *35*, 450–458.

Botuyan, M.V., Lee, J., Ward, I.M., Kim, J.-E., Thompson, J.R., Chen, J., and Mer, G. (2006). Structural Basis for the Methylation State-Specific Recognition of Histone H4-K20 by 53BP1 and Crb2 in DNA Repair. Cell *127*, 1361–1373.

Brameier, M., Krings, A., and MacCallum, R.M. (2007). NucPred Predicting nuclear localization of proteins. Bioinformatics *23*, 1159–1160.

Brown, E.J., and Baltimore, D. (2003). Essential and dispensable roles of ATR in cell cycle arrest and genome maintenance. Genes & Development *17*, 615–628.

Buis, J., Wu, Y., Deng, Y., Leddon, J., Westfield, G., Eckersdorff, M., Sekiguchi, J.M., Chang, S., and Ferguson, D.O. (2008). Mre11 Nuclease Activity Has

Essential Roles in DNA Repair and Genomic Stability Distinct from ATM Activation. Cell *135*, 85–96.

Bulavin, D.V., Demidov, O.N., Saito, S., Kauraniemi, P., Phillips, C., Amundson, S.A., Ambrosino, C., Sauter, G., Nebreda, A.R., Anderson, C.W., et al. (2002). Amplification of PPM1D in human tumors abrogates p53 tumor-suppressor activity. Nat. Genet. *31*, 210–215.

Bunting, S.F., Callen, E., Wong, N., Chen, H.-T., Polato, F., Gunn, A., Bothmer, A., Feldhahn, N., Fernandez-Capetillo, O., Cao, L., et al. (2010). 53BP1 Inhibits Homologous Recombination in Brca1-Deficient Cellsby Blocking Resection of DNA Breaks. Cell *141*, 243–254.

Burgers, P.M.J. (2009). Polymerase Dynamics at the Eukaryotic DNA Replication Fork. Journal of Biological Chemistry *284*, 4041–4045.

Burma, S., Chen, B.P., Murphy, M., Kurimasa, A., and Chen, D.J. (2001). ATM Phosphorylates Histone H2AX in Response to DNA Double-strand Breaks. Journal of Biological Chemistry *276*, 42462–42467.

Cai, Z., Chehab, N.H., and Pavletich, N.P. (2009). Structure and Activation Mechanismof the CHK2 DNA Damage Checkpoint Kinase. Molecular Cell *35*, 818–829.

Callen, E., Di Virgilio, M., Kruhlak, M.J., Nieto-Soler, M., Wong, N., Chen, H.-T., Faryabi, R.B., Polato, F., Santos, M., Starnes, L.M., et al. (2013). 53BP1 Mediates Productive and Mutagenic DNA Repair through Distinct Phosphoprotein Interactions. Cell *153*, 1266–1280.

Carlessi, L., Buscemi, G., Fontanella, E., and Delia, D. (2010). Biochimica et Biophysica Acta. BBA - Molecular Cell Research *1803*, 1213–1223.

Celeste, A., Difilippantonio, S., Difilippantonio, M.J., Fernandez-Capetillo, O., Pilch, D.R., Sedelnikova, O.A., Eckhaus, M., Ried, T., Bonner, W.M., and Nussenzweig, A. (2003). H2AX haploinsufficiency modifies genomic stability and tumor susceptibility. Cell *114*, 371–383.

Cha, H., Lowe, J.M., Li, H., Lee, J.S., Belova, G.I., Bulavin, D.V., and Fornace, A.J. (2010). Wip1 Directly Dephosphorylates gammaH2AX and Attenuates the DNA Damage Response. Cancer Research *70*, 4112–4122.

Chan, D.W., and Lees-Miller, S.P. (1996). The DNA-dependent protein kinase is inactivated by autophosphorylation of the catalytic subunit. J. Biol. Chem. *271*, 8936–8941.

Chang, K.E., Wei, B.R., Madigan, J.P., Hall, M.D., Simpson, R.M., Zhuang, Z., and Gottesman, M.M. (2015). The protein phosphatase 2A inhibitor LB100

sensitizes ovarian carcinaoma cells to cisplatin-mediated cytotoxicity. Mol Cancer Ther *14*, 90–100.

Chapman, J.R., and Jackson, S.P. (2008). Phospho-dependent interactions between NBS1 and MDC1 mediate chromatin retention of the MRN complex at sites of DNA damage. EMBO Rep *9*, 795–801.

Chapman, J.R., Taylor, M.R.G., and Boulton, S.J. (2012). Playing the End Game: DNA Double-Strand Break Repair Pathway Choice. Molecular Cell *47*, 497–510.

Chehab, N.H., Malikzay, A., and Appel, M. (2000). Chk2/hCds1 functions as a DNA damage checkpoint in G1 by stabilizing p53. Genes & Development *14*, 278–288.

Chen, G.I., Tisayakorn, S., and Jorgensen, C. (2008). PP4R4/KIAA1622 forms a novel stable cytosolic complex with phosphoprotein phosphatase 4. Journal of Biological Chemistry *283*, 29273–29284.

Chen, G., Yuan, S.S., Liu, W., Xu, Y., Trujillo, K., Song, B., Cong, F., Goff, S.P., Wu, Y., Arlinghaus, R., et al. (1999). Radiation-induced assembly of Rad51 and Rad52 recombination complex requires ATM and c-Abl. J. Biol. Chem. *274*, 12748–12752.

Chen, H., Lisby, M., and Symington, L.S. (2013). RPA Coordinates DNA End Resection and Prevents Formation of DNA Hairpins. Molecular Cell *50*, 589–600.

Chen, J. (2012). The Roles of MDM2 and MDMX Phosphorylation in Stress Signaling to p53. Genes & Cancer *3*, 274–282.

Chen, J., and Stubbe, J. (2005). Bleomycins: towards better therpeutics. Nature Reviews Cancer *5*, 102–112.

Chen, L., Trujillo, K.M., Van Komen, S., Roh, D.H., Krejci, L., Lewis, L.K., Resnick, M.A., Sung, P., and Tomkinson, A.E. (2005a). Effect of Amino Acid Substitutions in the Rad50 ATP Binding Domain on DNA Double Strand Break Repair in Yeast. Journal of Biological Chemistry *280*, 2620–2627.

Chen, L., Trujillo, K., Ramos, W., Sung, P., and Tomkinson, A.E. (2001). Promotion of Dnl4-catalyzed DNA end-joining by the Rad50/Mre11/Xrs2 and Hdf1/Hdf2 complexes. Molecular Cell *8*, 1105–1115.

Chen, L., Gilkes, D.M., Pan, Y., Lane, W.S., and Chen, J. (2005b). ATM and Chk2-dependent phosphorylation of MDMX contribute to p53 activation after DNA damage. The EMBO Journal *24*, 3411–3422.

Chen, M.X., and Cohen, P.T.W. (1997). Activation of protein phosphatase 5 by

limited proteolysis or the binding of polyunsaturated fatty acids to the TPR domain. FEBS Letters *400*, 136–140.

Chen, S., Xiao, Y., Ponnusamy, R., Tan, J., Lei, J., and Hilgenfeld, R. (2011). X-ray structure of the SH3 domain of the phosphoinositide 3-kinase p85β subunit. Structural Biology and Crystallization Communications *67*, 1328–1333.

Cheng, Q., Chen, L., Li, Z., Lane, W.S., and Chen, J. (2009). ATM activates p53 by regulating MDM2 oligomerization and E3 processivity. The EMBO Journal *28*, 3857–3867.

Cheung-Ong, K., Giaever, G., and Nislow, C. (2013). Perspective. Chemistry & Biology *20*, 648–659.

Chinkers, M. (2001). Protein phosphatase 5 in signal transduction. Trends Endocrinol. Metab. *12*, 28–32.

Chouinard, G., ment, I.C., Lafontaine, J., Rodier, F., and Schmitt, E. (2013). Cell cycle-dependent localization of CHK2 at centrosomes during mitosis. Cell Division *8*, 1–12.

Chowdhury, D., Keogh, M.-C., Ishii, H., Peterson, C.L., Buratowski, S., and Lieberman, J. (2005). γ-H2AX Dephosphorylation by Protein Phosphatase 2A Facilitates DNA Double-Strand Break Repair. Molecular Cell *20*, 801–809.

Chowdhury, D., Xu, X., Zhong, X., Ahmed, F., Zhong, J., Liao, J., Dykxhoorn, D.M., Weinstock, D.M., Pfeifer, G.P., and Lieberman, J. (2008). A PP4-Phosphatase Complex Dephosphorylates γ-H2AX Generated during DNA Replication. Molecular Cell *31*, 33–46.

Ciccia, A., and Elledge, S.J. (2010). The DNA Damage Response: Making It Safe to Play with Knives. Molecular Cell *40*, 179–204.

Ciotta, G. (2011). Tagging methods as a tool to investigate histone H3 methylation dynamics in mouse embryonic stem cells. Dresden University of Technology: Germany.

Cohen, P.T.W. (2002). Protein phosphatase 1--targeted in many directions. Journal of Cell Science *115*, 241–256.

Constantinescu, D., Csoka, A.B., Navara, C.S., and Schatten, G.P. (2010). Defective DSB repair correlates with abnormal nuclear morphology and is improved with FTI treatment in Hutchinson-Gilford progeria syndrome fibroblasts. Experimental Cell Research *316*, 2747–2759.

Cook, P.J., Ju, B.G., Telese, F., Wang, X., Glass, C.K., and Rosenfeld, M.G. (2009). Tyrosine dephosphorylation of H2AXmodulates apoptosis and survivaldecisions. Nature *458*, 591–596.

Costa, A., Ilves, I., Tamberg, N., Petojevic, T., Nogales, E., Botchan, M.R., and Berger, J.M. (2011). The structural basis for MCM2–7 helicase activation by GINS and Cdc45. Nat Struct Mol Biol *18*, 471–477.

Coster, G., and Goldberg, M. (2010). The cellular response to DNA damage: a focus on MDC1 and its interacting proteins. Nucleus *1*, 166–178.

Coster, G., Hayouka, Z., Argaman, L., Strauss, C., Friedler, A., Brandeis, M., and Goldberg, M. (2007). The DNA damage response mediator MDC1 directly interacts with the anaphase-promoting complex/cyclosome. J. Biol. Chem. *282*, 32053–32064.

Czornak, K., Chughtai, S., and Chrzanowska, K.H. (2008). Mystery of DNA repair: the role of the MRN complex and ATM kinase in DNA damage repair. J. Appl. Genet. *49*, 383–396.

D'Amours, D., and Jackson, S.P. (2002). The mre11 complex: at the crossroads of dna repair and checkpoint signalling. Nat. Rev. Mol. Cell Biol. *3*, 317–327.

Dai, Y., and Grant, S. (2010). New Insights into Checkpoint Kinase 1 in the DNA Damage Response Signaling Network. Clinical Cancer Research *16*, 376–383.

Darlington, Y., Nguyen, T.-A., Moon, S.-H., Herron, A., Rao, P., Zhu, C., Lu, X., and Donehower, L.A. (2011). Absence of Wip1 partially rescues Atm deficiency phenotypes in mice. *31*, 1155–1165.

Davies, A.A., Masson, J.Y., McIlwraith, M.J., Stasiak, A.Z., Stasiak, A., Venkitaraman, A.R., and West, S.C. (2001). Role of BRCA2 in control of the RAD51 recombination and DNA repair protein. Molecular Cell *7*, 273–282.

de Jager, M., van Noort, J., van Gent, D.C., Dekker, C., Kanaar, R., and Wyman, C. (2001). Human Rad50/Mre11 is a flexible complex that can tether DNA ends. Molecular Cell *8*, 1129–1135.

de Jager, M., Wyman, C., van Gent, D.C., and Kanaar, R. (2002). DNA end-binding specificity of human Rad50/Mre11 is influenced by ATP. Nucleic Acids Research *30*, 4425–4431.

DeFazio, L.G., Stansel, R.M., Griffith, J.D., and Chu, G. (2002). Synapsis of DNA ends by DNA-dependent protein kinase. The EMBO Journal *21*, 3192–3200.

Dehe, P.-M., Dichtl, B., Schaft, D., Roguev, A., Pamblanco, M., Lebrun, R., Rodriguez-Gil, A., Mkandawire, M., Landsberg, K., Shevchenko, A., et al. (2006). Protein interactions within the Set1 complex and their roles in the regulation of histone 3 lysine 4 methylation. J. Biol. Chem. *281*, 35404–35412.

Della-Maria, J., Zhou, Y., Tsai, M.S., Kuhnlein, J., Carney, J.P., Paull, T.T., and Tomkinson, A.E. (2011). Human Mre11/Human Rad50/Nbs1 and DNA Ligase

III /XRCC1 Protein Complexes Act Together in an Alternative Nonhomologous End Joining Pathway. Journal of Biological Chemistry *286*, 33845–33853.

Dephoure, N., Zhou, C., Villén, J., Beausoleil, S.A., Bakalarski, C.E., Elledge, S.J., and Gygi, S.P. (2008). A quantitative atlas of mitotic phosphorylation. Proceedings of the National Academy of Sciences *105*, 10762–10767.

Deriano, L., and Roth, D.B. (2013). Modernizing the Nonhomologous End-Joining Repertoire: Alternative and Classical NHEJ Share the Stage. Annu. Rev. Genet. *47*, 433–455.

Desai-Mehta, A., Cerosaletti, K.M., and Concannon, P. (2001). Distinct Functional Domains of Nibrin Mediate Mre11 Binding, Focus Formation, and Nuclear Localization. Molecular and Cellular Biology *21*, 2184–2191.

Diffley, J.F.X. (2011). Quality control in the initiation of eukaryotic DNA replication. Philosophical Transactions of the Royal Society B: Biological Sciences *366*, 3545–3553.

Digweed, M., and Sperling, K. (2004). Nijmegen breakage syndrome: clinical manifestation of defective response to DNA double-strand breaks. DNA Repair *3*, 1207–1217.

Dinant, C., de Jager, M., Essers, J., van Cappellen, W.A., Kanaar, R., Houtsmuller, A.B., and Vermeulen, W. (2007). Activation of multiple DNA repair pathways by sub-nuclear damage induction methods. Journal of Cell Science *120*, 2731–2740.

Dinkel, H., Van Roey, K., Michael, S., Davey, N.E., Weatheritt, R.J., Born, D., Speck, T., Kruger, D., Grebnev, G., Kuban, M., et al. (2013). The eukaryotic linear motif resource ELM: 10 years and counting. Nucleic Acids Research *42*, D259–D266.

Dohoney, K.M., Guillerm, C., Whiteford, C., Elbi, C., Lambert, P.F., Hager, G.L., and Brady, J.N. (2004). Phosphorylation of p53 at serine 37 is important for transcriptional activity and regulation in response to DNA damage. Oncogene *23*, 49–57.

Doil, C., Mailand, N., Bekker-Jensen, S., Menard, P., Larsen, D.H., Pepperkok, R., Ellenberg, J., Panier, S., Durocher, D., Bartek, J., et al. (2009). RNF168 Binds and Amplifies Ubiquitin Conjugates on Damaged Chromosomes to Allow Accumulation of Repair Proteins. Cell *136*, 435–446.

Donzelli, M., and Draetta, G.F. (2003). Regulating mammalian checkpoints through Cdc25 inactivation. EMBO Rep *4*, 671–677.

Dou, Y., Milne, T.A., Ruthenburg, A.J., Lee, S., Lee, J.W., Verdine, G.L., Allis,

C.D., and Roeder, R.G. (2006). Regulation of MLL1 H3K4 methyltransferase activity by its core components. Nat Struct Mol Biol *13*, 713–719.

Douglas, P., Zhong, J., Ye, R., Moorhead, G.B.G., Xu, X., and Lees-Miller, S.P. (2010). Protein Phosphatase 6 Interacts with the DNA-Dependent Protein Kinase Catalytic Subunit and Dephosphorylates -H2AX. Molecular and Cellular Biology *30*, 1368–1381.

Douglas, P., Moorhead, G.B.G., Ye, R., and Lees-Miller, S.P. (2001). Protein Phosphatases Regulate DNA-dependent Protein Kinase Activity. Journal of Biological Chemistry *276*, 18992–18998.

Douglas, P., Sapkota, G.P., Morrice, N., Yu, Y., Goodarzi, A.A., Merkle, D., Meek, K., Alessi, D.R., and Lees-Miller, S.P. (2002). Identification of in vitro and in vivo phosphorylation sites in the catalytic subunit of the DNA-dependent protein kinase. Biochem. J. *368*, 243–251.

Dozier, C., Bonyadi, M., Baricault, L., Tonasso, L., and Darbon, J.-M. (2004). Regulation of Chk2 phosphorylation by interaction with protein phosphatase 2A via its B' regulatory subunit. Biology of the Cell *96*, 509–517.

Dueva, R., and Iliakis, G. (2013). Alternative pathways of non-homologous end joining (NHEJ) in genomic instability and cancer. Translational Cancer Research *2*, 163–177.

Duong, H.-Q., Hong, Y.B., Kim, J.S., Lee, H.-S., Yi, Y.W., Kim, Y.J., Wang, A., Zhao, W., Cho, C.H., Seong, Y.-S., et al. (2013). Inhibition of checkpoint kinase 2 (CHK2) enhances sensitivity of pancreatic adenocarcinoma cells to gemcitabine. J. Cell. Mol. Med. *17*, 1261–1270.

Eissenberg, J.C., and Shilatifard, A. (2010). Histone H3 lysine 4 (H3K4) methylation in development and differentiation. Developmental Biology *339*, 240–249.

Eliezer, Y., Argaman, L., Kornowski, M., Roniger, M., and Goldberg, M. (2014). Interplay between the DNA damage proteins MDC1 and ATM in the regulation of the spindle assembly checkpoint. Journal of Biological Chemistry *289*, 8183–8193.

Eliezer, Y., Argaman, L., Rhie, A., Doherty, A.J., and Goldberg, M. (2008). The Direct Interaction between 53BP1 and MDC1 Is Required for the Recruitment of 53BP1 to Sites of Damage. Journal of Biological Chemistry *284*, 426–435.

Escribano-Diaz, C., Orthwein, A., Fradet-Turcotte, A., Xing, M., Young, J.T.F., Tkáč, J., Cook, M.A., Rosebrock, A.P., Munro, M., Canny, M.D., et al. (2013). A Cell Cycle-Dependent Regulatory Circuit Composed of 53BP1-RIF1 and BRCA1-CtIP Controls DNA Repair Pathway Choice. Molecular Cell *49*, 872–

883.

Falck, J., Mailand, N., Syljuåsen, R.G., Bartek, J., and Lukas, J. (2001). The ATM-Chk2-Cdc25A checkpoint pathway guards against radioresistant DNA synthesis. Nature *410*, 842–847.

Falck, J., Coates, J., and Jackson, S.P. (2005). Conserved modes of recruitment of ATM, ATR and DNA-PKcs to sites of DNA damage. Nature *434*, 605–611.

Falck, J., Petrini, J.H.J., Williams, B.R., Lukas, J., and Bartek, J. (2002). The DNA damage-dependent intra -S phase checkpoint is regulated by parallel pathways. Nat. Genet. *30*, 290–294.

Fan, J., and Pavletich, N.P. (2012). Structure and conformational change of a replication protein A heterotrimer bound to ssDNA. Genes & Development *26*, 2337–2347.

Fan, R., Kumaravel, T.S., Jalali, F., Marrano, P., Squire, J.A., and Bristow, R.G. (2004). Defective DNA strand break repair after DNA damage in prostate cancer cells: implications for genetic instability and prostate cancer progression. Cancer Research *64*, 8526–8533.

Farmer, H., McCabe, N., Lord, C.J., Tutt, A.N.J., Johnson, D.A., Richardson, T.B., Santarosa, M., Dillon, K.J., Hickson, I., Knights, C., et al. (2005). Targeting the DNA repair defect in BRCA mutant cells as a therapeutic strategy. Nature *434*, 917–921.

Faucher, D., and Wellinger, R.J. (2010). Methylated H3K4, a Transcription-Associated Histone Modification, Is Involved in the DNA Damage Response Pathway. PLoS Genet *6*, e1001082.

Fekairi, S., Scaglione, S., Chahwan, C., Taylor, E.R., Tissier, A., Coulon, S., Dong, M.-Q., Ruse, C., Yates, J.R., III, Russell, P., et al. (2009). Human SLX4 Is a Holliday Junction Resolvase Subunit that Binds MultipleDNA Repair/Recombination Endonucleases. Cell *138*, 78–89.

Field, C.M., Oegema, K., Zheng, Y., Mitchison, T., and Walczak, C. (1998). Purification of cytoskeletal proteins using peptide antibodies. Methods Enzymol *298*, 525–541.

Fiscella, M., Zhang, H., Fan, S., Sakaguchi, K., Shen, S., Mercer, W.E., Vande Woude, G.F., O'Connor, P.M., and Appella, E. (1997). Wip1, a novel human protein phosphatase that is induced in response to ionizing radiation in a p53-dependent manner. Proc. Natl. Acad. Sci. U.S.a. *94*, 6048–6053.

Foley, E.A., Maldonado, M., and Kapoor, T.M. (2011). Formation of stable attachments between kinetochoresand microtubules depends on the B56-

PP2Aphosphatase. Nature Cell Biology *13*, 1265–1271.

Forbes, S.A., Beare, D., Gunasekaran, P., Leung, K., Bindal, N., Boutselakis, H., Ding, M., Bamford, S., Cole, C., Ward, S., et al. (2015). COSMIC: exploring the world's knowledge of somatic mutations in human cancer. Nucleic Acids Research *43*, D805–D811.

Frappart, P.-O., and McKinnon, P.J. (2006). Ataxia-Telangiectasia and Related Diseases. Nmm *8*, 495–512.

Freeman, A.K., and Monteiro, A.N. (2010). Phosphatases in the cellular response to DNA damage. Cell Commun. Signal *8*, 27.

Freeman, A.K., Dapic, V., and Monteiro, A.N.A. (2010). Negative regulation of CHK2 activity by protein phosphatase 2A is modulated by DNA damage. Cell Cycle *9*, 736–747.

Fridman, J.S., and Lowe, S.W. (2003). Control of apoptosis by p53. Oncogene *22*, 9030–9040.

Fugmann, S.D., Lee, A.I., Shockett, P.E., Villey, I.J., and Schatz, D.G. (2000). The RAG proteins and V(D)J recombination: complexes, ends, and transposition. Annu. Rev. Immunol. *18*, 495–527.

Fujimoto, H., Onishi, N., Kato, N., Takekawa, M., Xu, X.Z., Kosugi, A., Kondo, T., Imamura, M., Oishi, I., Yoda, A., et al. (2005). Regulation of the antioncogenic Chk2 kinase by the oncogenic Wip1 phosphatase. Cell Death Differ *13*, 1170–1180.

Galanty, Y., Belotserkovskaya, R., Coates, J., and Jackson, S.P. (2012). RNF4, a SUMO-targeted ubiquitin E3 ligase, promotes DNA double-strand break repair. Genes & Development *26*, 1179–1195.

Galanty, Y., Belotserkovskaya, R., Coates, J., Polo, S., Miller, K.M., and Jackson, S.P. (2010). Mammalian SUMO E3-ligases PIAS1 and PIAS4 promote responses to DNA double-strand breaks. Nature *462*, 935–939.

Garrett, M.D., and Collins, I. (2011). Anticancer therapy with checkpointinhibitors: what, where and when? Trends in Pharmacological Sciences *32*, 308–316.

Gatei, M., Scott, S.P., Filippovitch, I., Soronika, N., Lavin, M.F., Weber, B., and Khanna, K.K. (2000a). Role for ATM in DNA damage-induced phosphorylation of BRCA1. Cancer Research *60*, 3299–3304.

Gatei, M., Young, D., Cerosaletti, K.M., Desai-Mehta, A., Spring, K., Kozlov, S., Lavin, M.F., Gatti, R.A., Concannon, P., and Khanna, K. (2000b). ATM-dependent phosphorylation of nibrin in response to radiation exposure. Nat. Genet. *25*, 115–119.

Gatti, R.A., Becker-Catania, S., Chun, H.H., and Sun, X. (2001). The pathogenesis of ataxia-telangiectasia. Clinical Reviews in Allergy and Immunology *20*, 87–108.

Germani, A., Prabel, A., Mourah, S., Podgorniak, M.-P., Carlo, A.D., Ehrlich, R., Gisselbrecht, S., Varin-Blank, N., Calvo, F., and Bruzzoni-Giovanelli, H. (2003). SIAH-1 interacts with CtIP and promotes its degradation by the proteasome pathway. Oncogene *22*, 8845–8851.

Gharbi-Ayachi, A., Labbé, J.-C., Burgess, A., Vigneron, S., Strub, J.-M., Brioudes, E., Van-Dorsselaer, A., Castro, A., and Lorca, T. (2010). The substrate of Greatwall kinase, Arpp19, controls mitosis by inhibiting protein phosphatase 2A. Science *330*, 1673–1677.

Gingras, A.-C., Caballero, M., Zarske, M., Sanchez, A., Hazbun, T.R., Fields, S., Sonenberg, N., Hafen, E., Raught, B., and Aebersold, R. (2005). A novel, evolutionarily conserved protein phosphatase complex involved in cisplatin sensitivity. Mol. Cell Proteomics *4*, 1725–1740.

Giunta, S., Belotserkovskaya, R., and Jackson, S.P. (2010). DNA damage signaling in response to double-strand breaks during mitosis. The Journal of Cell Biology *190*, 197–207.

Giunta, S., and Jackson, S.P. (2011). Give me a break, but not in mitosis: The mitotic DNA damage response marks DNA double-strand breaks with early signaling events. Cell Cycle *10*, 1215–1221.

Goldberg, M., Stucki, M., Falck, J., D'Amours, D., Rahman, D., Pappin, D., Bartek, J., and Jackson, S.P. (2003). MDC1 is required for the intra-S-phase DNA damage checkpoint. Nature *421*, 952–956.

Goodarzi, A.A., Jonnalagadda, J.C., Douglas, P., Young, D., Ye, R., Moorhead, G.B.G., Lees-Miller, S.P., and Khanna, K.K. (2004). Autophosphorylation of ataxia-telangiectasia mutated is regulated by protein phosphatase 2A. The EMBO Journal *23*, 4451–4461.

Gordon, I.K., Lu, J., Graves, C.A., Huntoon, K., Frerich, J.M., Hanson, R.H., Wang, X.F., Hong, C.S., How, W., Feldman, M.J., et al. (2015). Protein phosphatase 2A inhibition with LB100 enhances radiation-induced mitotic catastrophe and tumor growth delay in glioblastoma. Mol Cancer Ther *4*, epub.

Gottlieb, T.M., and Jackson, S.P. (1993). The DNA-dependent protein kinase: requirement for DNA ends and association with Ku antigen. Cell *72*, 131–142.

Gravel, S., Chapman, J.R., Magill, C., and Jackson, S.P. (2008). DNA helicases Sgs1 and BLM promote DNA double-strand break resection. Genes & Development *22*, 2767–2772.

Grawunder, U., Wilm, M., Wu, X., Kulesza, P., Wilson, T.E., Mann, M., and Lieber, M.R. (1997). Activity of DNA ligase IV stimulated by complex formation with XRCC4 protein in mammalian cells. Nature *388*, 492–495.

Greenman, C., Stephens, P., Smith, R., Dalgliesh, G.L., Hunter, C., Bignell, G., Davies, H., Teague, J., Butler, A., Stevens, C., et al. (2007). Patterns of somatic mutation in human cancer genomes. Nature *446*, 153–158.

Gumy-Pause, F., Wacker, P., and Sappino, A.-P. (2003). ATM gene and lymphoid malignancies. Leukemia *18*, 238–242.

Guo, C.Y., Brautigan, D.L., and Larner, J.M. (2002a). Ionizing Radiation Activates Nuclear Protein Phosphatase-1 by ATM-dependent Dephosphorylation. Journal of Biological Chemistry *277*, 41756–41761.

Guo, C.Y., Brautigan, D.L., and Larner, J.M. (2002b). ATM-dependent Dissociation of B55 Regulatory Subunit from Nuclear PP2A in Response to Ionizing Radiation. Journal of Biological Chemistry *277*, 4839–4844.

Guo, X., Ward, M.D., Tiedebohl, J.B., and Oden, Y.M. (2010). Interdependent phosphorylation within the kinase domain T-loop Regulates CHK2 activity. J. Biol. Chem. *285*, 33348–33357.

Gutiérrez-González, A., Belda-Iniesta, C., Bargiela-Iparraguirre, J., Dominguez, G., García Alfonso, P., Perona, R., and Sanchez-Perez, I. (2012). Targeting Chk2 improves gastric cancer chemotherapy by impairing DNA damage repair. Apoptosis *18*, 347–360.

Guzzo, C.M., Berndsen, C.E., Zhu, J., Gupta, V., Datta, A., Greenberg, R.A., Wolberger, C., and Matunis, M.J. (2012). RNF4-dependent hybrid SUMO-ubiquitin chains are signals for RAP80 and thereby mediate the recruitment of BRCA1 to sites of DNA damage. Sci Signal *5*.

Haesen, D., Sents, W., Lemaire, K., Hoorne, Y., and Janssens, V. (2014). The basic biology of PP2A in hematologic cells and malignancies. Frontiers in Oncology *4*, 1–11.

Hammel, M., Yu, Y., Mahaney, B.L., Cai, B., Ye, R., Phipps, B.M., Rambo, R.P., Hura, G.L., Pelikan, M., So, S., et al. (2010). Ku and DNA-dependent Protein Kinase Dynamic Conformations and Assembly Regulate DNA Binding and the Initial Non-homologous End Joining Complex. Journal of Biological Chemistry *285*, 1414–1423.

Hammond, D., Zeng, K., Espert, A., Nunes Bastos, R., Baron, R.D., Gruneberg, U., Barr, F.A. (2013) Melanoma-associated mutations in protein phosphatase 6 cause chromosome instability and DNA damage owing to dysregulated Aurora-A. J. Cell Sci. *126*, 3429-3440.

Hanahan, D., and Weinberg, R.A. (2000). The hallmarks of cancer. Cell *100*, 57–70.

Hanahan, D., and Weinberg, R.A. (2011). Hallmarks of Cancer: The Next Generation. Cell *144*, 646–674.

Haneda, M., Kojima, E., Nishikimi, A., Hasegawa, T., Nakashima, I., and Isobe, K.-I. (2004). Protein phosphatase 1, but not protein phosphatase 2A, dephosphorylates DNA-damaging stress-induced phospho-serine 15 of p53. FEBS Letters *567*, 171–174.

Hanlon Newell, A.E., Hemphill, A., Akkari, Y.M.N., Hejna, J., Moses, R.E., and Olson, S.B. (2008). Loss of homologous recombination or non-homologous end-joining leads to radial formation following DNA interstrand crosslink damage. Cytogenet Genome Res *121*, 174–180.

Hartlerode, A.J., and Scully, R. (2009). Mechanisms of double-strand break repair in somatic mammalian cells. Biochem. J. *423*, 157–168.

Hartwell, L.H., and Kastan, M.B. (1994). Cell cycle control and cancer. Science *266*, 1821–1828.

Heideker, J., Lis, E.T., and Romesberg, F.E. (2014). Phosphatases, DNA Damage Checkpoints and Checkpoint Deactivation. Cell Cycle *6*, 3058–3064.

Helleday, T., Petermann, E., Lundin, C., Hodgson, B., and Sharma, R.A. (2008). DNA repair pathways as targets for cancer therapy. Nature Reviews Cancer *8*, 193–204.

Heyer, W.-D., Ehmsen, K.T., and Liu, J. (2010). Regulation of Homologous Recombination in Eukaryotes. Annu. Rev. Genet. *44*, 113–139.

Higgs, M.R., Reynolds, J.J., Winczura, A., Blackford, A.N., Borel, V., Miller, E.S., Zlatanou, A., Nieminuszczy, J., Ryan, E.L., Davies, N.J., et al. (2015). BOD1L Is Required to Suppress Deleterious Resection of Stressed Replication Forks. Molecular Cell 1–17.

Hirao, A., Kong, Y.Y., Matsuoka, S., Wakeham, A., Ruland, J., Yoshida, H., Liu, D., Elledge, S.J., and Mak, T.W. (2000). DNA damage-induced activation of p53 by the checkpoint kinase Chk2. Science *287*, 1824–1827.

Hoeijmakers, J.H. (2001). Genome maintenance mechanisms for preventing cancer. Nature *411*, 366–374.

Hoeijmakers, J.H.J. (2009). DNA Damage, Aging, and Cancer. N Engl J Med *361*, 1475–1485.

Honkanen, R.E., and Golden, T. (2002). Regulators of Serine / Threonine Protein

Phosphatases at the Dawn of a Clinical Era? Current Medicinal Chemistry *9*, 2055–2075.

Hopfner, K.P., Karcher, A., Shin, D.S., Craig, L., Arthur, L.M., Carney, J.P., and Tainer, J.A. (2000). Structural biology of Rad50 ATPase: ATP-driven conformational control in DNA double-strand break repair and the ABC-ATPase superfamily. Cell *101*, 789–800.

Houtgraaf, J.H., Versmissen, J., and van der Giessen, W.J. (2006). A concise review of DNA damage checkpoints and repair in mammalian cells. Cardiovascular Revascularization Medicine *7*, 165–172.

Hsu, L.-C. (2007). Identification and functional characterization of a PP1-binding site in BRCA1. Biochemical and Biophysical Research Communications *360*, 507–512.

Hu, C., Zhang, S., Gao, X., Gao, X., Xu, X., Lv, Y., Zhang, Y., Zhu, Z., Zhang, C., Li, Q., et al. (2012). Roles of Kruppel-associated Box (KRAB)-associated Co-repressor KAP1 Ser-473 Phosphorylation in DNA Damage Response. Journal of Biological Chemistry *287*, 18937–18952.

Huen, M.S.Y., Grant, R., Manke, I., Minn, K., Yu, X., Yaffe, M.B., and Chen, J. (2007). RNF8 Transduces the DNA-Damage Signal via Histone Ubiquitylation and Checkpoint Protein Assembly. Cell *131*, 901–914.

Huen, M.S.Y., Sy, S.M.H., and Chen, J. (2009). BRCA1 and its toolbox for the maintenance of genome integrity. Nature Publishing Group *11*, 138–148.

Huyen, Y., Zgheib, O., DiTullio, R.A., Gorgoulis, V.G., Zacharatos, P., Petty, T.J., Sheston, E.A., Mellert, H.S., Stavridi, E.S., and Halazonetis, T.D. (2004). Methylated lysine 79 of histone H3 targets 53BP1 to DNA double-strand breaks. Nature *432*, 406–411.

Iles, N., Rulten, S., El-Khamisy, S.F., and Caldecott, K.W. (2007). APLF (C2orf13) Is a Novel Human Protein Involved in the Cellular Response to Chromosomal DNA Strand Breaks. Molecular and Cellular Biology *27*, 3793–3803.

Inoue, K.-I., Nakanjishi, M., Kikuchi, H., Yamamoto, H., Todo, S., Nakagawara, A., and Ozaki, T. (2008). NFBD1/MDC1 stabilizes oncogenic MDM2 to contribute to cell fate determination in response to DNA damage. Biochemical and Biophysical Research Communications *371*, 829–833.

Ip, S.C.Y., Rass, U., Blanco, M.G., Flynn, H.R., Skehel, J.M., and West, S.C. (2008). Identification of Holliday junction resolvases from humans and yeast. Nature *456*, 357–361.

Jackson, S.P. (2002). Sensing and repairing DNA double-strand breaks. Carcinogenesis *23*, 687–696.

Jackson, S.P., and Bartek, J. (2009). The DNA-damage response in human biology and disease. Nature *461*, 1071–1078.

Janicki, S.M., Tsukamoto, T., Salghetti, S.E., Tansey, W.P., Sachidanandam, R., Prasanth, K.V., Ried, T., Shav-Tal, Y., Bertrand, E., Singer, R.H., et al. (2004). From silencing to gene expression: real-time analysis in single cells. Cell *116*, 683–698.

Janssens, V., Longin, S., and Goris, J. (2008). PP2A holoenzyme assembly: in cauda venenum (the sting is in the tail). Trends in Biochemical Sciences *33*, 113–121.

Jungmichel, S., Clapperton, J.A., Lloyd, J., Hari, F.J., Spycher, C., Pavic, L., Li, J., Haire, L.F., Bonalli, M., Larsen, D.H., et al. (2012). The molecular basis of ATM-dependent dimerization of the Mdc1 DNA damage checkpoint mediator. Nucleic Acids Research *40*, 3913–3928.

Jungmichel, S., and Stucki, M. (2010). MDC1: The art of keeping things in focus. Chromosoma *119*, 337–349.

Kakarougkas, A., and Jeggo, P.A. (2014). DNA DSB repair pathway choice: an orchestrated handover mechanism. Bjr *87*, 20130685.

Kalev, P., Simicek, M., Vazquez, I., Munck, S., Chen, L., Soin, T., Danda, N., Chen, W., and Sablina, A. (2012). Loss of PPP2R2A Inhibits Homologous Recombination DNA Repair and Predicts Tumor Sensitivity to PARP Inhibition. Cancer Research *72*, 6414–6424.

Kang, Y., Lee, J.-H., Hoan, N.N., Sohn, H.-M., Chang, I.-Y., and You, H.J. (2009). Protein phosphatase 5 regulates the function of 53BP1 after neocarzinostatin-induced DNA damage. J. Biol. Chem. *284*, 9845–9853.

Kay, B.K., Williamson, M.P., and Sudol, M. (2000). The importance of being proline: the interaction of proline-rich motifs in signaling proteins with their cognate domains. Faseb J. *14*, 231–241.

Khanna, A., Kauko, O., Bockelman, C., Laine, A., Schreck, I., Partanen, J.I., Szwajda, A., Bormann, S., Bilgen, T., Helenius, M., et al. (2013). Chk1 Targeting Reactivates PP2A Tumor Suppressor Activity in Cancer Cells. Cancer Research *73*, 6757–6769.

Kim, H., Lee, O.-H., Xin, H., Chen, L.-Y., Qin, J., Chae, H.K., Lin, S.-Y., Safari, A., Liu, D., and Songyang, Z. (2009). TRF2 functions as a protein hub and regulates telomere maintenance by recognizing specific peptide motifs. Nat

Struct Mol Biol *16*, 372–379.

Kim, J.-S., Krasieva, T.B., Kurumizaka, H., Chen, D.J., Taylor, A.M.R., and Yokomori, K. (2005). Independent and sequential recruitment of NHEJ and HR factors to DNA damage sites in mammalian cells. The Journal of Cell Biology *170*, 341–347.

Kim, S.S., Cao, L., Li, C., Xu, X., Huber, L.J., Chodosh, L.A., and Deng, C.X. (2004). Uterus Hyperplasia and Increased Carcinogen-Induced Tumorigenesis in Mice Carrying a Targeted Mutation of the Chk2 Phosphorylation Site in Brca1. Molecular and Cellular Biology *24*, 9498–9507.

Kim, S.T., Lim, D.S., Canman, C.E., and Kastan, M.B. (1999). Substrate Specificities and Identification of Putative Substrates of ATM Kinase Family Members. Journal of Biological Chemistry *274*, 37538–37543.

Kobayashi, J., Tauchi, H., Sakamoto, S., Nakamura, A., Morishima, K.-I., Matsuura, S., Kobayashi, T., Tamai, K., Tanimoto, K., and Komatsu, K. (2002). NBS1 localizes to gamma-H2AX foci through interaction with the FHA/BRCT domain. Curr. Biol. *12*, 1846–1851.

Kolas, N.K., Chapman, J.R., Nakada, S., Ylanko, J., Chahwan, R., Sweeney, F.D., Panier, S., Mendez, M., Wildenhain, J., Thomson, T.M., et al. (2007). Orchestration of the DNA-damage response by the RNF8 ubiquitin ligase. Science *318*, 1637–1640.

Koniaras, K., Cuddihy, A.R., Christopoulos, H., Hogg, A., and O'Connell, M.J. (2001). Inhibition of Chk1-dependent G2 DNA damage checkpoint radiosensitizes p53 mutant human cells. Oncogene *20*, 7453–7463.

Kozlov, S.V., Graham, M.E., Jakob, B., Tobias, F., Kijas, A.W., Tanuji, M., Chen, P., Robinson, P.J., Taucher-Scholz, G., Suzuki, K., et al. (2011). Autophosphorylation and ATM Activation: ADDITIONAL SITES ADD TO THE COMPLEXITY. Journal of Biological Chemistry *286*, 9107–9119.

Kozlov, S.V., Graham, M.E., Peng, C., Chen, P., Robinson, P.J., and Lavin, M.F. (2006). Involvement of novel autophosphorylation sites in ATM activation. The EMBO Journal *25*, 3504–3514.

Kumareswaran, R., Ludkovski, O., Meng, A., Sykes, J., Pintilie, M., and Bristow, R.G. (2012). Chronic hypoxia compromises repair of DNA double-strand breaks to drive genetic instability. Journal of Cell Science *125*, 189–199.

Küntziger, T., Landsverk, H.B., Collas, P., and Syljuåsen, R.G. (2014). Protein phosphatase 1 regulators in DNA damage signaling. Cell Cycle *10*, 1356–1362.

Lamarche, B.J., Orazio, N.I., and Weitzman, M.D. (2010). The MRN complex in

double-strand break repair and telomere maintenance. FEBS Letters *584*, 3682–3695.

Landsverk, H.B., dez, F.M.-B.U., Landsverk, O.J.B., Hasvold, G., Naderi, S., Bakke, O., Ellenberg, J., Collas, P., sen, R.G.S.A., and ntziger, T.K.U. (2010). scientific report. EMBO Rep *11*, 868–875.

Landsverk, H.B., Kirkhus, M., Bollen, M., Küntziger, T., and Collas, P. (2005). PNUTS enhances in vitro chromosome decondensation in a PP1-dependent manner. Biochem. J. *390*, 709.

Lavin, M.F. (2008). Ataxia-telangiectasia: from a rare disorder to a paradigm for cell signalling and cancer. Nature Publishing Group *9*, 759–769.

LeBron, C., Chen, L., Gilkes, D.M., and Chen, J. (2006). Regulation of MDMX nuclear import and degradation by Chk2 and 14-3-3. The EMBO Journal *25*, 1196–1206.

Lee, D.-H., and Chowdhury, D. (2011). What goes on must come off: phosphatases gate-crash the DNA damage response. Trends in Biochemical Sciences *36*, 569–577.

Lee, D.-H., Acharya, S.S., Kwon, M., Drane, P., Guan, Y., Adelmant, G., Kalev, P., Shah, J., Pellman, D., Marto, J.A., et al. (2014). Dephosphorylation Enables the Recruitment of 53BP1 to Double-Strand DNA Breaks. Molecular Cell *54*, 512–525.

Lee, D.-H., Goodarzi, A.A., Adelmant, G.O., Pan, Y., Jeggo, P.A., Marto, J.A., and Chowdhury, D. (2012). Phosphoproteomic analysis reveals that PP4 dephosphorylates KAP-1 impacting the DNA damage response. The EMBO Journal *31*, 2403–2415.

Lee, D.-H., Pan, Y., Kanner, S., Sung, P., Borowiec, J.A., and Chowdhury, D. (2010). A PP4 phosphatase complex dephosphorylates RPA2 to facilitate DNA repair via homologous recombination. Nat Struct Mol Biol *17*, 365–372.

Lee, J.H., Mand, M.R., Deshpande, R.A., Kinoshita, E., Yang, S.H., Wyman, C., and Paull, T.T. (2013). Ataxia Telangiectasia-Mutated (ATM) Kinase Activity Is Regulated by ATP-driven Conformational Changes in the Mre11/Rad50/Nbs1 (MRN) Complex. Journal of Biological Chemistry *288*, 12840–12851.

Lee, J.S., Collins, K.M., Brown, A.L., Lee, C.H., and Chung, J.H. (2000). hCds1-mediated phosphorylation of BRCA1 regulates the DNA damage response. Nature *404*, 201–204.

Lee, J.-H., and Paull, T.T. (2005). ATM activation by DNA double-strand breaks through the Mre11-Rad50-Nbs1 complex. Science *308*, 551–554.

Lee, K.-J., Jovanovic, M., Udayakumar, D., Bladen, C.L., and Dynan, W.S. (2004). Identification of DNA-PKcs phosphorylation sites in XRCC4 and effects of mutations at these sites on DNA end joining in a cell-free system. DNA Repair *3*, 267–276.

Lee, M.S., Edwards, R.A., Thede, G.L., and Glover, J.N.M. (2005). Structure of the BRCT Repeat Domain of MDC1 and Its Specificity for the Free COOH-terminal End of the -H2AX Histone Tail. Journal of Biological Chemistry *280*, 32053–32056.

Lee, S.-J., Lim, C.-J., Min, J.-K., Lee, J.-K., Kim, Y.-M., Lee, J.-Y., Won, M.-H., and Kwon, Y.G. (2007). Protein phosphatase 1 nuclear targeting subunit is a hypoxia inducible gene: its role in post-translational modification of p53 and MDM2. Cell Death Differ *14*, 1106–1116.

Leung-Pineda, V., Ryan, C.E., and Piwnica-Worms, H. (2006). Phosphorylation of Chk1 by ATR Is Antagonized by a Chk1-Regulated Protein Phosphatase 2A Circuit. Molecular and Cellular Biology *26*, 7529–7538.

Levine, A.J. (1997). p53, the cellular gatekeeper for growth and division. Cell *88*, 323–331.

Li, D.W.-C., Liu, J.-P., Schmid, P.C., Schlosser, R., Feng, H., Liu, W.-B., Yan, Q., Gong, L., Sun, S.-M., Deng, M., et al. (2006). Protein serine/threonine phosphatase-1 dephosphorylates p53 at Ser-15 and Ser-37 to modulate its transcriptional and apoptotic activities. Oncogene *25*, 3006–3022.

Li, H.-H., Cai, X., Shouse, G.P., Piluso, L.G., and Liu, X. (2007). A specific PP2A regulatory subunit, B56γ, mediates DNA damage-induced dephosphorylation of p53 at Thr55. The EMBO Journal *26*, 402–411.

Li, M., Makkinje, A., and Damuni, Z. (1996). The myeloid leukemia-associated protein SET is a potent inhibitor of protein phosphatase 2A. J. Biol. Chem. *271*, 11059–11062.

Li, X., Nan, A., Xiao, Y., Chen, Y., and Lai, Y. (2015). PP2A–B56ϵ complex is involved in dephosphorylation of γ-H2AX in the repair process of CPT-induced DNA double-strand breaks. Toxicology *331*, 57–65.

Liang, X., Reed, E., and Yu, J.J. (2006). Protein phosphatase 2A interacts with Chk2 and regulates phosphorylation at Thr-68 after cisplatin treatment of human ovarian cancer cells. Int. J. Mol. Med. *17*, 703–708.

Lieber, M.R. (2010). The Mechanism of Double-Strand DNA Break Repair by the Nonhomologous DNA End-Joining Pathway. Annu. Rev. Biochem. *79*, 181–211.

Lin, Y.-H., Chang, C.-C., Wong, C.-W., and Teng, S.-C. (2009). Recruitment of Rad51 and Rad52 to Short Telomeres Triggers a Mec1-Mediated Hypersensitivity to Double-Stranded DNA Breaks in Senescent Budding Yeast. PLoS ONE *4*, e8224.

Liu, J., Luo, S., Zhao, H., Liao, J., Li, J., Yang, C., Xu, B., Stern, D.F., Xu, X., and Ye, K. (2012). Structural mechanism of the phosphorylation-dependent dimerization of the MDC1 forkhead-associated domain. Nucleic Acids Research *40*, 3898–3912.

Liu, J., Xu, L., Zhong, J., Liao, J., Li, J., and Xu, X. (2014). Protein phosphatase PP4 is involved in NHEJ-mediated repair of DNA double-strand breaks. Cell Cycle *11*, 2643–2649.

Liu, P., Barkley, L.R., Day, T., Bi, X., Slater, D.M., Alexandrow, M.G., Nasheuer, H.-P., and Vaziri, C. (2006). The Chk1-mediated S-phase checkpoint targets initiation factor Cdc45 via a Cdc25A/Cdk2-independent mechanism. J. Biol. Chem. *281*, 30631–30644.

Liu, Q., Guntuku, S., Cui, X.S., Matsuoka, S., Cortez, D., Tamai, K., Luo, G., Carattini-Rivera, S., DeMayo, F., Bradley, A., et al. (2000). Chk1 is an essential kinase that is regulated by Atr and required for the G(2)/M DNA damage checkpoint. Genes & Development *14*, 1448–1459.

Liu, Y., Virshup, D.M., White, R.L., and Hsu, L.-C. (2002). Regulation of BRCA1 phosphorylation by interaction with protein phosphatase 1alpha. Cancer Research *62*, 6357–6361.

Llorente, B., Smith, C.E., and Symington, L.S. (2008). Break-induced replication: What is it and what is it for? Cell Cycle *7*, 859–864.

Lloyd, J., Chapman, J.R., Clapperton, J.A., Haire, L.F., Hartsuiker, E., Li, J., Carr, A.M., Jackson, S.P., and Smerdon, S.J. (2009). A Supramodular FHA/BRCT-Repeat Architecture Mediates Nbs1 Adaptor Function in Response to DNA Damage. Cell *139*, 100–111.

Lord, C.J., and Ashworth, A. (2012). The DNA damage response and cancer therapy. Nature *481*, 287–294.

Lou, Z., Chen, B.P.C., Asaithamby, A., Minter-Dykhouse, K., Chen, D.J., and Chen, J. (2004). MDC1 Regulates DNA-PK Autophosphorylation in Response to DNA Damage. Journal of Biological Chemistry *279*, 46359–46362.

Lou, Z., Minter-Dykhouse, K., Franco, S., Gostissa, M., Rivera, M.A., Celeste, A., Manis, J.P., van Deursen, J., Nussenzweig, A., Paull, T.T., et al. (2006). MDC1 Maintains Genomic Stability by Participating in the Amplification of ATM-Dependent DNA Damage Signals. Molecular Cell *21*, 187–200.

Lou, Z., Minter-Dykhouse, K., Wu, X., and Chen, J. (2003). MDC1 is coupled to activated CHK2 in mammalian DNA damage response pathways. Nature *421*, 957–961.

Lu, J., Kovach, J.S., Johnson, F., Chiang, J., Hodes, R., Lonser, R., and Zhuang, Z. (2009). Inhibition of serine/threonine phosphatase PP2A enhances cancer chemotherapy by blocking DNA damage induced defense mechanisms. Proceedings of the National Academy of Sciences *106*, 11697–11702.

Lu, X., Ma, O., Nguyen, T.-A., Jones, S.N., Oren, M., and Donehower, L.A. (2007). The Wip1 Phosphatase Acts as a Gatekeeper in the p53-Mdm2 Autoregulatory Loop. Cancer Cell *12*, 342–354.

Lu, X., Nannenga, B., and Donehower, L.A. (2005). PPM1D dephosphorylates Chk1 and p53 and abrogates cell cycle checkpoints. Genes & Development *19*, 1162–1174.

Lu, X., Nguyen, T.-A., and Donehower, L.A. (2014). Reversal of the ATM/ATR-Mediated DNA Damage Response by the Oncogenic Phosphatase PPM1D. Cell Cycle *4*, 4060–4064.

Lu, X., Nguyen, T.-A., Moon, S.-H., Darlington, Y., Sommer, M., and Donehower, L.A. (2008). The type 2C phosphatase Wip1: An oncogenic regulator of tumor suppressor and DNA damage response pathways. Cancer Metastasis Rev *27*, 123–135.

Luijsterburg, M.S., Dinant, C., Lans, H., Stap, J., Wiernasz, E., Lagerwerf, S., Warmerdam, D.O., Lindh, M., Brink, M.C., Dobrucki, J.W., et al. (2009). Heterochromatin protein 1 is recruited to various types of DNA damage. The Journal of Cell Biology *185*, 577–586.

Lukas, C., Bartek, J., and Lukas, J. (2005). Imaging of protein movement induced by chromosomal breakage: tiny ‘local’ lesions pose great ‘global’ challenges. Chromosoma *114*, 146–154.

Lukas, C., Falck, J., Bartkova, J., Bartek, J., and Lukas, J. (2003). Distinct spatiotemporal dynamics of mammalian checkpoint regulators induced by DNA damage. Nature Cell Biology *5*, 255–260.

Lukas, C., Melander, F., Stucki, M., Falck, J., Bekker-Jensen, S., Goldberg, M., Lerenthal, Y., Jackson, S.P., Bartek, J., and Lukas, J. (2004a). Mdc1 couples DNA double-strand break recognition by Nbs1 with its H2AX-dependent chromatin retention. The EMBO Journal *23*, 2674–2683.

Lukas, J., Lukas, C., and Bartek, J. (2004b). Mammalian cell cycle checkpoints: signalling pathways and their organization in space and time. DNA Repair *3*, 997–1007.

Luo, G., Yao, M.S., Bender, C.F., Mills, M., Bladl, A.R., Bradley, A., and Petrini, J.H. (1999). Disruption of mRad50 causes embryonic stem cell lethality, abnormal embryonic development, and sensitivity to ionizing radiation. Proc. Natl. Acad. Sci. U.S.a. *96*, 7376–7381.

Luo, K., Yuan, J., and Lou, Z. (2011). Oligomerization of MDC1 Protein Is Important for Proper DNA Damage Response. Journal of Biological Chemistry *286*, 28192–28199.

Luo, K., Zhang, H., Wang, L., Yuan, J., and Lou, Z. (2012). Sumoylation of MDC1 is important for proper DNA damage response. The EMBO Journal *31*, 3008–3019.

Luo, S., and Ye, K. (2012). Dimerization, but not phosphothreonine binding, is conserved between the forkhead-associated domains of Drosophila MU2 and human MDC1. FEBS Letters *586*, 344–349.

Luo, S., Xin, X., Du, L.-L., Ye, K., and Wei, Y. (2015). Dimerization mediated by a divergent FHA domain is essential for the DNA damage and spindle functions of fission yeast Mdb1. Journal of Biological Chemistry.

Lv, P., Wang, Y., Ma, J., Wang, Z., Li, J.-L., Hong, C.S., Zhuang, Z., and Zeng, Y.-X. (2014). Inhibition of protein phosphatase 2A with a small molecule LB100 radiosensitizes nasopharyngeal carcinoma xenografts by inducing mitotic catastrophe and blocking DNA damage repair. Oncotarget *5*, 7512–7524.

Ma, Y., Pannicke, U., Lu, H., Niewolik, D., Schwarz, K., and Lieber, M.R. (2005a). The DNA-dependent protein kinase catalytic subunit phosphorylation sites in human Artemis. J. Biol. Chem. *280*, 33839–33846.

Ma, Y., Schwarz, K., and Lieber, M.R. (2005b). The Artemis:DNA-PKcs endonuclease cleaves DNA loops, flaps, and gaps. DNA Repair *4*, 845–851.

Macurek, L., Lindqvist, A., Voets, O., Kool, J., Vos, H.R., and Medema, R.H. (2010). Wip1 phosphatase is associated with chromatin and dephosphorylatescH2AX to promote checkpoint inhibition. Oncogene *29*, 2281–2291.

Mahaney, B.L., Meek, K., and Lees-Miller, S.P. (2009). Repair of ionizing radiation-induced DNA double-strand breaks by non-homologous end-joining. Biochem. J. *417*, 639–650.

Mailand, N., Falck, J., Lukas, C., Syljuåsen, R.G., Welcker, M., Bartek, J., and Lukas, J. (2000). Rapid destruction of human Cdc25A in response to DNA damage. Science *288*, 1425–1429.

Mailand, N., Bekker-Jensen, S., Faustrup, H., Melander, F., Bartek, J., Lukas, C.,

and Lukas, J. (2007). RNF8 Ubiquitylates Histones at DNA Double-Strand Breaks and Promotes Assembly of Repair Proteins. Cell *131*, 887–900.

Maser, R.S., Mirzoeva, O.K., Wells, J., Olivares, H., Williams, B.R., Zinkel, R.A., Farnham, P.J., and Petrini, J.H.J. (2001). Mre11 Complex and DNA Replication: Linkage to E2F and Sites of DNA Synthesis. Molecular and Cellular Biology *21*, 6006–6016.

Matsuoka, S., Ballif, B.A., Smogorzewska, A., McDonald, E.R., Hurov, K.E., Luo, J., Bakalarski, C.E., Zhao, Z., Solimini, N., Lerenthal, Y., et al. (2007). ATM and ATR Substrate Analysis Reveals Extensive Protein Networks Responsive to DNA Damage. Science *316*, 1160–1166.

Matsuoka, S., Rotman, G., Ogawa, A., Shiloh, Y., Tamai, K., and Elledge, S.J. (2000). Ataxia telangiectasia-mutated phosphorylates Chk2 in vivo and in vitro. Proc. Natl. Acad. Sci. U.S.a. *97*, 10389–10394.

Mattiroli, F., Vissers, J.H.A., van Dijk, W.J., Ikpa, P., Citterio, E., Vermeulen, W., Marteijn, J.A., and Sixma, T.K. (2012). RNF168 Ubiquitinates K13-15 on H2A/H2AX to Drive DNA Damage Signaling. Cell *150*, 1182–1195.

McConnell, J.L., Gomez, R.J., McCorvey, L.R.A., Law, B.K., and Wadzinski, B.E. (2007). Identification of a PP2A-interacting protein that functions as a negative regulator of phosphatase activity in the ATM/ATR signaling pathway. Oncogene *26*, 6021–6030.

McCright, B., Rivers, A.M., Audlin, S., and Virshup, D.M. (1996). The B56 family of protein phosphatase 2A (PP2A) regulatory subunits encodes differentiation-induced phosphoproteins that target PP2A to both nucleus and cytoplasm. J. Biol. Chem. *271*, 22081–22089.

McCulloch, S.D., and Kunkel, T.A. (2008). The fidelity of DNA synthesis by eukaryotic replicative and translesion synthesis polymerases. Cell Res *18*, 148–161.

McKinnon, P.J. (2004). ATM and ataxia telangiectasia. EMBO Rep *5*, 772–776.

McKinnon, P.J. (2009). DNA repair deficiency and neurological disease. Nature Reviews Neuroscience *10*, 100–112.

McLean, J.R., Chaix, D., Ohi, M.D., and Gould, K.L. (2011). State of the APC/C: Organization, function, and structure. Critical Reviews in Biochemistry and Molecular Biology *46*, 118–136.

Melander, F., Bekker-Jensen, S., Falck, J., Bartek, J., Mailand, N., and Lukas, J. (2008). Phosphorylation of SDT repeats in the MDC1 N terminus triggers retention of NBS1 at the DNA damage-modified chromatin. The Journal of Cell

Biology *181*, 213–226.

Melo, J., and Toczyski, D. (2002). A unified view of the DNA-damage checkpoint. Curr. Opin. Cell Biol. *14*, 237–245.

Mi, J., Bolesta, E., Brautigan, D.L., and Larner, J.M. (2009a). PP2A regulates ionizing radiation-induced apoptosis through Ser46 phosphorylation of p53. Molecular Cancer Therapeutics *8*, 135–140.

Mi, J., Dziegielewski, J., Bolesta, E., Brautigan, D.L., and Larner, J.M. (2009b). Activation of DNA-PK by Ionizing Radiation Is Mediated by Protein Phosphatase 6. PLoS ONE *4*, e4395.

Miller, T., Krogan, N.J., Dover, J., Erdjument-Bromage, H., Tempst, P., Johnston, M., Greenblatt, J.F., and Shilatifard, A. (2001). COMPASS: a complex of proteins associated with a trithorax-related SET domain protein. Proc. Natl. Acad. Sci. U.S.a. *98*, 12902–12907.

Mirzayans, R., Andrais, B., Scott, A., and Murray, D. (2012). New Insights into p53 Signaling and Cancer Cell Response to DNA Damage: Implications for Cancer Therapy. Journal of Biomedicine and Biotechnology *2012*, 1–16.

Mochan, T.A., Venere, M., DiTullio, R.A., and Halazonetis, T.D. (2003). 53BP1 and NFBD1/MDC1-Nbs1 function in parallel interacting pathways activating ataxia-telangiectasia mutated (ATM) in response to DNA damage. Cancer Research *63*, 8586–8591.

Mochida, S., Maslen, S.L., Skehel, M., and Hunt, T. (2010). Greatwall phosphorylates an inhibitor of protein phosphatase 2A that is essential for mitosis. Science *330*, 1670–1673.

Moon, S.-H., Nguyen, T.-A., Darlington, Y., Lu, X., and Donehower, L.A. (2010). Dephosphorylation of γ-H2AX by WIP1: an important homeostatic regulatory event in DNA repair and cell cycle control. Cell Cycle *9*, 2092–2096.

Moreno-Herrero, F., de Jager, M., Dekker, N.H., Kanaar, R., Wyman, C., and Dekker, C. (2005). Mesoscale conformational changes in the DNA-repair complex Rad50/Mre11/Nbs1 upon binding DNA. Nature *437*, 440–443.

Morgan, A.A., and Rubenstein, E. (2013). Proline: The Distribution, Frequency, Positioning, and Common Functional Roles of Proline and Polyproline Sequences in the Human Proteome. PLoS ONE *8*, e53785.

Morris, J.R., Boutell, C., Keppler, M., Densham, R., Weekes, D., Alamshah, A., Butler, L., Galanty, Y., Pangon, L., Kiuchi, T., et al. (2010). The SUMO modification pathway isinvolved in the BRCA1 response togenotoxic stress. Nature *462*, 886–890.

Moynahan, M.E., Pierce, A.J., and Jasin, M. (2001). BRCA2 is required for homology-directed repair of chromosomal breaks. Molecular Cell *7*, 263–272.

Munoz, I.M., Hain, K., clais, A.-C.C.D., Gardiner, M., Toh, G.W., Sanchez-Pulido, L., Heuckmann, J.M., Toth, R., Macartney, T., Eppink, B., et al. (2009). Coordination of Structure-Specific Nucleasesby Human SLX4/BTBD12 Is Required for DNA Repair. Molecular Cell *35*, 116–127.

Munoz, I.M., Jowsey, P.A., Toth, R., and Rouse, J. (2007). Phospho-epitope binding by the BRCT domains of hPTIP controls multiple aspects of the cellular response to DNA damage. Nucleic Acids Research *35*, 5312–5322.

Musacchio, A., Gibson, T., Lehto, V.P., and Saraste, M. (1992). SH3--an abundant protein domain in search of a function. FEBS Letters *307*, 55–61.

Myers, K., Gagou, M.E., Zuazua-Villar, P., Rodriguez, R., and Meuth, M. (2009). ATR and Chk1 Suppress a Caspase-3–Dependent Apoptotic Response Following DNA Replication Stress. PLoS Genet *5*, e1000324.

Nakada, S., Chen, G.I., Gingras, A.-C., and Durocher, D. (2008). PP4 is a γH2AX phosphatase required for recovery from the DNA damage checkpoint. EMBO Rep *9*, 1019–1026.

Nakamura, K., Kato, A., Kobayashi, J., Yanagihara, H., Sakamoto, S., Oliveira, D.V.N.P., Shimada, M., Tauchi, H., Suzuki, H., Tashiro, S., et al. (2011). Regulation of Homologous Recombination by RNF20-Dependent H2B Ubiquitination. Molecular Cell *41*, 515–528.

Nakanishi, M., Ozaki, T., and Yamamoto, H. (2007). NFBD1/MDC1 associates with p53 and regulates its function at the crossroad between cell survival and death in response to DNA damage. J. Biol. Chem. *282*, 22993–23004.

Negrini, S., Gorgoulis, V.G., and Halazonetis, T.D. (2010). Genomic instability — an evolving hallmark of cancer. Nature Publishing Group *11*, 220–228.

Nick McElhinny, S.A., Snowden, C.M., McCarville, J., and Ramsden, D.A. (2000). Ku recruits the XRCC4-ligase IV complex to DNA ends. Molecular and Cellular Biology *20*, 2996–3003.

Nimonkar, A.V., Genschel, J., Kinoshita, E., Polaczek, P., Campbell, J.L., Wyman, C., Modrich, P., and Kowalczykowski, S.C. (2011). BLM-DNA2-RPA-MRN and EXO1-BLM-RPA-MRN constitute two DNA end resection machineries for human DNA break repair. Genes & Development *25*, 350–362.

Nimonkar, A.V., and Kowalczykowski, S.C. (2009). Second-end DNA capture in double-strand break repair: how to catch a DNA by its tail. Cell Cycle *8*, 1816–1817.

Nobumori, Y., Shouse, G.P., Wu, Y., Lee, K.J., Shen, B., and Liu, X. (2013). B56 Tumor-Associated Mutations Provide New Mechanisms for B56 -PP2A Tumor Suppressor Activity. Mol Cancer Res *11*, 995–1003.

O'Neill, T., Dwyer, A.J., Ziv, Y., Chan, D.W., Lees-Miller, S.P., Abraham, R.H., Lai, J.H., Hill, D., Shiloh, Y., Cantley, L.C., et al. (2000). Utilization of Oriented Peptide Libraries to Identify Substrate Motifs Selected by ATM. Journal of Biological Chemistry *275*, 22719–22727.

Oliva-Trastoy, M., Berthonaud, V., Chevalier, A., Ducrot, C., Marsolier-Kergoat, M.-C., Mann, C., and Leteurtre, F. (2006). The Wip1 phosphatase (PPM1D) antagonizes activation of the Chk2 tumour suppressor kinase. Oncogene *26*, 1449–1458.

Orthwein, A., Fradet-Turcotte, A., Noordermeer, S.M., Canny, M.D., Brun, C.M., Strecker, J., Escribano-Diaz, C., and Durocher, D. (2014). Mitosis inhibits DNA double-strand break repair to guard against telomere fusions. Science *344*, 189–193.

Ou, Y.-H., Chung, P.-H., Sun, T.-P., and Shieh, S.-Y. (2005). p53 C-terminal phosphorylation by CHK1 and CHK2 participates in the regulation of DNA-damage-induced C-terminal acetylation. Mol. Biol. Cell *16*, 1684–1695.

Panier, S., and Boulton, S.J. (2013). Double-strand break repair:53BP1 comes into focus. Nature Publishing Group *15*, 7–18.

Patel, A., Dharmarajan, V., Vought, V.E., and Cosgrove, M.S. (2009). On the Mechanism of Multiple Lysine Methylation by the Human Mixed Lineage Leukemia Protein-1 (MLL1) Core Complex. J. Biol. Chem. *284*, 24242–24256.

Patil, M., Pabla, N., and Dong, Z. (2013). Checkpoint kinase 1 in DNA damage response and cell cycle regulation. Cell. Mol. Life Sci. *70*, 4009–4021.

Paull, T.T., and Gellert, M. (1998). The 3′ to 5′ exonuclease activity of Mre11 facilitates repair of DNA double-strand breaks. Molecular Cell *1*, 969–979.

Paull, T.T., and Gellert, M. (1999). Nbs1 potentiates ATP-driven DNA unwinding and endonuclease cleavage by the Mre11/Rad50 complex. Genes & Development *13*, 1276–1288.

Paull, T.T., Rogakou, E.P., Yamazaki, V., Kirchgessner, C.U., Gellert, M., and Bonner, W.M. (2000). A critical role for histone H2AX in recruitment of repair factors to nuclear foci after DNA damage. Current Biology *10*, 886–895.

Pawson, T. (1995). Protein modules and signalling networks. Nature *373*, 573–580.

Paz, A., Brownstein, Z., Ber, Y., Bialik, S., David, E., Sagir, D., Ulitsky, I., Elkon,

R., Kimchi, A., Avraham, K.B., et al. (2010). SPIKE: a database of highly curated human signaling pathways. Nucleic Acids Research *39*, D793–D799.

Pâques, F., and Haber, J.E. (1999). Multiple pathways of recombination induced by double-strand breaks in Saccharomyces cerevisiae. Microbiol. Mol. Biol. Rev. *63*, 349–404.

Peng, A. (2003). NFBD1, Like 53BP1, Is an Early and Redundant Transducer Mediating Chk2 Phosphorylation in Response to DNA Damage. Journal of Biological Chemistry *278*, 8873–8876.

Peng, A., and Maller, J.L. (2010). Serine/threonine phosphatases in the DNA damage response and cancer. Oncogene *29*, 5977–5988.

Peng, A., Lewellyn, A.L., Schiemann, W.P., and Maller, J.L. (2010). Repo-man controls a protein phosphatase 1-dependent threshold for DNA damage checkpoint activation. Curr. Biol. *20*, 387–396.

Peng, C.Y., Graves, P.R., Thoma, R.S., Wu, Z., Shaw, A.S., and Piwnica-Worms, H. (1997). Mitotic and G2 checkpoint control: regulation of 14-3-3 protein binding by phosphorylation of Cdc25C on serine-216. Science *277*, 1501–1505.

Petersen, B., Petersen, T., Andersen, P., Nielsen, M., and Lundegaard, C. (2009). A generic method for assignment of reliability scores applied to solvent accessibility predictions. BMC Struct Biol *9*.

Pierce, A.J., Johnson, R.D., Thompson, L.H., and Jasin, M. (1999). XRCC3 promotes homology-directed repair of DNA damage in mammalian cells. Genes & Development *13*, 2633–2638.

Pines, J. (1999). Four-dimensional control of the cell cycle. Nature Cell Biology *1*, E73–E79.

Pitts, S.A., Kullar, H.S., Stankovic, T., Stewart, G.S., Last, J.I., Bedenham, T., Armstrong, S.J., Piane, M., Chessa, L., Taylor, A.M., et al. (2001). hMRE11: genomic structure and a null mutation identified in a transcript protected from nonsense-mediated mRNA decay. Hum. Mol. Genet. *10*, 1155–1162.

Porter, I.M., McClelland, S.E., Khoudoli, G.A., Hunter, C.J., Andersen, J.S., McAinsh, A.D., Blow, J.J., and Swedlow, J.R. (2007). Bod1, a novel kinetochore protein required for chromosome biorientation. The Journal of Cell Biology *179*, 187–197.

Porter, I.M., Schleicher, K., Porter, M., and Swedlow, J.R. (2013). Bod1 regulates protein phosphatase 2A at mitotic kinetochores. Nature Communications *4*, 1–9.

Renkawitz, J., Lademann, C.A., and Jentsch, S. (2014). Mechanisms and principlesof homology search duringrecombination. Nature Publishing Group *15*, 369–383.

Reynolds, J.J., and Stewart, G.S. (2013). A nervous predisposition to unrepaired DNA double strand breaks. DNA Repair *12*, 588–599.

Rogakou, E.P., Boon, C., Redon, C., and Bonner, W.M. (1999). Megabase chromatin domains involved in DNA double-strand breaks in vivo. The Journal of Cell Biology *146*, 905–916.

Rogakou, E.P., Pilch, D.R., Orr, A.H., Ivanova, V.S., and Bonner, W.M. (1998). DNA double-stranded breaks induce histone H2AX phosphorylation on serine 139. J. Biol. Chem. *273*, 5858–5868.

Roos, W.P., and Kaina, B. (2006). DNA damage-induced cell death by apoptosis. Trends in Molecular Medicine *12*, 440–450.

Rothstein, R., Michel, B., and Gangloff, S. (2000). Replication fork pausing and recombination or “gimme a break.” Genes & Development *14*, 1–10.

Ruediger, R., Hentz, M., Fait, J., Mumby, M., and Walter, G. (1994). Molecular model of the A subunit of protein phosphatase 2A: interaction with other subunits and tumor antigens. J. Virol. *68*, 123–129.

Saberi, A., Hochegger, H., Szuts, D., Lan, L., Yasui, A., Sale, J.E., Taniguchi, Y., Murakawa, Y., Zeng, W., Yokomori, K., et al. (2007). RAD18 and Poly(ADP-Ribose) Polymerase Independently Suppress the Access of Nonhomologous End Joining to Double-Strand Breaks and Facilitate Homologous Recombination-Mediated Repair. Molecular and Cellular Biology *27*, 2562–2571.

Saitoh, H., Pizzi, M.D., and Wang, J. (2002). Perturbation of SUMOlation Enzyme Ubc9 by Distinct Domain within Nucleoporin RanBP2/Nup358. Journal of Biological Chemistry *277*, 4755–4763.

Sancar, A., Lindsey-Boltz, L.A., Ünsal-Kaçmaz, K., and Linn, S. (2004). Molecular mechanisms of mammalian DNA repair and the DNA damage checkpoints. Annu. Rev. Biochem. *73*, 39–85.

Sanchez, Y., Wong, C., Thoma, R.S., Richman, R., Wu, Z., Piwnica-Worms, H., and Elledge, S.J. (1997). Conservation of the Chk1 checkpoint pathway in mammals: linkage of DNA damage to Cdk regulation through Cdc25. Science *277*, 1497–1501.

Sanders, S.L., Portoso, M., Mata, J., Bähler, J., Allshire, R.C., and Kouzarides, T. (2004). Methylation of histone H4 lysine 20 controls recruitment of Crb2 to

sites of DNA damage. Cell *119*, 603–614.

Schumacher, A.J., Mohni, K.N., Kan, Y., Hendrickson, E.A., Stark, J.M., and Weller, S.K. (2012). The HSV-1 Exonuclease, UL12, Stimulates Recombination by a Single Strand Annealing Mechanism. PLoS Pathogens *8*, e1002862.

Schwarz, J.K., Lovly, C.M., and Piwnica-Worms, H. (2003). Regulation of the Chk2 protein kinase by oligomerization-mediated cis- and trans-phosphorylation. Mol Cancer Res *1*, 598–609.

Seiler, D.M., Rouquette, J., Schmid, V.J., Strickfaden, H., Ottmann, C., Drexler, G.A., Mazurek, B., Greubel, C., Hable, V., Dollinger, G., et al. (2011). Double-strand break-induced transcriptional silencing is associated with loss of tri-methylation at H3K4. Chromosome Res *19*, 883–899.

Sents, W., Ivanova, E., Lambrecht, C., Haesen, D., and Janssens, V. (2012). The biogenesis of active protein phosphatase 2A holoenzymes: a tightly regulated process creating phosphatase specificity. FEBS Journal *280*, 644–661.

Seo, G.-J., Kim, S.-E., Lee, Y.-M., Lee, J.-W., Lee, J.-R., Hahn, M.-J., and Kim, S.-T. (2003). Determination of substrate specificity and putative substrates of Chk2 kinase. Biochemical and Biophysical Research Communications *304*, 339–343.

Sfeir, A., and de Lange, T. (2012). Removal of shelterin reveals the telomere end-protection problem. Science *336*, 593–597.

Shafman, T., Khanna, K.K., Kedar, P., Spring, K., Kozlov, S., Yen, T., Hobson, K., Gatei, M., Zhang, N., Watters, D., et al. (1997). Interaction between ATM protein and c-Abl in response to DNA damage. Nature *387*, 520–523.

Shahar, O.D., Ram, E.V.S.R., Shimshoni, E., Hareli, S., Meshorer, E., and Goldberg, M. (2011). Live imaging of induced and controlled DNA double-strand break formation reveals extremely low repair by homologous recombination in human cells. *31*, 3495–3504.

Shaltiel, I.A., Krenning, L., Bruinsma, W., and Medema, R.H. (2015). The same, only different - DNA damage checkpoints and their reversal throughout the cell cycle. Journal of Cell Science *128*, 607–620.

Shang, Y.L., Bodero, A.J., and Chen, P.L. (2003). NFBD1, a Novel Nuclear Protein with Signature Motifs of FHA and BRCT, and an Internal 41-Amino Acid Repeat Sequence, Is an Early Participant in DNA Damage Response. Journal of Biological Chemistry *278*, 6323–6329.

Sharma, K., D'Souza, R.C.J., Tyanova, S., Schaab, C., Wiśniewski, J.R., Cox, J.,

and Mann, M. (2014). Ultradeep Human Phosphoproteome Reveals a Distinct Regulatory Nature of Tyr and Ser/Thr-Based Signaling. CellReports *8*, 1583–1594.

Shi, W., Ma, Z., Willers, H., Akhtar, K., Scott, S.P., Zhang, J., Powell, S., and Zhang, J. (2008). Disassembly of MDC1 Foci Is Controlled by Ubiquitin-Proteasome-dependent Degradation. Journal of Biological Chemistry *283*, 31608–31616.

Shibata, A., Conrad, S., Birraux, J., Geuting, V., Barton, O., Ismail, A., Kakarougkas, A., Meek, K., Taucher-Scholz, G., brich, M.L.O., et al. (2011). Factors determining DNA double-strand break repair pathway choice in G2 phase. The EMBO Journal *30*, 1079–1092.

Shibata, A., Moiani, D., Arvai, A.S., Perry, J., Harding, S.M., Genois, M.-M., Maity, R., van Rossum-Fikkert, S., Kertokalio, A., Romoli, F., et al. (2014). DNA Double-Strand Break Repair Pathway Choice Is Directed by Distinct MRE11 Nuclease Activities. Molecular Cell *53*, 7–18.

Shilatifard, A. (2012). The COMPASS Family of Histone H3K4 Methylases: Mechanisms of Regulation in Development and Disease Pathogenesis. Annu. Rev. Biochem. *81*, 65–95.

Shiloh, Y. (1997). Ataxia-telangiectasia and the Nijmegen breakage syndrome: related disorders but genes apart. Annu. Rev. Genet. *31*, 635–662.

Shiloh, Y., and Ziv, Y. (2013). The ATM protein kinase:regulating the cellular response togenotoxic stress, and more. Nature Publishing Group *14*, 197–210.

Shimada, M., and Nakanishi, M. (2013). Response to DNA damage: why do we need to focus on protein phosphatases? Frontiers in Oncology 1–14.

Shouse, G.P., Cai, X., and Liu, X. (2008). Serine 15 Phosphorylation of p53 Directs Its Interaction with B56 and the Tumor Suppressor Activity of B56 - Specific Protein Phosphatase 2A. Molecular and Cellular Biology *28*, 448–456.

Shouse, G.P., Nobumori, Y., Panowicz, M.J., and Liu, X. (2011). ATM-mediated phosphorylation activates the tumor-suppressive functionof B56y–PP2A. Oncogene *30*, 3755–3765.

Shreeram, S., Demidov, O.N., Hee, W.K., Yamaguchi, H., Onishi, N., Kek, C., Timofeev, O.N., Dudgeon, C., Fornace, A.J., Anderson, C.W., et al. (2006). Wip1 Phosphatase Modulates ATM-Dependent Signaling Pathways. Molecular Cell *23*, 757–764.

Shrivastav, M., De Haro, L.P., and Nickoloff, J.A. (2008). Regulation of DNA double-strand break repair pathway choice. Cell Res *18*, 134–147.

Shull, E.R.P., Lee, Y., Nakane, H., Stracker, T.H., Zhao, J., Russell, H.R., Petrini, J.H.J., and McKinnon, P.J. (2009). Differential DNA damage signaling accounts for distinct neural apoptotic responses in ATLD and NBS. Genes & Development *23*, 171–180.

Sidi, S., Sanda, T., Kennedy, R.D., Hagen, A.T., Jette, C.A., Hoffmans, R., Pascual, J., Imamura, S., Kishi, S., Amatruda, J.F., et al. (2008). Chk1 Suppresses a Caspase-2 Apoptotic Response to DNA Damage that Bypasses p53, Bcl-2, and Caspase-3. Cell *133*, 864–877.

Smetana, J.H.C., and Zanchin, N.I.T. (2007). Interaction analysis of the heterotrimer formed by the phosphatase 2A catalytic subunit, α4 and the mammalian ortholog of yeast Tip41 (TIPRL). FEBS Journal *274*, 5891–5904.

Smith, J., Tho, L.M., Xu, N., and Gillespie, D.A. (2010). The ATM–Chk2 and ATR–Chk1 Pathways in DNA Damage Signaling and Cancer (Elsevier Inc.).

Solinger, J.A., Kiianitsa, K., and Heyer, W.D. (2002). Rad54, a Swi2/Snf2-like recombinational repair protein, disassembles Rad51: dsDNA filaments. Molecular Cell *10*, 1175–1188.

Sommer, L., Cho, H., Choudhary, M., and Seeling, J. (2015). Evolutionary Analysis of the B56 Gene Family of PP2A Regulatory Subunits. Ijms *16*, 10134–10157.

Song, J.Y., Han, H.S., Sabapathy, K., Lee, B.M., Yu, E., and Choi, J. (2010). Expression of a Homeostatic Regulator, Wip1 (Wild-type p53-induced Phosphatase), Is Temporally Induced by c-Jun and p53 in Response to UV Irradiation. Journal of Biological Chemistry *285*, 9067–9076.

Spycher, C., Miller, E.S., Townsend, K., Pavic, L., Morrice, N.A., Janscak, P., Stewart, G.S., and Stucki, M. (2008). Constitutive phosphorylation of MDC1 physically links the MRE11-RAD50-NBS1 complex to damaged chromatin. The Journal of Cell Biology *181*, 227–240.

Stefansson, B., and Brautigan, D.L. (2006). Protein phosphatase 6 subunit with conserved Sit4-associated protein domain targets IkappaBepsilon. J. Biol. Chem. *281*, 22624–22634.

Stefansson, B., Ohama, T., Daugherty, A.E., and Brautigan, D.L. (2008). Protein Phosphatase 6 Regulatory Subunits Composed of Ankyrin Repeat Domains †. Biochemistry *47*, 1442–1451.

Stewart, G.S., Maser, R.S., Stankovic, T., Bressan, D.A., Kaplan, M.I., Jaspers, N.G., Raams, A., Byrd, P.J., Petrini, J.H., and Taylor, A.M. (1999). The DNA double-strand break repair gene hMRE11 is mutated in individuals with an ataxia-telangiectasia-like disorder. Cell *99*, 577–587.

Stewart, G.S., Panier, S., Townsend, K., Al-Hakim, A.K., Kolas, N.K., Miller, E.S., Nakada, S., Ylanko, J., Olivarius, S., Mendez, M., et al. (2009). The RIDDLE Syndrome Protein Mediates a Ubiquitin-Dependent Signaling Cascade at Sites of DNA Damage. Cell *136*, 420–434.

Stewart, G.S., Wang, B., Bignell, C.R., Taylor, A.M.R., and Elledge, S.J. (2003). MDC1 is a mediator of the mammalian DNA damage checkpoint. Nature *421*, 961–966.

Stiff, T., O'Driscoll, M., Rief, N., Iwabuchi, K., Löbrich, M., and Jeggo, P.A. (2004). ATM and DNA-PK function redundantly to phosphorylate H2AX after exposure to ionizing radiation. Cancer Research *64*, 2390–2396.

Strack, S., Cribbs, J.T., and Gomez, L. (2004). Critical Role for Protein Phosphatase 2A Heterotrimers in Mammalian Cell Survival. Journal of Biological Chemistry *279*, 47732–47739.

Stucki, M., and Jackson, S.P. (2006). γH2AX and MDC1: Anchoring the DNA-damage-response machinery to broken chromosomes. DNA Repair *5*, 534–543.

Stucki, M., Clapperton, J.A., Mohammad, D., Yaffe, M.B., Smerdon, S.J., and Jackson, S.P. (2005). MDC1 Directly Binds Phosphorylated Histone H2AX to Regulate Cellular Responses to DNA Double-Strand Breaks. Cell *123*, 1213–1226.

Sun, Y., Jiang, X., Chen, S., Fernandes, N., and Price, B.D. (2005). A role for the Tip60 histone acetyltransferase in the acetylation and activation of ATM. Proc. Natl. Acad. Sci. U.S.a. *102*, 13182–13187.

Sun, Y., Jiang, X., Xu, Y., Ayrapetov, M.K., Moreau, L.A., Whetstine, J.R., and Price, B.D. (2009). Histone H3 methylation links DNA damage detection to activation of the tumour suppressor Tip60. Nature Cell Biology *11*, 1376–1382.

Svendsen, J.M., Smogorzewska, A., Sowa, M.E., Connell, B.C.O., Gygi, S.P., Elledge, S.J., and Harper, J.W. (2009). Mammalian BTBD12/SLX4 Assembles A Holliday Junction Resolvaseand Is Required for DNA Repair. Cell *138*, 63–77.

Swann, P.F., Waters, T.R., Moulton, D.C., Xu, Y.Z., Zheng, Q., Edwards, M., and Mace, R. (1996). Role of postreplicative DNA mismatch repair in the cytotoxic action of thioguanine. Science *273*, 1109–1111.

Symington, L.S., and Gautier, J. (2011). Double-Strand Break End Resection and Repair Pathway Choice. Annu. Rev. Genet. *45*, 247–271.

Sørensen, C.S., Hansen, L.T., Dziegielewski, J., Syljuåsen, R.G., Lundin, C.,

Bartek, J., and Helleday, T. (2005). The cell-cycle checkpoint kinase Chk1 is required for mammalian homologous recombination repair. Nature *7*, 195–201.

Tang, J., Cho, N.W., Cui, G., Manion, E.M., Shanbhag, N.M., Botuyan, M.V., Mer, G., and Greenberg, R.A. (2013). Acetylation limits 53BP1 association with damaged chromatin to promote homologous recombination. Nat Struct Mol Biol *20*, 317–325.

Tang, X., Hui, Z.G., Cui, X.L., Garg, R., Kastan, M.B., and Xu, B. (2008). A Novel ATM-Dependent Pathway Regulates Protein Phosphatase 1 in Response to DNA Damage. Molecular and Cellular Biology *28*, 2559–2566.

Taniguchi, T., Garcia-Higuera, I., Andreassen, P.R., Gregory, R.C., Grompe, M., and D'Andrea, A.D. (2002). S-phase-specific interaction of the Fanconi anemia protein, FANCD2, with BRCA1 and RAD51. Blood *100*, 2414–2420.

Tasat, D.R., and Yakisich, J.S. (2010). DNA Damage Repair, Repair Mechanisms and Aging (Nova Science Publishers Inc).

Taylor, A.M.R., Groom, A., and Byrd, P.J. (2004). Ataxia-telangiectasia-like disorder (ATLD)—its clinical presentation and molecular basis. DNA Repair *3*, 1219–1225.

Terradas, M., Martín, M., Tusell, L., and Genescà, A. (2009). DNA lesions sequestered in micronuclei induce a local defective-damage response. DNA Repair *8*, 1225–1234.

Townsend, K., Mason, H., Blackford, A.N., Miller, E.S., Chapman, J.R., Sedgwick, G.G., Barone, G., Turnell, A.S., and Stewart, G.S. (2009). Mediator of DNA Damage Checkpoint 1 (MDC1) Regulates Mitotic Progression. Journal of Biological Chemistry *284*, 33939–33948.

Traven, A., and Heierhorst, J. (2005). SQ/TQ cluster domains: concentrated ATM/ATR kinase phosphorylation site regions in DNA-damage-response proteins. Bioessays *27*, 397–407.

Trinkle-Mulcahy, L., Andersen, J., Lam, Y.W., Moorhead, G., Mann, M., and Lamond, A.I. (2006). Repo-Man recruits PP1 gamma to chromatin and is essential for cell viability. The Journal of Cell Biology *172*, 679–692.

Trujillo, K.M., and Sung, P. (2001). DNA Structure-specific Nuclease Activities in theSaccharomyces cerevisiae Rad50-Mre11 Complex. Journal of Biological Chemistry *276*, 35458–35464.

Trujillo, K.M., Yuan, S.S., Lee, E.Y., and Sung, P. (1998). Nuclease activities in a complex of human recombination and DNA repair factors Rad50, Mre11, and p95. J. Biol. Chem. *273*, 21447–21450.

Uziel, T., Lerenthal, Y., Moyal, L., Andegeko, Y., Mittelman, L., and Shiloh, Y. (2003). Requirement of the MRN complex for ATM activation by DNA damage. The EMBO Journal *22*, 5612–5621.

van der Linden, E., Sanchez, H., Kinoshita, E., Kanaar, R., and Wyman, C. (2009). RAD50 and NBS1 form a stable complex functional in DNA binding and tethering. Nucleic Acids Research *37*, 1580–1588.

van Nuland, R., Smits, A.H., Pallaki, P., Jansen, P.W.T.C., Vermeulen, M., and Timmers, H.T.M. (2013). Quantitative Dissection and Stoichiometry Determination of the Human SET1/MLL Histone Methyltransferase Complexes. Molecular and Cellular Biology *33*, 2067–2077.

Varmuza, S.E.A. (1998). Spermiogenesis Is Impaired in Mice Bearing a Targeted Mutation in the Protein Phosphatase 1c. Developmental Biology *205*, 98–110.

Varon, R., Vissinga, C., Platzer, M., Cerosaletti, K.M., Chrzanowska, K.H., Saar, K., Beckmann, G., Seemanová, E., Cooper, P.R., Nowak, N.J., et al. (1998). Nibrin, a novel DNA double-strand break repair protein, is mutated in Nijmegen breakage syndrome. Cell *93*, 467–476.

Villarroel, M.C., Rajeshkumar, N.V., Garrido-Laguna, I., De Jesus-Acosta, A., Jones, S., Maitra, A., Hruban, R.H., Eshleman, J.R., Klein, A., Laheru, D., et al. (2011). Personalizing Cancer Treatment in the Age of Global Genomic Analyses: PALB2 Gene Mutations and the Response to DNA Damaging Agents in Pancreatic Cancer. Molecular Cancer Therapeutics *10*, 3–8.

Vodermaier, H.C. (2004). APC/C and SCF: Controlling Each Other and the Cell Cycle. Current Biology *14*, R787–R796.

Vousden, K., and Lu, X. (2002). Live or let die: the cell's response to p53. Nature Reviews Cancer *2*, 594–604.

Wakula, P., Beullens, M., Ceulemans, H., Stalmans, W., and Bollen, M. (2003). Degeneracy and Function of the Ubiquitous RVXF Motif That Mediates Binding to Protein Phosphatase-1. Journal of Biological Chemistry *278*, 18817–18823.

Walter, J., and Newport, J. (2000). Initiation of eukaryotic DNA replication: origin unwinding and sequential chromatin association of Cdc45, RPA, and DNA polymerase alpha. Molecular Cell *5*, 617–627.

Wang, B., and Elledge, S.J. (2007). Ubc13/Rnf8 ubiquitin ligases control foci formation of the Rap80/Abraxas/Brca1/Brcc36 complex in response to DNA damage. Proceedings of the National Academy of Sciences *104*, 20759–20763.

Wang, Q., Goldstein, M., Alexander, P., Wakeman, T.P., Sun, T., Feng, J., Lou, Z., Kastan, M.B., and Wang, X.F. (2014). Rad17 recruits the MRE11-RAD50-

NBS1 complex to regulate the cellular response to DNA double-strand breaks. The EMBO Journal *33*, 862–877.

Wang, Q., Gao, F., Wang, T., Flagg, T., and Deng, X. (2009a). A Nonhomologous End-joining Pathway Is Required for Protein Phosphatase 2A Promotion of DNA Double-Strand Break Repair. Neoplasia *11*, 1012–1021.

Wang, X., Kennedy, R.D., Ray, K., Stuckert, P., Ellenberger, T., and D'Andrea, A.D. (2007). Chk1-Mediated Phosphorylation of FANCE Is Required for the Fanconi Anemia/BRCA Pathway. Molecular and Cellular Biology *27*, 3098–3108.

Wang, Y., Ji, P., Liu, J., Broaddus, R.R., Xue, F., and Zhang, W. (2009b). Centrosome-associated regulators of the G2/M checkpoint as targets for cancer therapy. Mol Cancer *8*.

Ward, I.M., Wu, X., and Chen, J. (2001). Threonine 68 of Chk2 is phosphorylated at sites of DNA strand breaks. J. Biol. Chem. *276*, 47755–47758.

Wei, D., Parsels, L.A., Karnak, D., Davis, M.A., Parsels, J.D., Marsh, A.C., Zhao, L., Maybaum, J., Lawrence, T.S., Sun, Y., et al. (2013). Inhibition of Protein Phosphatase 2A Radiosensitizes Pancreatic Cancers by Modulating CDC25C/CDK1 and Homologous Recombination Repair. Clinical Cancer Research *19*, 4422–4432.

Westermarck, J., and Hahn, W.C. (2008). Multiple pathways regulated by the tumor suppressor PP2A in transformation. Trends in Molecular Medicine *14*, 152–160.

Williams, R.S., Dodson, G.E., Limbo, O., Yamada, Y., Williams, J.S., Guenther, G., Classen, S., Glover, J.N.M., Iwasaki, H., Russell, P., et al. (2009). Nbs1 Flexibly Tethers Ctp1 and Mre11- Rad50 to Coordinate DNA Double-Strand Break Processing and Repair. Cell *139*, 87–99.

Williamson, M.P. (1994). The structure and function of proline-rich regions in proteins. Biochem. J. *297 (Pt 2)*, 249–260.

Wu, H.-H., Wu, P.-Y., Huang, K.-F., Kao, Y.-Y., and Tsai, M.-D. (2012). Structural Delineation of MDC1-FHA Domain Binding with CHK2-pThr68. Biochemistry *51*, 575–577.

Wu, L., Luo, K., Lou, Z., and Chen, J. (2008). MDC1 regulates intra-S-phase checkpoint by targeting NBS1 to DNA double-strand breaks. Proceedings of the National Academy of Sciences *105*, 11200–11205.

Xia, B., Sheng, Q., Nakanishi, K., Ohashi, A., Wu, J., Christ, N., Liu, X., Jasin, M., Couch, F.J., and Livingston, D.M. (2006). Control of BRCA2 Cellular and

Clinical Functions by a Nuclear Partner, PALB2. Molecular Cell *22*, 719–729.

Xiao, A., Li, H., Shechter, D., Ahn, S.H., Fabrizio, L.A., Erdjument-Bromage, H., Ishibe-Murakami, S., Bin Wang, Tempst, P., Hofmann, K., et al. (2008). WSTF regulates the H2A.X DNA damageresponse via a novel tyrosine kinaseactivity. Nature *457*, 57–64.

Xiao, Y., and Weaver, D.T. (1997). Conditional gene targeted deletion by Cre recombinase demonstrates the requirement for the double-strand break repair Mre11 protein in murine embryonic stem cells. Nucleic Acids Research *25*, 2985–2991.

Xiao, Z., Xue, J., Semizarov, D., Sowin, T.J., Rosenberg, S.H., and Zhang, H. (2005). Novel indication for cancer therapy: Chk1 inhibition sensitizes tumor cells to antimitotics. Int. J. Cancer *115*, 528–538.

Xie, A., Hartlerode, A., Stucki, M., Odate, S., Puget, N., Kwok, A., Nagaraju, G., Yan, C., Alt, F.W., Chen, J., et al. (2007). Distinct Roles of Chromatin-Associated Proteins MDC1 and 53BP1 in Mammalian Double-Strand Break Repair. Molecular Cell *28*, 1045–1057.

Xu, X. (2003). NFBD1/MDC1 regulates ionizing radiation-induced focus formation by DNA checkpoint signaling and repair factors. The FASEB Journal *17*, 1842–1848.

Yamaguchi, H., Durell, S.R., Chatterjee, D.K., Anderson, C.W., and Appella, E. (2007). The Wip1 Phosphatase PPM1D Dephosphorylates SQ/TQ Motifs in Checkpoint Substrates Phosphorylated by PI3K-like Kinases †. Biochemistry *46*, 12594–12603.

Yan, Y., Cao, P.T., Greer, P.M., Nagengast, E.S., Kolb, R.H., Mumby, M.C., and Cowan, K.H. (2010). Protein phosphatase 2A has an essential role in the activationof c-irradiation-induced G2/M checkpoint response. Oncogene *29*, 4317–4329.

Yeung, Y.-G., and Stanley, E.R. (2009). Analytical Biochemistry. Analytical Biochemistry *389*, 89–91.

Yin, Y., Seifert, A., Chua, J.S., Maure, J.F., Golebiowski, F., and Hay, R.T. (2012). SUMO-targeted ubiquitin E3 ligase RNF4 is required for the response of human cells to DNA damage. Genes & Development *26*, 1196–1208.

Yoda, A., Xu, X.Z., Onishi, N., Toyoshima, K., Fujimoto, H., Kato, N., Oishi, I., Kondo, T., and Minami, Y. (2006). Intrinsic kinase activity and SQ/TQ domain of Chk2 kinase as well as N-terminal domain of Wip1 phosphatase are required for regulation of Chk2 by Wip1. J. Biol. Chem. *281*, 24847–24862.

Yong, W., Bao, S., Chen, H., Li, D., Sanchez, E.R., and Shou, W. (2007). Mice Lacking Protein Phosphatase 5 Are Defective in Ataxia Telangiectasia Mutated (ATM)-mediated Cell Cycle Arrest. Journal of Biological Chemistry *282*, 14690–14694.

Yoo, S., and Dynan, W.S. (1999). Geometry of a complex formed by double strand break repair proteins at a single DNA end: recruitment of DNA-PKcs induces inward translocation of Ku protein. Nucleic Acids Research *27*, 4679–4686.

You, Z., Chahwan, C., Bailis, J., Hunter, T., and Russell, P. (2005). ATM Activation and Its Recruitment to Damaged DNA Require Binding to the C Terminus of Nbs1. Molecular and Cellular Biology *25*, 5363–5379.

Yu, Y., Wang, W., Ding, Q., Ye, R., Chen, D., Merkle, D., Schriemer, D., Meek, K., and Lees-Miller, S.P. (2003). DNA-PK phosphorylation sites in XRCC4 are not required for survival after radiation or for V(D)J recombination. DNA Repair *2*, 1239–1252.

Yu, Y.-M., Pace, S.M., Allen, S.R., Deng, C.-X., and Hsu, L.-C. (2008). A PP1-binding motif present in BRCA1 plays a role in its DNA repair function. Int. J. Biol. Sci. *4*, 352–361.

Yuan, S.S., Lee, S.Y., Chen, G., Song, M., Tomlinson, G.E., and Lee, E.Y. (1999). BRCA2 is required for ionizing radiation-induced assembly of Rad51 complex in vivo. Cancer Research *59*, 3547–3551.

Zannini, L., Delia, D., and Buscemi, G. (2014). CHK2 kinase in the DNA damage response and beyond. Journal of Molecular Cell Biology *6*, 442–457.

Zgheib, O., Pataky, K., Brugger, J., and Halazonetis, T.D. (2009). An Oligomerized 53BP1 Tudor Domain Suffices for Recognition of DNA Double-Strand Breaks. Molecular and Cellular Biology *29*, 1050–1058.

Zhang, J., Willers, H., Feng, Z., Ghosh, J.C., Kim, S., Weaver, D.T., Chung, J.H., Powell, S.N., and Xia, F. (2004). Chk2 Phosphorylation of BRCA1 Regulates DNA Double-Strand Break Repair. Molecular and Cellular Biology *24*, 708–718.

Zhang, J., Ma, Z., Treszezamsky, A., and Powell, S.N. (2005). MDC1 interacts with Rad51 and facilitates homologous recombination. Nat Struct Mol Biol *12*, 902–909.

Zhao, H., and Piwnica-Worms, H. (2001). ATR-Mediated Checkpoint Pathways Regulate Phosphorylation and Activation of Human Chk1. Molecular and Cellular Biology *21*, 4129–4139.

Zhao, H., Traganos, F., Albino, A.P., and Darzynkiewicz, Z. (2008). Oxidative

stress induces cell cycle-dependent Mre11 recruitment, ATM and Chk2 activation and histone H2AX phosphorylation. Cell Cycle *7*, 1490–1495.

Zhong, J., Liao, J., Liu, X., Wang, P., Liu, J., Hou, W., Zhu, B., Yao, L., Wang, J., Li, J., et al. (2011). Protein phosphatase PP6 is required for homology-directed repair of DNA double-strand breaks. Cell Cycle *10*, 1411–1419.

Zhou, B.B., and Bartek, J. (2004). Targeting the checkpoint kinases: chemosensitization versus chemoprotection. Nature Reviews Cancer *4*, 216–225.

Zhou, B.B., and Elledge, S.J. (2000). The DNA damage response: putting checkpoints in perspective. Nature *408*, 433–439.

Zhu, J., Petersen, S., Tessarollo, L., and Nussenzweig, A. (2001). Targeted disruption of the Nijmegen breakage syndrome gene NBS1 leads to early embryonic lethality in mice. Current Biology *11*, 105–109.

Zou, Y., Liu, Y., Wu, X., and Shell, S.M. (2006). Functions of human replication protein A (RPA): From DNA replication to DNA damage and stress responses. J. Cell. Physiol. *208*, 267–273.